Use of Inertial Sensors to Measure Upper Limb Motion: Application in Stroke Rehabilitation

A Dissertation submitted to the
University of Oxford

In partial fulfilment of the requirement
For the Degree of
Doctor of Philosophy

Nour Shublaq

Keble College, Oxford

Michaelmas Term, 2010

Acknowledgements

First and foremost, I would like to gratefully thank both of my supervisors Dr. Penny Probert Smith and Dr. Julie Stebbins for their invaluable guidance and advice throughout, which helped shape the contents of this work. It is with your support that I have achieved this goal!

Thanks are extended to Dr. Rachel Buckingham, Dr. Jane Burridge, and Mr. Tim Theologis whose wise counsel and conversations helped enrich my understanding of the biomechanical problems in the upper limb community, and the movement limitations for stroke patients. Thanks must also go to Dr. Amy Zavatsky and Dr. Paul Newman whose advice and feedback in my first year transfer oral examination allowed me to revise my future plans, and think more about my PhD contributions. Many thanks to Dr. Nigel Harris at the University of Bath for showing me the SMART rehabilitation project for upper limb training, Dr. Helen Dawes at the Movement Science Group at Oxford Brookes University, and Dr. Charles Bibby for his practical advice with the inertial sensors. Also, special thanks to Mr. Eric Peasley at the Department of Engineering Science for his support with the mobile robot.

I would like to thank Dr. Gari Clifford for always having the time to listen to questions. Thanks to Dr. Anne Marie Hughes for her assistance with obtaining the research ethics to collect data from the stroke patient at the University of Southampton. Thanks to Dr. Cheryl Metcalf who showed me the facilities and the Vicon setup in the Biomechanics Laboratory at the University of Southampton, and Ms. Louise Johnson, a physiotherapist at the Western Community Hospital in Southampton, who helped me attend a physiotherapy session with stroke patients.

Thank you to the wonderful team at the Oxford Gait Laboratory (Jennifer, Jo, Mike, Martin, Rob, and Nicky); you have added a lot of fun to this PhD!! Thank you to all my friends in the Institute of Biomedical Engineering who kept me going, especially Katherine, Yasmina, and Simon for your companionship.

My utmost sincere thanks goes to the UK Engineering and Physical Sciences Research Council (EPSRC), whose funding allowed me to work on this project, and to the collaborators in the 'Motivating Mobility' Consortium (at the Universities of Nottingham, Dundee, Southampton, Sheffield-Hallam, and Sussex) for the enjoyable multi-disciplinary meeting discussions.

I would like to express my gratitude to the Khoury family of the Consolidated Contracting Company (CCC) and Dr. Nabil Qaddumi for funding my Masters studies at Oxford University. Special thanks to Mr. Yusuf Kanan for his significant role in the funding process, ongoing support, and his trust in my potential.

Finally, I would like to thank my parents (dad, mom and two sisters) for being great role models, and for the continuous support and encouragement.

Abstract

Use of Inertial Sensors to Measure Upper Limb Motion: Application in Stroke Rehabilitation[1]

Nour Shublaq
Keble College

Submitted in partial fulfilment of the requirements for the Degree of
Doctor of Philosophy at the University of Oxford

Michaelmas Term, 2010

Stroke is the largest cause of severe adult complex disability, caused when the blood supply to the brain is interrupted, either by a clot or a burst blood vessel. It is characterised by deficiencies in movement and balance, changes in sensation, impaired motor control and muscle tone, and bone deformity. Clinically applied stroke management relies heavily on the observational opinion of healthcare workers. Despite the proven validity of a few clinical outcome measures, they remain subjective and inconsistent, and suffer from a lack of standardisation. Motion capture of the upper limb has also been used in specialised laboratories to obtain accurate and objective information, and monitor progress in rehabilitation. However, it is unsuitable in environments that are accessible to stroke patients (for example at patients' homes or stroke clubs), due to the high cost, special set-up and calibration requirements.

The aim of this research project was to validate and assess the sensitivity of a relatively low cost, wearable, compact and easy-to-use monitoring system, which uses inertial sensors in order to obtain detailed analysis of the forearm during simple functional exercises, typically used in rehabilitation. Forearm linear and rotational motion were characterised for certain movements on four healthy subjects and a stroke patient using a motion capture system. This provided accuracy and sensitivity specifications for the wearable monitoring system. With basic signal pre-processing, the wearable system was found to report reliably on acceleration, angular velocity and orientation, with varying degrees of confidence. Integration drift errors in the estimation of linear velocity were unresolved. These errors were not straightforward to eliminate due to the varying position of the sensor accelerometer relative to gravity over time. The cyclic nature of rehabilitation exercises was exploited to improve the reliability of velocity estimation with model-based Kalman filtering, and least squares optimisation techniques. Both signal processing methods resulted in an encouraging reduction of the integration drift in velocity. Improved sensor information could provide a visual display of the movement, or determine kinematic quantities relevant to the exercise performance. Hence, the system could potentially be used to objectively inform patients and physiotherapists about progress, increasing patient motivation and improving consistency in assessment and reporting of outcomes.

[1] This work was made possible by a grant from the Engineering and Physical Sciences Research Council, UK

Contents

List of Figures ix

List of Tables xv

List of Abbreviations xvii

Chapter 1 Introduction 1

1.1 Introduction 1

1.2 Upper limb monitoring – Current situation and limitations 4

1.3 Research Methodology 6

1.4 Document structure 8

Chapter 2 The Upper Limb in Stroke Rehabilitation: Clinical Background 12

2.1 Introduction 12

2.2 An overview of the upper limb and the effect of stroke 13

2.1.1 The upper limb and region of interest 13

2.2.2 The upper limb: a kinematic chain 15

2.2.3 The effect of stroke 17

2.3 Rehabilitation schools of thought: Restoring proper movement versus function 22

2.4 Outcome measures for upper limb motor performance and function 23

2.5 Summary 26

Chapter 3 Measuring Upper Limb Kinematics: Technical Background 28

3.1 Introduction 28

3.2 Laboratory-based and wearable motion detection/tracking devices 29

3.2.1 Laboratory based systems 31

3.2.2 Wearable systems 36

3.2.3 Other devices 39

3.2.4 The choice of suitable motion detection/tracking devices 39

3.3 Standardising measurement of the upper limb 42

3.3.1 Types of markers and configurations 43

3.3.2 Marker placement 45

3.4 Modelling motion of the forearm 46

3.5 Clinical upper limb kinematic measures 50

3.6 Summary 52

Chapter 4 Measurement of Arm Movement using Vicon™ for Healthy Subjects and a Stroke Patient 54

4.1 Introduction 54

4.2 Upper limb motion data acquisition and pre-processing with Vicon 55

4.2.1 Recruitment of subjects and the research ethics process 56

4.2.2 Subjects 57

4.2.3 Subject preparation and marker placement protocol 58

4.2.4 System set-up and calibration 60

4.2.4.1 System "calibration" 61

4.2.4.2 Residuals 62

4.2.5 Data capture using Vicon 63

4.2.6 Movements 64
4.2.7 Data pre-processing using Vicon 66
4.2.7.1 Marker position reconstruction 66
4.2.7.2 Marker labelling 68
4.2.7.3 Data filtering 69
4.2.7.4 Gap filling: Static reconstruction 70
4.3 Upper limb kinematic model in BodyBuilder (Vicon, U.K.) 72
4.3.1 Segmental coordinate system definitions 72
4.3.2 Rotation angle order and Cardan angles 73
4.4 Results and discussion 73
4.4.1 Results – Three dimensional upper limb model 73
4.4.2 Specifications for wearable monitoring of the forearm performing functional movements 74
4.4.2.1 Normal upper limb movement 77
4.4.2.2 Pathological upper limb movement 80
4.4.3 Minimum sensitivity required to detect differences in pre/post- stroke intervention 81
4.4.4 Discussion 84
4.5 Summary 85

Chapter 5 Evaluation of Inertial Sensors for Upper Limb Monitoring 87
5.1 Introduction 87
5.2 System setup with Xsens^{TM} sensors 89
5.2.1 System calibration of inertial sensors with Vicon 92
5.3 Experiment 1: A mobile robot to evaluate sensor orientation estimates 99
5.4 Experiment 2: A rotating bar to evaluate sensor gyroscopic readings 110

5.5 Experiment 3: Sensor accelerometer accuracy from a simulated "reach" movement of a mobile robot 121

5.6 Experiment 4: Testing the performance of sensors on motion data of a stroke patient 127

5.6.1 Pre-stroke data (Accuracy testing) 127

5.6.2 Pre/Post change measurement (Sensitivity testing) 134

5.7 Summary of results 138

5.8 Summary 144

Chapter 6 Signal Processing Techniques to Improve the Sensor Motion Measurements 146

6.1 Introduction 146

6.2 Previous work 148

6.3 Summary of the motion profile 151

6.4 Model-based estimation 153

6.4.1 Kalman filter design 154

6.4.2 Experiment 1: Robot motion experiment 155

6.4.3 Experiment 2: Healthy upper limb reach experiment 158

6.4.4 Experiment 3: Upper limb reach experiment for a stroke patient 159

6.5 Results 160

6.5.1 Experiment 1: Robot motion experiment 160

6.5.2 Experiment 2: Healthy upper limb reach experiment 164

6.5.3 Experiment 3: Upper limb reach experiment for a stroke patient 165

6.6 Optimisation estimator 167

6.6.1 Optimisation estimator design 167

6.6.2 Healthy upper limb reach experiment 169

6.7 Comparison of the EKF and optimisation techniques 171

6.8 Discussion 172

6.9 Summary 175

Chapter 7 Conclusions, Recommendations, Limitations and Suggested Further Research 177

7.1 Conclusions 177

7.2 Thesis contributions and recommendations 182

7.2.1 Thesis contributions 182

7.2.2 Recommendations for use of inertial sensors 184

7.3 Limitations and suggested further research 186

7.3.1 Biomechanical modelling and markers 186

7.3.2 Movements and outcome measures 186

7.3.3 Sensor accuracy and sensitivity 187

7.3.4 Signal processing 188

7.3.5 Application improvements and more subjects 189

List of References 190

Appendix A Glossary 207

Appendix B Outcome Measures in Stroke Rehabilitation 209

List of Figures

Figure 2.1 The main bone components of upper limb motion (clavicle, scapula, humerus, ulna, and radius) 14

Figure 2.2 The upper body: thorax and sternum 15

Figure 2.3 The upper limb: a multi-link system or kinematic chain 16

Figure 2.4 The primary motor cortex in the forebrain 18

Figure 2.5 The primary motor cortex, the pyramidal tract (within the brain stem), and the descending brain 19

Figure 3.1 Biomechanical forearm model (as a single segment) 49

Figure 3.2 Biomechanical forearm model (as a double segment) 49

Figure 4.1 Healthy subject setup – reflective markers (black dots) 58

Figure 4.2 Stroke patient setup 58

Figure 4.3 Plug-in-Gait marker placement protocol (after adjustments) with positions and labels of passive 59

Figure 4.4 Diagram with an overview of the system setup 60

Figure 4.5 Static and dynamic calibration object 61

Figure 4.6 Vicon's capture volume with the position of cameras, gait lab floor, and in orange the upper limb markers on a subject 64

Figure 4.7 Diagram of the reach-and-grasp exercise from 1 to 2 64

Figure 4.8 Diagram of the forearm pronation/supination exercise from B to A 65

Figure 4.9 Diagram of the hand-to-mouth exercise from 1 to 2 65

Figure 4.10 Markers (before position reconstruction) 68

Figure 4.11 Markers (after position reconstruction) as white dots 68

Figure 4.12 Marker labelling 69

Figure 4.13 Marker set labels 69

Figure 4.14 RASI marker disappearance 72

Figure 4.15 Static reconstruction of the RASI marker 72

Figure 4.16 Development of a three dimensional upper body model (in Vicon Nexus) 74

Figure 4.17 The upper limb model (in BodyBuilder) for forearm pronation/supination 74

Figure 5.1 Diagram with an overview of the system set-up, both for the robot and the human patient 89

Figure 5.2 The Xsens sensor with its fixed local coordinate system overlaid (x,y,z) 90

Figure 5.3 Alignment of Xsens local coordinate system (S) with its fixed global coordinate system (G) 90

Figure 5.4 MTi Xsens sensor 91

Figure 5.5 MTx Xsens sensor 91

Figure 5.6 Determination of point *P* position located in coordinate system {B} relative to {A}, where {B} is a 93

Figure 5.7 Xsens sensors tracked in Vicon to determine ${}^{G}_{V}R$ relating the global coordinate systems of Vicon and Xsens. 95

Figure 5.8 The three forces plates fixed to the gait laboratory floor, NOC 95

Figure 5.9 Determination of ${}^{G}_{V}R$ from estimated sensor three dimensional orientation (roll, pitch, yaw) for sensor S1 96

Figure 5.10 The effect of magnetism on sensor orientation mis-estimation with force plates on for sensor S2. An 99

Figure 5.11 Robot actions presented from Vicon's orientation compution: one sequence was for robot to move straight, ... 101

Figure 5.12 Set-up of the mobile robot with sensor S1 and S1 tracked in Vicon using four markers 101

Figure 5.13 The robot angle about the vertical z-axis for the robot straight motion section: in green Vicon computation 105

Figure 5.14 The robot angle about the vertical z-axis for the robot straight motion section after data detrending: in 105

Figure 5.15 The robot angle about the vertical z-axis for the robot oscillatory/turning motion sections: in green Vicon 106

Figure 5.16 The error in sensor estimation in the robot angle about the vertical z-axis in the oscillatory/turning section 106

Figure 5.17 A linear increase of error in sensor estimation of the robot angle about the vertical z-axis in 107

Figure 5.18 The robot angular velocity about the vertical z-axis for the robot oscillatory/turning sections: in green 108

Figure 5.19 The robot angle about the longitudinal x-axis for the robot straight motion section: in green Vicon 109

Figure 5.20 The robot angle about the longitudinal x-axis for the robot oscillatory/turning motion sections: in green 109

Figure 5.21 Experiment setup: a rotating bar, Xsens sensors and Xbus Master 112

Figure 5.22 Reference point for locating the centres of sensor three dimensional gyroscopic 113

Figure 5.23 Plan view of an Xsens sensor with locations of 3-D gyroscopic centres relative to the red dot reference 114

Figure 5.24 Marker labels for one sensor (S2). The same marker labelling was used across sensor units S3 and S4 114

Figure 5.25 Markers' attachment positions (as 1, 2, 3 orange squares) shown in relation to the physical location of 115

Figure 5.26 Mid-point calculation of vectors joining markers 2 and 3 for three sensors shown as white dots 116
Figure 5.27 Sensor (S3) gyroscope-z accuracy for measuring low angular velocities (reach-and-grasp) for a setting of 119
Figure 5.28 Sensor (S4) gyroscope-z accuracy for measuring low angular velocities (reach-and-grasp) for a setting of 119
Figure 5.29 Sensor internal consistency of the accelerometers and gyroscopes 120
Figure 5.30 Mobile robot with inertial sensor S1: setup and both as tracked in Vicon 122
Figure 5.31 The simulated motion of a robot compared to the reach-and-grasp movement of a healthy upper limb 123
Figure 5.32 Sensor raw acceleration measurement (in blue) compared to Vicon's computation (in red) of the robot 125
Figure 5.33 Sensor acceleration measurement after detrending and high-pass filtering (in blue), compared to Vicon's 125
Figure 5.34 Velocity from integration of raw sensor accelerations (in blue) compared to Vicon's computation (in red) 126
Figure 5.35 Velocity from integration of detrended and high pass filtered sensor accelerations (in blue) compared to 126
Figure 5.36 Comparing the sensor acceleration measurements (in blue) to Vicon's computation (in red) for a stroke 131
Figure 5.37 Comparing the sensor acceleration measurements (in blue) after high pass filtering and detrending, to 131
Figure 5.38 Comparing the velocity estimation from integration of detrended high pass filtered sensor accelerations (in 132

Figure 5.39 Comparing the sensor estimation of pitch (in blue), to Vicon's computation (in red) for a stroke patient 132
Figure 5.40 Comparing the sensor estimation of pitch (in blue) after detrending, to Vicon's computation (in red) 133
Figure 5.41 Comparing the sensor estimation of pitch (in blue) after detrending, to Vicon's computation (in red) 133
Figure 6.1 The velocity profile of a repetitive forearm reach-and-grasp movement for a healthy subject along the 151
Figure 6.2 The velocity profile of a reach-and-grasp movement for a stroke patient 21 months after a stroke. The 152
Figure 6.3 A mobile robot with inertial sensor S1: setup, and both as tracked in Vicon 155
Figure 6.4 Calibrated sensor acceleration measurements along the longitudinal axis of the mobile robot during one 156
Figure 6.5 The marker/sensor placement on the upper limb of a healthy subject and model in Vicon 158
Figure 6.6 The marker/sensor placement on the upper limb of a stroke patient and model in Vicon 160
Figure 6.7 Plots of observed (sensor) and Kalman filter predicted accelerations of the mobile robot motion in blue and 161
Figure 6.8 Innovation in sensor acceleration of the mobile robot motion. Acceleration prediction error significantly 162
Figure 6.9 Comparison of velocity estimate from the Vicon system (in green) with the standard Simpson integration 163
Figure 6.10 Comparison of velocity estimate from the Vicon system (in green) with the Kalman filter (in red) for the 163

Figure 6.11 Plots of observed (sensor) and Kalman filter predicted accelerations of a healthy subject's forearm reach-.....164

Figure 6.12 Comparison of velocity estimate from the Vicon system (in green) with the Kalman filter (in red) for 165

Figure 6.13 Comparison of velocity estimate from the Vicon system (in green) with the Kalman filter (in red) for 166

Figure 6.14 Comparison of velocity estimate from the Vicon system (in green) with the optimisation estimator (in red) for.....170

List of Tables

Table 3.1 Classification of human motion tracking using sensor technologies 30

Table 3.2 Comparison of different motion tracking systems 31

Table 3.3 Clinical kinematic measures of performance 51

Table 4.1 Functional movements of interest 56

Table 4.2 Segment definitions and constituent marker labels 57

Table 4.3 Marker labels and positions of 9 mm spherical markers 59

Table 4.4 Marker reconstruction parameters in Vicon 67

Table 4.5 Segment definitions and constituent marker labels 69

Table 4.6 Coordinate system definitions for the upper body segments in BodyBuilder 73

Table 4.7 Effect of marker position on characterising forearm segment translational motion 76

Table 4.8 Characterisation of forearm motion during reach-and-grasp for four healthy subjects 78

Table 4.9 Characterisation of forearm motion during forearm pronation/supination for four healthy subjects 80

Table 4.10 Comparison of forearm motion during reach-and-grasp for a stroke patient, pre- and post- intervention 82

Table 4.11 Comparison of forearm motion during hand-to-mouth for a stroke patient, pre- and post- intervention 83

Table 5.1 Average value of sensor orientation computed in Vicon and estimated by sensors S2, S3 and S4 97

Table 5.2 Static sensor accuracy for estimating orientation (roll, pitch, yaw) 98

Table 5.3 Marker labels and positions on the robot 102

Table 5.4 Determining Xsens sensor placement based on motion analysis of forearm reach-and-grasp and 111

Table 5.5 Marker labels and positions on the robot and sensor 122

Table 5.6 Difference between sensor acceleration and Vicon computation of acceleration (mean error) for the mobile 124

Table 5.7 Difference between sensor measurement/estimation and Vicon computation (mean error) for a stroke patient 129

Table 5.8 Difference between sensor measurement/estimation and Vicon computation (mean error) for a stroke patient 129

Table 5.9 Sensor sensitivity to detect change in movement in pre/post- stroke intervention for the reach-and- 136

Table 5.10 Sensor sensitivity to detect change in movement in pre/post- stroke intervention for the hand-to-mouth 136

Table 5.11 Sensor 95% confidence interval (which is sensor RMS errors ± 2*σ_d, where σ_d is the standard deviation of 137

Table 5.12 The measurable difference to detect change in movement in pre/post- stroke intervention for the reach- 137

Table 5.13 Sensor sensitivity to detect change in movement for the reach- and-grasp and hand-to-mouth movement, ... 137

Table 6.1 Motion analysis of healthy subjects and a stroke patient 153

Table 6.2 The Kalman filter: Initialisation of variables (V_I) and noise co-variances (NC_I) 157

Table 6.3 Differences in the amplitude of velocity positive peaks before and after Kalman filtering across the four 167

Table 6.4 Error analysis to compare the performance of the EKF and optimisation techniques (as compared to Vicon) 172

List of Abbreviations

AC	acromio-clavicular
ADL	activities of daily living
ARAT	Action Research Arm Test
AV	average velocity
CP	coefficient of periodicity
BSRM	British Society of Rehabilitation Medicine
DH	Department of Health
EKF	Extended Kalman filtering
EMG	electromyography
GH	gleno-humeral
HR	humero-radial
IR-LED	Infrared light-emitting diode
MD	movement duration
MEM	microelectromechanical
MRC	Medical Research Council
MRI	magnetic resonance imaging
NMU	number of movement units
NOC	Nuffield Orthopaedic Centre
NJ	normalised jerk score
PLR	percent length ratio
PTMV	percent time to maximum velocity
RCT	randomised controlled trial
RMS	root mean square
ROM	range of motion
RT	reaction time
SC	sterno-clavicular
SHUEE	Shriners Hospital for Upper Extremity Evaluation
SMART	Self Management and Assistive Rehabilitative Technology
ST	scapulo-thoracic
UH	ulno-humeral
ULA	upper limb assessment
UR	ulno-radial
US	ultrasound
VR	virtual reality
WHO	World Health Organisation

Chapter 1
Introduction

1.1 Introduction

According to the Stroke Association in the UK, the American Stroke Association, and the National Stroke Foundation in Australia, stroke is the largest cause of severe adult complex disability (Adamson *et al.*, 2004), with 30.7 million people in the world living with the after-effects of stroke (World Health Organisation, 2004). The economic impact of stroke was estimated in 2007 to be at least five billion pounds in the UK (UK Department of Health). Concerns regarding the increasing prevalence of chronic disease, and the need to ensure that spending on long-term conditions is controlled, have led to explicit UK Department of Health (DH) agendas to find innovative, cost-effective, evidence-based ways of supporting the care of stroke and other chronic conditions, especially in older people (Singh, 2005).

In the UK, over two-thirds of stroke patients are impaired in activities of daily living (ADL) due to partial paralysis of the upper limb (Caimmi *et al.*, 2008). In general, one upper limb is affected by stroke. The physical after-effects of stroke include numbness or weakness, paralysis, impaired motor control, changes in sensation, deformity, and spasticity (an increase in muscle tone). These not only affect the upper limb's ability to execute general movements and perform everyday tasks, but also have a significant impact on the patient's quality of life. The aim of this work is to thoroughly assess the performance of a single sensor, as a monitoring and feedback tool, to measure forearm motion during functional movements.

In general, the goal of rehabilitation is to limit the impact of stroke related brain damage on daily life, using a mixture of therapeutic and problem solving approaches (Young & Foster, 2007), to enable a person who has experienced a stroke to regain as much movement as possible, and the highest level of independence. Full brain recovery following stroke is seen as a return to normal brain activation patterns (Krakauer, 2005); this is not always achieved during the course of the rehabilitation programme due to the extent of the damage to the brain. In such cases, additional areas in the brain are recruited to allow partial recovery (Krakauer, 2005). So undamaged parts of the brain learn to take over the functions of the damaged parts, and the patient must then re-learn how to perform various motor tasks (The Stroke Association, 2009).

Recent neuro-imaging evidence and randomised controlled trials (RCTs) suggest that the brain's responsiveness to achieve recovery of function is best and fastest at the early stages of stroke therapy (Biernaskie *et al.*, 2004, Baron *et al.*, 2004). This is because the brain's ability to reorganise, and plastic adaptation of the central nervous system, are both time-dependent, rehabilitation-induced processes. The activation of the reorganisation at different parts of the brain occurs at different phases of recovery, and for some parts, recruitment is only possible during the early post-stroke phase (Ward *et al.*, 2004).

While the most important predictor of recovery after stroke is the severity of the initial deficit (Krakauer, 2005), the effectiveness of stroke therapy and long term prognosis have been related to the quality and quantity (intensity and frequency) of treatment, especially in the months immediately following the stroke (Teasell & Kalra, 2005). There is agreement that a greater intensity of arm rehabilitation leads to small but lasting effects on arm fine movement and dexterity; however, the effect on arm function was not conclusive

according to Van der Lee et al. (2001). Later, Feys et al. (2004) showed that an early, repetitive, and targeted stimulation of the arm after a stroke resulted in a clinically meaningful and long-lasting effect on motor function in patients, even after five years. Specific treatment techniques that have shown promise in small-scale studies on highly-selected patients include constraint induced movement therapy (in which the unaffected arm is immobilised for a few hours each day), electro-stimulation, virtual reality based exercise training, and robot aided therapy (in which the affected limb is guided through movements, or a resistive force is provided to exercise against). But there is no clear evidence on the duration, intensity, or the type of therapy most likely to be beneficial (Van der Lee *et al.*, 2001).

Patient motivation (Van Vliet *et al.*, 2001), goal setting, specificity (Krebs *et al.*, 1998, World Health Organisation, 2004), and the degree of relevance of the rehabilitation exercises to the patient (Department of Health, 2007) have been found to have a positive influence on patient adherence to exercise programmes, and participation in physical activity. Also, organisation and coordination of stroke care are recognised to be crucially important in rehabilitation outcome (Maclean *et al.*, 2002, Stroke Unit Trialists' Collaboration, 2001).

While appropriate available treatments, including physiotherapy and occupational therapy (Stroke Association, 2008), can help improve or regain function, standard treatment planning remains empirical, and treatment recommendations are not based on sufficient evidence (Quinn *et al.*, 2009). The assessment of the patient's progress may vary between assessors (Blair & Stanley, 1985). In addition, the patient is likely to be given skilled feedback only occasionally. For instance, in England less than half of patients admitted

with a stroke are treated on stroke units which provide specialised care, and therefore outcomes for many patients at medical non-specialist wards are compromised (Intercollegiate Working Party for Stroke, 2004).

The idea that abnormal movement patterns are inherent in dysfunction has motivated the use of movement analysis and human motion tracking as clinical, diagnostic tools to assess impairment, and to plan treatment. This area emerged with the analysis of abnormal gait (Whittle, 1996, Allard *et al.*, 1995), facilitated by the repetitive nature of the gait cycle. This aims to identify abnormal gait patterns, guide treatment such as the design for corrective footwear and orthoses, among other applications. It has been actively applied in several research areas, like sports science, veterinary science, and clinical rehabilitation since the 1980s (Zhou & Hu, 2008).

In comparison with gait analysis, research in upper limb movement analysis is a relatively recent phenomenon. It is also more difficult to perform due to the complexity and variability of upper limb mechanics. Nonetheless, the same basic concept of measuring movement patterns during specific functional tasks, to understand the fundamental mechanisms involved applies, and is important as a basis for observing impairment.

1.2 Upper limb monitoring – Current situation and limitations

Several clinical upper limb assessments (ULAs) are used, prior to and in conjunction with therapy, to aid clinicians in making a better informed diagnosis, assessing the effectiveness of a rehabilitation technique, recommending a treatment or intervention, and revisiting goals as the therapy progresses. These assessments may be grouped into the categories

clinical examination, and upper limb motion measurements with motion tracking systems (for example, multi-camera motion capture systems, and inertial sensors).

Clinical examination includes visual-based and video-based assessments, which tend to use hierarchical scoring to measure the impairment, loss of function, or degree of patient's dependence/quality of life. The assessments are qualitative even though they give a quantitative score. Also despite the established clinical validity of some, they mostly depend on subjective judgement. This not only undermines the objectivity of measurements, but can also lead to variation in task scoring for one patient between multiple assessors (Blair & Stanley, 1985). There is also a lack of standardisation when it comes to the choice of activities to be assessed. The British Society of Rehabilitation Medicine (BSRM), and the World Health Organisation (WHO, 2002), agree on the importance of providing a standardised framework for comparison and analysis of chosen activities. Video-based clinical assessments also rank the patients' impairment and degree of functional loss based on clinical judgement, but they have the capacity to provide relatively objective scores (as the video can be re-played and the patient assessed by multiple experts). Nonetheless, these video-based assessments still depend on visual observation, and are therefore not entirely quantitative.

The use of multi-camera motion capture systems for upper limb motion tracking has been shown to provide better accuracy and objectivity of measurement compared to video-based systems (Ehara *et al.*, 1995, Ehara, 2002, Eliot *et al.*, 2007, Richards, 1999). The method is widely used in specialised laboratories and in clinical environments, but it is unsuitable in a home based environment due to the high cost, special setup and calibration requirements.

A facility to gather clinically relevant kinematic[2] metrics from wearable sensors as patients exercise at home is an attractive possibility for monitoring performance, and providing real-time feedback to encourage motivation. The portability, compactness and low cost of these sensors make them ideal for wearable monitoring in clinics, or at patients' homes. However, despite major advances in the measurement capabilities of inertial sensors, driven by new developments in the computer games technology and virtual reality industry, there are some known systematic problems (such as gravity bias, and drift) that can affect sensor readings.

1.3 Research Methodology

To date, clinical assessments (described in section 1.2) have been used to provide essential information to measure the upper limb, and monitor progress in rehabilitation. However, the methods either suffer from subjectivity, and variation between assessors (clinical examination), or are too costly and require special expertise to operate (multi-camera motion capture systems). As a result, neither method is suitable to use in a non-clinical environment (for example at patients' homes or stroke clubs); in agreement with the findings of the EPSRC SMART Rehabilitation Project.

The work described here aims to address this issue, and presents the information necessary to develop a possible alternative to current upper limb monitoring methods used in stroke rehabilitation. The alternative system will not only be applicable in a clinical research setting, but could potentially be part of a home-based rehabilitation system. The aim is to validate and assess the sensitivity of a simple measurement technique based on wearable sensors, to obtain detailed analysis of upper limb motion, in particular the forearm segment,

[2] to do with pure motion, without reference to the masses or forces involved

during simple functional exercises typically used in rehabilitation. Several signal processing methods are developed and implemented to improve the sensor measurements, and assessed over a small set of the functional exercises. The performance of the system (inertial sensors combined with signal processing methods) is investigated on a small group of healthy volunteers and a stroke patient. In addition, the system's performance is investigated and discussed for application in a clinical setting, and potentially at patients' homes. It should be emphasised that the aim of this work is to investigate the performance of a single sensor, and not to design a system for home use.

The work deploys the following specific methodologies to the area of human movement monitoring and analysis using inertial sensors, applied to healthy upper limb movements and movements performed during rehabilitation from stroke, including reach-and-grasp, forearm pronation/supination and hand-to-mouth movements.

1. An assessment of the precision and sensitivity of state-of-the-art inertial sensors as compared to a sophisticated multi-camera motion capture system (taken as the gold standard), over motion regimes typical of relevant rehabilitation exercises (both for rigid body tracking, and on human motion data).
2. Establishment of a sensor placement protocol on the arm through validating the sensor readings, by comparing them to motion capture data over the same range of exercises as above.
3. Deployment of signal processing methods, which include a model-based method suitable for cyclic movements and an optimisation technique, to improve the performance of inertial sensors by reducing/removing artefacts, and using improved methods of data integration with application of motion constraints.

4. An evaluation of the system on a small group of healthy volunteers and a stroke patient, with proposed recommendations for system use inside and outside the clinic.

Long-term or potential outcomes of the work are that the improved sensor measurements may be used to provide a visual display of movement, or to determine kinematic quantities relevant to the performance of the exercise (as in (Caimmi *et al.*, 2008)). Consequently, the system could potentially be able to inform patients and physiotherapists objectively about progress, increasing patient motivation (Caimmi *et al.*, 2008, Cozens & Bhakta, 2002, Maclean *et al.*, 2002), and improving consistency in assessment and reporting of outcomes.

1.4 Document structure

An outline of the bony anatomy of the upper limb is presented in Chapter 2, identifying the underlying skeletal body structures. The undesirable physical after-effects of stroke on upper limb motor performance and functionality are highlighted. Concepts related to functional rehabilitation strategies of the upper limb are also provided, along with the outcome measures clinically applied on a daily basis. Finally, the chapter provides insight into the choice of the protocol used to define the arm movements.

Chapter 3 provides a review of research and commercially based motion detection/tracking devices, with a focus on existing or potential application to stroke rehabilitation. The devices are grouped into laboratory-fixed and wearable categories for comparison purposes. The results of the comparison are later used to identify a motion tracking device that meets the requirements of this research. The chapter briefly discusses marker placement methods,

and provides the literature to model and assess forearm movements. A list of relevant, clinical kinematic measures accumulated from a review of the literature is also provided.

Chapter 4 presents the development and implementation of a computational method to describe the kinematic associations of segments and joints of the right and left upper limbs, the trunk and pelvis, with a main focus on the forearm. This method is based on motion data measured by a multi-camera motion capture system (chosen in Chapter 3). Motion regimes for three functional movements, typical in stroke rehabilitation, are characterised, which relate to forearm linear motion (position) and its derivatives, and forearm rotational motion (orientation) and its derivative. The computational method (kinematic model) is later applied both to data from the motion capture system, and data collected from a number of wearable inertial sensors (also chosen in Chapter 3). Specifications of accuracy and sensitivity for wearable monitoring of the forearm, while performing the functional movements are defined, for both healthy subjects and stroke patients. This information is necessary to determine whether wearable motion sensors are suitable (accurate and sensitive enough) to measure the functional movements, and to quantify movement differences in pre/post- stroke intervention. Subjects' demographics, inclusion/exclusion criteria, details on the movements, and the process of obtaining research ethics are all included.

Chapter 5 assesses the dynamic and static measurement accuracy of inertial sensors for rigid body tracking, with known movement parameters. Sensor measurement errors in linear and rotational motion are then determined, as a basic accuracy measure. The sensor accuracy is also determined for human motion data, when measuring the forearm motion of a stroke patient. In both scenarios, the gold standard is data acquired from the motion

capture system, used in Chapter 4. The sensors' sensitivity within certain confidence intervals is found for linear and rotational motion, and compared to the sensitivity requirements determined in Chapter 4. Simple signal processing methods to manage the sensor measurement errors are presented, along with their effect on the sensor accuracy and sensitivity. The effect of environmental conditions and possible external magnetism on sensor operation and data collection is investigated. Appropriate and practical considerations are given in this chapter, in terms of establishing a sensor mounting method, and determining the best conditions for sensor operation and data collection. Consequently, the strengths and limitations of the sensor performance are discussed. The sensor internal consistency of its components is also investigated.

Chapter 6 presents the development of a model-based method suitable for cyclic movements, and an optimisation technique to improve the raw sensor measurements using data integration and application of motion constraints, for a typical rehabilitation movement. The model-based algorithm is first evaluated on the simulated movement data of a rigid body. Later, the algorithm's efficiency is tested on healthy and pathological motion data measured by a sensor on the forearm. The optimisation technique is developed and tested on the healthy motion data of the sensor placed on the forearm. The performance of the two signal processing methods is then compared, and discussed in the context of their suitability for different applications.

Chapter 7 summarises the conclusions that can be drawn from this work, and re-visits the main thesis contributions. It comments on the practicalities of sensor mounting. It advises on suitable environmental conditions for sensor operation and data collection, in terms of minimising sensor measurement errors and increasing accuracy. Also, recommendations

on the signal processing methods to reduce the effect of error, and improve the raw sensor measurements are given. These cover recommendations for system use inside the clinic, and potentially outside the clinic. Finally, possible areas of further research are outlined.

Chapter 2

The Upper Limb in Stroke Rehabilitation: Clinical Background

2.1 Introduction

The human skeleton, and in particular the upper body, is a highly articulated structure, with joints capable of rotations incorporating many degrees of freedom (Morecki *et al.*, 1971). In comparison to gait analysis, the development of kinematic measurement of the upper limb is more complex, given the intrinsic, composite, non-cyclic, redundant, and complementary nature of upper limb movement. In this chapter, the bony anatomy of the upper limb is briefly introduced, as it forms the basis of its functional capability, together with the mechanisms involved in functional movements. The undesirable after-effect of stroke to upper limb motor performance and functionality is also reviewed.

In addition, an overview of stroke rehabilitation for the upper limb is presented. Two main rehabilitation schools of thought exist, which primarily focus on restoring either movement or function. In the context of rehabilitation, function refers to a day-to-day activity. Hence, protocols for arm movement restoration are either based on specific movement exercises or on day-to-day activities. The concepts related to these functional rehabilitation strategies are briefly described.

Relevant and appropriate outcome measures, which are clinically applied on a daily basis, are summarised. For definitions of the technical terms appearing in this chapter, and indicated at first use in italics, refer to the Glossary (in Appendix A).

2.2 An overview of the upper limb and the effect of stroke

2.2.1 The upper limb and region of interest

Neglecting the hand, the human upper limb may be described as being composed of five bones, the clavicle, the scapula, the humerus, the ulna and the radius (Figure 2.1), forming two joints, the shoulder mechanism and the elbow joint. The upper limb is attached to the trunk via a set of bones, called the pectoral girdle. The girdle also provides an attachment point for the muscles that allow the shoulder and the elbow to move.

Considering bones in pairs, seven joints may be distinguished (Figure 2.1 and Figure 2.2): the sterno-clavicular (SC) joint (which *articulates* the clavicle by its *proximal* end onto the sternum), the acromio-clavicular (AC) joint (which articulates the scapula by its acromion onto the *distal* end of the clavicle), the scapulo-thoracic (ST) joint (which allows the scapula to glide on the thorax), the gleno-humeral (GH) joint (which allows the humeral head to rotate in the *glenoid fossa* of the scapula), the ulno-humeral (UH) and humero-radial (HR) joints (which articulate both ulna and radius with the distal end of the humerus), and the ulno-radial (UR) joint (where both proximal and distal ends of the ulna and radius articulate).

Upper limb motion, as in Figure 2.1, is divided into three main components: upper arm (between the shoulder mechanism and the elbow joint), forearm (between the elbow and

the wrist joints), and hand with two surfaces (the anterior or palmar surface, and the posterior or dorsal surface). The work of this thesis is mainly concerned with the forearm segment.

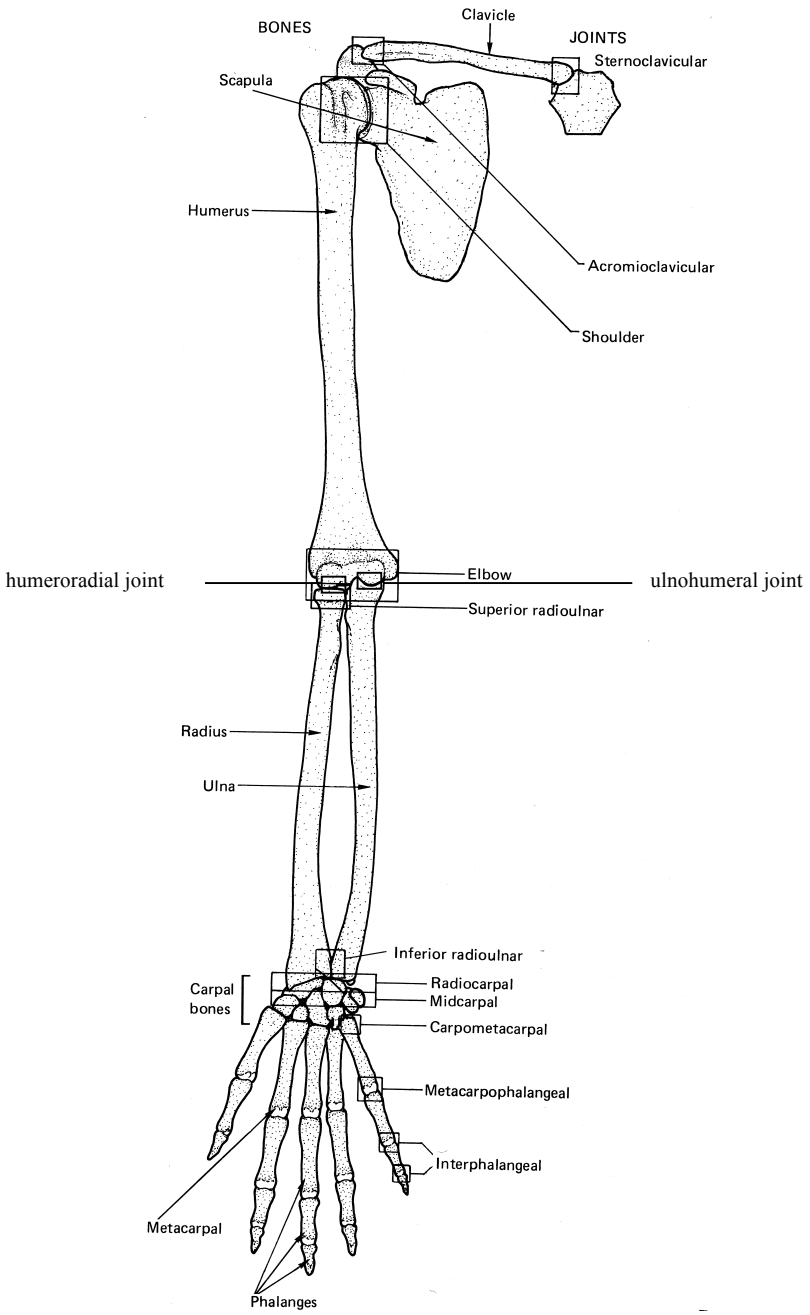

Figure 2.1 The main bone components of upper limb motion (clavicle, scapula, humerus, ulna and radius).
Adapted from (Palastanga *et al.*, 1989)

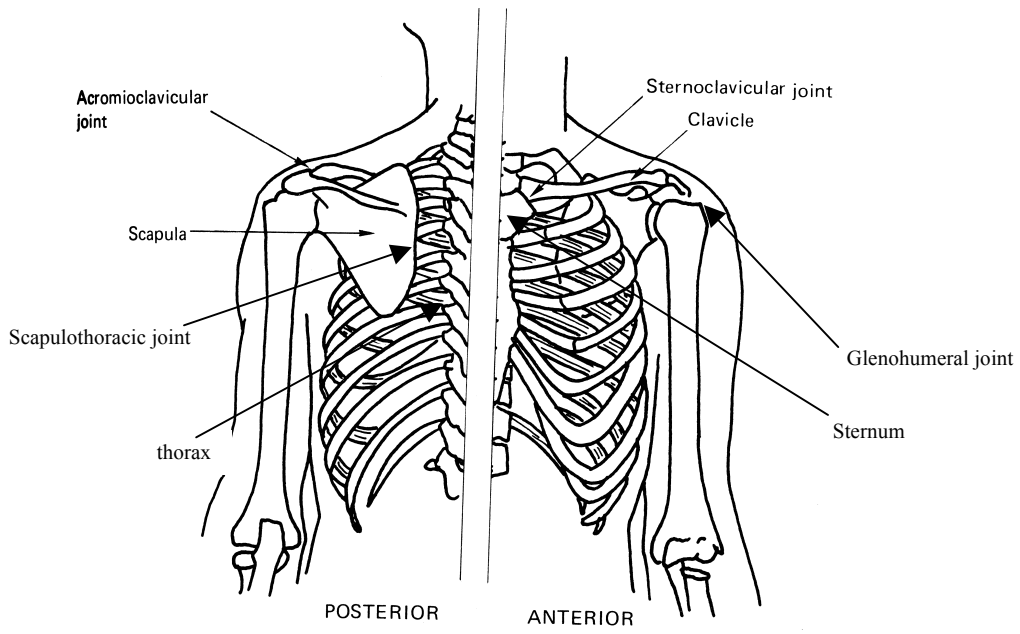

Figure 2.2 The upper body: thorax and sternum.
Adapted from (Palastanga *et al.*, 1989)

2.2.2 The upper limb: a kinematic chain

In the framework of modelling, bones are regarded as rigid bodies, in contrast to surrounding soft tissues (e.g. muscles and ligaments). These rigid bodies (links) are connected by joints to form a "kinematic chain" (a multilink system). The simplest kinematic chain, consisting of two links connected by a single joint, is known as a "kinematic pair". The upper arm – forearm pair is one example connected by the elbow. A rigid body segment can be defined as a limb segment, for instance the upper arm (anatomically, the humerus). The forearm is also assumed to be a single segment in most upper limb modelling literature (Figure 2.3) even though anatomically it is comprised of two bones, the radius and the ulna (Figure 2.1).

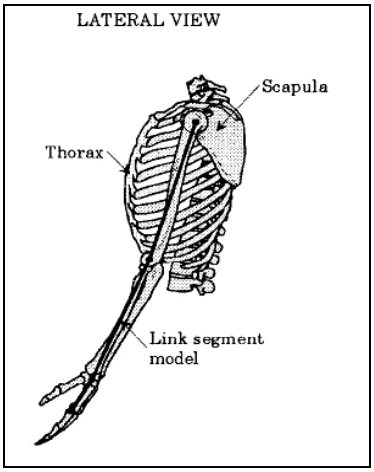

Figure 2.1 The upper limb: a multi-link system or kinematic chain
Reproduced from (Anglin & Wyss, 2000b)

Assuming a gross body model (where the main joints are included), the upper limb is considered to have seven degrees of freedom, namely three at the shoulder, two at the elbow and two at the wrist; the scapula and clavicle are each considered to have three degrees of freedom (Anglin & Wyss, 2000b).

This introduces the components and the basic structure of an upper limb skeletal model. Soft tissues (e.g. muscles, skin) surrounding the skeletal structure ideally should also be accounted for (considering skin properties and muscle activity), given their effect on skeletal motion. They introduce skin motion artefacts, and represent uncertainty in the rigid body assumption of the behaviour of the model segments.

Nonetheless, when conducting upper limb motion analysis, studying the bones in isolation from their surrounding soft tissue counterparts is crucial. This is permitted under the assumption that both bones and soft tissues behave in a similar rigid body manner, and soft tissue deformation does not significantly affect the rigid body properties of the segment. Therefore, the forearm model in this work is only based on the rigid body skeletal motion. This approach in modelling is commonly used as it provides a good representation of the

segment motion, and sufficient computational detail of the kinematics to inform clinicians. The effect of muscles and skin is not included here.

Another consideration is the degrees of freedom joints are assumed to have for different movements. In general, simplifications to the degrees of freedom available to joints are made. These are recognised as limitations to the upper limb model.

In considering forearm motion, which is the segment of interest to this work, translation and rotation are facilitated by the degrees of freedom at the wrist and elbow joints. For a relatively simple movement like reach-and-grasp, forearm translation occurs along the longitudinal axes of the forearm, facilitated by elbow and shoulder flexion/extension. The rotation of the forearm is mainly about the longitudinal axis, and occurs along the whole length of the forearm. It is made possible by the arrangement of the ulna and radius bones, and the way in which the two bones can twist relative to one another, mainly at the distal end.

2.2.3 The effect of stroke

When the blood supply to an area in the brain is interrupted, either by a clot or a burst blood vessel (haemorrhage), the brain cells are deprived of oxygen and eventually die. Positive and negative motor symptoms including sensory and neural dysfunction occur as a result, usually just affecting one side of the body, which neurologists collectively refer to with the term “hemiparesis” (Krakauer, 2005). Understanding the physiology of hemiparesis and motor recovery was the interest of several studies in the 1960s and 1970s (Beck & Chambers, 1970, Lawrence & Kuypers, 1968b). The primary motor cortex (highlighted in pink in Figure 2.4) supports a host of body segment representations. Motor

control output is provided by the motor cortex, area residing in the forebrain, to the spinal cord either directly, or through the *pyramidal tract* in the brain stem and the *descending brain stem pathways* (Figure 2.5). Hence, damage imposed on the pyramidal tract for instance, was found to lead to a permanent loss of independent movements (like finger movements) with unaffected grip strength, whereas lesions of the descending brain stem pathways produced postural abnormalities, but distal limb control was preserved. These results were reported to be congruent with bedside findings in post-stroke patients (Krakauer, 2005).

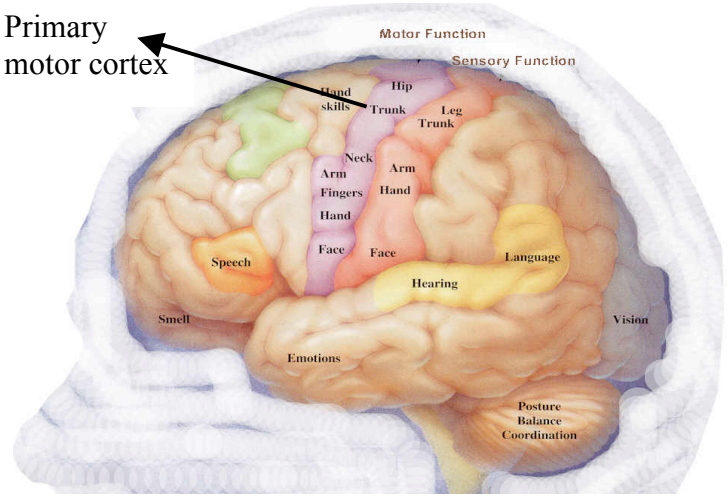

Figure 2.2 The primary motor cortex in the forebrain.
Reproduced from (Canadian Institute of NeuroSciences, 2005)

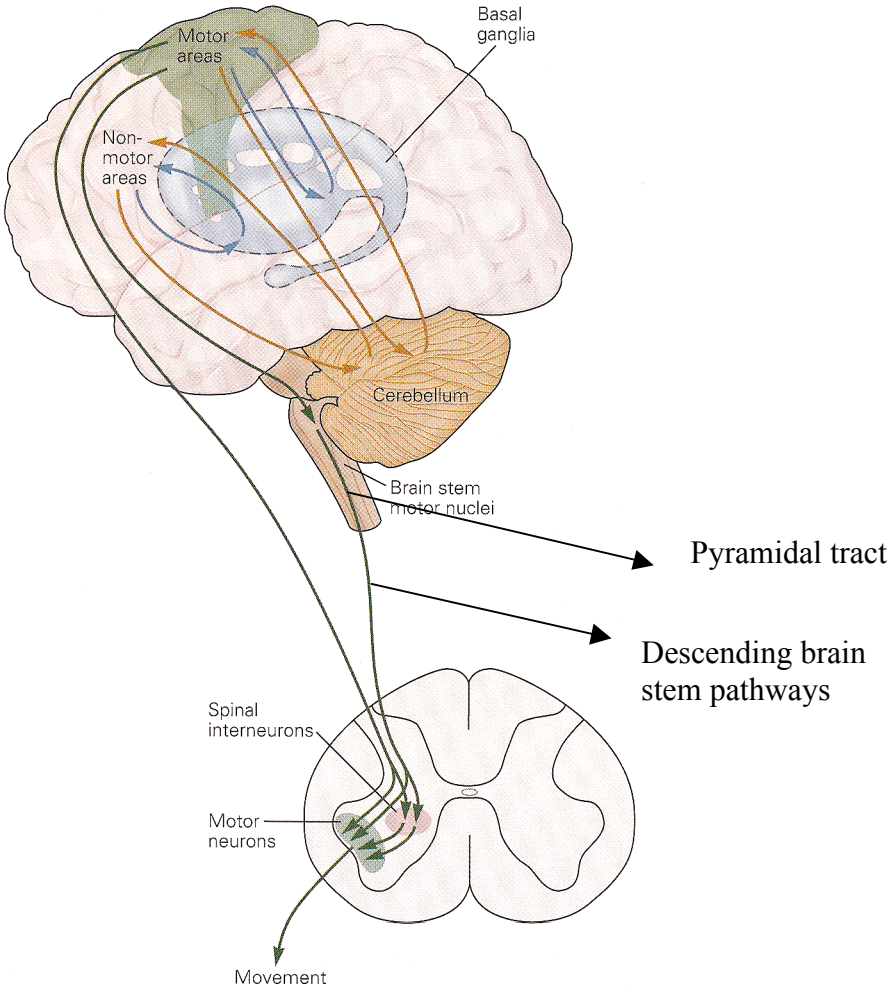

Figure 2.3 The primary motor cortex, the pyramidal tract (in the brain stem), and the descending brain stem pathways. Adapted from (Kandel *et al.*, 2000)

Later, motor control theorists studied arm reaching movements in healthy subjects and stroke patients to further understand the processes involved in motor function deficit due to stroke. Reaching was studied as an important, functional task. It was thought to be modular (i.e. made of simple elements, which can be separately affected by a lesion) (Mussa-Ivaldi, 1999), and consisting of two distinct parts, the geometry of the movement (kinematics) and the forces needed to generate it (dynamics) (Shadmehr & Wise, 2005). As the kinematic characteristics and velocity profiles did not vary for multiple reaching movements involving several joints, *advance planning* was suggested to drive the movements, irrespective of the manipulation of limb dynamics (Morasso, 1981). Target location is encoded into a planned motor movement with an extent and direction relative to the

starting point (Ghez *et al.*, 2000). Then motor commands are generated, given the configuration and inertial properties of the multi-jointed limbs, to produce the forces needed to execute the desired movement.

The arm was also found to have greatest inertia in directions that required rotation of the elbow and shoulder joints, and lowest inertia when only the elbow joint rotated (Hogan, 1985). So uncontrolled reaching following stroke was hypothesised to be related to errors in these direction-dependent changes in the inertial resistance to forearm motion (inertial anisotropy), or a difficulty in controlling torques produced by multi-articulated limbs, which were dependent (the problem of interaction torques) (Hollerbach & Flash, 1982). It was hypothesised that the latter occurred due to a de-calibration of an internal model of limb dynamics, due to non-use, similar to the concept of loss of skill due to non-use of a limb.

Studies on cats and monkeys revealed many aspects of stroke, and its effect on motor performance (Ashby *et al.*, 1972, Lawrence & Kuypers, 1968a). Pure pyramidal lesions cause hemiparesis without increased *muscle tone*. Spasticity is a velocity-dependent increase in muscle tone, combined with an increased excitability of the resting stretch reflex (hyperreflexia), and an increase in muscle flexor tone with sudden relaxation (the clasp-knife phenomenon) (Lance, 1980). Spasticity might be problematic but there is little evidence that it contributes to impairment of voluntary movement, as reported by (Krakauer, 2005, Thilman *et al.*, 1991). Motor synergies could also occur after stroke, which are stereotypic patterns of muscle co-activation that limit independent control of single joints (Brunnstrom, 1994, Dewald *et al.*, 1995, Twitchell, 1950). With the flexor synergy, there is forearm *supination* and elbow *flexion* when the shoulder flexes and

abducts, while with the extensor synergy, there is forearm *pronation* and elbow *extension* when the shoulder extends and *adducts*. By contrast, healthy subjects can contract and activate isolated muscles on demand.

Other than spasticity and muscle synergies, weakness and abnormalities in interjoint coordination between the elbow and shoulder are prominent (Levin, 1996), resulting from a deficit in transforming the planned movement trajectory into the corresponding joint angles (known as the inverse dynamic problem). A loss of *proprioception* or *tactile* sensation is possible, which reduces the probability of recovery when combined with hemiparesis (Krakauer, 2005); in addition to an inappropriate temporal sequencing of muscle activity. Finally, Brodal (1973) highlighted the involvement of the unaffected arm with the deterioration of the stroke-affected arm. These deficits depend on whether the *infarct* is in the dominant or nondominant *hemisphere* (Bernspang & Fisher, 1995, Winstein & Pohl, 1995). This implies that bilateral hemisphere activation takes place even during unilateral arm movements (Kim *et al.*, 1993). This also means that the patient's unaffected arm is unsuitable to be used as an experimental control for the affected arm. Instead, age-matched healthy subjects should be used (Krakauer, 2005).

Specific reported after-effects of stroke on forearm motion include limited active range of motion, muscle synergies, stiffness, weakness and tiring, painful muscle spasms, involuntary rhythmic contractions, and exaggerated reflexes (Krakauer, 2005, The Stroke Association, 2009).

Human movements are generally constrained by anatomic[3], actual[4], mechanical[5] and motor task[6] type constraints, and other factors relating to pathology and functional synergies[7]. These constraints reduce the redundant degrees of freedom (multiple routes) for the execution of a particular movement. According to the work of Latash and Levin (2004), a healthy individual will always adopt the simplest and most energy cost-effective solution to complete a given task. Stroke patients or individuals with impairment have extra limitations to their movement, which vary depending on the motor deficit. So despite similar optimisation strategies as outlined above, movement strategies adopted by stroke patients will be different from healthy subjects, given their extra movement constraints (De Quervain *et al.*, 1996).

2.3 Rehabilitation schools of thought: Restoring proper movement versus function

There is evidence that chronic stroke patients (six months after a stroke) tend to continue to respond to rehabilitation (Krakauer, 2005). Some patients do not show significant progress by the sixth month period, and may need more extended periods of rehabilitation. Rehabilitation techniques vary depending on the lesion location (Feys *et al.*, 2000, Shelton & Reding, 2001), but overall the aim is to enhance learning-related changes after stroke, and contribute to recovery. There are two main rehabilitation schools of thought to restore movement after upper limb impairment. The first promotes the restoration and improvement of upper limb function (to regain patient's independence), while the second

[3] imposed by the structure of the musculoskeletal system (e.g. a joint has to preserve its integrity by a limited range of motion)
[4] incurred by physical obstacles, preventing motion beyond a given border or limit (like the supporting contact pedal surfaces during bicycling)
[5] are those that are necessitated by limited friction or balance demands
[6] are imposed both voluntarily and involuntarily during movement execution
[7] joints' movement is coupled over the duration of the action

defines patient's progress by checking whether the sequence of motion components followed is correct. A good balance between these two viewpoints can optimise upper limb rehabilitation.

Protocols used in rehabilitation are therefore based either on functional tasks, with emphasis on subject functionality and everyday life (known as activities of daily living, ADLs), or individual isolated movements prioritising fine movement and dexterity aspects of motor ability. Examples of functional tasks are reaching, reaching-and-grasping, combing hair, hand-to-mouth/drinking, and hand-to-back pocket motions (Van Andel *et al.*, 2008). Isolated upper limb movements include elbow flexion/extension, forearm pronation/supination, and shoulder flexion/extension/abduction (Johnson & Anderson, 1990).

2.4 Outcome measures for upper limb motor performance and function

The need to measure outcome in rehabilitation, to assess the upper-extremity limitations of stroke patients, and measure their progress in rehabilitation is undisputed. Duncan et al. (1992) showed that the Fugl-Meyer score (an outcome measure) at one month predicted 86 percent of the variance in recovery of motor function at six months. According to the British Society of Rehabilitation Medicine (Turner-Stokes, 2000), no one single instrument can be used as a common measure in different rehabilitation settings. Still, all outcome measures should be scientifically sound and validated, reliable, sensitive to change, clinically useful and applicable, feasible to use, and relevant to the intervention pursued.

In choosing an appropriate outcome measure, it is important to identify the progression of the condition to be measured (impairment, disability, dependency), determine the problem nature (neurological, musculoskeletal, amputation) and the setting (hospital, community), and check for any time constraints in the routine clinical practice (Turner-Stokes, 2000). A scale's usefulness can be predicted by considering issues such as consistent scoring, and standardisation among different users.

Established clinical examination based rehabilitation outcome measures are in practice categorised as generalised (e.g. Motricity Index and Motor Assessment Scale), mobility (e.g. Rivermead Mobility), and upper limb function tests (e.g. Nine-hole Peg Test) (Turner-Stokes, 2000). Other widely used measures, with proven reliability and validity, include the Action Research Arm Test (ARAT) that assesses upper limb function, and Fugl-Meyer test that measures the upper limb impairment (Platz *et al.*, 2005). These are often used to evaluate the efficacy of treatment for one patient or for a study population, by categorising their tests using, for example, pass/fail (known as hierarchical scoring). Appendix B gives a brief description to all these different outcome measures.

Despite the simplicity and clinical suitability of clinical examination based outcome measures, there are some serious issues associated with these measures. A lack of sensitivity at the upper and lower ends of arm function and ability is sometimes apparent, which is known as the ceiling and floor (or basement) effect respectively. The measures are also dependent on subject effort and observer ratings, which introduce bias. Ways to improve these issues include timing the patients' test activities, incorporating nominal cut-off activity times into the scoring criteria (so it is not simply pass or fail) and using a double-blind protocol.

None of the clinically proven scales mentioned above is appropriate to quantitatively assess upper limb impairment or loss in function. This is informed by the work of Gresham et al. (1995), which found that only seven out of 32 recommendations in stroke rehabilitation practice were based on experimental evidence. Recent advances in imaging have informed the rehabilitation process, providing better understanding of the adult brain reorganisation after injury (Krakauer, 2005). Current research has shown that better outcome measures, attainable using motion capture technology and inertial sensors, support accelerated recovery in stroke in the clinical environment (Zhou & Hu, 2008). However, there is still a need for outcome measures to reflect the isolated components of movements that are clinically relevant.

One video-based and recently developed tool is the Shriners Hospital for Upper Extremity Evaluation (SHUEE) protocol (Shriners Hospital Upper Extremity Evaluation (SHUEE) protocol, 2005), which provides a detailed description of the position of the thumb, fingers, wrist, forearm and elbow (Klingels *et al.*, 2010). It assesses the level of body function (e.g. range of motion from shoulders to fingers, muscle tone, and activities of daily living). It also analyses the motion of the involved extremity during functional activities in terms of the spontaneous functionality, dynamic positioning, and grasp-release (with wrist in flexion, neutral and extension).

Outcome measures for the work in this thesis used movements which were chosen in line with the SHUEE protocol, given its emphasis on measuring skeletal motion within functional tasks, and its established validity in assessing the motion of the upper extremity for children with cerebral palsy (Davids *et al.*, 2006). Despite the SHUEE protocol not

having been validated for stroke patients, it helped to identify the individual components of the functional movements of interest clinically.

Three movements, which were functional and typical of upper limb rehabilitation, were chosen in this work for upper limb monitoring. These were reach-and-grasp, forearm pronation/supination (e.g. accepting a coin), and hand-to-mouth (e.g. drinking/eating) movements. The first two movements had primarily translational and rotational components of forearm motion respectively, while the third was a combination. The movements could be performed in a predefined and repeatable manner. They were also constrained, which ensured that the movements' components in translation and rotation could be quantified, and better measured (for more detail, see section 4.2.6).

2.5 Summary

This chapter provided background of the bony anatomy of the upper limb, and the effect of stroke. Statistically significant improvement was seen in stroke patients in the first three to six months as reported by (Goldstein & Matchar, 1994, Krakauer, 2005, Wade *et al.*, 1983), with the initial severity of paresis as the best predictor of recovery of arm function. In restoring upper limb movement, two main schools of rehabilitation exist; one prioritised arm function, and the other motor performance.

Different outcome measures were used to assess the efficacy of therapeutic interventions and the progress of stroke patients. Their strengths and weaknesses were provided. It was concluded that none of these clinically proven scales was adequate to quantitatively assess upper limb impairment or loss in function. Outcome measures for this work needed to be objective, quantitative, and reflect the isolated components of movements that were

clinically relevant. Functional movements of the forearm were chosen in line with the SHUEE protocol, given its emphasis on measuring skeletal motion within functional tasks, and its established validity in assessing motion of the upper extremity in children with cerebral palsy. These movements were reach-and-grasp, forearm pronation/supination, and hand-to-mouth.

Chapter 3
Measuring Upper Limb Kinematics: Technical Background

3.1 Introduction

A reliable, accurate and sensitive system that can measure upper limb motion, and gather clinically relevant kinematic metrics, is an attractive possibility to monitor performance, and provide feedback to stroke patients as they exercise. The system should be wearable, so it is not restricted to the clinical environment, and could potentially be part of a home-based rehabilitation system. However, proper validation and assessment of the wearable system is needed before this can be implemented, by comparing the wearable system's measurements to those of an accurate laboratory-based motion tracking system.

The variety, complexity and range of upper extremity movements (as discussed in Chapter 2) make the measurement, assessment, and interpretation of upper limb motion data a real challenge, which becomes even more complicated with pathological motion. However, the equipment and well-established procedures from decades of gait analysis have guided the development of possible approaches for the three dimensional analysis of upper extremity movements. This chapter briefly summarises the efforts and challenges of previous research in upper limb motion analysis, while providing an overview of the pathology groups of interest, areas of application, movements studied, and the outcomes used for upper limb motion assessment.

The chapter reviews research and commercially based motion detection and tracking devices, with a focus on existing or potential application to stroke rehabilitation. The devices are classified in terms of their measurement function and setting of operation (laboratory-based versus wearable). Based on the results of the review, two motion detection and tracking systems are chosen, that meet the requirements of this work. The systems include a wearable system, and a laboratory based system for validation purposes. Drawbacks of the wearable system are stated, along with the research where these problems have been identified, and the methods developed to improve the motion data measurements.

Methods for standardising upper limb kinematics, in terms of marker systems, configurations and placement, are presented with a view to choosing a suitable marker system and placement protocol to capture forearm movements. Research on upper limb kinematics, mainly to model the forearm and calculate its movement, is provided. A list of relevant clinical, kinematic measures accumulated from a review of the literature is given. Technical terms, and the terminology used to describe limb movement in relation to the body are defined in the Glossary (in Appendix A), and are indicated in italics.

3.2 Laboratory-based and wearable motion detection/tracking devices

The use of tracking devices has been demonstrated to contribute to an accelerated recovery in stroke, in particular the laboratory-based systems (Zhou & Hu, 2008). Despite this capacity, and the favourable performance of some systems, there are also some limitations. These are mainly due to the complexity of human motion, and the existence of noise

sources or measurement errors. This gives rise to system design challenges for monitoring upper limb motion.

Traditionally, motion detection and tracking systems are classified based on the sensing technologies employed, as given in Table 3.1. Table 3.2 provides an overview of the different types of tracking systems. The criteria adopted in this work to define a wearable monitoring system is if the system's output is immediately available without complicated computation or need of expertise, its cost is low, and compactness is high. By this definition and as given in Table 3.2, systems are discussed separately as laboratory-based and wearable systems.

Table 3.1 Classification of human motion tracking using sensor technologies Reproduced from (Zhou & Hu, 2008)

Human Motion Tracking	
a. Non-visual tracking	
1	*Inertial based*
2	*Magnetic based*
3	*Other sensors*
4	*Glove based*
b. Visual tracking	
1	*Visual marker based (passive or active)*
2	*Marker-free visual based*
3	*Combinatorial tracking*
c. Robot-aided tracking	

Table 3.2 Comparison of different motion tracking systems
Adapted from (Zhou & Hu, 2008)

Systems	***Accuracy***	***Compactness***	***Computation***[A]	***Cost***	***Drawbacks***	***Setting***
Inertial	high	high	efficient	low	drift	wearable
Acoustic	medium	low	efficient	low	occlusion/latency	lab-based
Magnetic	medium	high	efficient	low	ferromagnetic materials	wearable/ lab-based
Goniometry	medium	medium	efficient	low	alignment/cross talk	wearable/ lab-based
Ultrasound	medium	low	efficient	low	occlusion	lab-based
Glove	high	high	efficient	medium	partial pressure	wearable
Marker	high	low	inefficient	medium	occlusion	lab-based
Marker-free	high	high	inefficient	low	occlusion	lab-based
Combinatorial	high	low	inefficient	high	multi-disciplinary	lab-based
Robot	high	low	inefficient	high	limited motion	lab-based

[A] if the system's output is immediately available without complicated computation or need for expertise

3.2.1 Laboratory based systems

Vision based systems are used for position estimation via optical sensors (cameras). The two main classes for these systems are marker based and markerless, depending on whether or not indicators are attached to the body for motion tracking. Markerless visual systems are more concerned with the silhouettes and boundaries of human bodies (Zhou & Hu, 2008). On the other hand, the unique appearance of markers for the marker based visual systems helps to minimise the uncertainty in tracking human movements. Given the interest is to compute forearm kinematics rather than obtain general boundary information, the focus here is on the marker based visual systems.

Marker based visual systems exploit optical sensors to track movements with identifiers placed on the body. Locations of the identifiers (also known as markers) are detected, and reconstructed in two or three dimensions. Early work on the upper limb was by Johansson (1975) who attached small flashlight bulbs to the joints of human subjects (shoulders, elbows, wrists, hips, knees, and ankles), and recorded the moving light streaks on motion picture film, during a person walking and a couple dancing. He theorised that tracking the

motion of particular joints allowed motion estimation and recognition of whole body movement. Although Johansson's work established a solid ground for human movement tracking, marker based vision systems still face challenges to date, including space constraints, occlusion (mutual[8] or self [9]), and the need for pre-calibration. Markers are susceptible to skin motion artefacts leading to noisy motion data, and unreliable repeat marker positioning can compromise the comparability of assessments, taken across multiple sessions using the same marker set. Nonetheless, the accuracy of visual marker based tracking systems has been established in clinical trials, with tracking errors around 1 mm (clinically seen as acceptable (Zatsiorsky, 1998 p. 355, Zhou & Hu, 2008)). Hence, they are often used by human motion analysis studies as a gold standard.

The marker based visual tracking systems can be passive, active or hybrid in style (a combination). The passive marker based systems use markers that do not generate light; instead the markers reflect incoming light from cameras acting both as the infrared light emitter and receiver. A number of these systems have been commercialised; examples are Vicon™ (Oxford Metrics Limited, UK), Qualysis™ (Qualisys Medical AB, Sweden), and Elite™ (BTS Engineering Technology and Systems, Italy). For example, the Vicon™ system has been used by Rao et al. (1996) to model upper extremity movement patterns during wheel chair propulsion for the most able customary wheel chair users.

By contrast, active marker based systems use infrared light-emitting diodes (IR-LEDs) as markers, with the receiver cameras sensitive to infrared lighting. These cameras use a unique pulse sequence for each diode, ensuring that each IR-LED marker is identified and

[8] usually occurs between different persons in a scene
[9] usually occurs between different body segments of a person in a scene
Park, S. and J. Aggarwal (2006). "Simultaneous tracking of multiple body parts of interacting people." Computer Vision and Image Understanding **102**: 1-21.

known during the data capture. One of the most common commercial systems described in the literature is CODA™ (Charndyn Inc. UK), used in (Zhou *et al.*, 2008) to validate upper extremity motion trajectory measurements of inertial sensors. Another system is OPTOTRAK™ (Northern Digital Inc., Canada) that has been used for arm motion and load analysis of sit-to-stand, stand-to-sit, and lifting tasks (Anglin & Wyss, 2000a). Generally speaking and in practice, the passive class of vision based systems is preferable to the active for a number of reasons. Passive systems require less wiring than active systems. Also, active optical systems have the possibility for subject distraction and motion alteration, because the system of cables that powers and controls the LEDs, trails the subjects as they move. This might also raise the issue of additional "phantom" marker artefacts, due to reflection of LED pulses from the testing surfaces.

Virtual Reality (VR) is an active area, based on markerless vision based systems, and suited to achieve effective rehabilitation intervention when the virtual reality experience is relevant to the rehabilitation process. It uses a video camera and software to generate the user's image in a simulated, animated environment, where the user's movements are tracked while interacting with the environment. It has been used to pre-record the movements of a virtual teacher to conduct upper limb repetitive training, as patients are asked to imitate typical rehabilitation-like movement templates. Aspects of the teacher-patient relationship, such as the frequency of visual feedback, speed of motion, and degree of movement synchronisation can be modulated. There is evidence that training with the virtual teacher can lead to variable improvements of upper extremity function and strength from a study on eight chronic post-stroke patients (Holden & Dyar, 2002).

Other systems that directly measure position can use acoustic or ultrasonic sensors, or goniometry to collect body movement information. Certain environmental limitations (e.g. temperature, illumination, or line of sight) may arise when such non-vision systems are used. Acoustic sensor systems transmit and sense sound waves to collect data, where the flight duration of a short travelling ultrasonic pulse is timed and calculated. One application of this sensing technology is the tracking of brain deformations in time sequences of three dimensional ultrasound (US) images (Pennec *et al.*, 2001). A number of problematic issues with acoustic systems exist, limiting their application for motion tracking. Given that the efficiency of an acoustic transducer is proportional to the active capture surface area, large transducers are generally required affecting the system's compactness. Secondly, the choice of low-frequency ultrasonic waves (e.g. 10 Hz) might help improve the range detection, but the system's *latency* is then compromised. Lastly, a line of sight between the emitters and receivers for acoustic systems is a requirement, and not always possible to maintain.

Ultrasonic sensors are similar to acoustic sensors in the general principle of functioning, except that they employ ultrasound waves. An example of this technology is (Sonoace, PICO, Medison, South Korea) used by Ko et al. (2006) to estimate the difference between measured and actual pelvic inclinations for standing and lying positions. This difference is due to marker measurement errors caused by the thick soft tissue at anatomical landmarks of the pubic bone.

For systems based on goniometry, direct position measurements focus mainly on joint range of motion (ROM). Compared to other technologies, goniometric methods are simple and cheap (Laskoski *et al.*, 2009). Despite being originally limited to generating static data

with manual goniometry, recent developments in electrogoniometry have enabled dynamic uni- and bi-axial joint movement to be acquired. A limitation is the cross-talk between axes which interferes with the movement capture itself, although recent models appear to be more flexible. A tri-axial electrogoniometer was developed to measure the three dimensional angular motion of the shoulder joint during daily activities, for the purpose of understanding the effect of arthritic impairment on joint control and coordination strategies (Barker *et al.*, 1996). Two parameters, the slope and movement area, were derived and used in the interpretation of results.

Other motion detection and tracking systems use magnetic, radio or microwave sensors. The magnetic sensor based systems have been widely used in virtual reality due to their size, high-sampling rate and lack of occlusion. Inherent weaknesses of such systems comprise of operational range limitations, latency due to the asynchronisation of measurements, and jitter mainly from sensitivity to magnetically permeable materials (such as in the vicinity of metals). One application is the work of Molet et al. (1997) where magnetic sensor measurements were converted into human anatomical rotations in real-time. Commonly used systems available commercially are FASTRAK™ and LIBERTY™ (Polhemus Inc., USA). Radio and micro-wave systems are also used, but due to their low resolution and large space requirements to accommodate equipment, in most cases they are found as unfit for human motion tracking.

Robot-guided systems use the manipulative ability of a robot and the incorporated sensor technologies to guide limb motion within the framework of 'sense-measure-feedback'. Several studies (Lum *et al.*, 2002, Masiero *et al.*, 2007) confirm that robot-assisted movement training leads to large recovery improvements of upper limb function in stroke

patients, mainly in terms of strength gains and increase in reach extent within two months of treatment. The three main robotic devices that are used in randomised controlled trials (RCTs) are MIT-MANUS™, the ARM Guide™, and the MIME™.

3.2.2 Wearable systems

Glove-based systems are used for position measurement, primarily to analyse hand gestures. By measuring finger flexion and abduction via glove-mounted sensors, and converting the measurements into electrical signals, these devices provide valuable information on the current state of the hand, which can be ultimately used in hand therapy to assess hand impairment. Attractive features of this technology include flexibility, easy donning and removal, light weight, and accuracy (Zhou & Hu, 2008).

Early investigations using accelerometry to examine locomotion, and to distinguish normal and pathological gait were by Liberson in the 1930s (Liberson, 1936, Liberson *et al.*, 1962). Later, as reviewed by Kavanagh and Menz (2008), accelerometers were used for many purposes; to discriminate types of walking patterns, quantify the rhythmicity of walking patterns, study dynamic postural control and stability during normal and impaired walking, monitor activities of daily living and obtain spatio-temporal variables. The increase in the use of accelerometers was driven by improvements in the sensitivity, frequency response, and dynamic range of the devices, hence their measurement accuracy, as well as a reduction in the cost, size, and measurement noise of the apparatus. For instance, the Microtron™ 7290A (Endevco MEGGITT, USA) utilises unique variable capacitance accelerometers designed for measuring low-level accelerations in aerospace and automobile environments. This sensor is also suitable for biomedical applications, as it can measure low-frequency long-duration motion events while maintaining a high sensitivity.

In a study by Codd et al. (2005), it was used to examine muscle activity in the giant Canada goose. The G-link^{TM} (MicroStrain Inc., USA) is a wireless tri-axial accelerometer. It has been used in geotechnical engineering and intelligent construction to continuously monitor lateral deformations in embankments and landslide areas (Furlani *et al.*, 2005).

New developments in the computer games technology, animation and virtual reality industry, as well as microelectromechanical (MEMs) and wireless technologies have led to the release of a new generation of inertial sensors, composed of accelerometers and gyroscopes. The use of this structure has become very widespread in medicine, especially in recent years. In the area of human motion tracking, inertial sensors have been used for two types of measurements.

The first type of measurement involves assessing gross movement, such as detecting falls in the elderly (Hwang *et al.*, 2004), quantifying physical activity levels and energy expenditure (Crouter *et al.*, 2006, Pober *et al.*, 2006), and activity classification (e.g. sitting, standing, and lying) using pre-determined fixed threshold levels (Lyons *et al.*, 2005, Veltink *et al.*, 1996). For instance, Coley et al. (2008) defined shoulder mobility using inertial sensors, based on the angular velocities and accelerations of the humerus for 31 healthy subjects, with no shoulder disorder and during eight hours of daily living. The proposed method quantified shoulder three dimensional kinematics, and was used to differentiate a dominant from a non dominant shoulder, based on objective upper limb usage. Also, Hwang et al. (2004) proposed a real-time ambulatory monitoring system comprised of a tri-axial accelerometer, tilt sensor and gyroscope to conduct a study on falls in the elderly. The system was attached to the chest, and used a fall detection algorithm to detect three cases of falls: forward fall, backward fall, and side fall. After collecting data

on three people aged over 26 years, the system could distinguish between falling and daily life activity, with fall detection accuracy of 96.7%.

The second type of measurement is detecting small changes in motion, such as the incremental changes in daily activities achieved by rehabilitation, or obtaining detailed three dimensional arm position information. One very popular sensor is the Xsens^{TM} MT9 (newly MTx) (Motion Technologies, the Netherlands), which is a digital measurement unit that measures three dimensional rate of turn, linear acceleration, and Earth magnetic field data. The Xsens sensor (MTx model) has been used by Zheng et al. (2007) for home-based monitoring of stroke patients, as part of the Self Management and Assistive Rehabilitative Technology (SMART) Consortium, due to its good accuracy as quoted by the manufacturer (root-mean-square angular resolution = 0.05°, static accuracy < 1.0°, dynamic accuracy < 2.0°). Later, Roetenberg et al. (2009) developed a sensor suit with 17 Xsens sensors, as a new motion capture method for any type of movement, including running, jumping, and crawling. Zhou et al. (2008) used two Xsens sensors to measure the upper extremity motion trajectory. They developed algorithms using least squares filtering to improve the sensor measurements (Zhou *et al.*, 2005), and compared the sensor outputs before and after filtering. Results show a favourable performance of their filtering algorithm, with a mean wrist position error of 2.45 cm before filtering and 1.79 cm after, with a sensor measurement range of 20 cm.

Another recent sensor is DynaPort$^{MiniMod\ TM}$ GaitTest and GaitMonitor (McRoberts, the Netherlands) which comes as one of three products: variable capacitor tri-axial accelerometers (DynaPort^{MiniMod} TriAcc), tri-axial gyroscopes (DynaPort^{MiniMod} TriGyro), or two accelerometers and one gyroscope (DynaPort^{MiniMod} AccGyro). The validity of the

DynaPort GaitMonitor sensor has been established for detecting spatio-temporal parameters of normal gait (Brandes, 2006).

3.2.3 Other devices

In addition to the motion detection and tracking devices described in sections 3.2.1 and 3.2.2, other tools exist that can be used in conjunction. For human motion tracking, imaging modalities have been mainly used to locate joint centres, ensure the repeatability of marker placements, or for model validation. The work of Beaulieu et al. (1999) used open magnetic resonance imaging (MRI) on ten subjects to establish the normal ranges of motion of the glenohumeral head during shoulder *abduction*/*adduction* and *internal*/*external rotation*.

3.2.4 The choice of suitable motion detection/tracking devices

To assess upper limb movement in all degrees of freedom, and gain a greater understanding of upper limb function, movement analysis systems that are vision based are preferred to other devices in a laboratory based environment. These systems can offer unlimited information with regard to the three dimensional position and pose of objects. In a meeting of the Clinical Gait Analysis Forum in Japan, eight vision-based movement analysis systems were tested to compare the validity and system performance in constrained conditions (Ehara, 2002). The systems were Vicon[10], Eagle Digital System, Visualeyez, ProReflex, Peak Motus, PhaseSpace, CODA and FASTRAK. The systems were set-up and calibrated by the manufacturers or trading houses, and there was no

[10] Vicon 512 (Oxford Metrics Co. Ltd, U.K.), Eagle Digital System (Motion Analysis Corporation, California, U.S.A.), Visualeyez (VisualEYEZ, U.K.), ProReflex (Qualysis AB, Sweden), Peak Motus (Peak Performance Technologies, Japan), PhaseSpace (PhaseSpace, California, U.S.A), CODA (Codamotion, U.K.), and FASTRAK (Polhemus, Colchester, U.S.A.)

restriction on the number of cameras used. Four tests were conducted to assess the system's validity using a bar with markers placed upon it at uniform distances. The first two tests compared the difference between actual and measured distances, and angles generated from the movement analysis system between the two markers placed at either end of the bar (900 mm). The third test assessed the ability of each system to generate virtual markers, with certain virtual marker placements pre-identified on the bar and measured. The fourth and final test assessed the processing time required by each system.

For the first test, Vicon was the only system out of the eight capable of producing results accurate to less than 1 mm (0.42 mm average absolute error). For the second test, only seven systems generated an average absolute error smaller than 1°, topping that list was Vicon with 0.16° error. With the third test, five out of the eight systems were capable of generating virtual marker placements. Two of these five systems generated an average absolute error less than 1 mm; these were Vicon (0.50 mm) and Eagle Digital System (0.77 mm). With the final test, three systems were capable of real time processing, with ProReflex, Vicon and Peak Motus processing in 42, 1.94 and 5.78 seconds respectively. The results of that meeting, supported by the findings of Richards (1999), favour the Vicon motion capture system in terms of a commercial movement analysis system, to obtain upper limb kinematics in three dimensions. With that said, its availability as a clinical and research tool at the Oxford Gait laboratory of the Nuffield Orthopaedic Centre (NOC) makes it even more suitable to meet the requirements of this work, for upper limb investigation and assessment in a clinical environment. It should be noted that in (Richards, 1999) the systems were compared with the number of cameras used per system fixed to six cameras.

To assess upper limb motion outside the laboratory environment, a wearable system is required. Out of the four possible wearable systems given in Table 3.2, only inertial sensors provide high measurement accuracy to measure upper limb motion. Inertial sensors offer an alternative sensing solution to the multi-camera vision system which is compact, easy-to-use and relatively low cost. The sensors do not suffer from the 'line-of-sight' problem, which is hard to effectively deal with in a real world scenario (such as a home based environment). It is therefore better suited for wearable monitoring, applicable both in specialised laboratories or clinics and at patients' homes. The Xsens system provides state-of-the-art tracking for wearable monitoring systems, and was therefore chosen for this work.

It should be stated that the direct measurement of three dimensional accelerations from the sensors eliminates errors associated with differentiating displacement and velocity motion data; errors that would be introduced when visual based systems (like Vicon) are used. Nonetheless, a body-mounted sensor accelerometer measures the movement acceleration, along with a gravity component (Kavanagh & Menz, 2008). The accelerometer data could also suffer cross talk from physiological systems, electronic and motion artefacts, as well as signal offset due to temperature changes, fluctuations in gain or general mechanical wear (Kavanagh & Menz, 2008). These readings are sometimes dominated by gravity, especially in low acceleration regimes, typical of rehabilitation exercises. This can lead to an erroneous sensor reading, and hence integration drifts in the velocity and position estimation (Nebot & Durrant Whyte, 1999).

Equally, sensor gyroscopes could suffer from drift due to temperature changes, changes in the mechanical structure and presence of ferromagnetic devices (metals, magnets or

electronic devices). As a result, orientation estimated by the sensors (to provide joint angle information for static and dynamic full-body activities) is not accurately determined. The performance of inertial sensors could then degrade after a long execution time, from the accumulation of errors (or drift) due to the sensor noise or offsets. Brodie et al. (2008) assessed the dynamic accuracy of orientation estimations by an inertial sensor during simple pendulum motion with the Vicon capture data as a reference. They found the orientation estimated by the vendor's propriety software had a root mean square error of between 8.5º and 11.7º, while the orientation estimated by the authors' own data fusion algorithm resulted into a root mean square error of between 0.8º and 1.3º.

Different approaches to manage errors in estimating position and orientation have been previously investigated; for example vision based corrections (You *et al.*, 1999), error models for drift estimation (Nebot & Durrant Whyte, 1999), and adaptive motion modelling (Luinge & Vetlink, 2005). Dealing with accelerometer errors associated with certain functional movements, and the problem of integration drift in the velocity estimation are yet to be systematically addressed. The relevant literature to this is introduced in Chapter 6 (section 6.2).

3.3 Standardising measurement of the upper limb

If the multi-camera motion capture system is to be used as a gold standard, this needs to be optimised to give best possible results, in terms of the choice of marker set and configuration, marker placement and modelling assumptions.

A rigid body segment, freely suspended in three dimensional space, requires six parameters to identify its location and orientation in space (Craig, 2004). Three parameters determine

its origin by means of *xyz* coordinates, and three parameters determine the individual rotations around the three independent axes (longitudinal, vertical and frontal).

The Vicon system depends on attaching retro-reflective marker balls to the surface of body segments, with the markers aligned with particular bony landmarks found by palpation. Each marker is detected and recorded on camera (resolution reaching 16 million pixels), with its movement associated with a bone segment. Stereometric techniques (Woltring & Huiskes, 1990) and frame-by-frame analysis are then used to combine the two dimensional camera images, and determine the instantaneous three dimensional coordinates of markers relative to a fixed laboratory coordinate system. The three dimensional path of each marker, commonly referred to as a trajectory, permits segment displacements and rotations to be calculated along with the joint movements.

Many attempts have been made to standardise the method of applying markers to the upper limb, to ensure repeat positioning, as has been done for the lower limb (Rau *et al.*, 2000). Although standards have been proposed for upper limb analysis (Van der Helm, 1996), they are based on bony anatomical landmarks; some of which are beyond those directly attainable from surface markers. In addition, comparisons are difficult between upper limb studies, due to the multitude of methods employed to provide kinematics and analyse the movements. The types of markers and their configurations as well as marker placement are provided below, with the choices made in this work.

3.3.1 Types of markers and configurations

As stated earlier, a passive marker system was utilised for this research. The two types of passive marker systems described in the literature are surface and invasive marker systems.

The former is more popular, as invasive systems, although more accurate and reliable, are not convenient or applicable in a clinical research setting to assess living participants (i.e. not cadavers). Despite the susceptibility of surface marker systems to displacement from skin movement (disrupting marker positions mainly above joint centres), surface marker systems are adopted in this work as a viable marker system method.

Passive marker systems are available in a wide range of different configurations depending on the application. These range from single or pairs of surface markers joined together to denote a rigid body segment, *marker triads* which are sets of three markers placed in a triangle, and marker clusters (otherwise known as technical arrays or marker trees) defined by placing markers on the end of rods (Anglin & Wyss, 2000b).

The first two types of marker systems can suffer from skin displacement errors and inter-marker movements, and therefore may not accurately represent segment motion. However, they do not encumber the natural movement of the upper limb. By contrast, marker clusters serve to increase visibility of marker positions during video capture, and reduce potential errors of inter-marker movements depending on the cluster rigidity. However, these can affect the way in which the participant naturally undertakes a movement, especially at small surfaces like the hand or when the markers are attached in close proximity. Marker clusters are also more likely to move as a whole relative to the bone, and often do not have an anatomical reference point for repeat positioning.

So as not to interfere with or obstruct the natural movement being measured, individual surface markers were selected in this work to track body segments, and marker triads to track the wearable sensors. Both were taped directly onto the object being tracked, which was the skin for body segments and external packaging for the sensors.

3.3.2 Marker placement

Based on the locations of attached marker positions, body-fixed coordinate systems are defined, commonly known as technical coordinate systems. By contrast, coordinate systems which are based on locations of actual bony landmarks or joint centre positions are known as anatomical coordinate systems (Cappozzo, 1984). In general, calculations of a moving limb segment are best represented when made as closely as possible to where the natural movement took place, i.e. relative to the anatomical coordinate systems. Hence, a challenge of kinematic modelling is to find the ideal marker set (on which to base the local coordinate system definitions) such that the relationship between the technical and anatomical coordinate systems is best identified.

A standard marker set for upper limb analysis has not yet been agreed upon, as this depends on several factors. These are the type of optical system used (passive or active), the tasks being performed (which has an effect on marker visibility), whether the relevant measurements are static or dynamic, the setting for data capture (clinical or research), and how the data will eventually be used (Anglin & Wyss, 2000b). However, the main concerns with regard to marker location are to avoid excessive errors due to skin movement under the marker, and to keep the markers in view at all times.

General guidelines, especially in a clinical setting, are to ensure that marker application time is kept to a minimum, and that the chosen marker system does not hinder or interfere with the movement itself (Rau *et al.*, 2000). For optical systems, a minimum of three non-collinear markers are required to determine the six degrees of freedom associated with the position and spatial orientation (pose) of a rigid body. Thus at least three markers must be visible to at least two cameras at all times for a given segment. The markers should ideally

be well-spaced, and should rest on locations with minimal skin movement, to ensure greatest visibility and minimum noise. Redundancy is possible if more than three markers are used per segment with sufficient visibility over time. In an attempt to standardise marker placements and upper limb biomechanical models, the International Society of Biomechanics has proposed coordinate system definitions for upper limb segments and joints, joint centres, and rotation axes (Wu *et al.*, 2005). This proposal followed the standardisation work by Wu et al. (2002) for the joints of the lower limb.

3.4 Modelling motion of the forearm

The existing research on movement analysis of the upper limb concentrates on gross movement, such as shoulder and elbow movements. Rao et al. (1996) used a six camera Vicon system to develop a three dimensional model of trunk, shoulder, elbow and wrist movements, based on ten anatomic surface markers using sixteen male subjects. Definitions of joint axes for the wrist and elbow along with coordinate frames and planes of motion for the movement of the trunk, upper arm (humerus), forearm, and hand were described. As it is clinically useful to analyse gross upper limb movements, the authors made assumptions about joint axes to adequately measure the movement. For example to calculate the wrist angle, they created a forearm coordinate frame and a hand coordinate frame. Then, they computed the wrist joint movement about an axis positioned at the *distal* end of the forearm coordinate frame.

Schmidt et al. (1999) studied the effects of unconstrained movements of the elbow and wrist during a tracking task set on a table. They found that forearm pronation/supination is particularly susceptible to skin movement. To reduce the erroneous effect of skin movement, sets of triad markers were employed. They used a marker placement method

similar to Rao et al. (1996). Additional markers were placed to mark approximately the joint centre locations, derived from a priori knowledge of plausible locations. Using static calibrations, they identified the location of joint centres more accurately relative to the sets of triad markers on the humeral and forearm segments. To reduce the variability between inter-marker distances, they decided to place the marker triads on flexible cuffs. However, the potential error due to skin movement was compounded by error due to movement of the cuff.

The level of detail of forearm models, as given in the literature, generally depends on the application area and the movements performed. Although the forearm is correctly modelled by two segments (the ulna and the radius) as supported by evidence from imaging (Nakamura *et al.*, 1994) and observation (Weinberg *et al.*, 2000), most upper limb studies have simplified the forearm, and modelled it as a single segment. This could have implications on forearm kinematic analysis during certain movements. For instance, the single segment model treats a forearm *pronation/supination* movement as a rotation of the distal end of the radius about a fixed ulna. So for an unconstrained elbow, the movement would be a combination of an internal/external rotation of the humerus, and a pronation/supination at the elbow joint (Figure 3.1). By contrast, the two segment model extends the single segment model, stating that the ulna does in fact move (an axial rotation about itself). So there is a relative motion between the radius and the ulna, which is prominent at the extremes of pronation and supination. This makes forearm pronation/supination the resultant motion of internal/external rotation of the humerus at the shoulder joint, axial rotation of the ulna at the humero-ulnar joint, and pronation/supination of the radius relative to the ulna at the radio-ulnar joint (Figure 3.2).

Most upper limb modelling literature treats the forearm as a rigid single segment body to compute kinematics (Biryukova *et al.*, 2000, Nakamura *et al.*, 1994, Schmidt *et al.*, 1999, Van Andel *et al.*, 2008, Weinberg *et al.*, 2000, Williams *et al.*, 2006). For instance, Van Andel et al. (2008) used an Optotrack system with three cameras, and recorded an average pronation/supination range of approximately 161º from motion data of ten healthy subjects. Nakamura et al. (1994) reported a similar range finding of about 163º, with twenty healthy subjects using a goniometer. On the other hand, the work of Peterson (1994) and a review by Anglin and Wyss (2000b) stress that the ulna and radius should be treated separately, as a single joint at the elbow does not represent forearm pronation/supination accurately. An internal report in Oxford, (Lievesley, 2010) found that a model where the ulna and radius are treated separately does not uniquely measure the different rotation elements of the overall pronation/supination motion of the forearm. Also, the small rotation of the ulna, reported as about 6º by Nakamura et al. (1994), does not warrant measuring it separately. Hence, there is little benefit or clinical value in pursuing the two segment forearm model, and the single segment model was chosen for this study.

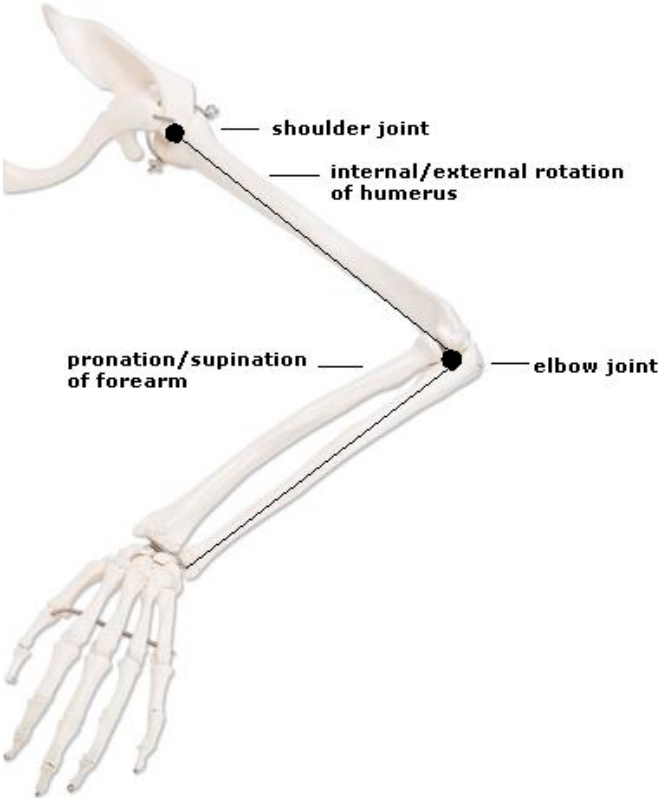

Figure 3.1 Biomechanical forearm model (as a single segment)
Adapted from (a3bs.com)

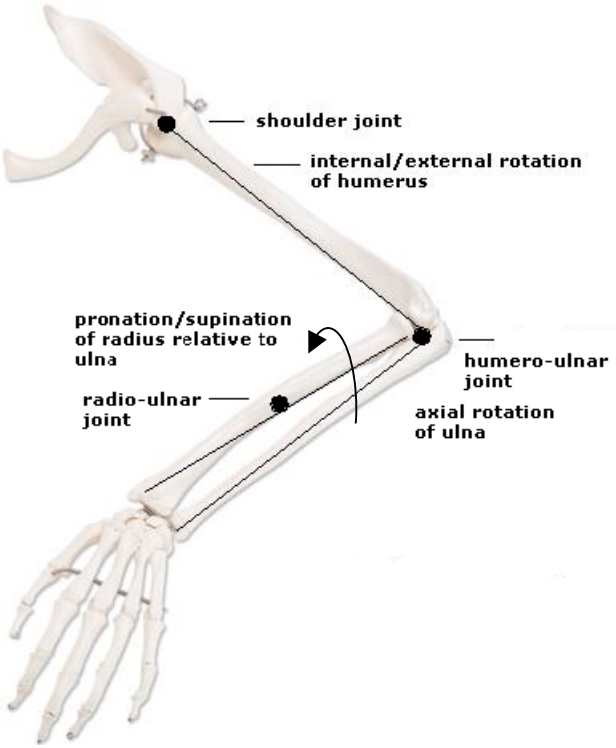

Figure 3.2 Biomechanical forearm model (as a double segment)
Adapted from (a3bs.com)

Another issue is whether to calculate absolute or relative forearm kinematics. Relative kinematics represents forearm motion relative to the upper arm (rotation at the elbow joint). On the other hand, absolute kinematics (the simpler solution) is forearm segment rotation about a fixed coordinate system.

In this work, absolute kinematics are reported (in Chapter 4), given that the absolute forearm kinematics should correspond to the absolute sensor measurements at the forearm.

3.5 Clinical upper limb kinematic measures

Measuring motor performance kinematically, to assess improvement or provide real-time feedback to patients, can promote the understanding of related changes in underlying motor control mechanisms. This relationship is still poorly understood (Wu, Chen *et al.*, 2007). Most upper extremity function assessment studies rely on subjective clinical evaluations and measures. The main problems associated with these measures are possible subjectivity and non-repeatability (as explained in Chapter 1 and 2, sections 1.1 and 2.4 respectively).

Recent research (Page *et al.*, 2005) has recommended the use of biomechanical (kinetic and kinematic) analysis during functional tasks for outcome evaluations, considering it a valid means to directly and objectively measure the spatio-temporal parameters and motor control of a given movement. Several measures can be extracted from upper limb kinematics to assess the effectiveness of a rehabilitation method or intervention, by comparing the pre- and post- measures of comparable movements in impaired participants. Also using these metrics, it is possible to compare two or more rehabilitation methods, and identify the method yielding the highest improvement in outcome.

Based on a literature review of studies conducted on stroke patients, children with cerebral palsy, and Parkinson's disease patients, several measures are extracted and presented in Table 3.3, along with the metric definition and significance. Most of these measures can only be derived from motion tracking systems.

In this work, three clinical kinematic measures were selected for computation (as later discussed in Chapter 4) to quantify performance during functional tasks; these were average velocity, movement duration and percent time to maximum velocity. These metrics were chosen as they are beneficial clinically and in stroke rehabilitation, mainly because they relate to temporal efficiency, motor control and overall quality of movement.

Table 3.3 Clinical kinematic measures of performance

Metric	***Definition***	***Significance***	***Paper***
Movement duration (MD)	the execution time of a movement in seconds	temporal efficiency	*(Wu, Chen et al., 2007)*
Average velocity (AV)	measured in mm/s when MD is inverted and multiplied by displacement	temporal efficiency	*(Wu, Chen et al., 2007)*
Percent length ratio (PLR)	the total displacement of a movement normalized by the actual start to target distance	spatial efficiency, movement directness	*(Wu, Chen et al., 2007)*
Reaction time (RT)	the time taken to initiate the movement	motor control strategy adopted	*(Wu, Chen et al., 2007)*
Percent time to maximum velocity (PTMV)	the ratio of time when peak velocity occurs to total movement duration; (the proportion of MD spent in acceleration)	motor control strategy adopted	*(Wu, Chen et al., 2007)*
Number of movement units (NMU)	a pair of adjacent minimum and maximum points on a velocity plot where the increase between minimum and adjacent maximum exceed a threshold (set as 15% of the movement peak velocity).	movement smoothness	*(Kamper et al., 2002)*
Normalised jerk score (NJ)	score based on jerk (the third derivative of position)	movement smoothness/ irregularity	*(Cozens & Bhakta, 2002)*
Coefficient of periodicity (CP)	a value between 0 and 1 computed using singular value decomposition from displacement, velocity or acceleration	movement periodicity	*(Caimmi et al., 2008)*

3.6 Summary

This chapter provided a review of several motion detection and tracking systems. These systems were introduced in terms of their measurement function and environment of operation, reflecting their different purposes in the areas of biomechanics and movement analysis. On the basis of the review, a comparison of the devices' performance, and the requirements of this work, two systems were chosen.

Vicon was chosen as a suitable laboratory-based system to act as a gold standard. In order to ensure the best possible data, methods for standardising upper limb kinematics in general, and specifically measuring forearm movements, were presented in terms of marker systems and configurations, and marker placement. As a result, a surface marker system, implied by using Vicon, was selected and considerations for nominal marker placements to capture upper limb movements were identified. Existing research on upper limb kinematics, mainly to model the forearm and calculate its movement, was also described.

In addition, Xsens inertial sensors were chosen as a wearable system, which could potentially be used in a home environment. Despite this potential, current limitations of the wearable system were identified, which include sensor accelerometer bias due to gravity, and sensor gyroscopic drift. These could lead to integration drift in the estimation of linear velocity, position and orientation. The research where these problems were identified and methods developed to deal with them were briefly stated. More work on improving the sensor data is still needed, mainly to estimate linear velocity.

The chapter also identified a set of clinical kinematic measures that could be used to quantify motor performance, or the effectiveness of a rehabilitation method. Three clinical kinematic measures were selected for computation (Chapter 4); these were average velocity, movement duration and percent time to maximum velocity. These metrics were chosen as they are beneficial clinically in stroke rehabilitation.

Chapter 4

Measurement of Arm Movement Using Vicon™ for Healthy Subjects and a Stroke Patient

4.1 Introduction

This chapter presents the development and implementation of a computational method for describing the kinematic associations of segments and joints of the right and left upper limbs, the trunk and pelvis, with a main focus on the forearm, using Vicon. It develops specifications for wearable monitoring of the forearm, while performing certain functional movements, for healthy subjects and stroke patients. Also, it aims to quantify the minimum sensitivity requirement of wearable devices to detect movement differences in pre/post-stroke intervention.

The protocol defines specific placement for the markers, and measurement generates vectors and coordinate frames based on marker positions. The technique is applied to track upper limb motion of four healthy subjects and one stroke patient; with motion data collected twice from the latter to measure change of movement following a rehabilitation program. The two data collection sessions for the patient are referred to as pre- and post-intervention, separated by a month. The subjects' demographics, along with a description of a typical data capture session conducted using the Vicon system are provided, with details on data pre-processing and processing stages. Definitions and choices made to

develop the computational measurement technique in BodyBuilder software (Vicon, Oxford, UK) are presented. Results are summarised to characterise forearm reach-and-grasp and pronation/supination movements for four healthy subjects and a stroke patient. Hand-to-mouth movement is also reported due to its further three dimensional complexity. Necessary specifications for wearable monitoring of the forearm, while performing certain functional movements, are highlighted in the results section. For the stroke patient, results are also used to quantify the minimum sensitivity requirement of wearable devices to detect movement differences in pre/post- stroke intervention. The process of obtaining the research ethics is provided.

4.2 Upper limb motion data acquisition and pre-processing with Vicon

As concluded in Chapter 3, Vicon (Oxford, UK) was chosen for human motion tracking and kinematic analysis due to its utilisation of optical technology, thereby reducing the test's invasiveness and the subject's inconvenience, and its high-quality motion capture capabilities (reaching 16 million pixels in terms of camera resolution). It has been widely used by researchers in the literature (Schmidt *et al.*, 1999, Rao *et al.*, 1996) as a gold standard for position data, both for clinical gait analysis and upper limb biomechanical modelling and movement analysis studies.

Under the ethics approval described in section 4.2.1, four upper limb motion tracking sessions were carried out at the Nuffield Orthopaedic Centre (NOC) to track and measure upper limb, trunk and pelvis movements in three dimensions for four healthy subjects. Similarly, motion data of a male patient, 21 months after a stroke, were collected on two occasions at the Biomechanics Laboratory at University of Southampton to represent pre-

and post- stroke intervention. Comparison of the pre- and post- data measured the change in movement following a home-based rehabilitation program. The subjects' demographics are provided in section 4.2.2.

Each session comprised three functional movements (Table 4.1), selected in Chapter 2 which are typical of upper limb rehabilitation. Each movement was repeated at least five times to assess upper limb motion. A 12-camera Vicon (MX F40) system was used to capture the movements of the healthy subjects, while motion data of the stroke patient were collected using a 12-camera Vicon (TX) system, of which six cameras were T40 and the remaining six were T160. The main focus was on characterising motion of the forearm segment.

Table 4.1 Functional movements of interest

Functional Movements
Forearm pronation/supination (accepting a coin)
Reach-and-grasp
Hand-to-mouth (drinking/eating)

4.2.1 Recruitment of subjects and the research ethics process

Postgraduate students at the University of Oxford, aged over 20 years, with no history of neurological disorders and no recent upper limb disorders or injuries, were targeted as primary test subjects for ease of availability (for more details, see section 4.2.2). To collect the motion data of these healthy subjects, ethics approval was obtained from the Medical Sciences Divisional Ethics Committee at the University of Oxford (Ref. MSD/IDREC/C1/2009/33).

For the stroke patient (age 48 years), ethics approval was obtained from the Research Governance Office at the University of Southampton (Ref. SoHS-ETHICS-09-028). The

patient was identified and recruited by a physiotherapist at the University of Southampton, who contacted participants of private neuro-gyms[11] and interviewed them. Based on the participants' willingness to take part in the study, informed consent was obtained from the patient, and motion data were collected on two occasions, as was explained earlier.

4.2.2 Subjects

The study participants were four healthy subjects, one female (Subject 1) and three males (Subjects 2-4), (ages 25 – 30 years), and a male stroke patient (age 48 years). Clinical measurements, given in Table 4.2, were taken from all participants prior to motion data capture. These measurements were necessary for the upper limb model to be a good representation of the skeletal structure being tracked, by reflecting the size and anatomical proportions of upper limb segments.

Table 4.2 Segment definitions and constituent marker labels

Measurement	**Subject 1 (left)**[A]	**Subject 2 (right)**	**Subject 3 (right)**	**Subject 4 (left)**	**Stroke (left)**
Height (cm)	171	178	180	178	182
Weight (kg)	60	74	87	67	100
Right Shoulder offset (cm)	5.0	6.5	7.0	5.5	5.5
Right Elbow width (cm)	8.8	9.7	10.4	8.7	7.6
Right Wrist width (cm)	5.5	6.5	6.3	5.4	6.4
Right Hand thickness (cm)	3.0	3.6	3.5	3.1	2.6
Left Shoulder offset (cm)	4.9	6.5	6.7	6.0	5.4
Left Elbow width (cm)	8.8	9.5	10.3	8.8	7.4
Left Wrist width (cm)	5.3	6.2	6.2	5.4	6.4
Left Hand thickness (cm)	3.0	2.8	3.4	3.2	3.1

[A] in brackets is the side measured (i.e. the dominant side for healthy subjects, or the affected side for the stroke patient)

What follows is a detailed description of the subject preparation (marker placement), motion capture system set-up and calibration, as well as the stages of data capture, pre-processing and processing using Vicon.

[11] physiotherapy clinics utilising neural stimulation

4.2.3 Subject preparation and marker placement protocol

The thirty-nine (9 mm diameter) passive spherical retro-reflective markers (black dots, Figure 4.1) were placed on the right and left upper limbs, the trunk, and pelvis of the healthy subjects. Each upper limb side was defined as three separate segments: upper arm, forearm, and hand. For the stroke patient, the pelvis was not tracked, so thirty-one markers (9 mm) were used (Figure 4.2). The marker attachment followed was according to the Vicon Plug-In-Gait marker placement protocol (Figure 4.3) whose clinical validity was originally established for gait analysis (Davis *et al.*, 1991). To provide a better model for the upper limb, adjustments to the Plug-In-Gait marker set were made in adherence to the International Society of Biomechanics recommendations for the upper body (Wu *et al.*, 2005). The additional markers were one on the medial epicondyle of the humerus (to better estimate the elbow joint axis) and the other on the spinous process of the 8th thoracic vertebrae. All marker labels and positions are summarised in Table 4.3. Markers that were not attached to the forearm are not needed to measure the forearm motion, but data were collected for analysis beyond the main scope of this work.

Figure 4.1 Healthy subject setup – reflective markers (black dots)

Figure 4.2 Stroke patient setup

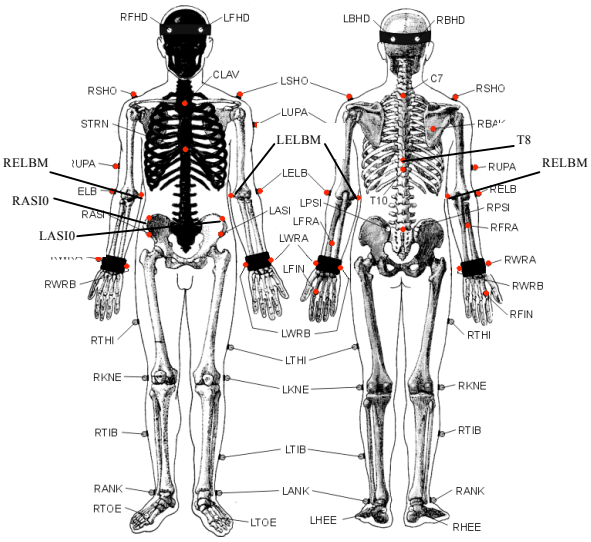

Figure 4.3 Plug-in-Gait marker placement protocol (after adjustments) with positions and labels of passive retro-reflective 9 mm spherical marker for the whole body- the red dots represent the markers used to track upper body motion. Adapted from (Vicon Motion Systems, 2005)

Table 4.3 Marker labels and positions of 9 mm spherical markers

	Marker Description of Placement
C7	Spinous process of the 7th cervical vertebrae
T8	Spinous process of the 8th thoracic vertebrae
T10	Spinous process of the 10th thoracic vertebrae
CLAV	Jugular notch where the clavicles meet the sternum
STRN	Xiphoid process of the sternum
RBAK	Placed in the middle of the right scapula (anti-symmetry for automatic labelling)
RSHO[1]	Dorsal point on the acromioclavicular joint
RUPA[1]	Placed on the upper arm between the elbow and the shoulder
RELB[1]	Lateral epicondyle of the humerus at the elbow
RELBM[1]	Medial epicondyle of the humerus at the elbow
RFRA[1]	Placed on the forearm between the wrist and the elbow
RWRA[1]	Medial point on the ulnar styloid
RWRB[1]	Lateral point on the radial styloid
RFIN[1]	Distal head of the 2nd metacarpal
LSHO[2]	same as RSHO
LUPA[2]	same as RUPA (only placed asymmetrically)
LELB[2]	same as RELB
LELBM[2]	same as RELBM
LFRA[2]	same as RFRA (only placed asymmetrically)
LWRA[2]	same as RWRA
LWRB[2]	same as RWRB
LFIN[2]	same as RFIN
SACR	Sacral marker placed midway between the posterior superior iliac spines (PSIS)
RASI	right anterior superior iliac spine (ASIS)
LASI	left anterior superior iliac spine (ASIS)
RASI0	Proximal displacement of RASI along the ASIS-ASIS axis
LASI0	Proximal displacement of LASI along the ASIS-ASIS axis

[1] right side, [2] left side

4.2.4 System set-up and calibration

The Vicon systems used (MX F40 and TX) consisted of 12 infrared cameras each (capture frequency: 100 Hz). These cameras surround the subject and each camera emits strobed infrared light which is then reflected back by the markers attached to the skin, as specified in section 4.2.3 (system set-up shown in Figure 4.4).

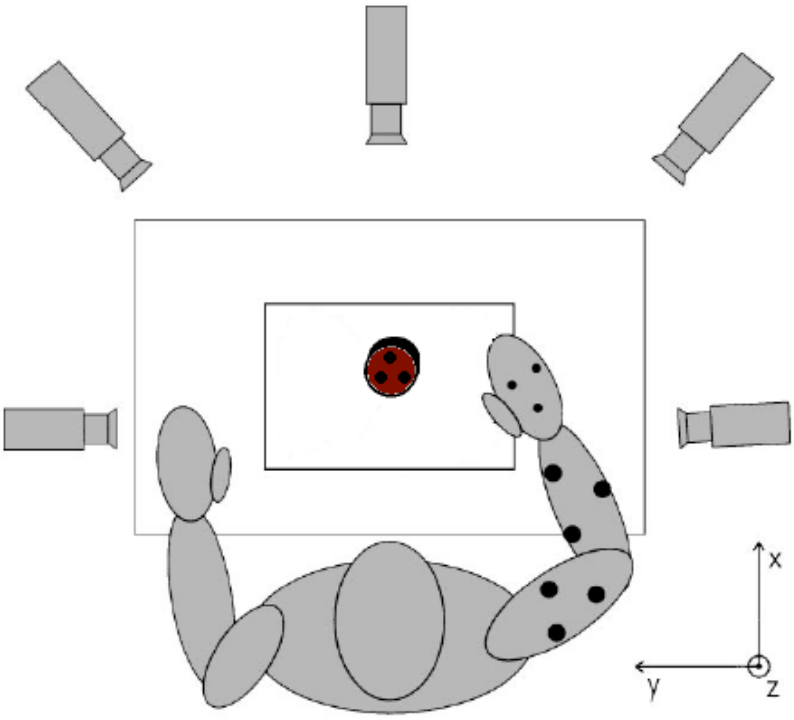

Figure 4.4 Diagram with an overview of the system set-up; in the centre in red is an object

Not only do markers have to be distinguished by the cameras separately but also consistently, ensuring the most appropriate angle of vision for clusters of markers. If this condition is not satisfied, the markers will be seen by the cameras as an undesired reflection and will be affected by noise after reconstruction. In order to avoid this problem, cameras should be placed adequately above the plane where the markers will be moving, and camera sensitivity should be adjusted accordingly. Inappropriate system set-up and calibration can lead to unstable, reconstructed data, adding noise and inaccuracy to the data. The camera placement, marker position and marker size are therefore the three underlying factors that affect the accuracy of the data, as explained in section 4.2.7.1.

4.2.4.1 System "calibration"

Once the user has checked that each of the twelve cameras can clearly see reflective markers placed within the capture volume (defined in section 4.2.5) it is necessary to "calibrate" the system (more correctly orient the system). This is a vital step that allows the software to define a global origin and a capture volume as well as calculate the relative location and global orientation of all the cameras. These measurements are used during the reconstruction process to calculate the accurate positions of the reflective markers tracked in space. The calibration process consists of two main parts:

- **Static Calibration:** A static calibration is taken to calculate the origin of the capture volume and to determine the orientation of the three dimensional workspace. The calibration object used is a small metal L-shaped frame comprising five accurately spaced markers. The L-frame is made from two metal rods fixed at 90°, that being the zero-point (or origin), as shown in Figure 4.5. One arm has three reflective spheres attached, and the other also has three reflective spheres, with one sphere common to both arms.

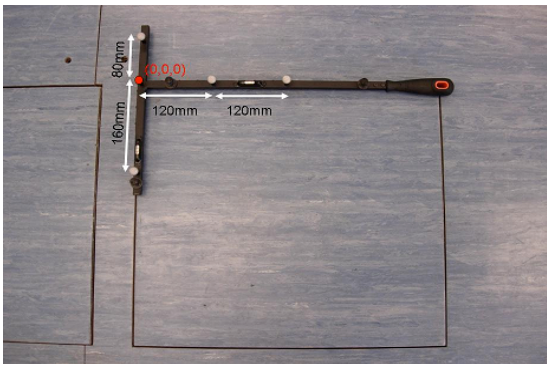

Figure 4.5 Static and dynamic calibration object

- **Dynamic Calibration:** By moving the same L-shaped frame through the whole capture volume the system can calculate the relative positions and orientations of

the cameras (Cerveri *et al.*, 1998). The frame is waved within the capture volume to encompass a wide range of positions and orientations.

It is important that the capture volume is free from reflective surfaces which can alter the amount of light reflected to the cameras and create non-existent markers or "phantom" markers when the data is visualised. The main contributors to this type of distortion are flat reflecting surfaces, such as the room floor.

4.2.4.2 Residuals

Having collected sufficient data for the static and dynamic calibration, the system's accuracy can be examined. If the angular error (in radians) is defined as "the amount by which a ray from the calibrated camera misses a reference marker", the *calibration residual* (mm) is "the angle error multiplied by the mean distance from the camera to the reference marker" (Woolard and Lyster 1999). The calibration residual constitutes therefore a measure of system accuracy, and a well-calibrated system has a low residual (due to a small angular error). In Vicon, residuals are computed as the root mean square of the distance between two rays; the first being that from the centre of the strobe ring (that emits the infrared light) to the centroid (geometric centre) of the marker, and the second being the reflected ray from the marker to the camera lens (Vicon Motion Systems, 2006). A "Calibrate Cameras" window displays a residual for each of the twelve infrared cameras, that is to say a measure of the accuracy of any single camera. In general, Vicon recommends that the residuals should be less than 0.1% of the distance from the camera to the centre of the capture volume, and for this work a residual less than 2 mm was found acceptable. A calibration is only valid for the arrangement of cameras for which it was done. If a camera is knocked out of its original position at any point in time, it is necessary to recalibrate the cameras.

4.2.5 Data capture using Vicon

The coordinate location of each marker, given by the marker centroid, is calculated within each camera for every frame of data from the greyscale image of the marker and the edges of any bright spots in the image. All coordinate information is forwarded to ultranets that manage data flow to a central Workstation PC (each ultranet can manage up to ten cameras). Initially there is no way to associate a particular marker centroid with a particular physical marker but the process of marker tracking across frames, also known as trajectory following or tracking, allows to a certain degree of accuracy, appropriate identification of markers. Using marker coordinates forwarded by all cameras, Vicon's capture software Nexus™, can reconstruct the position of markers in three dimensions and visualise their centres on the screen as a group of points. It allows marker trajectory data to be edited, and three dimensional coordinates of the markers to be exported for further analysis.

Cameras collect data over a volume called the *capture volume*. This is a three dimensional space that contains all movements made by a subject in the laboratory. The white rhomboid shown in Figure 4.6 is the capture volume for motion capture. The white squares represent the gait laboratory floor, and the orange part in the middle represents markers on a subject. The twelve cameras (Figure 4.6) were conveniently distributed in the laboratory to ensure marker movements were captured from different angles using Nexus V1.4.116 (Vicon, Oxford, UK).

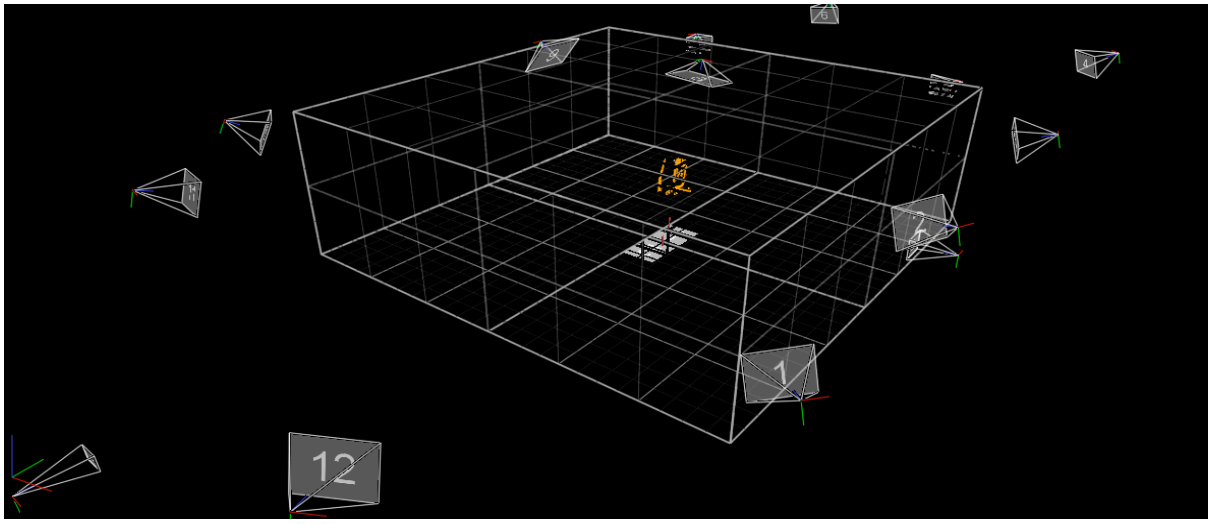

Figure 4.6 Vicon's capture volume with the position of cameras, gait lab floor, and in orange the upper limb markers on a subject

4.2.6 Movements

While seated, participants were instructed to perform certain functional movements as given below. Each movement was repeated at least five times.

1. Reach and grasp (Figure 4.7): The healthy subjects reached forward with the dominant arm to pick up a light object (placed centrally, 24 cm away from the edge of a table), moved the arm 15 cm backwards, and then forwards again to release the object at its original location. The patient however, right side dominant, was asked to reach with his affected left arm (to reflect pathological upper limb movement which is also of interest) to a comfortable position (38 cm away from his body) and then return his arm to the exercise starting point.

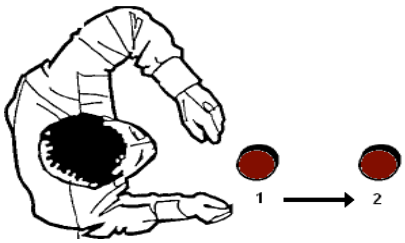

Figure 4.7 Diagram of the reach-and-grasp exercise from 1 to 2

2. Forearm pronation/supination (Figure 4.8): Starting from an inferior-facing palm position of the hand and elbow flexed at about 135º, healthy subjects were asked to turn their hands 180º into a superior-facing position (resulting in forearm supination) and vice versa (known as forearm pronation). The patient was not capable of performing this movement.

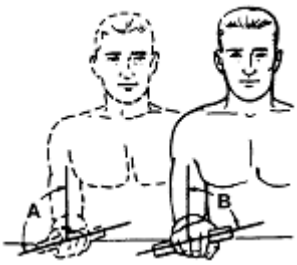

Figure 4.8 Diagram of the forearm pronation/supination exercise from B to A

3. Hand-to-mouth (Figure 4.9): The healthy subjects picked up a light object (placed centrally, 17.5 cm away from body) which was then taken up to mouth and back. The patient, however, used his unaffected arm to place the object (also placed centrally, 56.5 cm away from his body) into the affected hand, and lifted the object to his mouth and back.

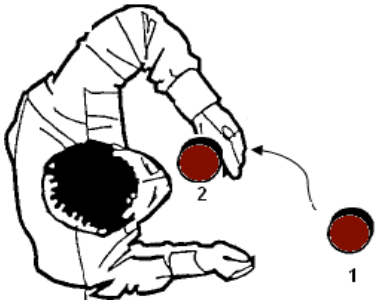

Figure 4.9 Diagram of the hand-to-mouth exercise from 1 to 2

4.2.7 Data pre-processing using Vicon

A pre-processing stage using Vicon generally follows the data capture. Below is a description of the four necessary steps to complete this stage; these being marker position reconstruction, marker labelling, data filtering and gap filling.

4.2.7.1 Marker position reconstruction

Marker position reconstruction is frame-by-frame analysis to combine two dimensional camera images and determine instantaneous three dimensional coordinates of each marker (Figure 4.11). A common problem with vision systems is marker disappearance, which becomes obvious in the reconstruction of a marker position. During capturing, any marker should be simultaneously located in space by at least two cameras to be able to reconstruct its position in three dimensions. In this work, every marker during capturing was tracked by twelve cameras with a minimum of three cameras contributing to a marker location during its position reconstruction, ensuring stereoscopic vision and any required correction of spatial reconstruction. This redundancy of marker position information from the twelve cameras can be exploited to improve accuracy. The determining factors for marker position reconstruction in Vicon, known as reconstruction parameters, are given in Table 4.4 (Vicon Motion Systems, 2006).

Table 4.4 Marker reconstruction parameters in Vicon (Vicon Motion Systems, 2006)

Parameter	Description
Dimensions of reconstruction volume (mm)	typically, the reconstruction volume is larger than the capture volume. Setting it too large leads to slow reconstruction and ghost trajectories may appear, while if it is set too small useful trajectories may be lost.
Predictor radius (mm)	it sets a limit on the space surrounding a given marker used as a search area to predict where it might appear in the next frame. If this is set to a large value, marker trajectory will break less number of times as compared to when the radius is set to a small value but it may associate an incorrect marker with the trajectory resulting in a false swap. The faster the markers move the larger the predictor radius needs to be. Typical values of this parameter (mm) are 20 for walking, 20-30 for running and 60 for golf swinging.
Marker movement speed (mm/s)	is accounted for because speed of marker movement affects continuity of marker trajectories. This can have a value between 0 (slow) and 10 (fast) with a default value of 6 sufficient for normal movement captures where markers move at 1-3 m/s. Choosing the fastest setting can ensure continuous marker trajectories even when markers move at high speeds, but can cause undesired cross-overs if markers are in close proximity. The slowest setting is suitable when the markers are in close proximity but do not move very much.
Subject acceleration (mm/s^2)	is the maximum acceleration expected which is essential when creating new trajectories for markers (default value is 50 mm/s^2). If it set too low, new trajectories will not start, leading to missing data but if it set too high, points may be assigned to the wrong trajectory.
Model rigidity	is informative of how rigid are the markers attached to the subject (default value is 6) but the parameter range is 0 (rigid when there is no significant movement of markers with respect to the underlying segment) to 10 (loose when markers are expected to move significantly relative to the segment beneath, possibly due to excessive skin movement artefacts).
Maximum noise factor	is relevant when a marker position is determined by circle fitting from the camera image recordings. In general, it is set to 7 but for the MX system, which was used in this work, image recordings from cameras are saved as 10-bit gray-scale instead of black and white (increasing the system's accuracy to fit a circle more accurately around the marker image and best locate it), so 2 is found suitable.
Intersection limit	is defined as the upper limit on the separation of the rays from two cameras in order for them to contribute to the reconstruction of a marker. This is related to the size of markers; the smaller the markers the smaller is the intersection limit (should be set to 12 for calibration residuals around 2.0 mm or less, set higher for higher calibration residuals and lower if trajectories start to crossover or fail to start).
Residual factor	is set such that multiplying by the intersection limit and then dividing by the average camera residual yields a result between 3 and 10.

As markers were moving at one to three m/s (which is similar to average movement speed during walking), predictor radius was set to 20, a typical value for walking. Despite the default value six, marker movement speed was set to five, at the middle of its [0-10] range, as some markers were in close proximity and a slightly lower setting was found to be more suitable. Subject acceleration was set to the default value 50 mm/s^2; no higher accelerations were expected for the upper limb movements captured. Model rigidity was set to six (default value), maximum noise factor set to two as found suitable for MX cameras, intersection limit set to 12 (as calibration residuals were less than two mm), and residual factor set to one.

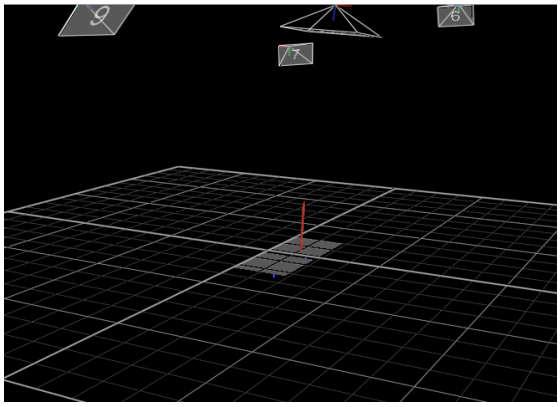

Figure 4.10 Before marker position reconstruction

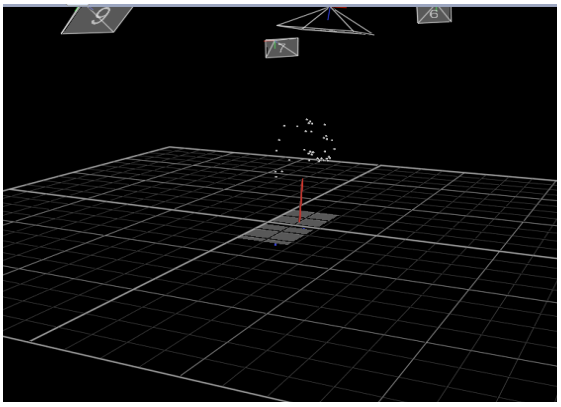

Figure 4.11Markers (after position reconstruction) as white dots

4.2.7.2 Marker labelling

For the pre-processing of the data, the markers are initially unlabelled and therefore unidentified by Vicon after position reconstruction. This is depicted in Figures 4.10 and 4.11 with the markers shown as white dots. To label these dots so they become orange in colour (as shown in Figure 4.12), all marker labels should be listed by the user in a file called the “Marker Set” making them available to the Vicon Nexus application (Figure 4.13) and only then can they be manually or automatically associated with the markers.

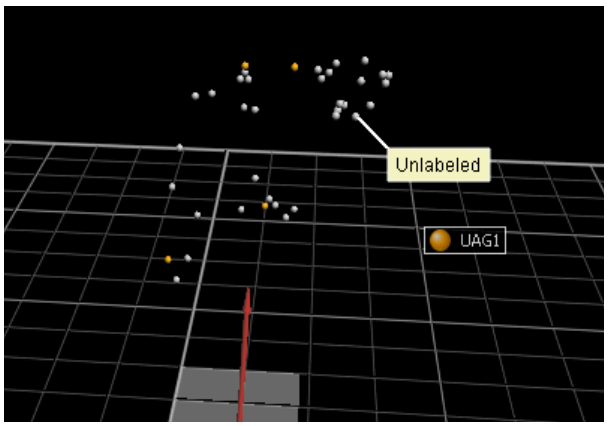

Figure 4.12 Marker labelling

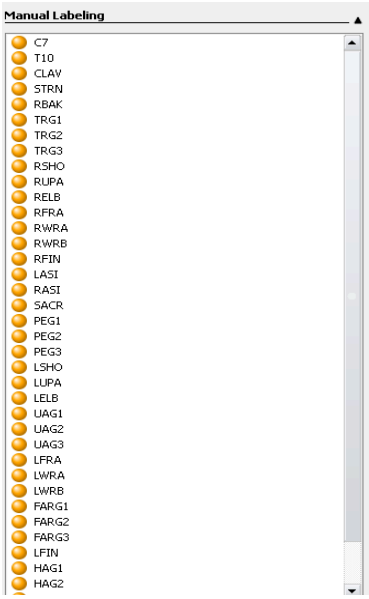

Figure 4.13 Marker set labels

Specific markers can be grouped together to represent segments of the tracked upper body. Fourteen segments were created, of which nine were anatomical segments and are detailed below in Table 4.5 (refer to Figure 4.3 and Table 4.3 for marker locations and labels). The rest, related to wearable sensors, are introduced in Chapter 5.

Table 4.5 Segment definitions and constituent marker labels

Segment	**Constituent Marker Labels**
Pelvis	SACR, LASI, RASI, LASI0, RASI0
Thorax	C7, T8, T10, CLAV, STRN
Shoulders	LSHO, RSHO, C7
Right Upper Arm	RSHO, RUPA, RELB, RELBM
Right Forearm	RELB, RELBM, RFRA, RWRA, RWRB
Right Hand	RWRA, RWRB, RFIN
Left Upper Arm	LSHO, LUPA, LELB, LELBM
Left Forearm	LELB, LELBM, LFRA, LWRA, LWRB
Left Hand	LWRA, LWRB, LFIN

4.2.7.3 Data filtering

Filtering to reduce high-frequency noise (for example from an electromagnetic signal generation source or floor vibration) in the marker motion data and to smooth trajectories is essential to proper data processing and calculating kinematics. Noise content should be

minimised prior to differentiation (calculation of displacement derivatives such as velocity or acceleration) because differentiation magnifies small signal variations, and hence the signal noise component. The aim is to only allow low frequency components, and remove sharp features from marker trajectories.

The filtering algorithm which was applied to data within the Vicon Nexus application was the Woltring (1995) routine, popular in gait analysis. It uses a low pass filter to retain the low frequency components of the movement signal under the assumption that general random noise which is "white" noise is a result of laboratory equipment interference, and is characterised by a high frequency content. This does not overcome systematic noise due to skin-marker movement which may include low and high frequency components depending on speed of movement. Optimal cut-off frequencies can be determined using residual analysis plots, which are plots of the root-mean-square error of the raw and filtered data at several cut-off frequencies to determine when the residual is a linear function of the cut-off frequency. According to Woltring (1995), this is when the noise residual is best estimated.

4.2.7.4 Gap filling: Static reconstruction

Despite the measures taken to avoid a marker not being tracked by the cameras during data capture, this may still occur. The missing positions of a marker over time can be reconstructed using mathematical interpolation by applying algorithms of cubic spline fitting or piecewise cubic Hermite interpolation. An alternative is the reconstruction procedure adopted here, known as static reconstruction, which reconstructs marker positions on the basis of information obtained from static trials usually acquired before capturing any dynamic trials.

Two static trials were taken with the subject stationary and wearing the full markers setup; one with the subject standing in anatomical position and the other with the subject seated. The visibility of all markers was ensured in the static trial. A missing marker position was determined in the dynamic trial based on the known relative position in the static trial to the other markers belonging to the same segment. First, a local segment based coordinate system, known as a 'dummy' segment, was defined using the other markers from the static trial. Using the known static position of the marker (dynamically missing) relative to the dummy segment, the missing marker position was statically parameterised. These static parameters, which represent where the missing marker is located relative to the dummy segment, were then used to generate the dynamic three dimensional marker coordinate within the same dummy segment, as that dummy segment moved from frame to frame in the dynamic trial.

Static reconstruction is generally found to be more reliable than interpolation, as interpolation has more overshoot at the start and end of the fitted data set. Interpolation forces a smoothing effect to satisfy continuity of the second derivative (Hanselman & Littlefield, 2004) which can lead to departure from the accuracy in measurements in some situations. In that sense, interpolation resembles filtering in its smoothing effect; however, repeated interpolation, unlike repeated filtering, maintains marker trajectory curvature.

Figure 4.14 is one example of the marker disappearance problem where the RASI marker was occluded from camera view in the pelvis segment. This example corresponds to a healthy subject (Subject 1) abducting the left shoulder with the elbow flexed, which caused the marker to be obscured. To solve this, the two markers LASI0 and RASI0, from the revised marker set (refer to Figure 4.3 and Table 4.3 for marker locations and labels), were

used to define a 'dummy' pelvis with the posterior SACR marker. The RASI marker was parameterised in terms of its three dimensional static position relative to the dummy pelvis. Then, these static parameters were used in the dynamic trial to generate a virtual RASI marker point (Figure 4.15) in space, which moved with the 'dummy' pelvis segment.

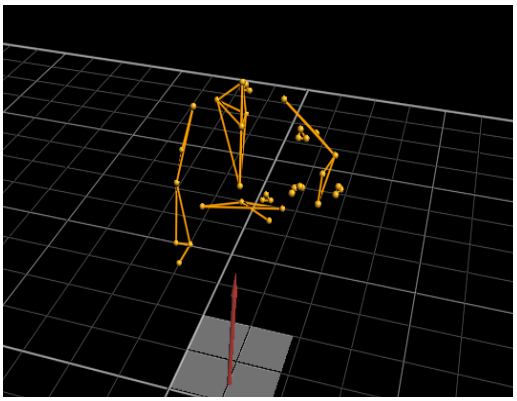

Figure 4.14 RASI marker disappearance

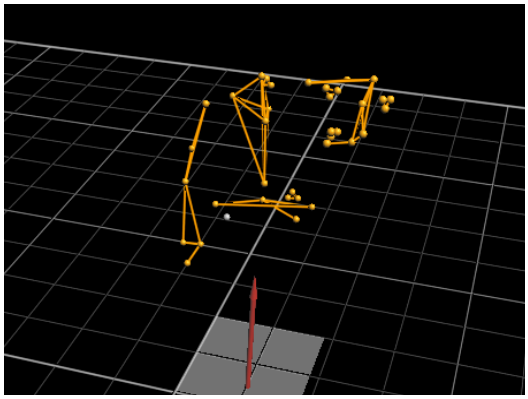

Figure 4.15 Static reconstruction of the RASI marker

4.3 Upper body kinematic model in BodyBuilder (Vicon, U.K.)

4.3.1 Segmental coordinate system definitions

Table 4.6 below summarises the segmental local coordinate system definitions adopted in the development of the upper body kinematic model in BodyBuilder (Vicon, Oxford, U.K.), a specialised body modelling programming language (refer to Figure 4.3 and Table 4.3 for marker locations and labels). The principles upon which these definitions are made are explained in Chapter 3 (section 3.3). Generally speaking, the z-direction is taken as vertically upwards, the x-axis longitudinally forwards, and the y-axis laterally pointing leftwards.

Table 4.6 Coordinate system definitions for the upper body segments in BodyBuilder[1]

Coordinate System[2]	***Origin***	***First Axis***	***Second Axis***	***Third Axis***
Pelvis[3] (y-z-x)	mid[4](LASI0-RASI0) if not (LASI-RASI)	(LASI0-RASI0) if not (LASI-RASI)	1st axis ⊗ v; v = (Origin-SACR)	1st axis ⊗ 2nd axis
Thorax (z-y-x)	CLAV	mid(CLAV-C7) – mid(STRN-T10)	1st axis ⊗ v; v = mid(CLAV-STRN) – mid(C7-T10)	1st axis ⊗ 2nd axis
Shoulder Complex (x-z-y)	mid(LSHO-RSHO)	C7– mid(LSHO-RSHO)	1st axis ⊗ v; v = LSHO-RSHO	1st axis ⊗ 2nd axis
Right Humerus[5] *(Upper arm)* (z-x-y)	RSHO	RSHO– mid(RELB-RELBM)	1st axis ⊗ v; v = RELBM – RELB	1st axis ⊗ 2nd axis
Right Ulna/Radius (Forearm) (x-z-y)	RWRA	RWRA–mid(RELB-ELBM)	1st axis ⊗ v; v = RWRA-RWRB	1st axis ⊗ 2nd axis
Right Hand (y-z-x)	RWRA	RWRA–RWRB	1st axis ⊗ v; v = RFIN–RWRA	1st axis ⊗ 2nd axis

[1] The definitions of segments Left Humerus (upper arm), Left Ulna & Radius (forearm), and Left Hand are the same as their right side counterpart but using the equivalent left marker as opposed to the right one.
[2] (y-z-x) for instance corresponds to the coordinate system definition of an upper body segment, given in the order first axis, second axis and third axis respectively
[3] the pelvis origin specified above is a simplification to the origin anatomical position, which is the hip joint centre of rotation. This can be determined using a functional approach (Leardini *et al.*, 1999) or a prediction method (Seidel *et al.*, 1995).
[4] mid is midpoint operator; also the vector definition a – b is a vector from marker b to marker a
[5] the humerus origin specified above is also a simplification. The anatomical origin is the glenohumeral joint GH that can be estimated using regression analysis (Meskers *et al.*, 1998).

4.3.2 Rotation angle order and Cardan angles

The angles are computed in the BodyBuilder software as Cardan (roll, pitch, yaw) angles with the rotation sequence $x - y - z$. These Cardan angles are calculated relative to Vicon's global coordinate frame using a dedicated code written in BodyBuilder, since this is not a standard Vicon Nexus output. Angular velocity in three dimensions was computed as first order differentiation of the Cardan (roll, pitch, yaw) angles.

4.4 Results and discussion

4.4.1 Results – Three dimensional upper body model

Figure 4.16 below presents the three dimensional upper body model developed using BodyBuilder. It is a stick figure[12] representation with eight segments tracking the upper

[12] a skeletal structure as a collection of segments

limbs (left and right upper arm, forearm, and hand), the trunk and pelvis, as seen in the Vicon Nexus application.

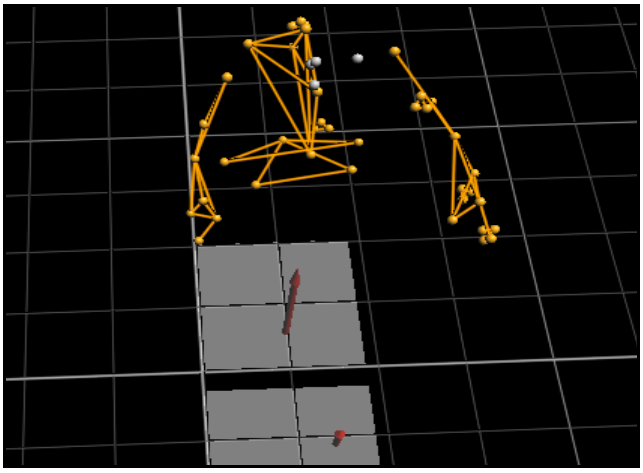

Figure 4.16 Development of a three dimensional upper body model (in Vicon Nexus)

Figure 4.17 shows the same stick figure as seen in BodyBuilder, for the computation of segmental (absolute) and joint (relative) angles for the upper limb movement, forearm pronation/supination.

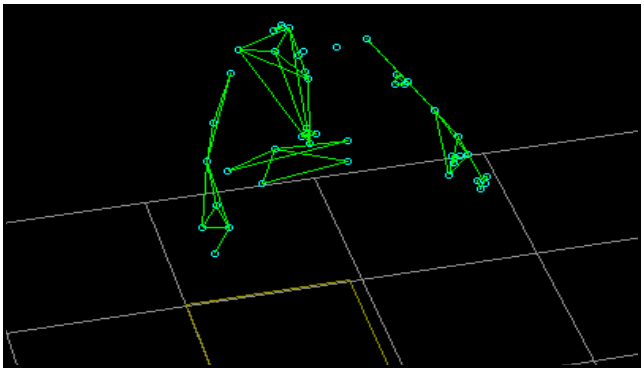

Figure 4.17 The upper limb model (in BodyBuilder) for forearm pronation/supination

4.4.2 Specifications for wearable monitoring of the forearm performing functional movements

Using the three dimensional upper body model from section 4.4.1, typical ranges (mean and standard deviation) of position, velocity, acceleration, orientation and angular velocity of the forearm were determined, along with the minimum and maximum absolute value for

some parameters, for movements of a set of healthy subjects and a stroke patient. Clinical metrics were also computed, which were derived from the literature and chosen in section 3.5. These were movement duration and percent time to maximum velocity (which corresponds to the time spent in the acceleration phase). This data were used to specify the accuracy and sensitivity requirements of wearable devices for forearm monitoring during certain functional movement tasks.

For optical systems, a minimum of three non-collinear markers are required to determine the six degrees of freedom associated with the position and spatial orientation (pose) of a three dimensional rigid body. Thus at least three markers must be visible in at least two cameras at all times for a given segment. Forearm kinematics are generally characterised by taking into account motion data of all rigid markers placed on the forearm segment. It is possible, however, to track the forearm segment movement using data from an individual marker only, when characterising just the translational parameters of forearm motion (i.e. position and its derivatives). Nonetheless, different markers estimate motion of the same segment differently depending on marker location; i.e. if markers are located on rigid anatomical positions (e.g. wrist bones), or on areas of more skin motion (e.g. mid forearm). As a result, it was important to investigate the relationship between marker position and characterising forearm translational motion. A better understanding of this relationship would facilitate choosing from the three forearm markers, the marker yielding forearm translation in best agreement with actual motion (comparison with the other two markers).

Table 4.7 shows forearm translational motion computed from individual markers for a healthy subject (Subject 2) performing reach-and-grasp ten times with the dominant right side. It is worth noting that RWRA and RWRB were placed on the ulnar and radial styloid

processes respectively (wrist bones), while the RFRA marker was attached on the mid forearm (refer to Figure 4.3 for exact marker locations).

Table 4.7 Effect of marker position on characterising forearm segment translational motion

		Forearm Markers		
		RWRA	**RWRB**	**RFRA**
Position p-p[1] [m]	**μ[2]**	0.284	0.266	0.267
	σ[2]	0.008	0.008	0.008
Velocity p-p [m/s]	**μ**	0.971	0.970	0.885
	σ	0.086	0.092	0.078
Acceleration p-p [m/s^2]	**μ**	3.326	3.556	2.940
	σ	0.482	0.620	0.437

[1] p-p is the peak to peak value defined as the magnitude of range (minimum to maximum value) of a given quantity

[2] **μ** is the mean value; **σ** is the standard deviation for the ten cycles

It was found (Table 4.7) that the mean peak-to-peak (p-p) values of forearm linear velocity and acceleration for the reach-and-grasp movement across the ten trials compared more closely when calculated from motion data of RWRA and RWRB forearm markers; the same can not be said for the RFRA marker. This could possibly be due to the former markers being attached to bony landmarks of the wrist with little skin movement, while RFRA was located on the mid forearm, an area of relatively higher skin motion. Therefore, either RWRA or RWRB was found to be suitable to characterise forearm translational motion components (position, velocity, and acceleration).

Comparing forearm linear velocity and acceleration, which were obtained from differentiating RWRA and RWRB measured position data for all four healthy subjects, the plots derived from the RWRB position were found to be more smooth than those obtained from the RWRA (this can be interpreted by assuming RWRB position data were less influenced by skin motion artefacts compared to RWRA). In addition, the RWRB velocity and acceleration plots had values between corresponding plots of the two other forearm

markers, RWRA and RFRA. Hence, RWRB was chosen out of the three markers as the best to represent forearm translational motion.

Based on the RWRB marker position components, forearm translational movement for the four healthy subjects and the stroke patient was characterised, while they performed reach-and-grasp and forearm pronation/supination movements. Forearm rotational motion was based on the entire three dimensional movement of the segment using all its markers.

The numerical findings were intended as technical specifications for wearable devices that monitor the forearm while it performs the movements mentioned earlier. The translational aspect of forearm motion for reach-and-grasp movement guided the accelerometers' specifications. The rotational aspect (i.e. orientation and angular velocity) of forearm motion for reach-and-grasp and forearm pronation/supination movements provided low and high velocity requirements of the gyroscopes respectively.

4.4.2.1 Normal upper limb movement

Characterisation of forearm motion, both in translation and in rotation, for reach-and-grasp and forearm pronation/supination movements on a set of four healthy subjects is shown in Table 4.8 and Table 4.9. The mean (**μ**) and standard deviation (**σ**) of a given variable are computations within subject, using motion data from five trials (and ten trials for Subject 2). The 'Overall' column corresponds to the overall minimum or maximum of a variable across all four subjects, for the minimum and maximum rows respectively; for other rows it represents the overall mean value.

Table 4.8 Characterisation of forearm motion during reach-and-grasp for four healthy subjects

		Translation Kinematics: Based on the RWRB Marker Rotation Kinematics: Based on all Markers				
		Subject 1 (left) [1] **N = 5**	**Subject 2 (right)** **N = 10**	**Subject 3 (right)** **N = 5**	**Subject 4 (left)** **N = 5**	**Overall**[2]
Position p-p [m]	**μ**	0.419	0.266	0.321	0.316	**0.331**
	σ	0.016	0.008	0.003	0.004	
Velocity p-p [m/s]	**μ**	1.280	0.970	0.880	1.431	**1.140**
	σ	0.136	0.092	0.063	0.120	
	min[3]	1.145	0.767	0.804	1.234	**0.767**
	max[3]	1.487	1.066	0.964	1.562	**1.562**
Acceleration p-p [m/s^2]	**μ**	4.608	3.556	2.464	6.2700	**4.224**
	σ	0.875	0.620	0.315	0.549	
	min	3.885	2.406	2.197	5.365	**2.197**
	max	6.096	4.573	2.914	6.789	**6.789**
Velocity [m/s]	**min**	0.068	0.168	0.188	0.174	**0.068**
	max	0.184	0.326	0.320	0.589	**0.589**
Acceleration [m/s^2]	**min**	0.111	0.033	0.008	0.712	**0.008**
	max	1.206	1.302	0.989	2.931	**2.931**
Orientation p-p [deg]	**μ**	41.926	49.021	35.087	53.855	**44.972**
	σ	7.678	3.983	3.353	1.494	
Angular velocity p-p [rad/s]	**μ**	2.935	3.163	1.737	4.013	**2.962**
	σ	0.507	0.596	0.243	0.425	
Angular velocity(y) [rad/s]	**max abs**[3]	2.197	1.344	0.909	2.155	**2.197**
Movement duration [s]	**μ**	2.476	2.667	2.740	2.520	**2.650**
	σ	0.181	0.159	0.407	0.179	
Percent time to maximum velocity [%]	**μ**	43.483	48.350	46.356	42.048	
	σ	5.709	7.063	3.099	1.942	

[1] in brackets is the side measured (i.e. dominant side); N is the total number of trials
[2] the overall column contains the overall mean, standard deviation, minimum, maximum, or maximum absolute value across the four subjects depending on the column quantity
[3] min is the minimum value; max is the maximum value; and max abs is the maximum absolute value

The reach-and-grasp movement for a healthy subject is primarily a translation along the longitudinal axis of the forearm, with some rotation in the vertical plane about the lateral axis (due to unconstrained arm abduction/adduction at the elbow). This is accompanied by slight rotation about the longitudinal axis of the forearm. Comparing forearm position peak-to-peak across trials of the same subject, the standard deviation was found to be small (less than 1.7 cm), which implied a high intra-subject repeatability for the reach-and-grasp

movement at the forearm. However, comparing the mean value of forearm position peak-to-peak across subjects, suggested an inter-subject variability for this movement.

Movement velocity had absolute minimum and maximum values of 0.07 and 0.59 m/s respectively with mean p-p value of 1.14 m/s (given to three significant figures). The absolute minimum and maximum quantities for movement acceleration were 0.01 and 2.93 m/s^2 with mean p-p value of 4.22 m/s^2 (given to three significant figures). To monitor this movement with wearable devices like accelerometers, accelerations as small as 0.01 m/s^2 need to be measured, and up to 2.93 m/s^2.

As mentioned earlier, reach-and-grasp movement is primarily translational with the main rotational component in the vertical plane about the lateral axis, defined in this case as the y-axis. The mean p-p value of orientation was found to be 44.97º and the maximum absolute value of angular velocity about the lateral y-axis was 2.20 rad/s with 2.96 rad/s mean p-p value of total angular velocity. This would be the low-end requirement for gyroscopes as the rotational component of forearm reach-and-grasp movement is minimal, along with its derivative angular velocity.

A high-end requirement for gyroscopes was found to be 9.02 rad/s during motion analysis of forearm pronation/supination (mostly rotational movement) for the healthy subjects (Table 4.9). This is necessary to measure the significant rotational component of forearm pronation/supination motion, which is about the longitudinal axis of the forearm; in this case defined as the x-axis. The motion's accelerations (mainly longitudinal) were as small as 0.001 m/s^2, so a higher accuracy of accelerometers would now be required, to measure accelerations during this motion.

Table 4.9 Characterisation of forearm motion during forearm pronation/supination for four healthy subjects

		Translation Kinematics: Based on the RWRB Marker Rotation Kinematics: Based on all Markers				
		Subject 1 (left) N = 5	**Subject 2 (right) N = 10**	**Subject 3 (right) N = 5**	**Subject 4 (left) N = 5**	**Overall**
Velocity [m/s]	**min**	0.058	0.038	0.0002	0.00001	**0.00001**
	max	0.141	0.103	0.098	0.254	**0.254**
Acceleration [m/s^2]	**min**	0.001	0.011	0.020	0.055	**0.001**
	max	0.796	0.657	0.716	1.674	**1.674**
Angular velocity(x) [rad/s]	**max abs**	4.986	5.288	7.485	9.023	**9.023**
Movement duration [s]	**μ**	2.350	3.128	2.212	1.580	
	σ	0.232	0.300	0.164	0.089	
Percent time to maximum velocity [%]	**μ**	36.705	41.895	45.187	45.522	
	σ	12.505	5.288	7.485	4.356	

4.4.2.2 Pathological upper limb movement

Results of forearm motion analysis for the stroke patient pre-intervention, the translational and rotational segment motion parameters, for reach-and-grasp are shown in Table 4.10 (first column). The main finding was larger mean p-p acceleration (7.79 m/s^2) compared to overall p-p mean of 4.22 m/s^2 across the healthy subjects; caused mainly by jerkiness of the patient's reach-and-grasp movement. Similarly, the minimum and maximum values of acceleration p-p were larger (being 6.97 and 8.39 m/s^2 respectively). So to monitor pathological upper limb movement, a wider range of acceleration measurements is required. The previously recommended minimum requirement of 0.001 m/s^2 for accelerometers still holds, and should be adequate to measure pathological upper limb movement for this stroke patient.

In addition, the accelerometers should be able to measure at least 9 m/s^2. The maximum absolute value of angular velocity about the lateral y-axis was 0.48 rad/s. Unexpectedly a larger rotational component (of 1.20 rad/s) was measured about the longitudinal x-axis. This finding might be as a result of this patient's motor disability and constrained

rotational motion at the elbow. So in an attempt to achieve the reach-and-grasp movement, expected rotation about the lateral axis was compensated for by rotation about the longitudinal axis. Both values of computed angular velocity about the y- and x- axes for the patient could be measured with the previously recommended gyroscopic specifications, with low and high requirements of 2.20 and 9.02 rad/s respectively.

4.4.3 Minimum sensitivity required to detect differences in pre/post-stroke intervention

A comparison of forearm motion during reach-and-grasp for the stroke patient between pre- and post- intervention is given in Table 4.10. This comparison allowed identification of device (accelerometer and gyroscope) sensitivity required to detect subtle differences in movement that might occur following the rehabilitation exercise phase. The standard deviation of position peak-to-peak was found to reduce slightly, as the reach-and-grasp movement was performed more consistently post-intervention. Acceleration values (both mean peak-to-peak and absolute minimum and maximum) post-intervention were much lower (a drop from 7.79, 6.97, and 8.39 m/s^2 to 2.65, 1.67, and 3.35 m/s^2 respectively) and less jerkiness was measured. This implied better movement control and improvement in performing the translational aspect of reach-and-grasp post intervention. The measured changes in acceleration from pre- to post- intervention were significant, so the sensor accelerometer does not need to be very sensitive (in the order of 1.5 m/s^2). However, this is based on sensor motion data for one patient, so this sensitivity requirement of accelerometers might not be representative over a larger population. There was a slight improvement from the restricted rotation seen at the elbow pre-intervention, so sensitivity of the gyroscopes should be in the order of 0.1-0.5 rad/s.

The standard deviation for clinical metrics such as movement duration and percent time to maximum velocity significantly reduced, to one-third its original value for the latter. This

suggested a better, more consistent and controlled movement post-intervention, which was measurable by the chosen clinical metrics. An important clinical requirement was added as a result, which is that wearable devices should be able to reliably measure parameters like movement duration and movement periodicity, as well as accurately estimate movement velocity.

Table 4.10 Comparison of forearm motion during reach-and-grasp for a stroke patient, pre- and post-intervention

		Pre-Intervention N = 5	Post-Intervention N = 5
Position p-p [m]	**μ**	0.370	0.294
	σ	0.024	0.017
Velocity p-p [m/s]	**μ**	1.302	0.706
	σ	0.039	0.106
	min	1.261	0.592
	max	1.337	0.826
Acceleration p-p [m/s^2]	**μ**	7.788	2.653
	σ	0.598	0.752
	min	6.974	1.667
	max	8.390	3.346
Velocity [m/s]	**min**	0.158	0.004
	max	0.321	0.072
Acceleration [m/s^2]	**min**	0.106	0.002
	max	2.123	0.497
Orientation p-p [deg]	**μ**	43.238	22.752
	σ	4.627	2.476
Angular velocity p-p [rad/s]	**μ**	2.346	1.009
	σ	0.1889	0.063
Angular velocity(y) [rad/s]	**max abs**	0.483	0.426
Angular velocity(x) [rad/s]	**max abs**	1.204	0.811
Movement duration [s]	**μ**	3.215	3.417
	σ	1.199	0.829
Percent time to maximum velocity [%]	**μ**	44.757	41.511
	σ	15.341	5.539

Both arm reach-and-grasp and forearm pronation/supination movements are constrained, in the sense that movement mainly occurs in two dimensions. So to test whether the recommended specifications of wearable devices, extracted from analysis of these movements, were sufficient to measure a more complex movement in three dimensions, forearm motion during hand-to-mouth motion was analysed for the stroke patient, both

pre- and post- intervention (results given in Table 4.11). Very small changes in the patient's movement were measured post-intervention (in the order of 0.5 m/s^2 and 0.1 rad/s). The small change quantified the minimum sensitivity required of wearable devices to monitor a patient's movement and detect differences in pre/post- stroke intervention. In terms of the patient's performance and lack of improvement in this case, it should be stated that the post-intervention hand-to-mouth movement was measured at the end of the data collection session and the patient was possibly tired at that stage. The clinical metrics computed, movement duration and percent time to maximum velocity, supported the lack of improvement in performing this complex movement (larger standard deviations for both metrics were measured).

Table 4.11 Comparison of forearm motion during hand-to-mouth for a stroke patient, pre- and post-intervention

		Pre-Intervention N = 5	**Post-Intervention N = 5**
Position p-p [m]	**μ**	0.328	0.467
	σ	0.017	0.014
Velocity p-p [m/s]	**μ**	1.083	1.188
	σ	0.019	0.098
	min	1.062	1.105
	max	1.108	1.314
Acceleration p-p [m/s^2]	**μ**	4.912	5.461
	σ	0.234	0.883
	min	4.718	4.595
	max	5.248	6.562
Velocity [m/s]	**min**	0.173	0.146
	max	0.531	0.585
Acceleration [m/s^2]	**min**	0.020	0.054
	max	2.626	2.239
Orientation p-p [deg]	**μ**	41.508	44.379
	σ	2.792	2.964
Angular velocity p-p [rad/s]	**μ**	2.529	2.031
	σ	0.570	0.179
Angular velocity(y) [rad/s]	**max abs**	0.965	0.632
Angular velocity(x) [rad/s]	**max abs**	0.928	1.003
Movement duration [s]	**μ**	8.995	8.282
	σ	0.426	0.539
Percent time to maximum velocity [%]	**μ**	15.501	17.894
	σ	1.694	3.386

4.4.4 Discussion

A computational procedure to measure upper body movements and compute kinematics for healthy subjects and a stroke patient was described. Movements taking place at the forearm were analysed; these included reach-and-grasp, forearm pronation/supination and hand-to-mouth movements. To characterise normal and pathological upper limb movement, typical ranges (the mean and standard deviation) of forearm position, velocity, acceleration, orientation and angular velocity along with the minimum and maximum absolute values for some parameters were investigated for all participants. Findings provided specifications for wearable monitoring of the forearm while performing the functional movements listed above. Also, device sensitivity requirements were determined to detect subtle change in movement in pre/post- stroke intervention

In summary, the measurement accuracy for accelerometers was recommended to be high; the device should be able to measure accelerations as small as 0.001 m/s^2, with an upper limit of measuring at least 9 m/s^2 in the case of jerky movement. Gyroscopes should also measure angular velocities as small as 2.20 rad/s, and as large as 9.02 rad/s.

To detect differences in forearm movement between pre- and post- stroke intervention, minimum sensitivity requirement for accelerometers and gyroscopes was found to be of the order of 0.5 m/s^2 and 0.1-0.5 rad/s respectively. Changes in functional movements in pre/post- stroke intervention, due to frequent exercise at home, were detectable by two clinical metrics chosen from the literature; these were movement duration and percent time to maximum velocity. This finding added a clinical requirement that wearable devices should be able to reliably measure parameters like movement periodicity, as well as accurately estimate movement velocity.

The characterisation of forearm motion was found to be anatomically meaningful, mainly for angular computations, as values lie within the expected ranges for performing the different movements (Zhou *et al.*, 2008, Van Andel *et al.*, 2008). Marker based model accuracy was assumed to be satisfactory as a validation tool for wearable devices (Anglin & Wyss, 2000b, Godwin *et al.*, 2009, Zhou, Hu & Tao, 2006).

It is worth noting that the four healthy subjects naturally performed forearm reach-and-grasp with almost the same movement duration (on average 2.65 seconds). This could imply that despite the different strategies and trajectories individuals employ to achieve a given movement, movement duration is the parameter that is optimised, by varying the movement's velocity, acceleration, and a given rotational component.

It should be stated that the characterisation of pathological upper limb movement, and requirements for wearable monitoring of the forearm in pre/post- stroke intervention, were solely based on forearm motion data from a single stroke patient. Other stroke patients might have forearm movement profiles that are completely non-periodic or extremely jerky, so further studies on more patients are needed to ensure reliability of these findings.

4.5 Summary

A computational procedure to measure upper body movements mainly at the forearm, and compute kinematics was described. Key aspects in this section were first to provide necessary specifications for wearable monitoring of the forearm while performing certain functional movements for healthy subjects and a stroke patient; and second to quantify the minimum sensitivity requirement of wearable devices to detect movement differences in pre/post- stroke intervention. Improvements in movements were detectable using clinical

metrics; which in this work were movement duration and percent time to maximum velocity. Results were also found to be anatomically meaningful, but proper validation of the marker based model and determination of its accuracy should be done, for example using imaging techniques. The importance of this validation is stated in Chapter 7 (section 7.3) as suggested further research.

Chapter 5

Evaluation of Inertial Sensors for Upper Limb Monitoring

5.1 Introduction

Chapter 4 presented a gold standard for measuring and assessing reach-and-grasp, forearm pronation/supination, and hand-to-mouth movements. This was facilitated by the development of a computational method in Vicon for describing the kinematic associations of segments and joints of the right and left upper limbs, the trunk and pelvis, with a main focus on the forearm. Despite the method's accuracy (particularly for measuring position and estimating orientation), it can not be applied outside specialised laboratories (such as a home based environment) due to its high cost, special setup and calibration requirements.

As an alternative, this chapter describes the use of inertial sensors, specifically the Xsens system (chosen in Chapter 3, section 3.2.4) for upper limb motion estimation and monitoring. The portability, compactness and low cost of these sensors make them ideal for wearable monitoring. Despite major advances in the measurement capabilities of inertial sensors, driven by technological developments in the computer games and virtual reality industries, there are some known systematic problems (such as gravity bias, and drift) that affect readings of sensor accelerometers and gyroscopes. In addition, manufacturer reported sensor accuracies are given for general motion regimes, whereas for monitoring specific upper limb exercises, sensor performance in a particular motion regime is required.

Several experiments were performed at the Nuffield Orthopaedic Centre (NOC) to assess individual sensor components. The specific outcomes of each experiment are listed below.

- *System Calibration* (section 5.2): relates the global coordinate systems of Vicon and Xsens sensors, establishes static sensor accuracy for estimating orientation, and determines the effect of magnetism, produced by force plates, on sensor orientation estimation

Rigid Body Tests (Rotating Bar, Mobile Robot):

- *Experiment 1* (section 5.3): determines dynamic sensor accuracy for estimating orientation over a general motion regime
- *Experiment 2* (section 5.4): assesses the angular velocity measurements from the sensor gyroscopes in specific motion regimes (established in section 4.4.2.1 from motion data of healthy subjects) representing reach-and-grasp and forearm pronation/supination. Hence, a task-specific dynamic measurement accuracy of the gyroscopes is determined. Internal sensor consistency of the accelerometers and gyroscopes is also checked.
- *Experiment 3* (section 5.5): determines dynamic sensor baseline accuracy for measuring accelerations and obtaining velocity from accelerometers, in motion regimes of comparable accelerations to healthy upper limb movement (established in section 4.4.2.1). This is facilitated by the absence of skin motion artefacts and an ideal (vertical) setting of initial sensor mounting. The appropriateness of the sensor mounting method is also investigated.

Human Tests:

- *Experiment 4* (section 5.6): investigates the accuracy of sensors for measuring motion data of healthy subjects and a stroke patient prior to intervention. In the case of the patient, the sensors' sensitivity to detect change in movement

patterns following intervention is checked against the sensitivity requirements identified in section 4.4.3 using Vicon.

Based on the findings described, recommendations on how to improve the estimation of certain rehabilitation outcomes (movement velocity, forearm absolute orientation, movement duration, and percent time to maximum velocity) are provided in section 5.7.

5.2 System set-up with Xsens sensors

Figure 5.1 shows the system set-up with Xsens sensors for the human patient and the mobile robot.

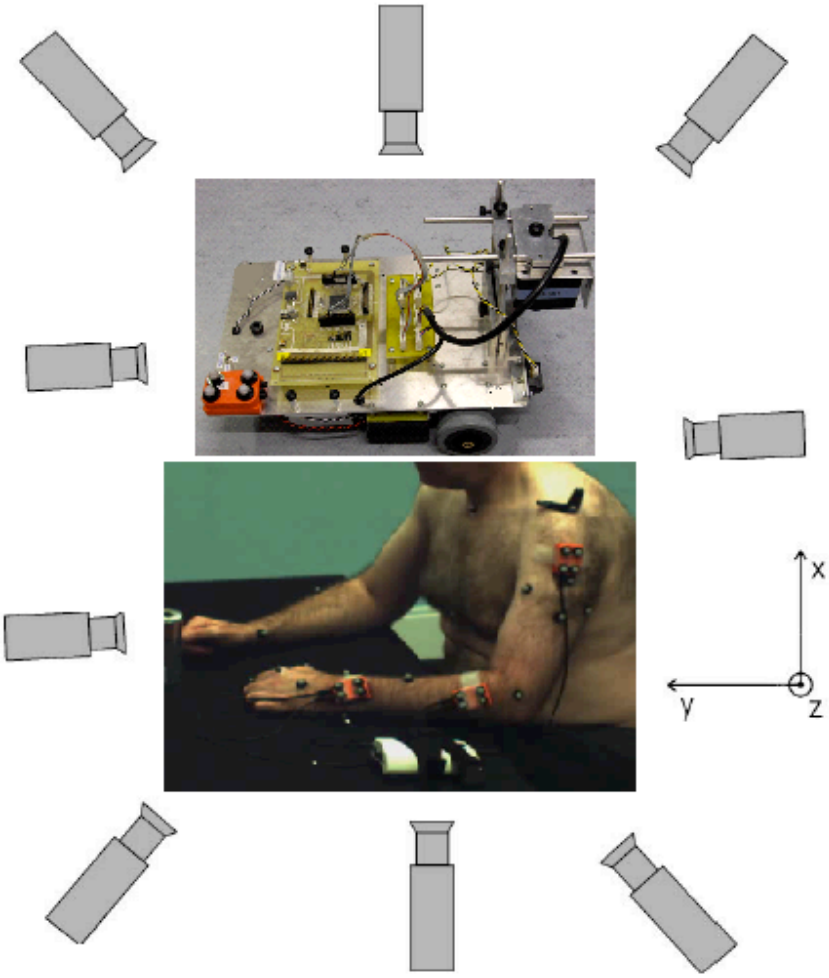

Figure 5.1 System set-up with Xsens sensors (in orange) for the human patient and the mobile robot

The Xsens sensor (Figure 5.2) is a miniature inertial measurement unit with integrated three dimensional magnetometers and an embedded processor that computes roll[13], pitch[14] and yaw[15] in real time. The sensor also measures local three dimensional kinematic data, which include linear acceleration, rate of turn (angular velocities measured by the gyroscopes), and Earth magnetic field data. The three dimensional orientation (roll, pitch, yaw), calculated using a fusion algorithm of sensor local readings, represent sensor pose with time in a fixed coordinate system. This fixed global coordinate system (labelled G in Figure 5.3) is defined as follows: x-axis positive pointing towards local magnetic North (determined by the sensor magnetometers), y-axis positive pointing West, and z-axis positive pointing upwards against gravity (determined by the vertical accelerometer).

The figure originally placed here has been removed for copyright reasons.

Figure 5.2 The Xsens sensor with its fixed local coordinate system overlaid (x,y,z) Reproduced from (Xsens Technologies, 2007)

The figure originally placed here has been removed for copyright reasons.

Figure 5.3 Alignment of Xsens local coordinate system (S) with its fixed global coordinate system (G) Reproduced from (Xsens Technologies, 2007)

[13] Rotational or oscillatory movement of a body about its longitudinal axis (McGRAW-Hill (2003). Dictionary of Engineering, second ed. New York: Licker, Mark D.)
[14] Angular displacement about an axis parallel to the lateral axis of a body (Ibid.)
[15] Rotational or oscillatory movement of a body about its vertical axis (Ibid.)

The Xsens system has two models, the MTi (Figure 5.4) and the MTx (Figure 5.5); the major difference between the two is in the casing shape and weight, connector, and general ruggedness. The MTi sensor is a miniature gyro-enhanced Attitude and Heading Reference System. It is popular in areas of robotics, aerospace, autonomous vehicles and the marine industry; mainly for stabilisation and control of cameras, robots, vehicles and similar equipment. The MTx model is smaller in size and is commonly used as a three dimensional inertial orientation tracker in areas of biomechanics, exercise and sports, virtual reality, animation and motion capture. Motion data in this work were acquired with four Xsens sensors, all of the MTx model.

The figure originally placed here has been removed for copyright reasons.

Figure 5.4 MTi Xsens sensor
Reproduced from (Xsens Technologies, 2007)

The figure originally placed here has been removed for copyright reasons.

Figure 5.5 MTx Xsens sensor
Reproduced from (Xsens Technologies, 2007)

Three of the Xsens sensors used (later referred to as S2, S3 and S4) could be connected to an Xbus Master, which allowed the sensors' data to be synchronised. These sensors belonged to a new sensor generation developed by Xsens Motion Technologies, and the Xbus Master supported two modes of data communication, connection via a USB cable, and connection via Bluetooth. Data from the fourth sensor S1 (an older model) could only be extracted serially with a USB cable for analysis. The four sensors were pre-calibrated at Xsens facilities to linearise the data, scale the data in S.I. units, and correct for misalignment and temperature effects. No extra sensor calibration was required prior to data collection.

5.2.1 System calibration with Vicon

For the Xsens system, accelerations, angular velocities and Earth's magnetic field data are measured relative to the sensor local coordinate system (S), while the sensor angular output (roll, pitch, yaw) is measured relative to the Xsens sensor global coordinate system (G) (defined in section 5.2). Computations of segments or objects tracked with Vicon are measured relative to Vicon's global coordinate system (V) in the gait laboratory. The local sensor measurements may be mapped from (S) to (G) using a transformation matrix ${}^{G}_{S}R$ based on sensor angular output.

To be able to validate sensor measurements (relative to (S)) and sensor angular output (relative to (G)) to computations of the sensor tracked with Vicon (relative to (V)), the two sets of sensor data needed to be related to a common coordinate system. Once the transformation matrix ${}^{G}_{V}R$ relating (V) and (G) was determined, data corrections could be made to accommodate for any deviation of one global coordinate system relative to the other.

In general, to map/transform a known point ${}^{B}P$ from one coordinate system {B} to another coordinate system {A} (Figure 5.6) and locate ${}^{A}P$, equation (5.1) is used. In this general case, {B} is translated with respect to {A} with a vector offset ${}^{A}P_{BORG}$ (relative to {A}) from its origin to the origin of {A}. Also, {B} is rotated with respect to {A} as described by ${}^{A}_{B}R$ (Craig, 2004).

$$ {}^{A}P = {}^{A}_{B}R\ {}^{B}P + {}^{A}P_{BORG} \tag{5.1} $$

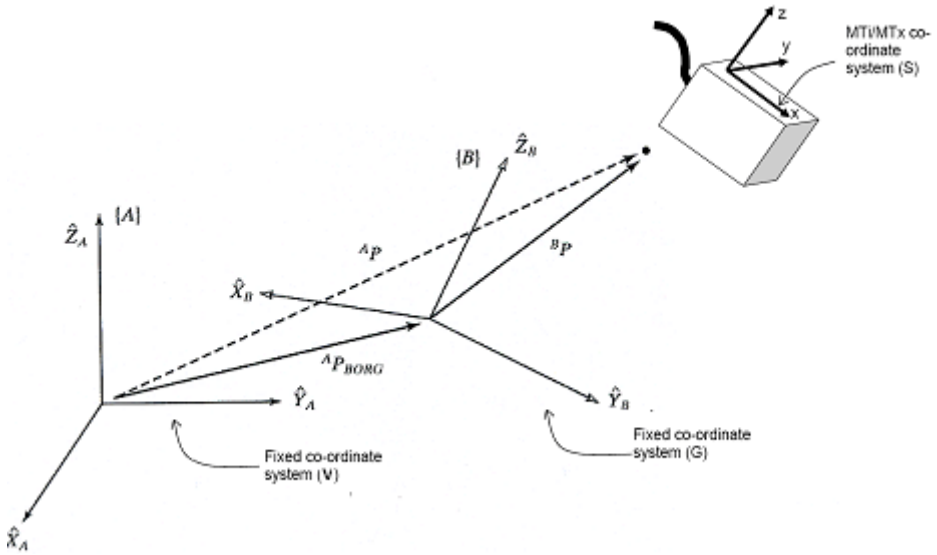

Figure 5.6 Determination of point *P* position located in coordinate system {B} relative to {A}, where {B} is a transformed version of {A} (translation and rotation in 3-D) Reproduced from (Craig, 2004)

To find ${}^{G}_{V}R$, the sets of rotations relating (V) and (G) were investigated (the offset vector ${}^{G}P_{VORG}$ between the origins of (V) and (G) is relevant to assess difference in translation and not rotation). Four Xsens sensors were securely attached on a table top of height 510 mm from the laboratory floor. Sensors were statically tracked in Vicon (i.e. with no sensor movement), each using three (9 mm diameter) markers (Figure 5.7). Two starting positions of (S) were adopted; the first with (S) aligned to (V) within 1º error, and the second with (S) aligned to (G) determined using a compass within 0.5º error. (V) was

defined in the gait lab as a horizontal x-y plane whose axes' directions as shown in Figure , and a vertical z axis pointing upwards.

When (S) and (V) were aligned using the Vicon position data of the markers on the sensors, the sensor angle output (roll, pitch, yaw) determined ${}^{G}_{V}R$. When (S) and (G) were aligned, the sensor angle output was close to zero (as expected), and ${}^{V}_{G}R$ was determined from sensor orientation computed in Vicon using markers on the sensors. The two rotation matrices ${}^{G}_{V}R$ and ${}^{V}_{G}R$ are transposed versions of each other, as in equation (5.2).

$$ {}^{G}_{V}R = ({}^{V}_{G}R)^{T} \tag{5.2} $$

Three force plates (Figure 5.8) are fixed to the laboratory floor, centrally located in the capture volume where upper limb motion is ideally captured in Vicon. So, it was also necessary to see the effect of magnetism (mainly produced by the force plates) on orientation estimation for the four sensors, by turning on and off the three force plates. The height of the table top on which the sensors were attached was carefully chosen to reflect the height of sensor mounting in a typical upper limb tracking session (the distance away from the force plates has been shown to affect the amount of magnetism seen by the sensors (de Veries *et al.*, 2009), hence the magnitude of distortion in sensor orientation estimation).

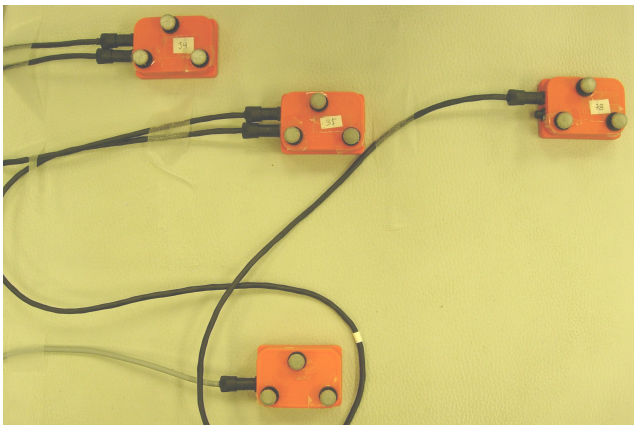

Figure 5.7 Xsens sensors tracked in Vicon to determine ${}^{G}_{V}R$ relating the global coordinate systems of Vicon and Xsens. Top (from left to right): sensors S2, S3, and S4 respectively; Bottom: sensor S1

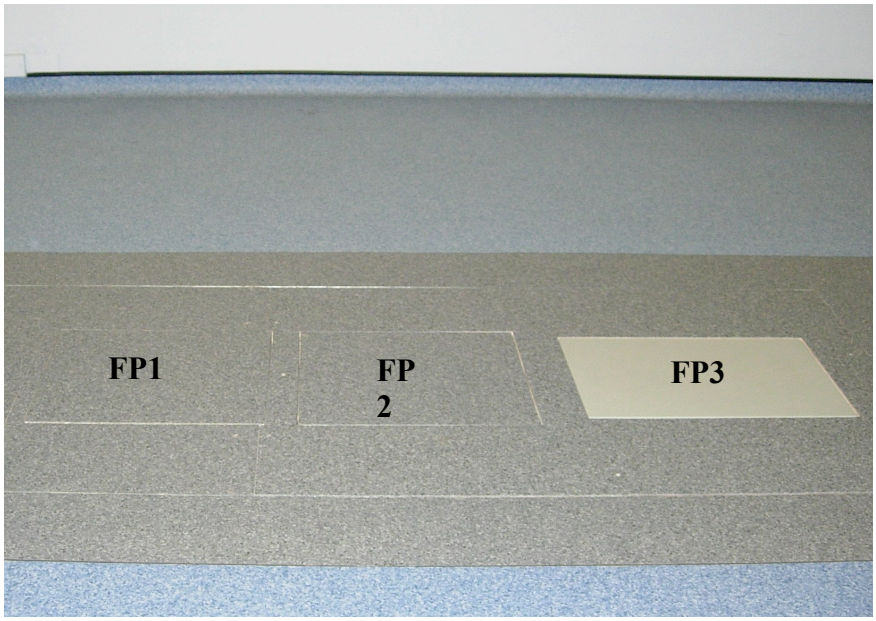

Figure 5.8 The three forces plates (labelled in the figure as FP1, FP2, and FP3) fixed to the gait laboratory floor, NOC. The plate FP3 is not externally covered hence the difference in its colour as compared to FP1 and FP2. The colour of the plates has no special meaning in the context of this work.

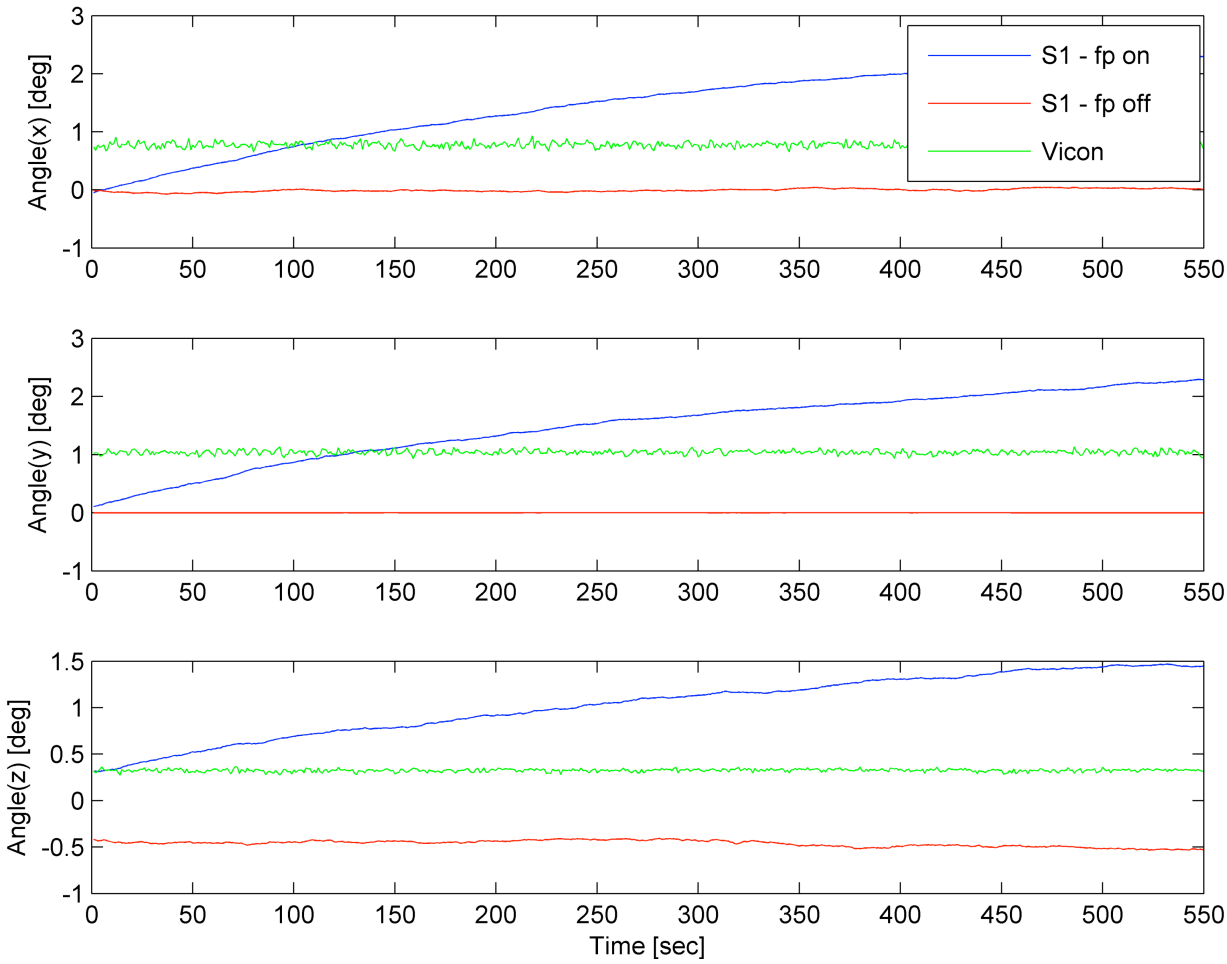

Figure 5.9 Determination of ${}^{G}_{V}R$ from estimated sensor three dimensional orientation (roll *x*, pitch *y*, yaw *z*) for sensor S1 (compare plots in red and green). The effect of magnetism produced by the force plates (fp) on sensor orientation misestimation (compare plots in red and blue).

Figure 5.9 shows in red sensor S1 estimation of its three dimensional orientation (roll, pitch, yaw) relative to (G), with force plates turned off and (S) of S1 aligned to (G). For S1, the x- and y- axes of (S) were perfectly aligned to the x- and y- axes of (G). The z-axis of (S) differed from the z-axis of (G) by 0.4º. Sensor orientation computed in Vicon relative to (V) is given in green. Correcting for the z-axis of (S), the x-, y- and z- axes of (V) and (G) differed by 0.75º, 1.03º and 0.32º respectively.

Similarly, with force plates turned off and (S) of sensors S2, S3 and S4 best aligned to (V) (by ensuring Vicon's position measurement of the two longitudinal sensor markers in Figure 5.10 gave approximately equal y-components, alignment was within 1º error),

average values of the three dimensional sensor orientation were computed in Vicon and are summarised in Table 5.1. In addition, average values of (roll, pitch, yaw) estimated by the sensors are indicated. These would describe ${}^{G}_{V}R$ for each sensor had the sensor orientation computed in Vicon given zero values (a perfect alignment of the sensor's (S) and (V)).

The results for the best sensor local alignment to (V) along the x-, y-, and z- axes are highlighted in red bold. Corresponding (roll, pitch, yaw) of the sensors relative to (G) are marked in black bold. By correcting the marked sensor estimations of orientation (in black bold) by the highlighted Vicon computations (in red bold) such that a perfect alignment of (S) and (V) had been achieved, the best relationship possible of (V) and (G) could be determined. This was found to be 0.84º, 0.54º, and 0.06º for the x-, y-, and z- axes of sensors S2, S3, and S4 respectively. On average for all sensors, (V) and (G) were related by about 1º difference for the x- and y- axes and 0º for the z-axis.

Table 5.1 Average value of sensor orientation computed in Vicon and estimated by sensors S2, S3 and S4

	Sensor orientation: Average value of components x, y, z					
	Vicon computation [deg]			**Sensor estimation [deg]**		
	Orientation (x)	**Orientation (y)**	**Orientation (z)**	**Roll**	**Pitch**	**Yaw**
S2	4.9	**-0.14**	-0.25	1.88	**0.40**	-0.10
S3	**0.7**	-0.6	-0.84	**1.54**	0.09	-1.00
S4	5.8	-0.77	**-0.16**	1.46	0.88	**-0.10**

The static sensor accuracy for estimating roll, pitch, and yaw, given in Table 5.2 with the force plates turned off, was found to be less than 4.5º, 1.8º, and 0.2º respectively. The root-mean-square errors given in Table 5.2 are obtained from the difference between Vicon and Xsens.

Table 5.2 Static sensor accuracy for estimating orientation (roll, pitch, yaw)

	Root-mean-square errors [deg]		
	Roll	**Pitch**	**Yaw**
S2	3.1038	0.6009	0.1269
S3	0.8257	0.7157	0.1641
S4	4.4099	1.7196	0.0608

The blue plot in Figure 5.9 shows sensor S1 estimation of roll, pitch, and yaw with the force plates turned on, and the sensor mounted 510 mm from the plates. With no sensor movement, orientation was incorrectly estimated by S1 due to magnetism produced by the force plates, with drift errors reaching about 2.5º in the x- and y- directions, and 1.2º in the z- direction.

Sensors S2 (Figure 5.10), S3, and S4, belonging to the new generation of Xsens sensors, showed a similar effect of magnetism on sensor estimation of roll, pitch, and yaw when the force plates were on. However, orientation estimation was seen to improve for the new generation sensors, as less orientation drift was detected when the force plates were on as compared to S1 (compare blue plots of Figure 5.9 and Figure 5.10).

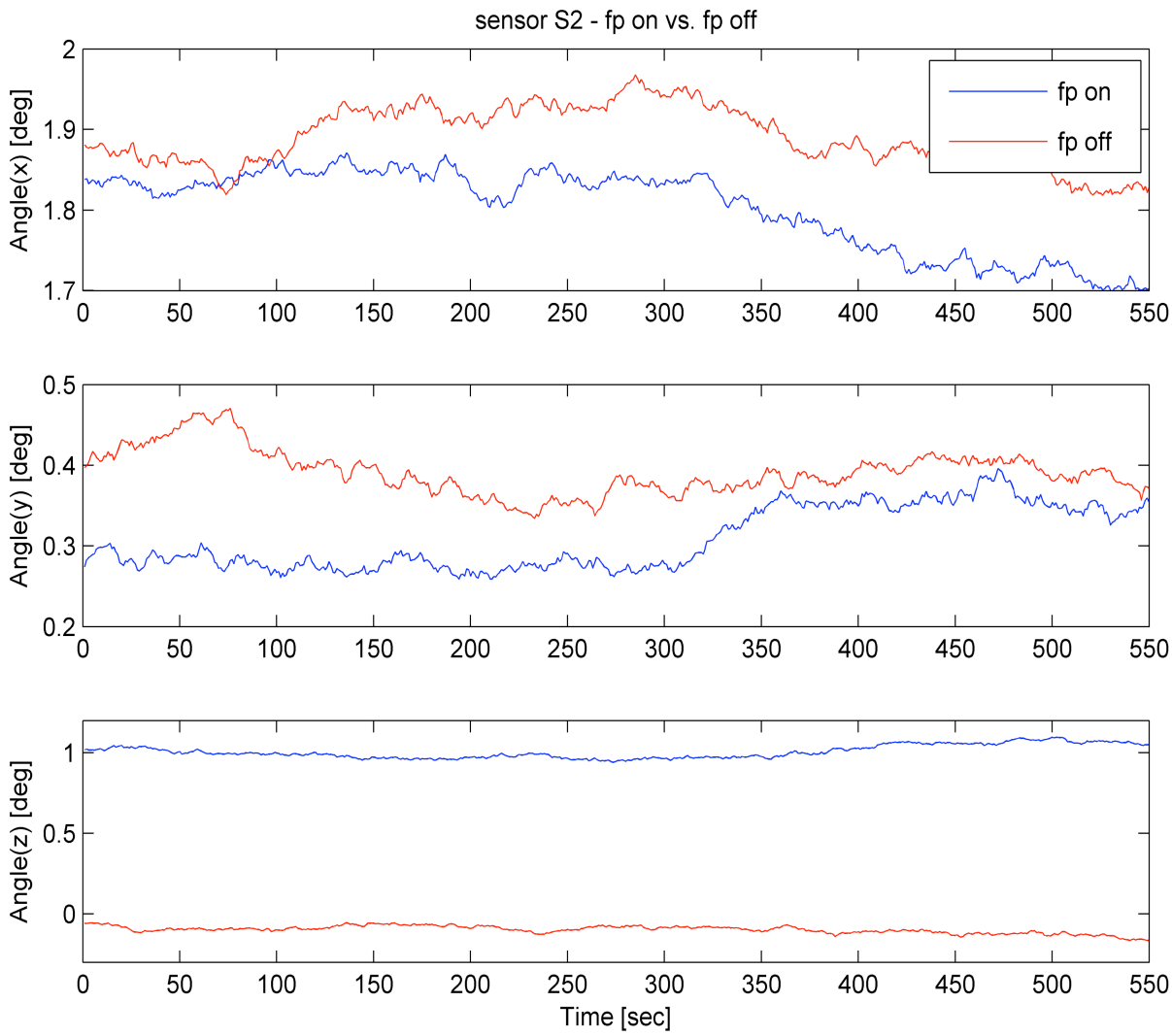

Figure 5.10 The effect of magnetism on sensor orientation misestimation with force plates on for sensor S2. An improvement was noted in orientation estimation for the new generation sensors (sensors S2, S3, and S4) with less orientation drift when the force plates were on, as compared to the sensor S1.

5.3 Experiment 1: A mobile robot to evaluate sensor orientation estimation

To determine the dynamic sensor accuracy for estimating orientation, over a general motion regime and with no skin motion artefacts, true rigid body movement of a mobile robot was measured. The mobile robot (30 cm x 20.5 cm) was driven by two DC motors, with a speed reduction gear box of ratio 60:1. Each motor was controlled by a Boolean signal (to control motor direction) and a pulse width modulation signal (to control motor speed); and both signals were generated by a microcontroller. The latter was programmed

in C language using CodeWarrior™ (Metrowerks, U.S.), so the robot performed a straight motion at constant speed, turned 180º about its vertical axis, oscillated, then turned another 180º about the vertical axis, before repeating this whole sequence once more. The robot's uniform straight motion represented translational reach motion of a healthy upper limb at relatively constant speed. The 180º turning motion represented healthy forearm pronation/supination rotational movement. It may be true that anatomical forearm pronation/supination maximal rotation does not achieve a full 180º (Anglin & Wyss, 2000b), however, given the elbow and shoulder are not constrained, the rotation of the distal forearm relative to the laboratory global coordinate system is approximately 180º. The robot oscillation represented jerkiness in upper limb movement for a stroke patient.

Sensor S1 was mounted on the top left corner of the robot (Figure 5.12) to measure its motion. The sensor was tracked by Vicon through four (9 mm diameter) passive reflective markers placed on it. Markers were labelled depending on attachment position (as specified in Table 5.3). Sensor mounting on the robot was such that the axes of (S) were defined as: x-axis along the longitudinal axis of the robot pointing backwards, y-axis along the lateral axis pointing to the right, and z-axis along the vertical axis positive upwards. The different robot actions (shown in Figure 5.11 from Vicon's orientation computation) were specified by controlling the input signal to the motors (i.e. the velocity).

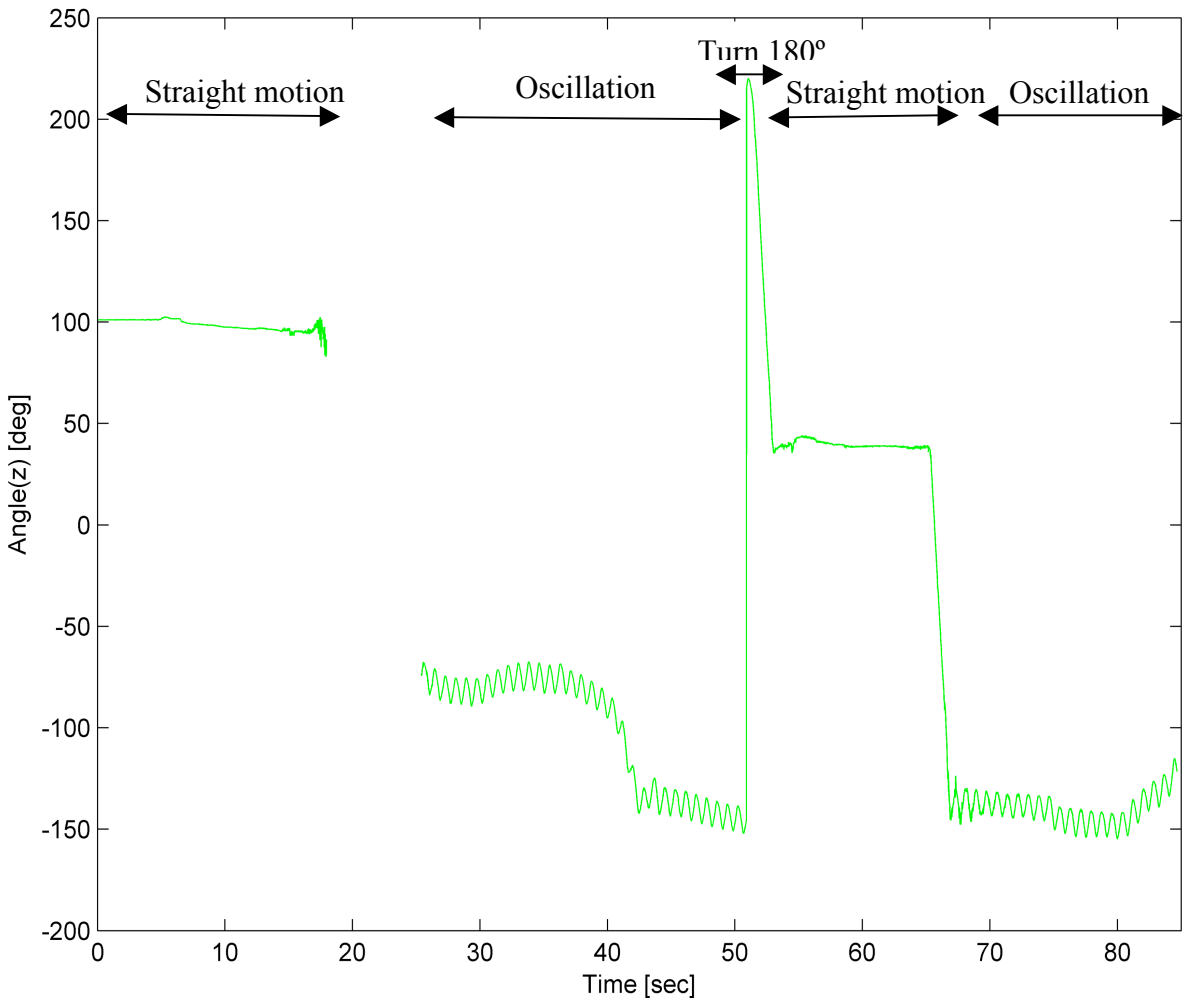

Figure 5.11 Robot actions presented from Vicon's orientation computation: one sequence was for robot to move straight, oscillate, turn 180 about the robot's vertical z axis, move straight again, then the same sequence was repeated

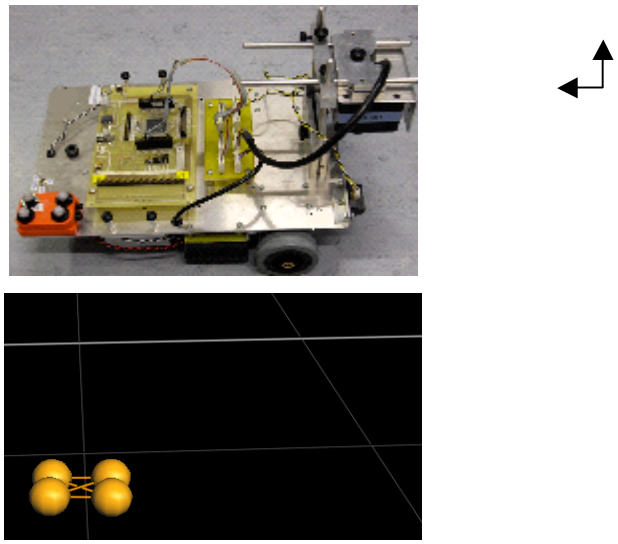

Figure 5.12 Set-up of the mobile robot with sensor S1; S1 tracked in Vicon using four markers

Table 5.3 Marker labels and positions on the robot

Marker	Description of Placement
FTLT	Front left
BKLT	Back left
FTRT	Front right
BKRT	Back right

Sensor orientation was computed in BodyBuilder software using markers mounted on the sensor, and angles output relative to (V). Transformation of sensor orientation from (V) to (G) was performed using ${}^{G}_{V}R$ (determined in section 5.2.1) and equation (5.3). Time synchronisation of the two systems' data was done manually by matching the point of movement initiation. Also, data analysis of the straight and oscillatory/turning movement sections was performed separately, due to a change in the frequency content of the motion data. Results for the robot angle made about the vertical z- and longitudinal x- axes for both straight and oscillatory/turning sections are given below, in Figure 5.13, Figure 5.15, Figure 5.19, and Figure 5.20 respectively.

$$ {}^{G}q = ({}^{G}_{V}R).{}^{V}q \text{, for a variable } q \qquad (5.3) $$

For the robot straight motion section, taking place along the longitudinal axis of the robot (which is the x-axis) in the time period 5.6 - 17 seconds, a slight rotation was observed about the vertical z-axis of about 4.5º by Vicon (green plot, Figure 5.13). This was possibly caused by differences between the two motors driving the robot. These changes in robot orientation about z were not seen to the same extent by the sensor S1 (red plot, Figure 5.13). Absolute sensor estimation of the z-component of robot orientation (yaw) was higher than that computed by Vicon, with a maximum angle difference over time of 2º. Evidence of a small amount of drift was suggested by Figure 5.14 which shows the data plots in Figure 5.13 detrended (with 0.16º root mean square (RMS) error after data detrending compared to 1.44º before). Data detrending removed the best straight-line fit

linear trend from the data (the “detrend” function was used in MATLAB). Given that computation of sensor orientation in Vicon was dependant on marker position data that do not drift, it was safe to conclude that this drift was due to the sensor gyroscopic measurements.

The robot oscillatory/turning motion sections took place in the time period 18.5 - 53 seconds. For the oscillatory part, there was a high correlation of 0.99 between Vicon computation and sensor estimation of the robot angle about the z-axis (green and red plots of Figure 5.15 respectively). At about 40 seconds, a larger oscillatory component was measured; this component was caused by the robot motion being obstructed by sensor S1 USB cable. The robot turning motion of 180º about the vertical axis, during the time period 51 - 53 seconds, led to a direction flip in (S), which S1 converted into a 360º overshoot in the orientation estimate. For comparison purposes, 360º were subtracted from the Vicon computation of sensor motion. Due to manual data synchronisation, a slight shift in time existed between the two plots, and was mainly evident from the 360º data overshoot at about 51 seconds.

The second sequence of robot motion started in the time period 53 – 85 seconds, which consisted of straight motion, turning and oscillating. During this sequence, the difference between the Vicon and Xsens plots was larger; probably owing to the sensor gyroscopes drifting over time. It should be noted that during the second turning in the time period 65 - 66.8 seconds, the robot slightly turned from its original longitudinal path due to differences between the two motors driving the robot. A similar data overshoot of 360º was not detected on this occasion.

Subtracting the two plots in Figure 5.15 gave the error in sensor S1 estimation of the robot angle about the vertical z-axis for the oscillatory/turning sections, shown in Figure 4.16. Both the error corresponding to the 360º data overshoot at about 51 seconds, and the linear increase in time of the sensor orientation error from 30 seconds onwards are clearly shown. The slight oscillations in sensor orientation error are likely to be from a phase offset in the orientation plots due to manual synchronisation of Vicon and sensor S1.

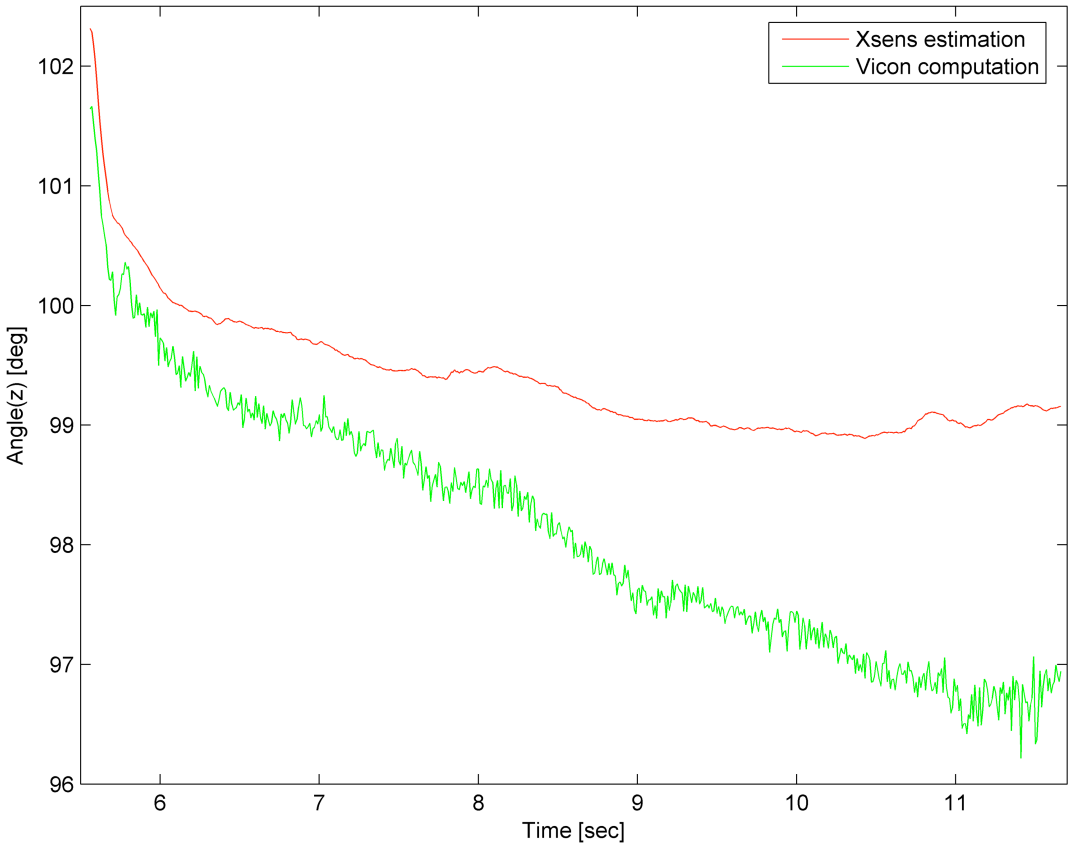

Figure 5.13 The robot angle about the vertical z-axis for the robot straight motion section: in green Vicon computation while in red sensor S1 estimation

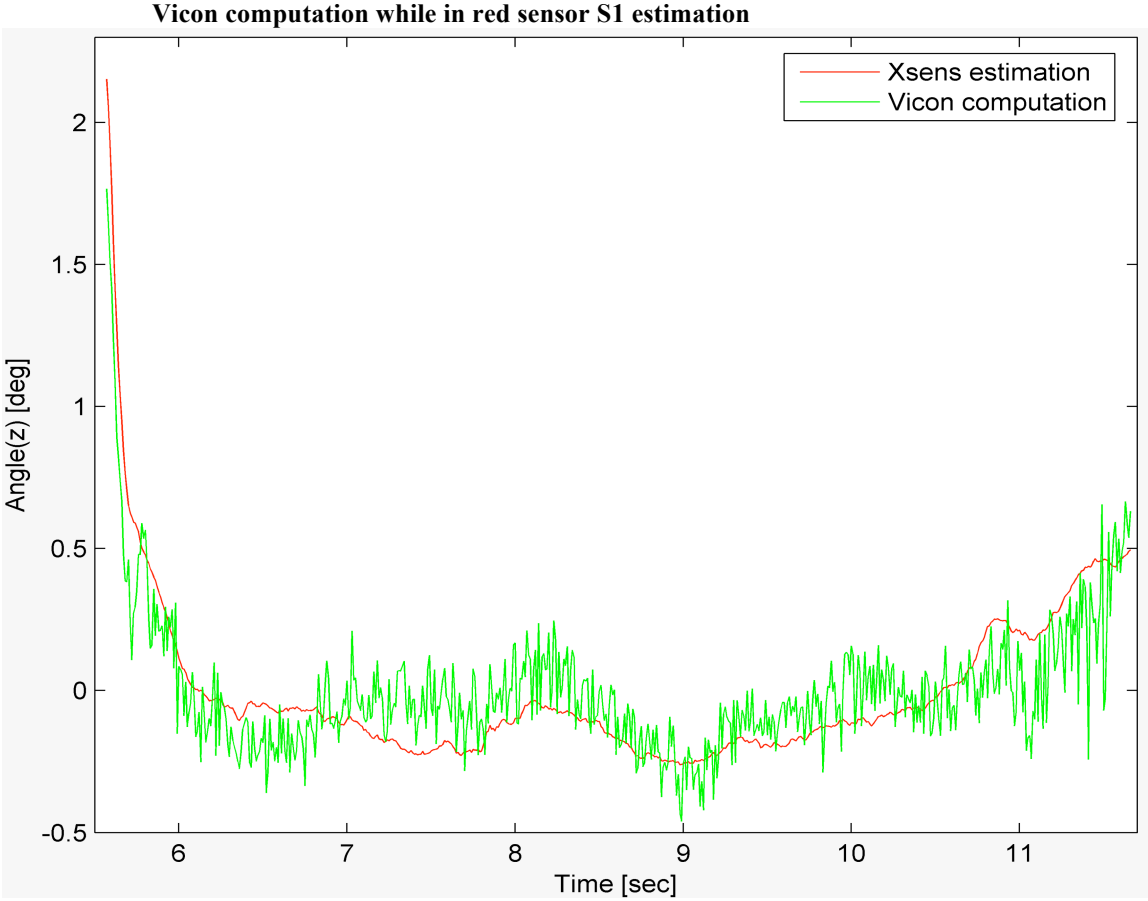

Figure 5.14 The robot angle about the vertical z-axis for the robot straight motion section after data detrending: in green Vicon computation while in red Xsens sensor S1 estimation

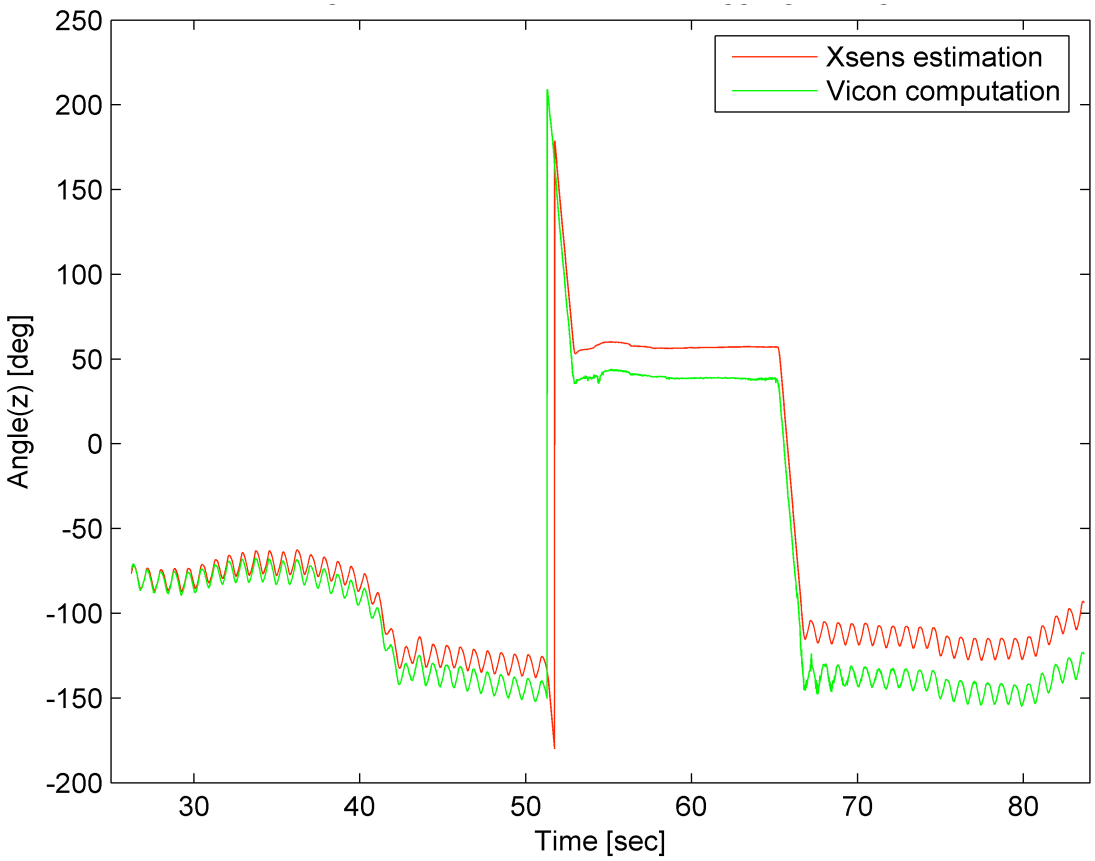

Figure 5.15 The robot angle about the vertical z-axis for the robot oscillatory/turning motion sections: in green Vicon computation while in red Xsens sensor estimation

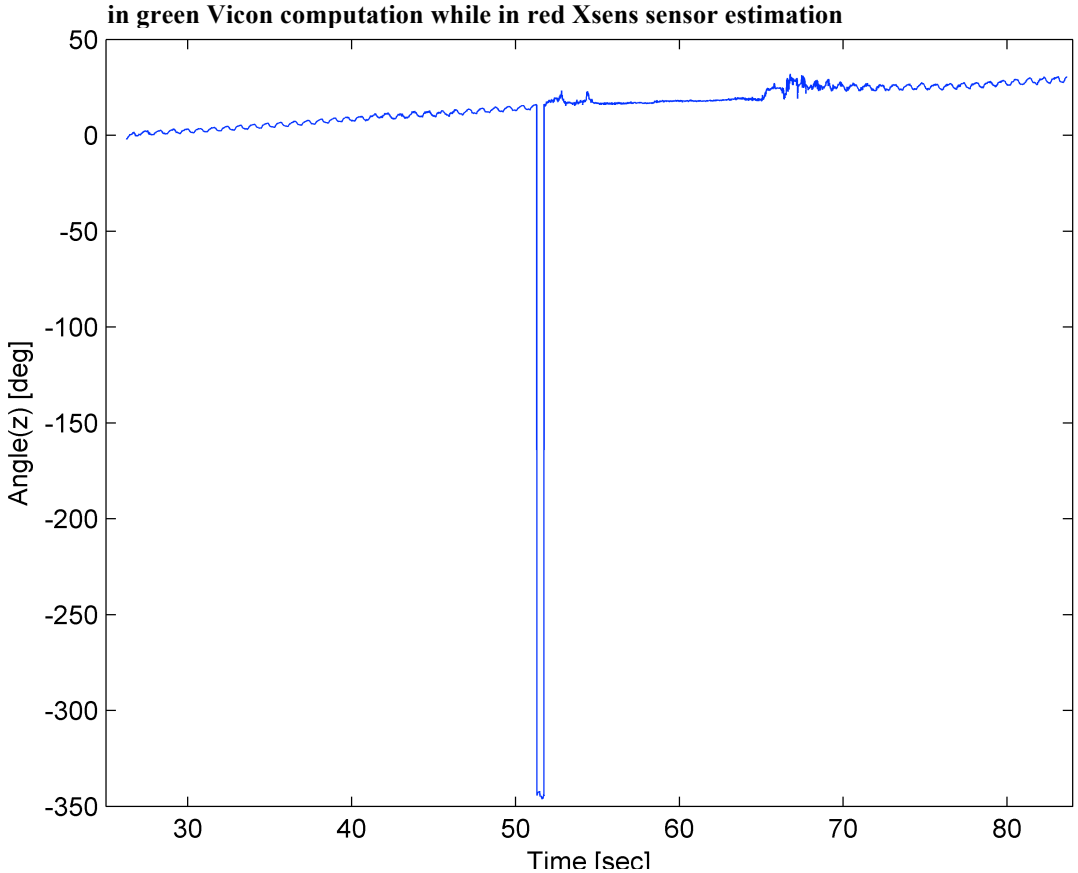

Figure 5.16 The error in sensor estimation in the robot angle about the vertical z-axis in the oscillatory/turning section

Removing the error corresponding to the 360º data overshoot (caused by manual data synchronisation of the Vicon and sensor systems), and linearly interpolating data in the time period 51 – 53 seconds, the plot in Figure 5.17 was obtained. A linear function (red plot, Figure 5.17) was fitted to the error in sensor data (blue plot, Figure 5.17). The slope of the error function was found to be 0.51º per second, and 0.035º per second after data detrending. This implies that sensor yaw (of robot motion) was mis-estimated due to an increasing drift, probably from the sensor gyroscopes. To check if this was the case, sensor gyroscopic measurements were compared to Vicon's computation of angular velocities of the sensor (obtained from first order differentiation of computed sensor orientation in Vicon). The z-components of angular velocities are shown in Figure 5.18. The RMS error of sensor gyroscope z was found to be 0.55º per second, almost equal to the slope of the fitted error function (0.51º per second). So, the linear error increase of sensor orientation was caused by a gyroscopic drift over time, but detrending the gyroscopic readings helped reduce this error.

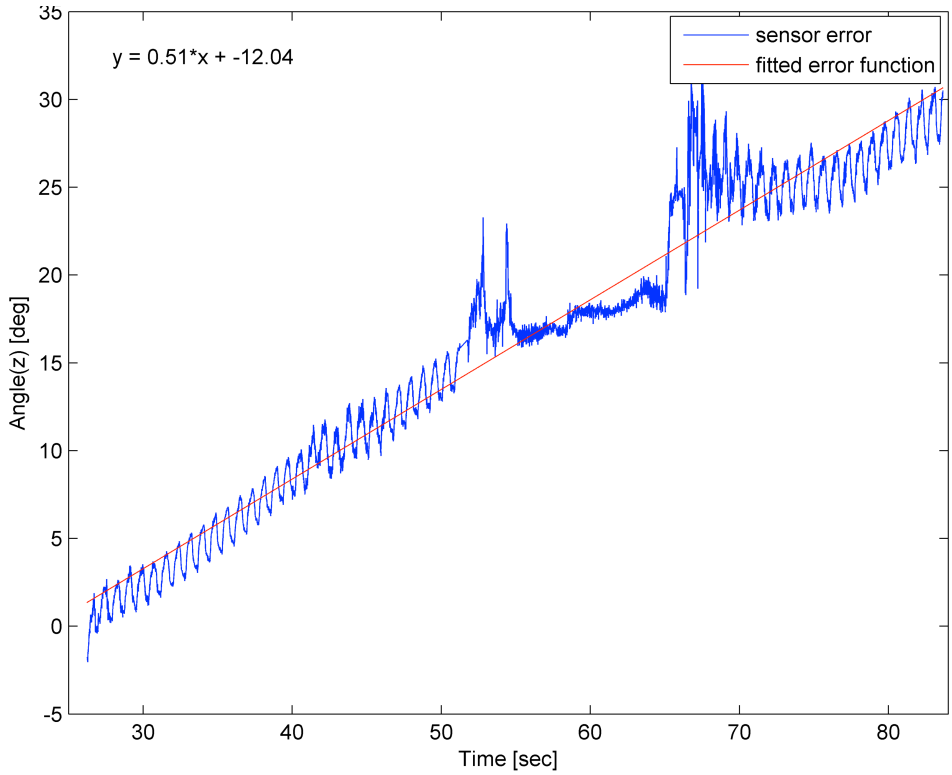

Figure 5.17 A linear increase of error in sensor estimation of the robot angle about the vertical z-axis in oscillatory/turning sections, fitted to a function of slope 0.51º/second.

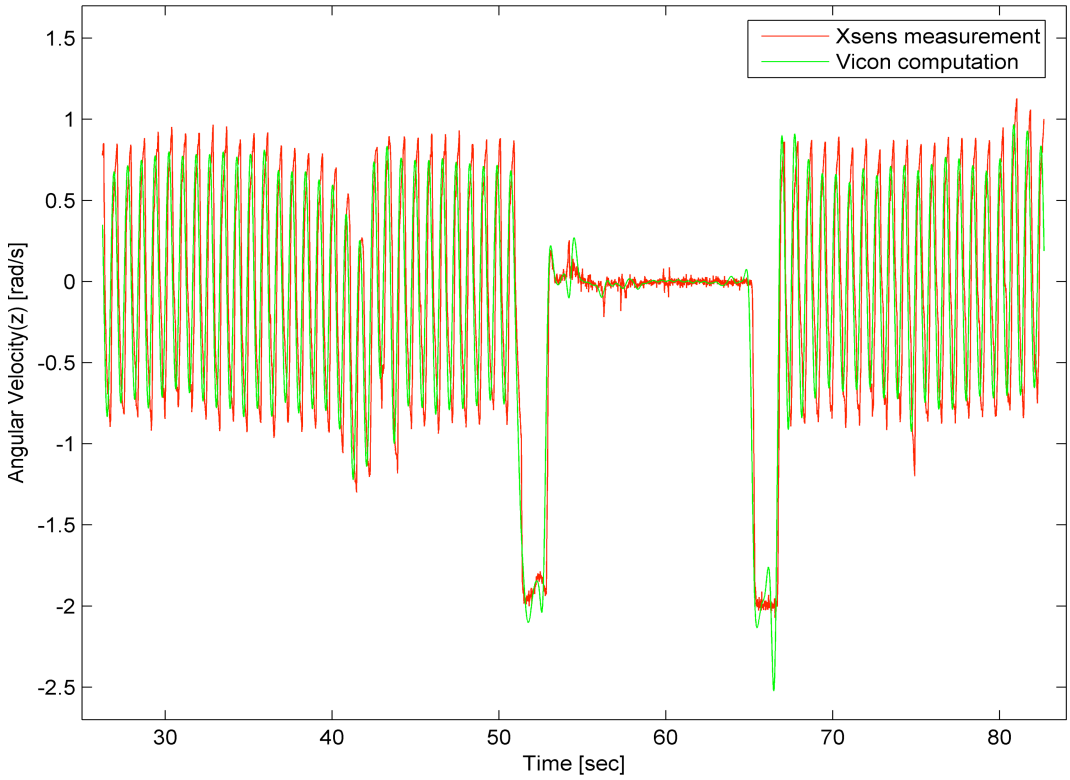

Figure 5.18 The robot angular velocity about the vertical z-axis for the robot oscillatory/turning sections: in green Vicon computation while in red Xsens sensor estimation

For the robot straight motion section, the robot rotation angle about the longitudinal x-axis was found to be very small (Figure 5.19). As a result, Vicon's computation of orientation suffered from high frequency "white" noise components (green plot, Figure 5.19). Bearing in mind the sensor's limited measurement bandwidth as compared to Vicon's, it was necessary to filter Vicon orientation data prior to comparison with the sensor's estimation of roll (red plot, Figure 5.19). Results of the digital infinite impulse response filter applied (of type Direct Form II), using MATLAB's "filter" function (Oppenheim & Schafer, 1989), are shown in blue (Figure 5.19). The correlation of orientation about x that was computed from Vicon (after digital filtering), and that estimated by the sensor (roll) was found to be satisfactory. Given Vicon's large measurement bandwidth, the need to smooth Vicon orientation data and attenuate high frequency noise components, questions whether Vicon really is a gold standard when it comes to measuring small movements as compared to the sensor and its limited bandwidth. Finally for completeness, results for the

oscillatory/turning sections of the robot rotation about the longitudinal axis were given in Figure 5.20 (with an RMS error of 2.52º).

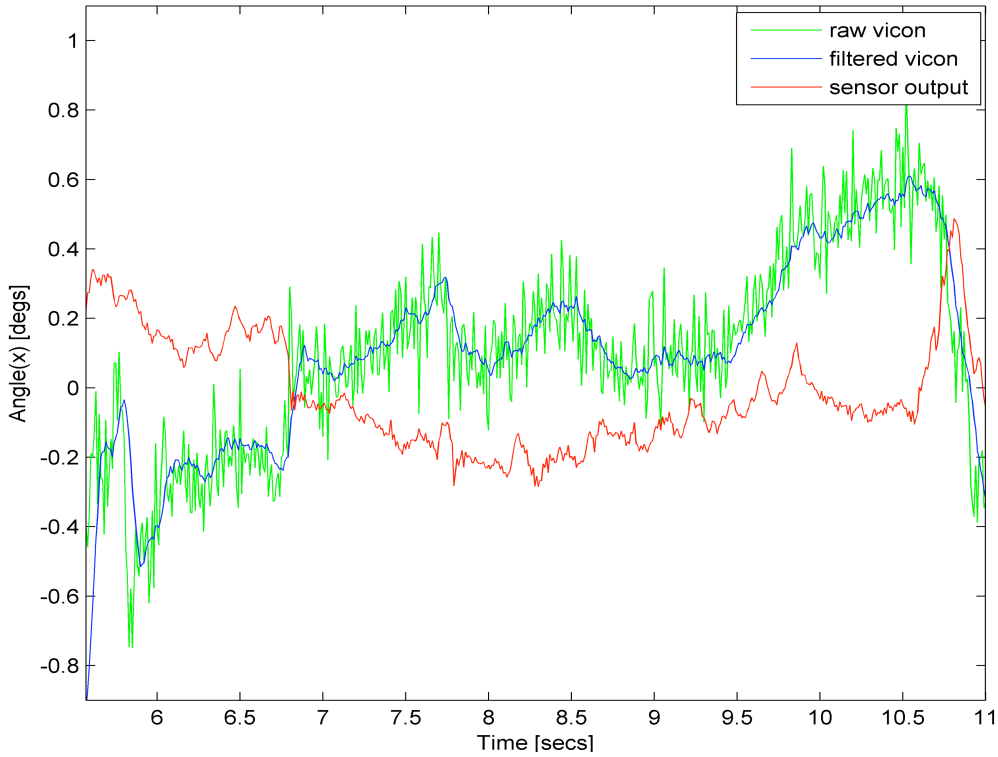

Figure 5.19 The robot angle about the longitudinal x-axis for the robot straight motion section: in green Vicon computation, in blue Vicon computation after digital filtering, and in red Xsens sensor estimation

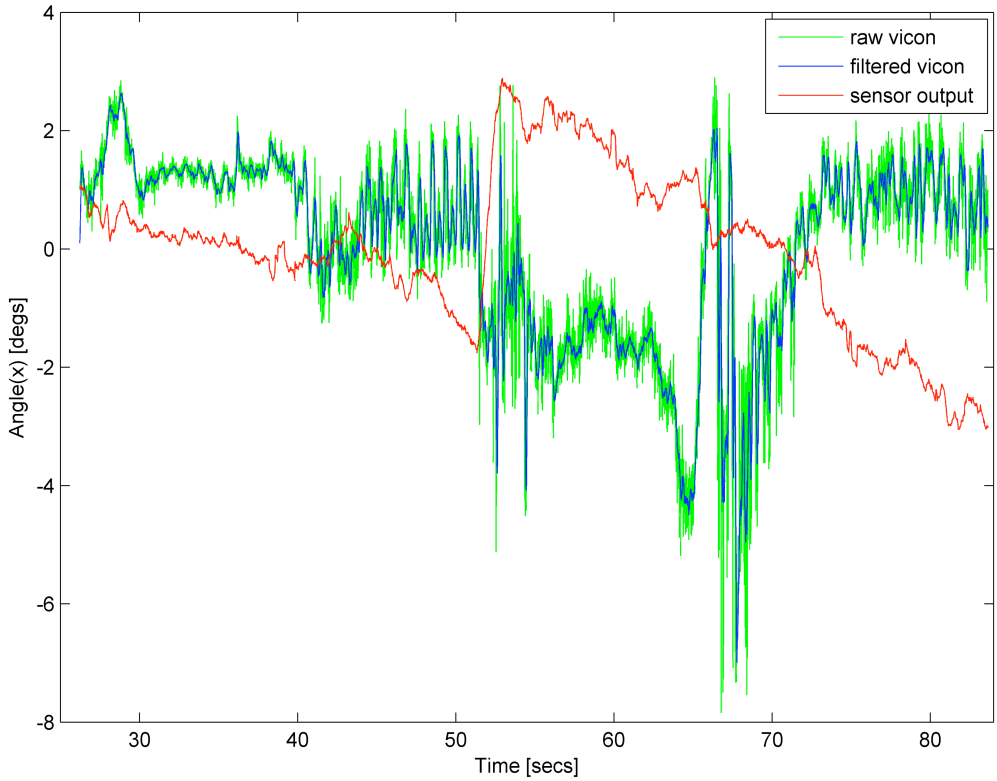

Figure 5.20 The robot angle about the longitudinal x-axis for the robot oscillatory/turning motion sections: in green Vicon computation, in blue Vicon computation after digital filtering, and in red Xsens sensor estimation

5.4 Experiment 2: A rotating bar to evaluate sensor gyroscopic readings

Sensor measurement accuracy varies with the motion regime it measures (Honeywell, 2010, Kavanagh & Menz, 2008). Previous results in sections 5.2 and 5.3 assessed the global sensor estimations of orientation (roll, pitch, yaw) over a general motion regime. In this section, the local sensor gyroscopic readings were assessed, and their task-specific dynamic measurement accuracy was determined for the chosen upper limb movements (reach-and-grasp and forearm pronation/supination), with motion regimes pre-determined in section 4.4.2.1. Table 5.4 summarises the relevant experiment parameters; which are the maximum absolute value of angular velocity, and the overall minimum and maximum absolute linear velocity required.

Three Xsens sensors (S2, S3 and S4) were attached to a 48 cm diameter bar that rotated in the horizontal x-y plane about the vertical z-axis, due to a small motor attached at the centre, whose output was controlled by a function generator (see Figure 5.21). Desired angular velocity information (from Table 5.4) determined the rate of turn of the rotating bar, hence the voltage control signal from the function generator to the motor. Sensor placement was determined from the relationship between linear and angular velocity for circular motion described in equation (5.4).

$$v = r.\omega \tag{5.4}$$

where v is linear velocity measured at a location r from the centre of an object rotating at angular velocity ω.

Sensor attachment positions (Table 5.4) were calculated based on required values of angular velocity and ranges of linear velocity for the reach-and-grasp and forearm

pronation/supination movements (from section 4.4.2.1). Three distinct positions for sensor attachment were identified to represent the two movements; these were at 0, 3 and 26 centimeters away from the bar's centre of rotation. It should be noted that due to the physical dimensions of the bar (of length 48 cm), the third sensor had to be placed 24 centimeters away from the bar centre instead of the computed 26 cm. The three sensors (S2, S3 and S4) were placed respectively in an outward direction from the bar's centre.

From the above calculation of sensor attachment positions, data from S3 and S4 represented measurement ranges for reach-and-grasp, while data from S2 and S3 represented forearm pronation/supination (Table 5.4). The whole setup was mounted on the gait laboratory floor with the force plates turned off. The five individual markers attached on the other arm of the rotating bar were not used as part of this study.

Table 5.4 Determining Xsens sensor placement based on motion analysis of forearm reach-and-grasp and pronation/supination movements summarised in section 4.4.2.1 (sensors S2, S3 and S4)

		Reach-and-Grasp	**Forearm Pronation/ Supination**
Max absolute of angular velocity (main component) [rad/s]		2.197	9.023
Velocity [m/s]	**overall min**	0.068	0.00001
	overall max	0.589	0.254
Computed sensor location [cm]	**min**	3.108 (sensor S3)	0.0001 (sensor S2)
	max	26.846 (sensor S4)	2.812 (sensor S3)

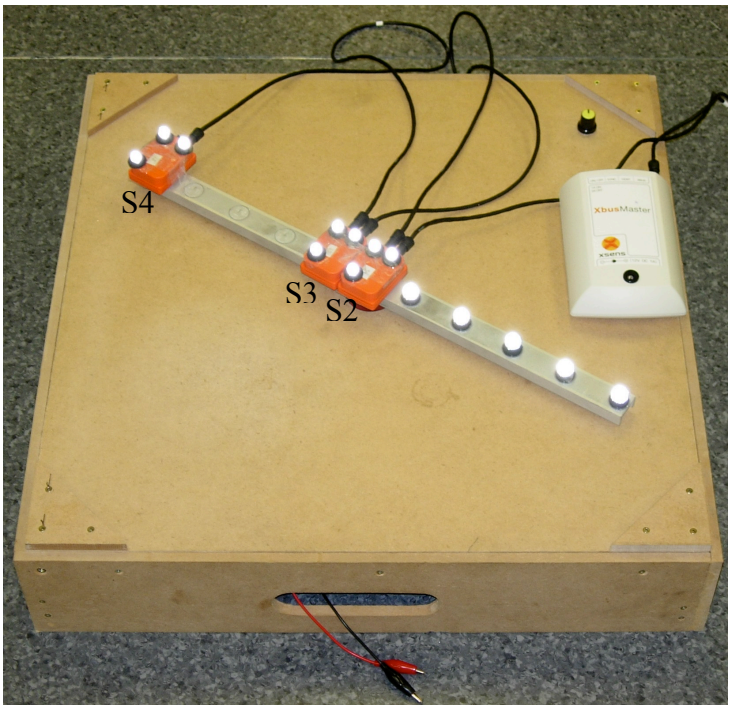

Figure 5.21 Experiment setup: the rotating bar, Xsens sensors and Xbus Master

The requirement of turn rates of 2.19 and 9.02 rad/s for the rotating bar (to respectively represent forearm reach-and-grasp and pronation/supination movements) corresponded to 20.913 and 86.135 rpm (revolutions per minute). The motor required a 15.9 Volt control signal to generate 132 rpm. So to obtain the desired rpm, the function generator control signal was set to 2.5 Volt for reach-and-grasp and 10.4 Volt for forearm pronation/supination.

The motor rpm output was checked for both cases using a tachometer. Also, velocity was obtained from first order differentiation of Vicon position data of markers placed on the sensors. This confirmed for both motor settings, that suitable ranges of velocity were generated (as indicated in Table 5.4). Following this, sensor data acquisition began using both the sensors and the Vicon system.

To validate the gyroscopic measurements (specifically the z component of rotation), linear velocity was computed from gyroscopic measurements at a given point using equation (5.4). These computations were compared to first order differentiation of Vicon marker position data at the same point. As angular velocity sensor measurements in the z direction were made about the centre of gyroscope-z, the physical location of gyroscope-z centre needed to be determined.

Figure 5.22 and Figure 5.23 were provided courtesy of Xsens Motion Technologies. Relative to the centre of the red dot (Figure 5.22; one of the sensor screw holes), physical locations of the three dimensional gyroscopic centres are given in Figure 5.23. The centre of gyroscope-z is located at a point (9, 18.5, 10.5) mm so is at a distance of 23.09 mm from the red dot.

The figure originally placed here has been removed for copyright reasons.

Figure 5.22 Reference point for locating the centres of sensor three dimensional gyroscopes Courtesy of (Xsens Technologies, 2010)

The figure originally placed here has been removed for copyright reasons.

Figure 5.23 Plan view of an Xsens sensor with locations of 3-D gyroscopic centres relative to the red dot reference (specified in Figure 5.22).
Courtesy of (Xsens Technologies, 2010)

The three markers attached at the edges on each of the three sensor units from Figure 5.21, are shown in orange in Figure 5.24. Markers were labelled 1, 2, and 3 with the sensor unit number as prefix. Marker labels for sensor S2 are shown in Figure 5.24; the same marker labelling was used for the other two sensors, S3 and S4. Marker attachment positions (given as 1, 2, 3 orange squares) in relation to the physical location of the centre of gyroscope-z (given as green square 'A') are shown in Figure 5.25.

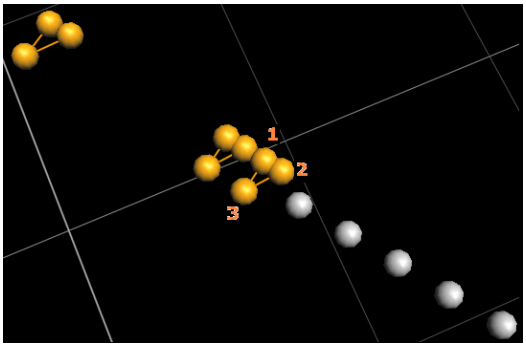

Figure 5.24 Marker labels for sensor S2. The same marker labelling was used across sensor units S3 and S4

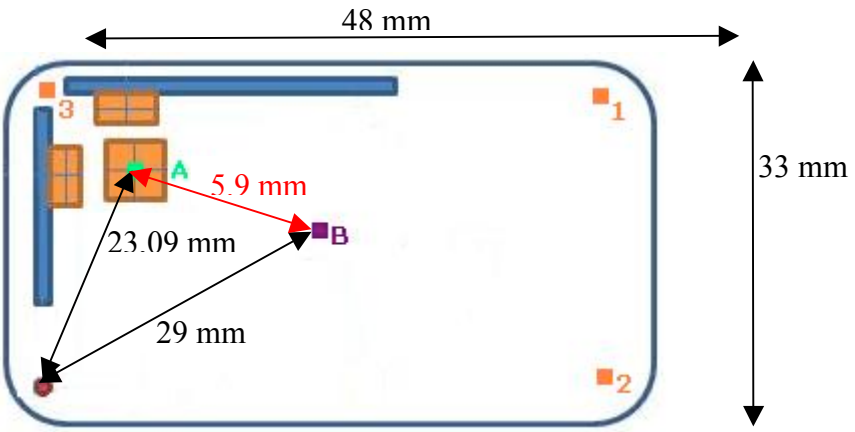

Figure 5.25 Markers' attachment positions (as 1, 2, 3 orange squares) shown in relation to the physical location of centre of gyroscope-z (as green square 'A') for one sensor unit. Also shown is the midpoint of the vector joining markers 2 and 3 (as violet square 'B')

Linear velocity of the sensor may be calculated using equation (5.4) at the exact centre of gyroscope-z (labelled as green square 'A' in Figure 5.25) where angular velocity is measured due to sensor rotation about the centre of the rotating bar. As the exact location of A was not marked in Vicon, an approximation was to find the midpoint of the vector joining markers 2 and 3, (labelled as violet square 'B' in Figure 5.25). Since the distance from A to B was very small (5.9 mm), r_{AB} was set to zero, relative linear velocity at B with respect to A was zero, and linear velocity at B and A were assumed equal (equation (5.5).

$$v_B = v_A + \omega . r_{AB} \tag{5.5}$$

So the midpoints of the vectors joining markers 2 and 3 for the three sensors were computed; shown as white dots in Figure 5.26. Sensor gyroscopic accuracy at low and high angular velocities was determined by comparing linear velocity computations at these midpoints obtained from the sensor gyroscopic measurements, to the first order differentiation of midpoint marker position data from Vicon. The midpoint of S2, attached to the midpoint of the rotating bar, was assumed to be the centre of the rotating bar. Distances from the midpoints of S3 and S4 were determined relative to midpoint of S2, as in Figure 5.26.

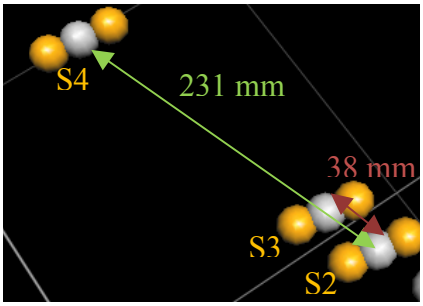

Figure 5.26 Mid-point calculation of vectors joining markers 2 and 3 for three sensors shown as white dots

For measuring low angular velocities (for the reach and grasp movement) and for a setting of minimum and maximum values of linear velocity (0.068 and 0.589 m/s respectively from Table 5.4), linear velocity was computed from the gyroscopic measurements of S3 and S4, and are shown in blue in Figure 5.27 and Figure 5.28 respectively. Velocity computations from Vicon (after filtering the position marker data with the (Woltring, 1995) routine) are also shown in red (Figure 5.27 and Figure 5.28); their values were comparable to the linear velocity settings (values achieved within 0.002 and 0.15 m/s respectively). After comparing the linear velocity computations from the two systems, at both settings of minimum and maximum linear velocities, the dynamic measurement accuracy of sensor gyroscope-z was found high for measuring low angular velocities, with RMS errors of 0.0095 and 0.0695 m/s at the minimum and maximum settings of linear velocity respectively. The difference between the red and blue plots in Figure 5.27 might appear larger than that in Figure 5.28 but this is due to different scaling used.

For measuring high angular velocities (for the forearm pronation/supination movement) and for a setting of maximum linear velocity (0.254 m/s from Table 4.9), linear velocity was computed at S3 and compared to velocity computed in Vicon. The maximum linear velocity setting was achieved to 0.096 m/s, with an RMS error of 0.038 m/s for gyroscope-z at this angular velocity.

Results for a setting of minimum linear velocity computed at S2 were not shown as these would be zero, bearing in mind that the sensor's midpoint (attached at the centre of the rotating bar) was taken as the centre of bar rotation. But angular velocity measured by S2 was found to be close to that measured by S3, with a steady-state value of about 8.5 rad/s. The linear velocity at S4 was also computed with the corresponding velocity computation in Vicon. No filtering was applied to the Vicon data as minimal high frequency signal content was present, and the root-mean-square error was found to be 0.347 m/s.

Reach-and-grasp low angular velocity = 2.197 rad/s	**RMS error [m/s]**
at minimum velocity = 0.068 m/s	0.0095
at maximum velocity = 0.589 m/s	0.0695

Forearm pronation/supination high angular velocity = 9.023 rad/s	**RMS error [m/s]**
at minimum velocity = 0.00001 m/s	-
at maximum velocity = 0.254 m/s	0.038
at maximum velocity >> 0.254 m/s (= 2.084 m/s)	0.347

The sources of error in this experiment included the sensors' vibrations relative to the rotating bar, computation of the radius distance (as measured by Vicon), and determination of the centre of rotation for the rotating bar, in addition to differentiation errors when computing velocity from Vicon. In spite of these errors, the dynamic measurement accuracy (task-specific) of sensor gyroscope-z was found to be high, for measuring low and high angular velocities (RMS errors were between 0.0095 and 0.0695 m/s for the low turn rate, and 0.038 m/s for the high turn rate). As the manufacturer reported accuracy for gyroscopes-x and -y to be similar to -z, the gyroscopes were deemed accurate enough to

measure turn rate for both reach-and-grasp and forearm pronation/supination movements. In principle, it is possible to re-orient and re-mount the sensors to check the -x and -y components.

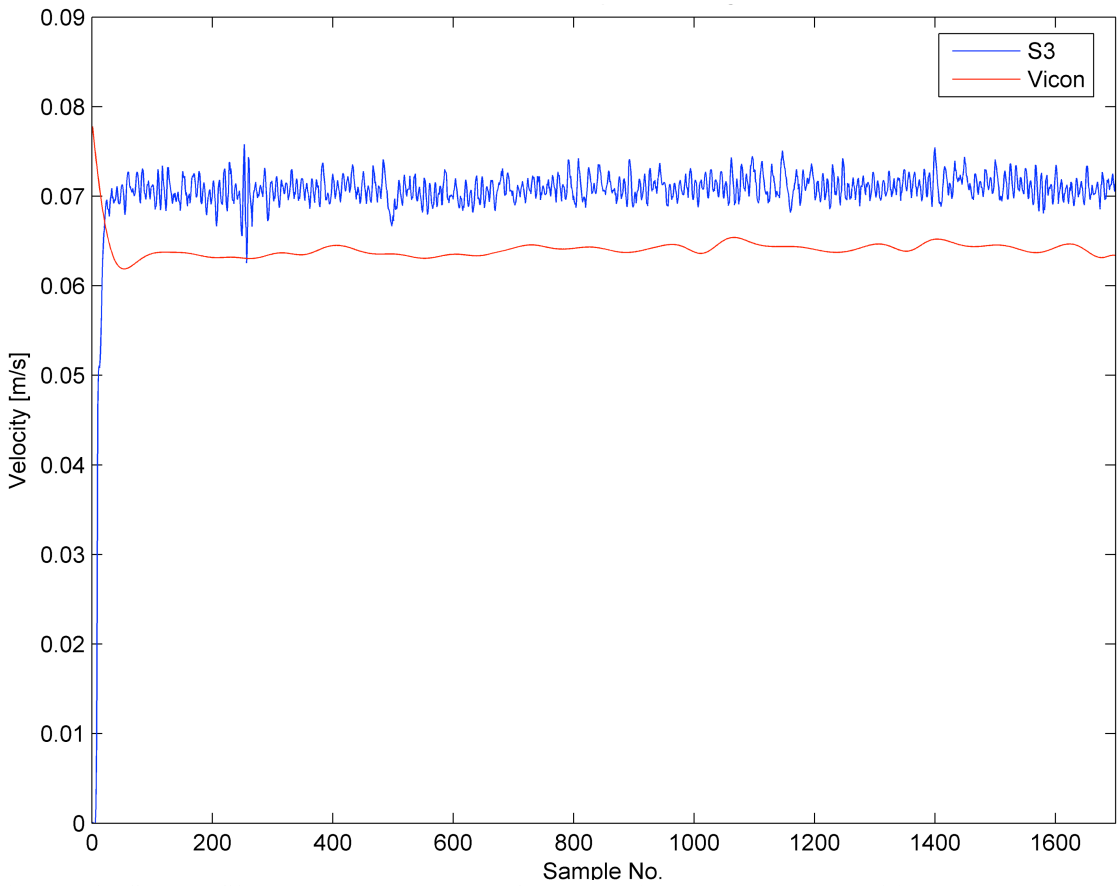

Figure 5.27 Sensor (S3) gyroscope-z accuracy for measuring low angular velocities (reach-and-grasp) for a setting of minimum linear velocity

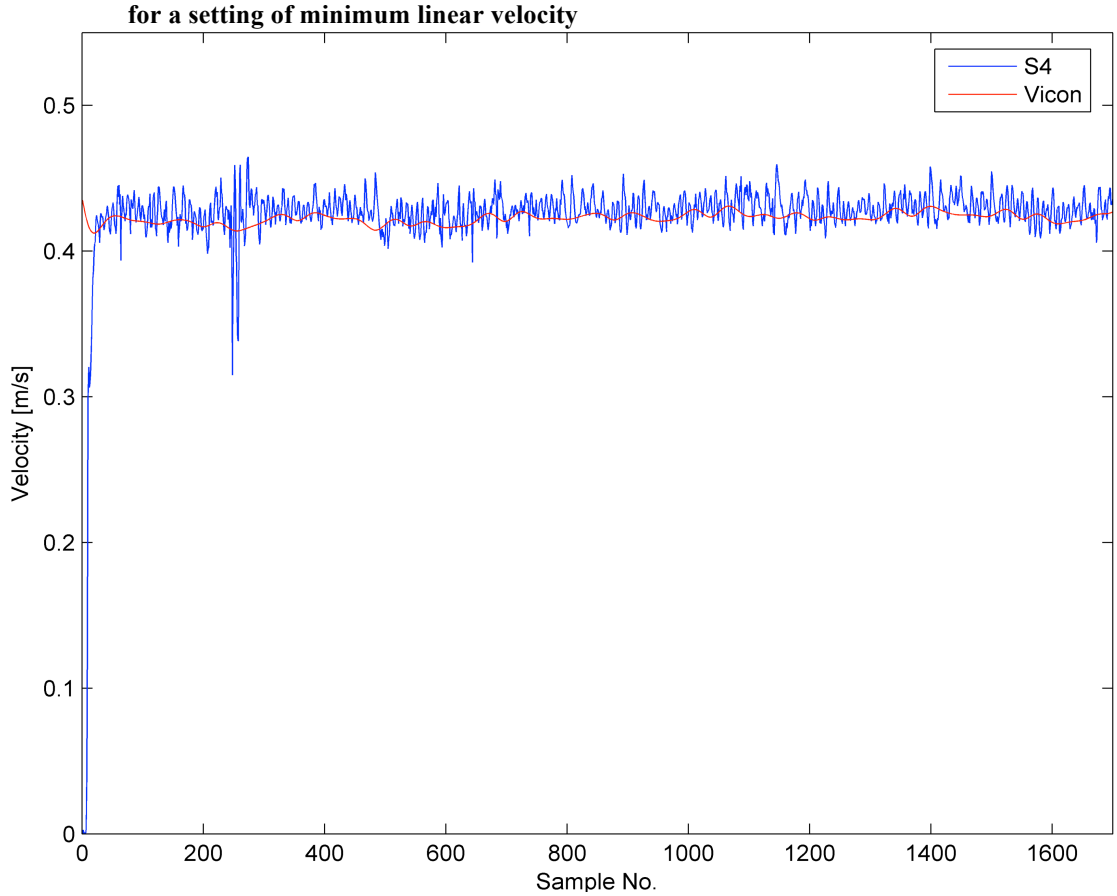

Figure 5.28 Sensor (S4) gyroscope-z accuracy for measuring low angular velocities (reach-and-grasp) for a setting of maximum linear velocity

Internal sensor consistency of accelerometers and gyroscopes:

Centripetal accelerations were computed from the gyroscopic measurements along z using equation (5.6).

$$a = \omega^2 . r \tag{5.6}$$

These accelerations were compared to acceleration measurements along the centripetal direction (the y axis) as measured by the sensor accelerometer-y. Results for S1 placed at the tip of the rotating bar (radius 240 mm) are given in Figure 5.29. From the plots, the sensor accelerometer-y and gyroscope-z took about 1 second to reach the steady state. If either accelerometers or gyroscopes were to be used clinically, this settling time should be considered. The sensor internal consistency was found to be high with an RMS error of 0.24 m/s^2. The 5 m/s^2 maximum peak-to-peak deviation in acceleration was due to a 1.4 rad/s maximum angular velocity peak-to-peak deviations measured by the gyroscope-z. This probably was actual vibrations in the rotating bar that the sensor measured, given its placement at the tip of the bar, or the motor velocity was not constant.

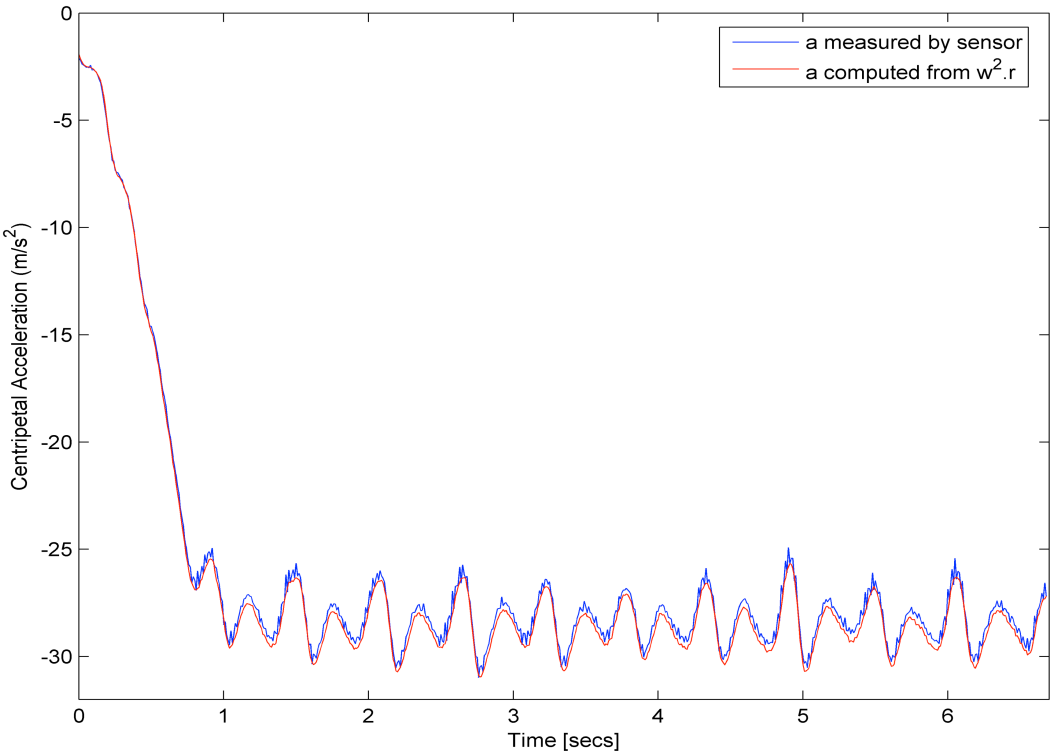

Figure 5.29 Sensor internal consistency of the accelerometers and gyroscopes

5.5 Experiment 3: Sensor accelerometer accuracy from a simulated "reach" movement of a mobile robot

The final sensor component whose accuracy was to be determined was the accelerometers. In this experiment, the sensor S1 measured simulated motion of the mobile robot (used in section 5.3) programmed to mimic a healthy reach-and-grasp movement (as established in section 4.4.2.1). It was not possible to programme the robot to mimic, along the longitudinal direction, a sinusoidal motion of comparable acceleration to a typical healthy reach-and-grasp movement, but the predominant acceleration during the periodic linear motion was found to be comparable (see Figure 5.31). The dynamic baseline sensor accuracy for measuring accelerations and obtaining velocity from accelerometer readings could then be established, for monitoring healthy upper limb movement, in the absence of skin motion artefacts and with an ideal (vertical) setting of initial sensor mounting.

Both S1 and the robot were tracked with the Vicon system using four and three (9 mm diameter) markers respectively (Figure 5.30), to compare the accuracy of the sensor to the Vicon system. Comparing the sensor and robot motion in Vicon allowed the appropriateness of the sensor attachment method (double sided tape) to be determined. Sensor and robot marker labels and positions are indicated in Table 5.5.

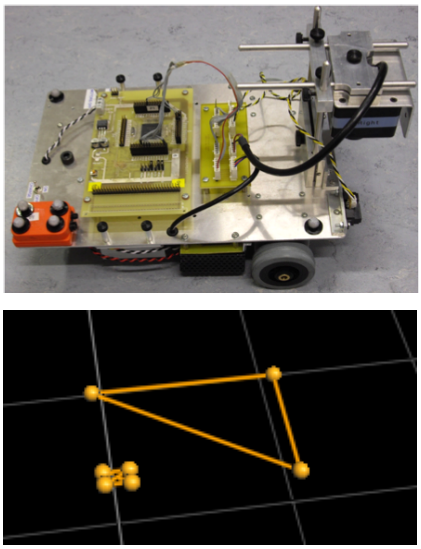

Figure 5.30 Mobile robot with inertial sensor S1: setup and both as tracked in Vicon

Table 5.5 Marker labels and positions on the robot and sensor

Marker	Description of Placement
FTLT	Sensor – Front left
BKLT	Sensor – Back left
FTRT	Sensor – Front right
BKRT	Sensor – Back right
RBT1	Robot – Back left
RBT2	Robot – Back right
RBT3	Robot – Front right

Figure 5.31 shows for three movement cycles a comparison of the velocity profiles of the robot simulated movement (in blue) and the reach-and-grasp movement of a typical healthy upper limb (in red). The robot velocity was computed in Vicon from first order differentiation of RBT3 (in Table 5.5) marker position data (which was found to have the least noise compared to RBT1 and RBT2). The reach-and-grasp movement of the healthy subject (Subject 2) was similarly obtained from the wrist marker LWRB (refer to marker label and position in section 4.2.3). With acceleration being a first order derivative of velocity, comparing the slopes of both velocity plots in Figure 5.31, as at the marked regions (at about samples 10 and 560), shows that the motion regimes for acceleration were comparable for the simulated robot movement and the reach-and-grasp movement of a typical healthy subject (as in section 4.4.2.1; with a maximum acceleration of about 1 m/s^2).

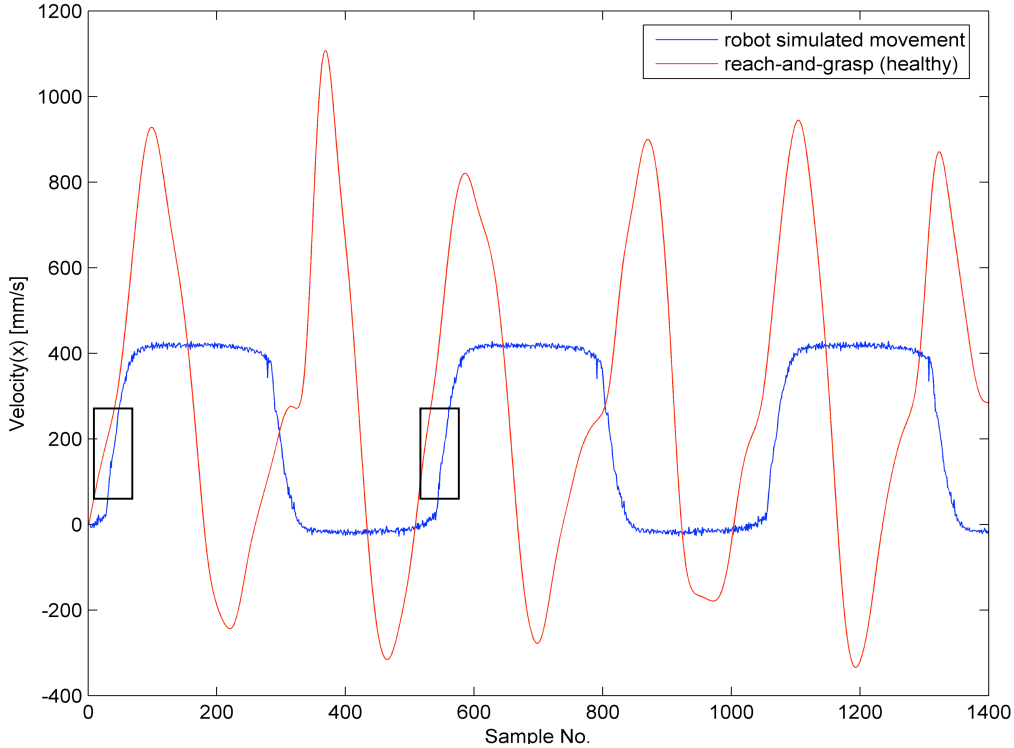

Figure 5.31 The simulated motion of a robot compared to the reach-and-grasp movement of a healthy upper limb (the rectangles at about samples 10 and 560 represent the marked regions)

To determine the dynamic baseline accuracy of the sensor accelerometers, in the motion regimes of healthy reach-and-grasp movement (identified from the peak-to-peak measurement of Vicon), Vicon computations were compared to sensor acceleration. Comparison was done for the main translational component of the robot's simulated movement (along the longitudinal x-axis of the robot). Vicon's computation of linear velocity and acceleration of sensor motion were obtained from the sensor marker BKLT (see Table 5.5). Acceleration was readily available as output from the sensor while linear velocity was computed from integration of accelerometer measurements. As the accelerometer data (Figure 5.32) were slightly biased due to gravity, the velocity estimation suffered some integration drift (Figure 5.34). Therefore the accelerometer data were high-pass filtered (using a median filter of order 17, necessary to attenuate the high-frequency noise) and detrended (to remove gravity offsets), as shown in Figure 5.33, and prior to integration. This resulted in a reduction of the drift in the velocity estimation (Figure 5.35). Results of the data analysis are summarised in Table 5.6, with the mean

error reported as the difference between the sensor measurement and Vicon's computation across the repeated simulated motion. The raw sensor data (with no pre-processing) was initially compared to Vicon's computation; this was repeated after some pre-processing (high pass filtering and detrending).

Table 5.6 Difference between sensor acceleration and Vicon computation of acceleration (mean error) for the mobile robot motion comparable to that of the reach-and-grasp movement of a healthy subject (d.f. = detrended and high pass filtered)

	Peak-to-peak (from Vicon)	Mean error (measure of bias or drift)		RMS error	
		raw	d.f.	raw	d.f.
Velocity (x) [m/s]	0.434	-0.078	-0.009	0.117	**0.054**
Acceleration (x) [m/s^2]	1.967	-0.0059	0.006	0.352	**0.127**

The sensor accelerometer data along x were slightly biased by the x-component of gravity (mean error of -0.0059 m/s^2), hence velocity suffered slight integration drift (-0.078 m/s). Applying the pre-processing to the sensor data reduced the gravity offset and the drift, and improved the RMS errors of acceleration and velocity to 0.127 m/s^2 and 0.054 m/s respectively. Experimenting with the robot, it was found that the minimum movement acceleration to obtain usable sensor accelerometer output should be larger than 0.5 m/s^2, to be able to correct the bias satisfactorily.

Source of error: Sensor attachment

In terms of the appropriateness of the sensor attachment method on the robot (using double sided tape), marker motion data for the sensor and the robot in Vicon were compared (for position, velocity and acceleration). A close relationship was found for the longitudinal, lateral, and vertical components of the movement. This meant that the sensor was well attached to the robot using double sided tape; its appropriateness to mount sensors on the forearm should be investigated. The vertical component for sensor velocity and acceleration did have slightly more noise than that of the robot. This could have been due

to the vertical component of sensor motion being small (with the movement being predominantly along the longitudinal axis), so sensor motion artefacts appeared more obvious when compared to this component.

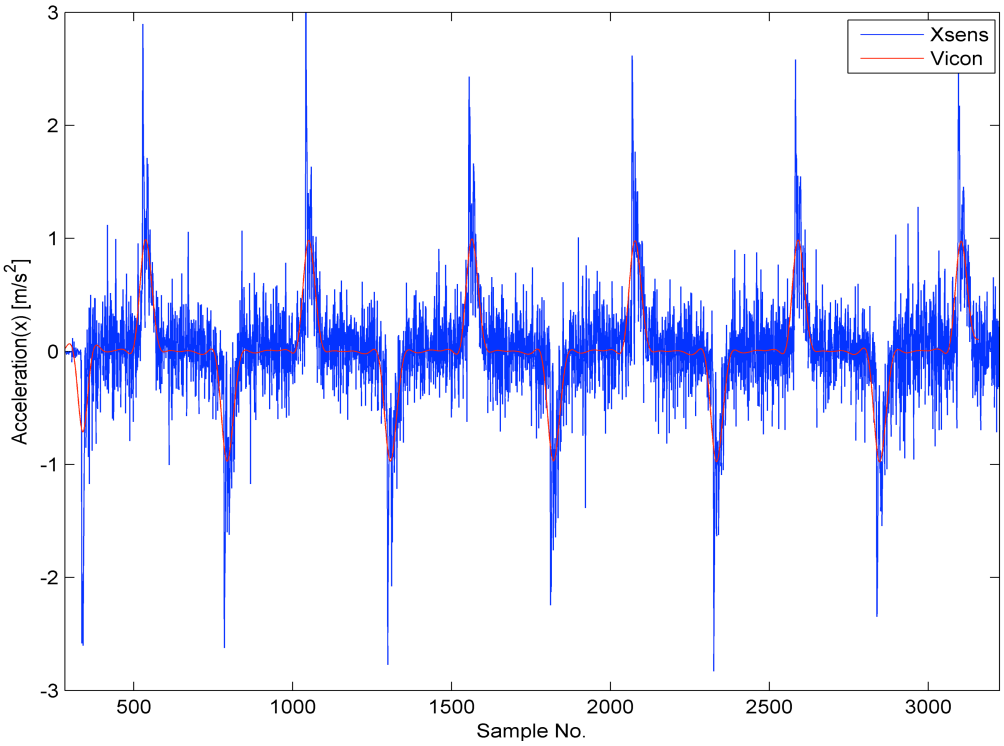

Figure 5.32 Sensor raw acceleration measurement (in blue) compared to Vicon's computation (in red) of the robot simulated motion

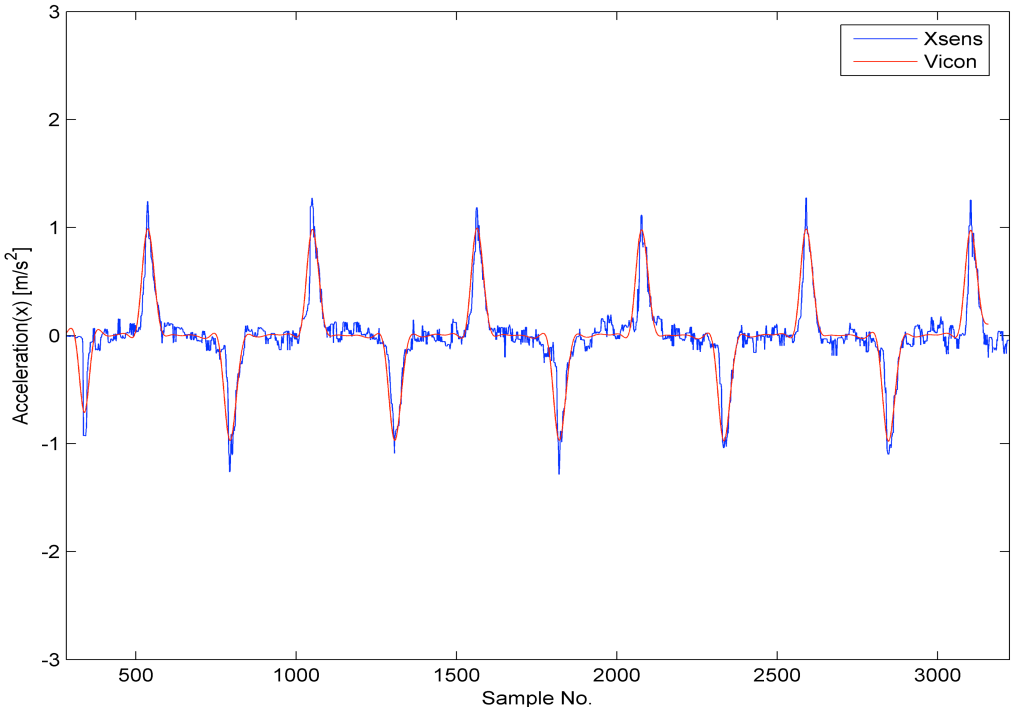

Figure 5.33 Sensor acceleration measurement after detrending and high-pass filtering (in blue), compared to Vicon's computation (in red) of the robot simulated motion

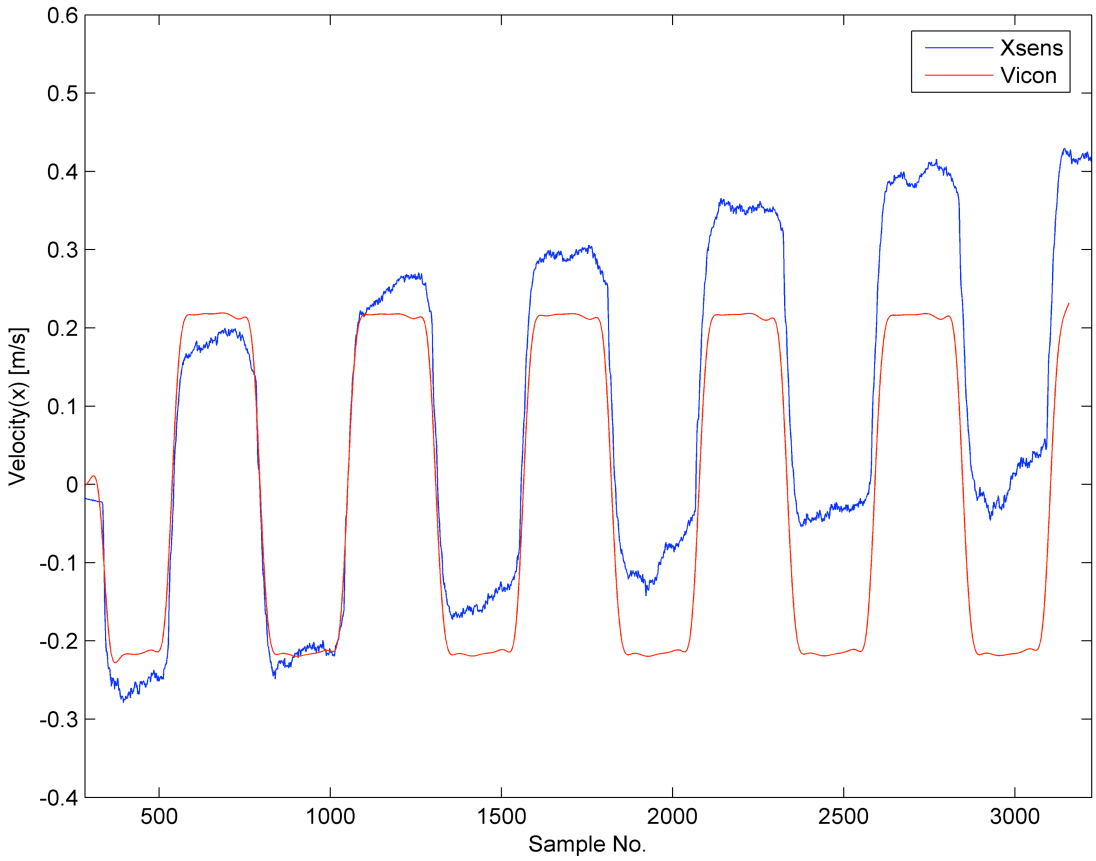

Figure 5.34 Velocity from integration of raw sensor accelerations (in blue) compared to Vicon's computation (in red) of the robot simulated motion

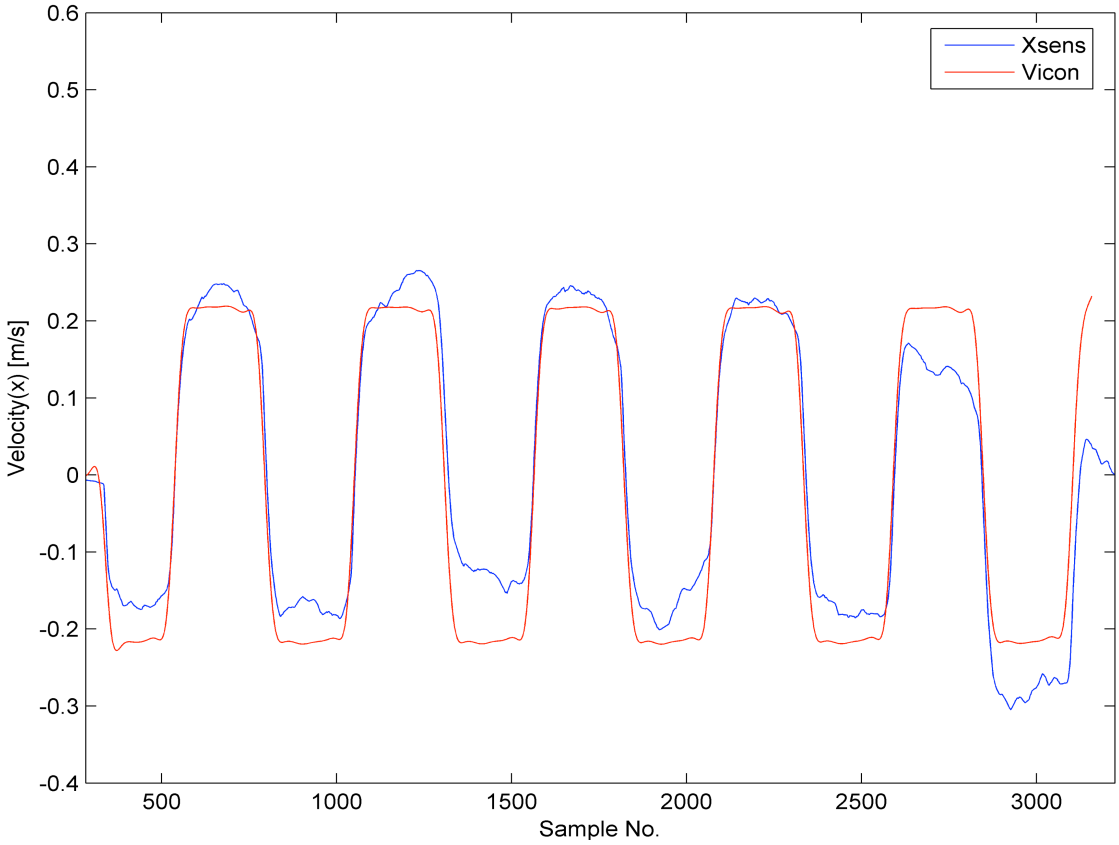

Figure 5.35 Velocity from integration of detrended and high pass filtered sensor accelerations (in blue) compared to Vicon's computation (in red) of the robot simulated motion

5.6 Experiment 4: Testing the performance of sensors on motion data of a stroke patient

5.6.1 Pre-stroke data (Accuracy testing)

Performance of the sensors was investigated on motion data of a stroke patient to see whether the sensors were suitable to measure and monitor jerky, uncontrolled movement (details on subject preparation and movements performed are provided in sections 4.2.3 and 4.2.6). Motion data was collected on two separate occasions from the patient, to measure change in movement following daily home exercise with personalised rehabilitative technology. The two data collection sessions are later referred to as pre- and post- stroke intervention, which were separated by a month.

Data from sensor S4 mounted on the distal forearm (near the wrist joint; Figure 4.9) were compared to Vicon computation of the sensor being tracked using three (9 mm diameter) markers placed on it. Quantities compared were linear velocity, acceleration, angular velocity and orientation (roll, pitch, yaw). The sensor measured linear accelerations and angular velocities in three dimensions, as well as estimated three dimensional orientations. To assess each sensor component measuring data along one dimension against Vicon, vector components of a given quantity were compared rather than absolute magnitudes. As the patient could not perform a full range forearm pronation/supination, the task was modified to hand-to-mouth motion, which is functional and contains a primary component of forearm pronation/supination. The focus in the analysis was on the main translational and rotational components of the movements the patient performed (reach-and-grasp and hand-to-mouth), which should take place along the longitudinal axis, and about the lateral axis of the forearm respectively. According to the sensor attachment, these axes were the x-axis and y-axis of the sensor local coordinate system. As a result, for both movements,

data from sensor accelerometer-x were analysed and compared to the x-component of Vicon's computation. Similarly, comparison was done for data from sensor gyroscope-y.

The measurement accuracy of sensor S4 was established for both movements in pre-stroke intervention, by calculating the mean sensor error and RMS error across the entire five repetitions of the movements (results given in Table 5.7 and Table 5.8). The mean sensor error was calculated as the difference between the sensor measurement and Vicon's computation, found as a result of accelerometer gravity bias and gyroscopic drift. So the raw sensor data (with no pre-processing) were compared to Vicon's computation, and the comparison was repeated after some pre-processing was applied to the sensor data (either by high pass filtering the data and detrending, or simply detrending). Motion regimes were identified from the peak-to-peak measurement of Vicon.

The sensor accelerometer data were high-pass filtered (using a median filter of order 17) to attenuate spikes and high frequency noise, then detrended to reduce the bias on accelerations from gravity. Velocity estimation from the sensor data was obtained by integrating the detrended and high-pass filtered sensor accelerometer data. The angular velocity from gyroscopes and sensor estimated orientation (roll, pitch, yaw) were only detrended to remove the effect of drift.

Table 5.7 Difference between sensor measurement/estimation and Vicon computation (mean error) for a stroke patient while performing the reach-and-grasp movement, pre-intervention (d. = detrended, d.f. = detrended and high pass filtered)

	Peak-to-peak (from Vicon)	Mean error (measure of bias or drift)		RMS error	
		raw	d. or d.f.	raw	d. or d.f.
Velocity (x) [m/s]	1.253	26.374	-0.009	30.593	**0.579**
Acceleration (x) [m/s^2]	6.140	3.723	0.012	3.876	**0.686**
Orientation (y) [deg]	18.200	21.127	-0.836	21.354	**3.504**
Angular velocity(y) [rad/s]	0.877	0.015	-0.007	0.443	**0.443**

Table 5.8 Difference between sensor measurement/estimation and Vicon computation (mean error) for a stroke patient while performing the hand-to-mouth movement, pre-intervention (d. = detrended, d.f. = detrended and high pass filtered)

	Peak-to-peak (from Vicon)	Mean error (measure of bias or drift)		RMS error	
		raw	d. or d.f.	raw	d. or d.f.
Velocity (x) [m/s]	0.551	41.107	-0.002	48.483	**1.133**
Acceleration (x) [m/s^2]	2.576	2.181	0.0001	2.467	**1.096**
Orientation (y) [deg]	19.000	22.415	-0.0007	22.861	**4.035**
Angular velocity(y) [rad/s]	1.616	0.012	-0.0005	0.283	**0.282**

For both movements in pre-stroke intervention, the mean and RMS errors for the sensor acceleration measurements along the x axis decreased, after the measurements were high pass filtered and detrended. For instance, the mean sensor error dropped from 3.72 to 0.012 m/s^2 and the RMS error from 3.88 to 0.69 m/s^2 for the movement reach-and-grasp. Similarly, the mean and RMS errors became 0.0001 and 1.10 m/s^2 for the hand-to-mouth movement. The sensor/Vicon comparison improved significantly after the pre-processing of raw sensor data, as shown in Figure 5.36 and Figure 5.37.

Velocity estimation along the x axis suffered from integration drift due to the gravity DC offsets of the raw sensor accelerations in the x direction. The mean error for raw sensor data was 26.37 m/s for reach-and-grasp. After the accelerations were high pass filtered and their DC shifts were removed (by detrending), the drift was significantly reduced to a mean

error of -0.009 m/s, and an RMS error of 0.58 m/s. A slight drift still existed as shown in Figure 5.38, which indicates that further work to improve the velocity estimation needs to be done. The velocity comparison between the sensor and Vicon showed a greater difference for hand-to-mouth movement than for reach-and-grasp, with the mean error dropping to -0.002 m/s, and the RMS error to 1.13 m/s after the pre-processing of sensor accelerations.

Detrending had the desired effect on sensor orientation estimation along y (pitch) and the gyroscopic measurements when these were compared to Vicon's computation (with corresponding RMS errors of 3.50º and 0.44 rad/s for reach-and-grasp, and 4.03º and 0.28 rad/s for hand-to-mouth). The sensor/Vicon comparison of orientation along y before and after detrending is shown in Figure 5.39 and Figure 5.40 for reach-and-grasp; the comparison after detrending is also shown in Figure 5.41 for hand-to-mouth. Despite the gyroscopes running for a longer time in the case of hand-to-mouth movement (40 seconds as compared to the 12 second run time for reach-and-grasp), RMS errors were found to be smaller after the detrending of angular velocities (0.28 rad/s as opposed to 0.44 rad/s). This was probably due to a larger angular velocity lateral component compared to reach-and-grasp (the peak-to-peak value from Vicon's measurement was 1.62 rad/s for hand-to-mouth and 0.88 rad/s for reach-and-grasp). It appears therefore that the larger the component of rotation (hence the angular velocity), the more effective detrending can be in reducing the drift, even for longer gyroscopic run times.

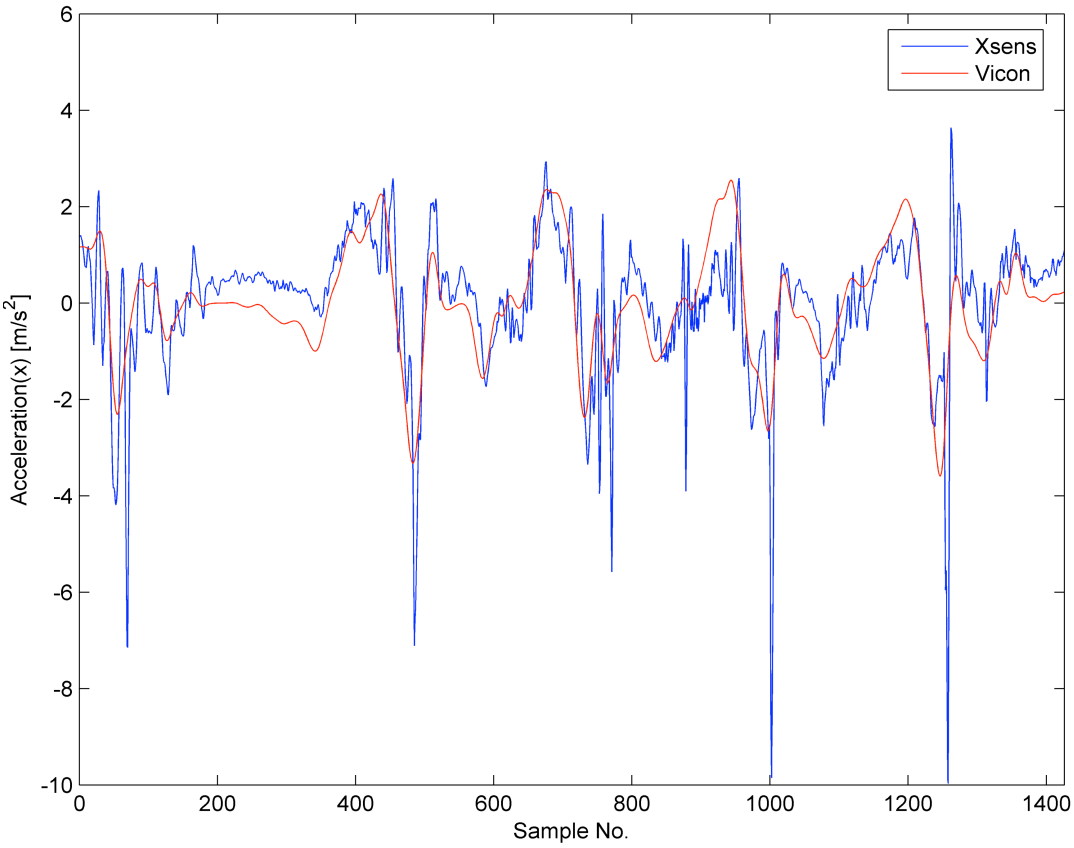

Figure 5.36 Comparing the sensor acceleration measurements (in blue) to Vicon's computation (in red) for a stroke patient performing reach-and-grasp, pre-intervention

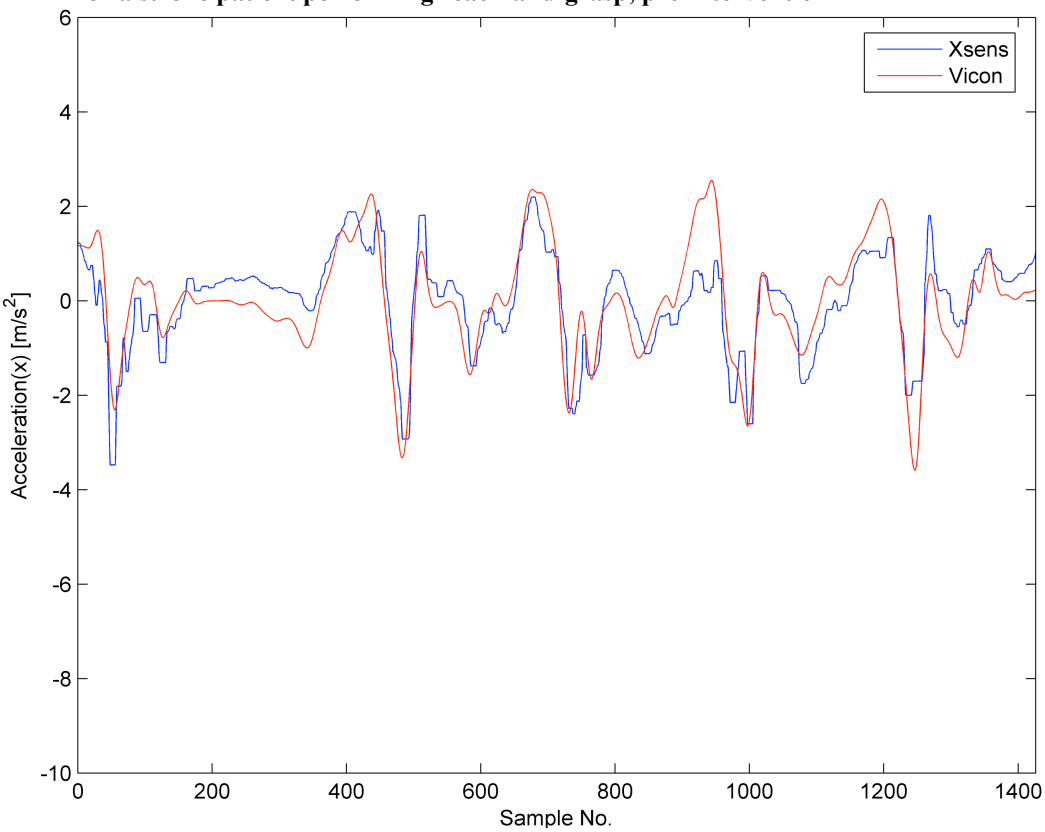

Figure 5.37 Comparing the sensor acceleration measurements (in blue) after high pass filtering and detrending, to Vicon's computation (in red) for a stroke patient performing reach-and-grasp, pre-intervention

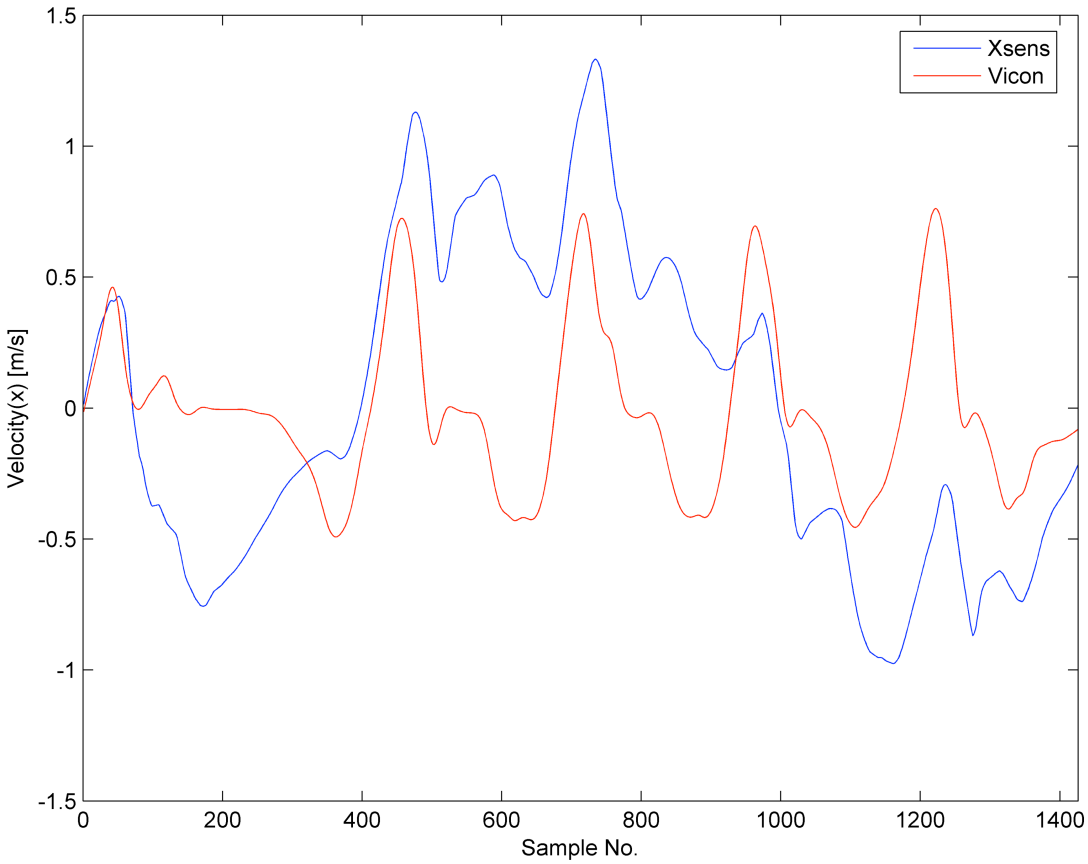

Figure 4 Comparing the velocity estimation from integration of detrended high pass filtered sensor accelerations (in blue), to Vicon's computation (in red) for a stroke patient performing reach-and-grasp, pre-intervention

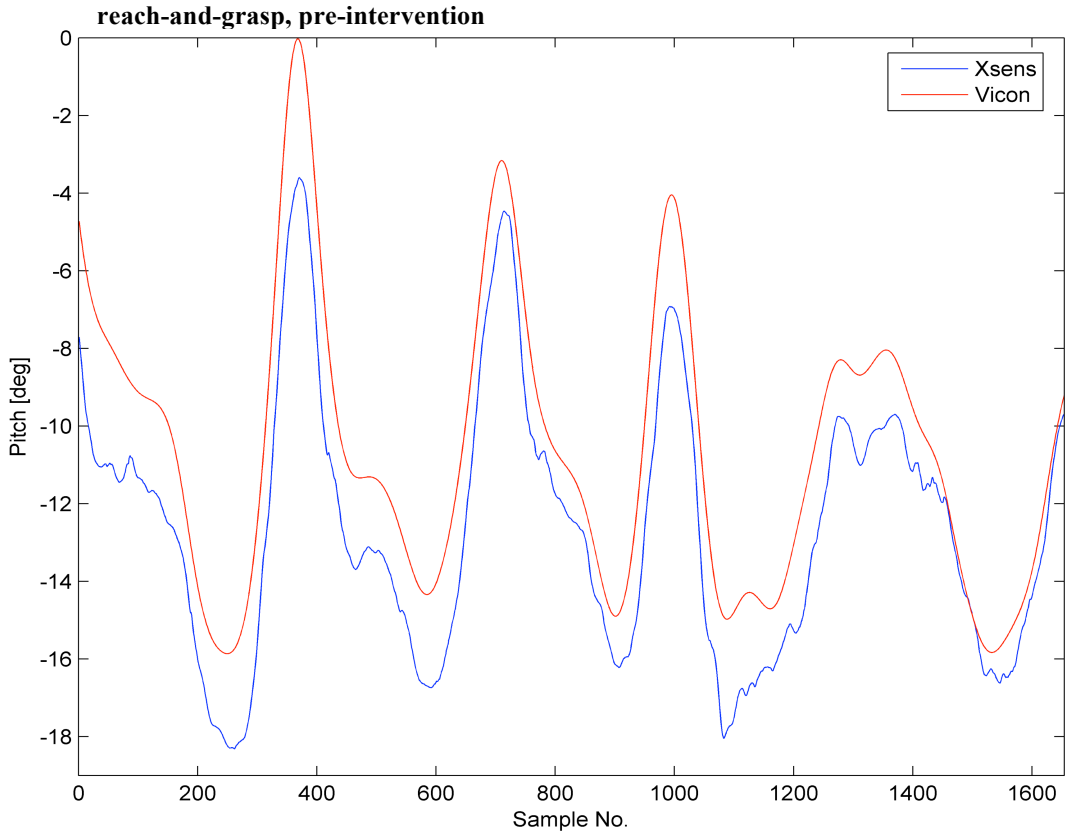

Figure 5.39 Comparing the sensor estimation of pitch (in blue), to Vicon's computation (in red) for a stroke patient performing reach-and-grasp, pre-intervention

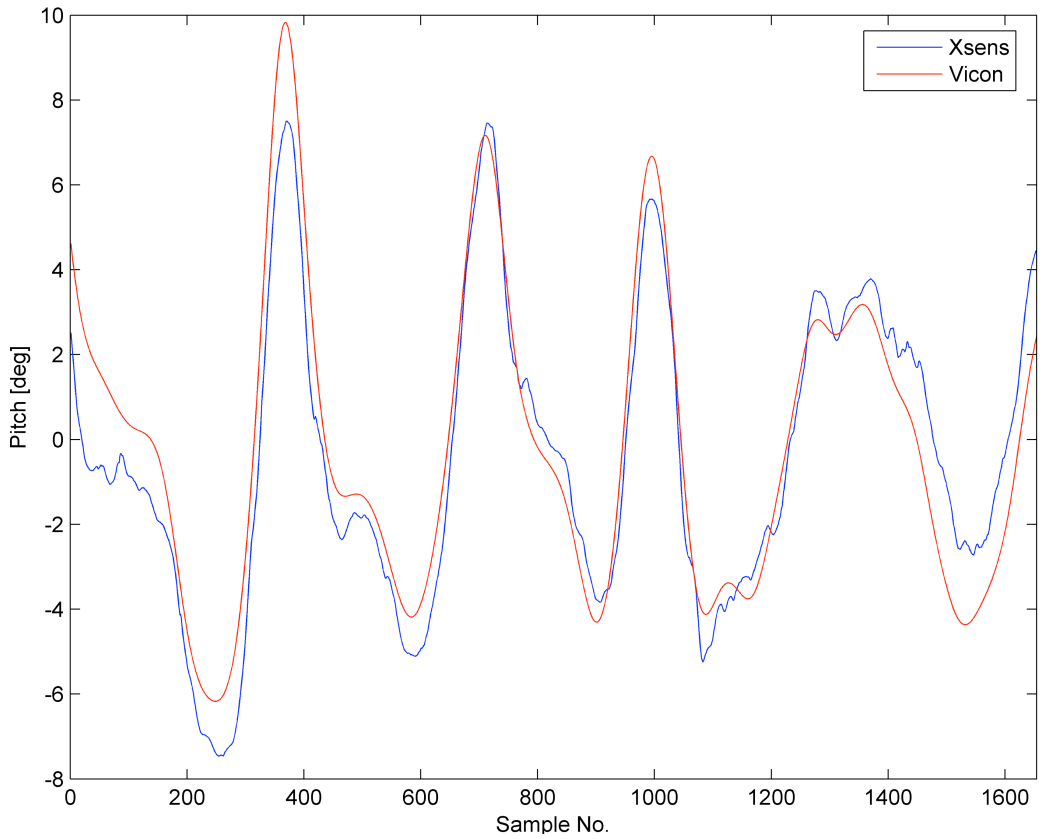

Figure 5.40 Comparing the sensor estimation of pitch (in blue) after detrending to Vicon's computation (in red) for a stroke patient performing reach-and-grasp, pre-intervention

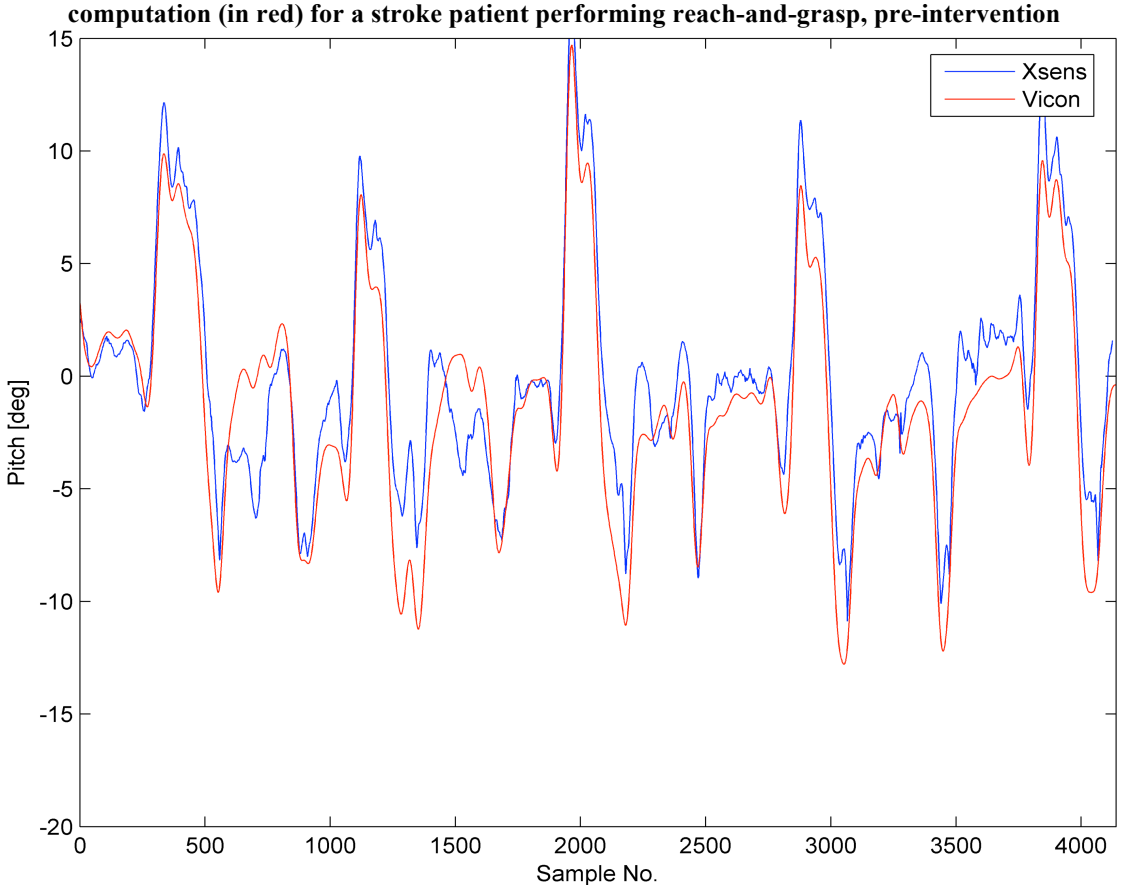

Figure 5.41 Comparing the sensor estimation of pitch (in blue)after detrending to Vicon's computation (in red) for a stroke patient performing hand-to-mouth, pre-intervention

5.6.2 Pre/Post change measurement (Sensitivity testing)

To determine the sensor sensitivity to measure change in movement, the RMS error of the sensor data, s_i, (compared to Vicon data, v_i), in pre- and post- stroke intervention, was calculated using equation (5.7), for the reach-and-grasp and hand-to-mouth movements, after the sensor data were pre-processed (as in section 5.6.1). Two sets of the distribution of sensor errors were obtained for each movement; the sets corresponded to the pre- and post- intervention data (Table 5.9 and Table 5.10 respectively). As shown in both tables, it was found that the pre-intervention sensor errors were larger or similar to the corresponding post-intervention error values, for the four quantities - velocity, acceleration, angular velocity and orientation. This could be the result of an improved movement strategy employed by the patient, or reduction of the noise component in the sensor data from a more effective sensor positioning.

Hence, a 95% confidence interval of the sensor errors was established for the pre-intervention data (to quantify the sensor sensitivity at its worst performance). The confidence interval was defined as the sum of the calculated RMS errors and twice the standard deviation of sensor errors, $\boldsymbol{\sigma_d}$; where sensor errors, d_i, were determined from the absolute difference between the sensor measurement and Vicon's computation across the entire duration of the movements (see equation (5.8), total number of samples for the movement is N). The upper limit of the 95% confidence interval of sensor errors, which represents the worst and largest possible error in the sensor measured data, is given in Table 5.11 for both movements, and indicated in bold. This was compared to the actual magnitude of change of the movements measured in Vicon from pre- to post- intervention (given in Table 5.12). It was then possible to determine whether the sensors were sufficiently sensitive to measure the movement change for the stroke patient. A findings' summary is given in Table 5.13, for the 68% and 95% confidence interval of sensor errors.

$$\text{RMS error} = \sqrt{\frac{1}{N}\sum_{i=1}^{N}(v_i - s_i)^2} \tag{5.7}$$

$$\sigma_d = \sqrt{\frac{1}{N}\sum_{i=1}^{N}(d_i - \mu)^2} \text{ where } d_i = abs(v_i - s_i) \text{ and } \mu = mean(d_i) \tag{5.8}$$

The upper limit of the sensor 95% confidence interval (within two $\boldsymbol{\sigma_d}$), at worst and after some pre-processing, was found to be smaller than the change in movement of the patient, for orientation for the reach-and-grasp and hand-to-mouth movements. Despite the pre-processing, the error in linear velocity exceeded the upper limit of the confidence interval, and was larger than the change in movement of the patient following intervention for both movements, even at the lower 68% confidence interval (which was within one $\boldsymbol{\sigma_d}$). The upper limit of the sensor confidence interval for angular velocity was found to be similar to the change in movement in the case of the hand-to-mouth movement; however this was with only 68% confidence. The upper limit of the sensor error confidence interval for acceleration was found to be smaller than the change in movement, with 95% confidence for the hand-to-mouth movement, and 68% confidence for the reach-and-grasp movement.

Therefore, after some pre-processing of the sensor raw data, the sensors were found to be adequate and sensitive for monitoring change in orientation, with 95% confidence, for the reach-and-grasp and hand-to-mouth movements. The sensors could reliably give feedback on acceleration and angular velocity, with 68% to 95% confidence, depending on the amount of accelerometer bias due to gravity (governed by the initial sensor mounting), and gyroscopic drift (affected by the run time of gyroscopes). However, despite the pre-processing, linear velocity was not accurately estimated by the sensors, and was not reported reliably for either movement, even within the 68% confidence interval.

The mean and standard deviation values for movement duration were also estimated from the sensor acceleration measurements (Table 5.9 and Table 5.10). Mean values were very close to the movement duration obtained from Vicon marker data (given in section 4.4.3). The standard deviation decreased for both movements following intervention, which implied a more consistent and controlled execution of the movements, which was measurable with the movement duration parameter. Percent time to maximum velocity was not compared between the two systems, as the velocity estimation from sensor acceleration measurements suffered from drift.

Table 5.9 Sensor sensitivity to detect change in movement in pre/post- stroke intervention for the reach-and-grasp movement (σ_d is the standard deviation of sensor errors determined from the absolute difference of sensor measurement and Vicon's computation, across the entire duration of the movement)

		Pre-Intervention		Post- Intervention	
		RMS error	σ_d	RMS error	σ_d
Velocity (x) [m/s]		0.5786	0.2875	0.4208	0.2670
Acceleration (x) [m/s^2]		0.6859	0.3786	0.6159	0.3712
Orientation (y) [deg]		3.5043	2.2554	1.2731	0.6775
Angular velocity(y) [rad/s]		0.4429	0.3035	0.1789	0.1126
Movement duration [s]	**μ**	3.170		3.422	
	σ	1.311		0.818	

Table 5.10 Sensor sensitivity to detect change in movement in pre/post- stroke intervention for the hand-to-mouth movement (σ_d is the standard deviation of sensor errors determined from the absolute difference of sensor measurement and Vicon's computation, across the entire duration of the movement)

		Pre-Intervention		Post-Intervention	
		RMS error	σ_d	RMS error	σ_d
Velocity (x) [m/s]		1.1331	0.7997	1.1300	0.7360
Acceleration (x) [m/s^2]		1.0962	0.7210	1.0914	0.7544
Orientation (y) [deg]		4.0352	2.6493	2.3820	1.3349
Angular velocity(y) [rad/s]		0.2818	0.2158	0.2774	0.1883
Movement duration [s]	**μ**	9.037		8.275	
	σ	0.605		0.389	

Table 5.11 Sensor 95% confidence interval (which is sensor RMS errors ± 2*σ_d, where σ_d is the standard deviation of sensor errors determined from the absolute difference of sensor measurement and Vicon's computation, across the entire duration of the movement) to detect change in movement at worst (in pre-stroke intervention) for the reach-and-grasp and hand-to-mouth movements

	Sensor 95% confidence interval (in pre-stroke intervention)	
	Reach-and-Grasp	**Hand-to-Mouth**
Velocity (x) [m/s]	[0.0036 – **1.1536**]	[-0.4663 – **2.7325**]
Acceleration (x) [m/s^2]	[-0.0713 – **1.4431**]	[-0.3458 – **2.5382**]
Orientation (y) [deg]	[-1.0065 – **8.0151**]	[-1.2634 – **9.3338**]
Angular velocity(y) [rad/s]	[-0.1641 – **1.0499**]	[-0.1499 – **0.7135**]

Table 5.12 The measurable difference to detect change in movement in pre/post- stroke intervention for the reach-and-grasp and hand-to-mouth movements, as measured by Vicon

	Movement change (RMS difference between pre- and post- intervention in Vicon)	
	Reach-and-Grasp	**Hand-to-Mouth**
Velocity (x) [m/s]	**0.3884**	**0.1846**
Acceleration (x) [m/s^2]	**1.3403**	**7.3559**
Orientation (y) [deg]	**10.242**	**13.346**
Angular velocity(y) [rad/s]	**0.2197**	**0.3178**

Table 5.13 Sensor sensitivity to detect change in movement for the reach- and-grasp and hand-to-mouth movement, with the sensor 68% confidence interval defined within one σ_d and the 95% confidence interval within 2*σ_d

	68% confidence interval	95% confidence interval
Velocity (x) [m/s]	✗ (both movements)	✗ (both movements)
Acceleration (x) [m/s^2]	✓(reach-and-grasp only)	✓(hand-to-mouth only)
Orientation (y) [deg]	✓ (both movements)	✓ (both movements)
Angular velocity(y) [rad/s]	✓ (hand-to-mouth only)	✗ (both movements)

Results are reported on the suitability (measurement accuracy in Table 5.7 and Table 5.8, and sensitivity testing summarised in Table 5.13) of using sensor accelerometer-x, and gyroscope-y for wearable monitoring of the forearm for the two movements, reach-and-grasp and hand-to-mouth. Given that sensor accelerometer-y and -z, as well as gyroscope-x

and -z were of similar characteristics and factory make, similar findings in terms of measurement accuracy and sensitivity to change in movement were expected. It should be stated that further sensor testing is needed on more stroke patients to confirm these results.

On the basis that monitoring jerky uncontrolled movement (of the stroke patient) was more difficult than monitoring smooth controlled movement, it was assumed the sensors would also be adequate (in terms of measurement accuracy and sensitivity) to monitor reach-and-grasp and hand-to-mouth movements of the healthy subjects.

5.7 Summary of results

Gravity, drift due to temperature changes or small changes in the structure of gyroscopes from mechanical wear, and magnetic disturbances produced by force plates, can all significantly affect sensor accelerometer and gyroscopic readings, as well as the estimated sensor angular output. Several experiments were therefore performed at the NOC to assess individual sensor components. Below is a review to the outcomes for each experiment in section 5.1, and a brief report on the findings.

- *Static Calibration* (section 5.2): **to relate the global coordinate systems of Vicon and Xsens sensors, establish static sensor accuracy for estimating orientation and check the effect of magnetism produced by the force plates on sensor orientation estimation**

On average, the two global coordinate systems of Vicon and Xsens sensors were able to be related by about 1º difference for the x- and y- axes and 0º for the z-axis. The static sensor accuracy for estimating roll, pitch, and yaw was found to be less than 4.5º, 1.8º, and 0.2º respectively. Sensor S1 orientation was incorrectly estimated due to magnetism produced

by active force plates; with drift errors reaching about 2.5º in the x- and y- directions, and 1.2º in the z- direction (with the sensor mounted 510 mm from the plates). However, an improvement in orientation estimation was seen for the new generation sensors (S2, S3 and S4), as less orientation drift was detected when the force plates were on as compared to S1.

- *Experiment 1* (section 5.3): **to determine dynamic sensor accuracy for estimating orientation over a general motion regime**

Dynamic sensor accuracy for estimating roll, pitch, and yaw over a general motion regime was found to be influenced by a systematic drift in the gyroscopes over time. For small rotations of about 3º, the RMS error of sensor yaw data was found to be 1.44º, but detrending the sensor data reduced this error to 0.16º. Similarly for larger rotations, detrending the sensor yaw data reduced the drift error from 0.51º to 0.035º per second. Sensor gyroscopic drift was found to linearly increase with time. When measuring small movements, the sensors could sometimes be more suitable than Vicon, given their limited measurement bandwidth, and the need to attenuate high frequency noise components on motion data from the latter.

- *Experiment 2* (section 5.4): **to determine the task-specific dynamic measurement accuracy of the sensor gyroscopes, in the motion regimes representing reach-and-grasp and forearm pronation/supination. Also, to check the internal sensor consistency of the accelerometers and gyroscopes**

In the motion regimes representing reach-and-grasp and forearm pronation/supination, the dynamic measurement accuracy of sensor gyroscope-z (task specific) was investigated, and

found to be high at low and high angular velocities (RMS errors were between 0.0095 and 0.0695 m/s for the low turn rate, and 0.038 m/s for the high turn rate). As the manufacturer reported accuracy for gyroscopes -x and -y were similar to -z, the gyroscopes were deemed accurate enough to measure turn rate for both reach-and-grasp and forearm pronation/supination movements. The internal sensor consistency of accelerometers and gyroscopes was found to be high with an RMS error of 0.24 m/s^2. Accelerometers and gyroscopes appear to require some time to settle down and reach steady state (about one second). So if either were to be used clinically, the settling time should be considered.

- *Experiment 3* (section 5.5): **to determine dynamic sensor baseline accuracy for measuring accelerations and obtaining velocity from accelerometer readings, in motion regimes of comparable accelerations of healthy upper limb movement. Also, to investigate the appropriateness of the sensor mounting method**

Due to the gravity offset on sensor accelerometer data, velocity estimates made by the sensors (obtained via integration) suffered slight integration drift. Detrending the accelerometer data, after a high-pass filter (median filter of order 17) was applied, helped to reduce this drift in velocity estimation. Applying the pre-processing to the sensor data reduced the gravity offset and the drift, and the RMS errors of acceleration and velocity improved to 0.127 m/s^2 and 0.054 m/s. It was found that the minimum movement acceleration to obtain usable sensor accelerometer output needs to be larger than 0.5 m/s^2, to be able to correct the bias satisfactorily. The sensor attachment method (double sided tape) was also found to be suitable in the case of the mobile robot, with very little motion artefact detected in the position, velocity and acceleration data in Vicon. The method's appropriateness to mount sensors on the forearm should be investigated.

- *Experiment 4* (section 5.6): **to investigate the measurement performance of sensors for measuring motion data of healthy subjects and a patient in pre-stroke intervention, and to check whether the sensors' sensitivity to detect change in movement in pre/post- stroke intervention met the requirements identified in section 4.4.3 using Vicon**

For a simple one dimensional movement like reach-and-grasp, the sensor accelerometer data, after high pass filtering and detrending, compared well to Vicon in pre-stroke intervention, and errors were within 0.69 m/s^2. For a more complex three dimensional movement like hand-to-mouth, errors were larger and reached 1.10 m/s^2. As a result, linear velocity estimation from the sensor accelerometer data suffered integration drift. Despite high-pass filtering the accelerations and removing the DC shift, errors in velocity estimation reached 0.58 and 1.13 m/s for the reach-and-grasp and hand-to-mouth movements respectively. The velocity comparison between the sensor and Vicon showed a greater difference for hand-to-mouth than for reach-and-grasp, for pre-stroke intervention.

Both the sensor gyroscopic readings and sensor orientation estimation compared well to Vicon when the rotation was large (about 19º). Errors in sensor orientation estimation in pre-stroke intervention after data detrending were about 3.50º and 4.03º for the reach-and-grasp and hand-to-mouth movements respectively.

Despite the gyroscopes running for a longer time in the case of hand-to-mouth movement (40 seconds as compared to the 12 second run time for reach-and-grasp), root-mean-square errors were found to be smaller after detrending the angular velocities (0.28 rad/s as opposed to 0.44 rad/s). This was probably due to a larger angular velocity component (the

peak-to-peak value from Vicon's measurement was 1.62 rad/s for hand-to-mouth and 0.88 rad/s for reach-and-grasp). Therefore, the larger the component of rotation (hence the angular velocity), the more effective detrending can be in reducing the drift, even for longer gyroscopic run times.

After some pre-processing of the sensor raw data, the sensors were found to be adequate (accurate) and sensitive enough for monitoring change in orientation, with 95% confidence, for the reach-and-grasp and hand-to-mouth movements. The sensors could reliably give feedback on acceleration and angular velocity, with 68% to 95% confidence, depending on the amount of accelerometer bias due to gravity (governed by the initial sensor mounting), and gyroscopic drift (affected by the run time of the gyroscopes). However, despite the pre-processing, linear velocity was not accurately estimated from the sensor readings, and was not reported reliably for either movement, even within the lower 68% confidence interval (see Table 5.13).

The mean value of movement duration, estimated from the sensor acceleration measurements, was found to be very close to the movement duration obtained from Vicon marker data (given in section 4.4.3). The standard deviation also decreased for both movements following intervention, which implied a more consistent and controlled execution of the movements, which was measurable with the movement duration parameter. Percent time to maximum velocity was not compared between the two systems, as the velocity estimation from sensor acceleration measurements suffered drift.

On the basis that monitoring jerky uncontrolled movement (of the stroke patient) was more difficult than monitoring smooth controlled movement, the sensors were assumed to be

adequate (in terms of measurement accuracy and sensitivity) to monitor reach-and-grasp and hand-to-mouth movements of the healthy subjects.

Finally, the rehabilitation outcomes of interest in this work were movement velocity, forearm orientation, movement duration and percent time to maximum velocity. Given the problems identified for the sensor components within the specific motion regimes of interest, below are recommendations to improve the estimation of these rehabilitation outcomes.

- To reduce the drift in gyroscopic readings, it is advisable to initially warm up sensor electronics for 15 minutes and leave the sensor for a rest period of two minutes between trials, so gyroscopes can settle down. The actual gyroscope settling parameters (15 minutes and two minutes) are based on a communicated recommendation of Motion Technologies, The Netherlands. Also, gyroscopes should not experience a major change in the temperature of the surroundings.

- To help reduce the effect of integration drift on sensor orientation estimation, it is recommended to keep the sensor away from any magnetic disturbance sources. So the force plates should be turned off, and ferromagnetic material should be kept to a minimum.

- Sensor accelerometer data are biased due to gravity, which leads to integration drift in the velocity estimation. Therefore, the sensors do not report reliably on velocity, particularly for complex exercises. The gravity bias on the accelerometer data, and its effect on velocity, could be controlled by the initial sensor mounting. Errors in

sensor placement and calibration could lead to measurement errors and noise, so a systematic mounting protocol should be developed and tested.

- Velocity estimation can also be improved through additional data pre-processing of the accelerometer data (high-pass filtering with median filters and detrending). However, better tracking algorithms like Kalman filters or optimisation techniques could also be used, as is later discussed in Chapter 6.

5.8 Summary

Results for a stroke patient while performing reach-and-grasp and hand-to-mouth movements, showed good agreement between Xsens inertial sensors and the Vicon multi-camera system in pre-stroke intervention. For simple one dimensional movements (like reach-and-grasp), data from the sensor accelerometer-x compared well to Vicon's computation, after median filtering and detrending. Velocity estimation via integrating the sensor acceleration suffered from integration drift; this drift was reduced after high-pass filtering and removing the DC offset from the accelerometer data. There were errors in orientation estimation by the sensor, mainly when the angle was small, probably caused by lack of sensor resolution, and from gyroscopic readings being susceptible to drift over time. These difficulties appeared when the angular velocity was low, and the rotation component was small (errors within 5° which is clinically seen as acceptable (Zatsiorsky, 1998, p. 355)). Detrending was sufficient to reduce these errors in orientation and angular velocity. Other smaller errors resulted from sensor positioning and mounting. Movement duration was well estimated from the sensor accelerometer measurements. Percent time to maximum velocity (from section 4.4.3) was not calculated or commented on, as velocity estimation from sensor accelerometer measurements suffered integration drift.

After processing the sensor data (either by high pass filtering and detrending or simply detrending), the upper limit of the sensor error 95% confidence interval for orientation was found to be smaller than the measurable difference to detect change in pre/post- stroke intervention (established in section 4.4.3). For acceleration and angular velocity, sensor sensitivity was found to be within 68% to 95% confidence, depending on the amount of accelerometer bias due to gravity (governed by the initial sensor mounting), and gyroscopic drift (affected by the run time of gyroscopes). Despite pre-processing, linear velocity was not accurately estimated by the sensor readings, and was not reported reliably for either movement, even within the lower 68% confidence interval. Hence the sensor sensitivity was found suitable with varying confidence extents for acceleration, angular velocity and orientation, but unacceptable for the estimation of linear velocity. The change of movement pattern following intervention was also detected by a decrease in the standard deviation of movement duration. Further sensor testing is needed on more stroke patients to confirm these findings.

The problem of integration drift was still evident in movement velocity obtained from integration of accelerometer data, even after high pass filtering and detrending. The exploitation of cyclic movement during exercise could reduce this drift problem in inertial sensors. Optimisation algorithms to model the movement and incorporate sensor readings (introduced in Chapter 6) could extend the useful range (Zhou *et al.*, 2008). Also, tracking algorithms (as in Chapter 6) could also help to resolve this drift in velocity estimation.

It is worth mentioning that a robotic arm (with Vicon markers and Xsens sensors) could be used to simulate a reach-and-grasp (or other) movement in a controlled manner without skin movement error for further accuracy testing.

Chapter 6
Signal Processing Techniques to Improve the Sensor Motion Measurements

6.1 Introduction

One of the most essential actions in stroke rehabilitation is reach-and-grasp, i.e. reaching to pick up an object on the table in front of a patient and releasing it to a position close-by (see Figure 4.9). Monitoring this action relies on the accelerometers rather than the gyroscopes within the inertial sensors, since the movements of the arm segments are primarily linear. In particular and as found in Chapter 3, movement velocity is considered a useful outcome measure and feedback metric in rehabilitation, as it relates to temporal efficiency, motor control, and overall quality of the movement (Wu, Lin *et al.*, 2007). This means that accurate measurement of velocity is crucial.

As reported by Kavanagh and Menz (2008), and found in Chapter 5 (section 5.6), a common problem with accelerometers is that measurements are dominated by gravity, especially in low movement acceleration regimes, as is typical of rehabilitation exercises. This can lead to an erroneous sensor accelerometer reading (with a gravity offset), and hence integration drift in velocity and position estimation. Similarly, as in section 5.3, gyroscopes drift as they gradually heat up during operation. This drift appears as a time-varying positive or negative bias depending on the ambient temperature (Barshan &

Durrant Whyte, 1995), which also leads to integration drift in orientation estimation. Different approaches to manage errors in estimating position and orientation have been previously investigated. However, the common problem of drift occurring in velocity estimation is yet to be systematically investigated. This chapter first presents a literature review of the different estimators and methods proposed to deal with the integration drift problem of inertial measurements.

In this chapter, a summary of the motion profile for a healthy subject and a stroke patient, performing reach-and-grasp, is provided. Two methods are described in sections 6.4 and 6.6 to improve the estimation of movement velocity, and reduce the integration drift. The first method is a dynamic model-based filtering strategy, based on extended Kalman filtering (EKF), which offers a linear and instantaneous solution (Bar-Shalom *et al.*, 2001). The EKF method is typically used to provide an optimal solution to the posterior of the state (where several variables such as orientation and position are stored to be estimated) (Brodie *et al.*, 2008), if the state space model and the sensor model are both linear and Gaussian (Hu & Gan, 2005). To practically cope with the non-linearity of most real-life problems (Hu & Gan, 2005), Kalman filters are usually based on linearised process models. The second method employs optimisation based on the non-linear least squares theorem (Bar-Shalom & Fortmann, 1988). In contrast to the Kalman filter, this technique estimates velocity by using all sensor measured data at the point of initialisation, and at each iteration of the estimator. It may therefore be considered to give the best estimate available from all the sensor data.

The algorithm for the EKF method is developed on the simulated, cyclic, two dimensional "reach" movement of a mobile robot, as this movement is fairly repeatable, with limited

sensor motion artefacts as compared to that in the presence of skin. It is then applied to upper limb motion data of a healthy subject during repetitive forearm reach-and-grasp. The EKF algorithm's performance is also tested on the motion data of a stroke patient.

The second signal processing method, which is the optimisation estimator, is applied to one data set to compare with the performance of the EKF method. The optimisation method is developed and applied to the upper limb motion data of a healthy subject during repetitive forearm reach-and-grasp. This set of motion data was chosen on the basis that it assesses the method's performance when applied to human motion data, without the extra artefacts that motion data of stroke patients usually suffer from. Finally, the two signal processing methods are compared and discussed in the context of their suitability for different applications.

6.2 Previous work

According to Barshan and Durrant Whyte (1995), "even very small errors in the velocity and angular rate information provided by inertial sensors, cause an unbounded growth in the error of integrated measurements". Methods to reduce drift in the tracking of human arms using inertial sensing have been classified into two groups - sensor fusion, and optimisation strategies (Zhou, Hu, Harris *et al.*, 2006).

The first group integrates sensors with a tracking system to compensate for the sensors' shortcomings, hence limiting the diffusion of estimation errors, and mitigating drift. For instance, by fusing visual measurements from three cameras with two inertial sensors, Foxlin et al. (2004) was able to track a pilot's head motion more accurately. Another hybrid system was proposed by Tao et al. (2007) to estimate the pose of the wrist joint,

from which the elbow joint pose information could be inferred (using kinematic models). The system combined visual information from one camera, and inertial information from two inertial sensors to track arm motion in predefined circular and rectangular paths. Two methods were developed for data fusion, a deterministic method based on upper arm geometry, and a probabilistic EKF method incorporating sensor noise and model uncertainty. When compared to commercial marker based systems like CODA and Qualysis, the EKF fusion method improved significantly the accuracy of the inertial data. However, best performance of the motion tracking system was achieved when additional constraints, related to upper arm geometry and wrist position re-projection and mapping onto camera images, were imposed on the EKF. These constraints defined an accuracy improvement model, and mean errors in estimated wrist position were less than one cm in all three dimensions, for both circular and rectangular path motions.

The second group, which include optimisation strategies, attempts to find an analytical or numerical solution to an appropriately chosen objective or cost function, without adding sensors or other measurement devices. Optimisation methods are used either to minimise errors, such as least squares and minimum mean square error, or to maximise expectation, such as maximum likelihood and maximum a posteriori (Bar-Shalom & Fortmann, 1988). For instance, Zhou et al. (2006, 2008) proposed a motion tracking system that allowed the position and pose of three joints (wrist, elbow and shoulder) to be determined using only two inertial sensors on the forearm and upper arm (two cms away from the wrist and elbow respectively). They considered this to be a unique feature of their motion tracking technique, on the basis that more sensors are normally required to achieve the same result. A kinematic model was devised, and an equality constrained Lagrangian optimisation was adopted to suppress potential drift in integrating wrist sensor data to obtain shoulder

position. Their optimisation incorporated upper limb geometry and structure constraints, as determined from anthropometric measurements. Three movements were studied by Zhou et al. (2006), each lasting about 45 seconds. These were forearm flexion/extension, forearm pronation/supination, and the reach test. Results of the three dimensional position and Euler angles of the three joints were in favour of their algorithm, as it provided stable and consistent arm motion tracking. No significant drift was found for the movement trials. Their system also had good performance at different movement speeds and sensor locations. Later, Zhou et al. (2008) quantified the system's accuracy for "target reaching", "shoulder shrugging", and "forearm rotation" using six CODA markers placed on the upper body. RMS position errors were reported to be less than 0.01 m, and RMS angle errors were 2.5 – 4.8º. The system was also found to be unable to detect small movements, for example less than 0.5 cm and 2º, similar to the outcomes of Luinge (2002). Other methods of optimisation have been adopted, such as Monte Carlo Sampling based optimisation (Zhou, Hu & Tao, 2006), and a total variation based minimisation to smooth out abrupt position amplitude changes (Zhou & Hu, 2007).

Measurement of orientation and position was found to be crucial by many researchers (Luinge & Vetlink, 2005, Zhou *et al.*, 2008, Schepers *et al.*, 2010) to measure human movement. Hence, much effort has gone into reducing the error associated with these measurements, to obtain accurate and stable position and orientation estimates. Approaches to manage these errors have included vision-based corrections (You *et al.*, 1999), error models for drift estimation (Nebot & Durrant Whyte, 1999), and adaptive motion modelling (Luinge & Vetlink, 2005). However, to the best of our knowledge, the common integration drift problem that velocity estimation suffers from is yet to be systematically investigated.

6.3 Summary of the motion profile

The velocity profile during a reach-and-grasp movement of a healthy subject (Subject 1, in Chapter 4) is shown in Figure 6.1, using measurements obtained from the Vicon system. Figure 6.2 shows the velocity profile of a patient 21 months after a stroke. The movement of the healthy subject is characterised by a periodic and almost sinusoidal velocity profile, as shown in Figure 6.1. The stroke patient's velocity, despite being jerky at times, is relatively periodic but with higher harmonic content.

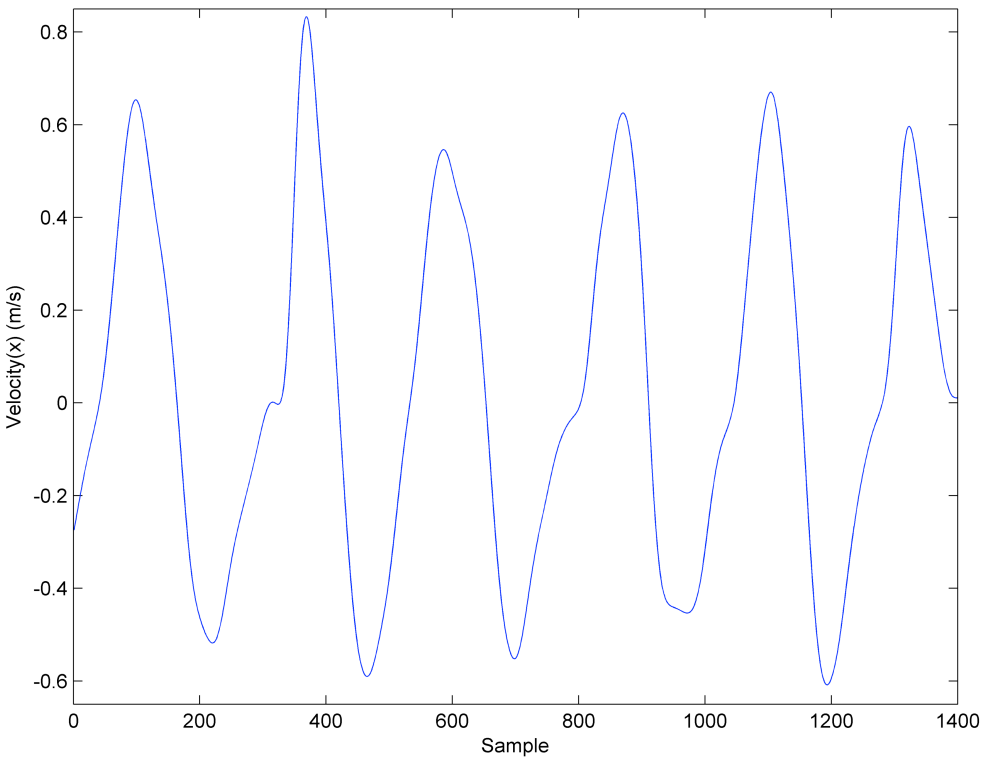

Figure 6.1 The velocity profile of a repetitive forearm reach-and-grasp movement for a healthy subject along the longitudinal axis of the forearm. The movement is periodic and almost sinusoidal.

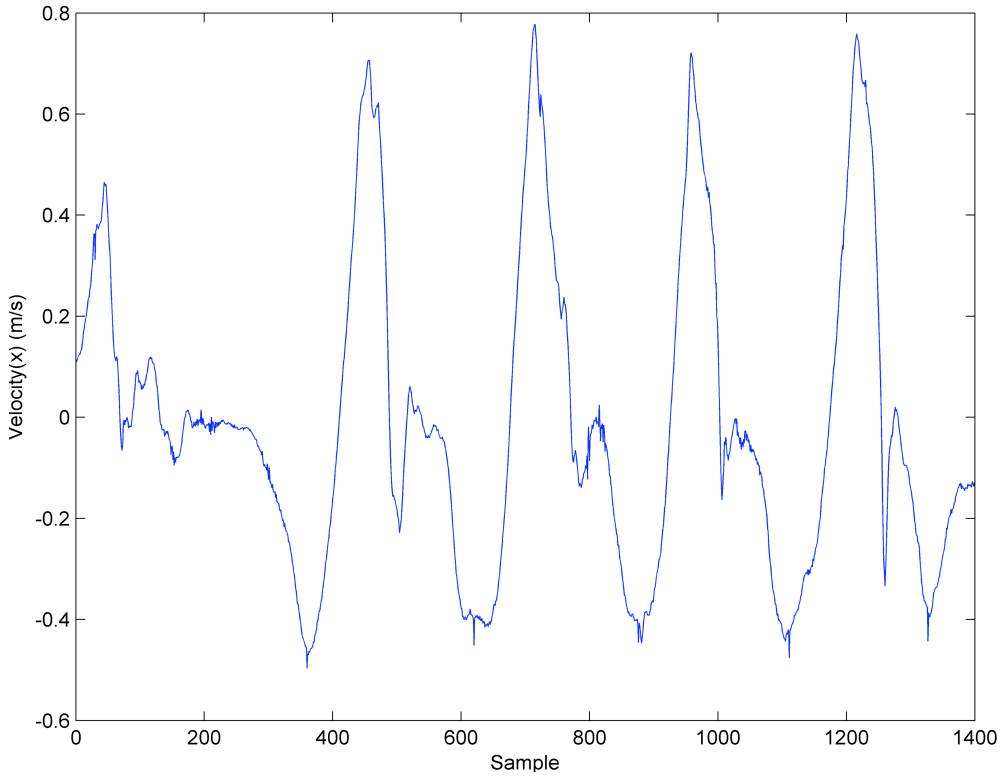

Figure 6.2 The velocity profile of a reach-and-grasp movement for a stroke patient 21 months after a stroke. The movement, despite being jerky at times, is still periodic.

Analysis of motion derived from Vicon's measurements (from Chapter 4, sections 4.4.2.1 and 4.4.2.2) for the four healthy subjects, one female (Subject 1) and three males (Subjects 2-4), (ages 25 – 30 years), and a male stroke patient (age 48 years) while performing forearm reach-and-grasp is summarised and shown in Table 6.1. This was performed with the dominant side for the healthy subjects, and the affected side for the stroke patient. The data presented was obtained from a single marker on the forearm segment, placed on the most caudal-medial point on the ulnar styloid (wrist joint). This information (Table 6.1) is later used to set the parameters of the two signal processing methods, the Kalman filtering strategy and the optimisation estimator.

Table 6.1 Motion analysis of healthy subjects and a stroke patient

Symbol	Quantity [A]	Subject 1 (left)[B]	Subject 2 (right)	Subject 3 (right)	Subject 4 (left)	Stroke (left)
T	movement period (in s)	2.48± 0.18	2.67± 0.16	2.74± 0.41	2.52± 0.18	2.66± 0.36
v_{xmin}	minimum movement velocity (in m/s)	0.07	0.17	0.19	0.17	0.16
v_{xmax}	maximum movement velocity (in m/s)	0.18	0.33	0.32	0.59	0.32
a_{xmin}	minimum movement acceleration (in m/s^2)	0.11	0.03	0.01	0.71	0.11
a_{xmax}	maximum movement acceleration (in m/s^2)	1.21	1.30	0.99	2.93	2.12

[A] m = meter, s = second
[B] in brackets is the side whose movement is measured

6.4 Model-based estimation

This section describes an extended Kalman filter to produce velocity estimation of the motion of the forearm segment. Three reach-and-grasp experiments are carried out to demonstrate the filter's performance on motion data of a mobile robot, a healthy upper limb, and a stroke patient. The mobile robot experiment allows the movement regime experienced by the sensor to be controlled, and the sensor is assessed over the motion regime of interest without mounting artefacts (such as skin movement). The EKF method is therefore able to be tested in a controlled environment. The two other experiments test the performance of the EKF when applied to human motion data of a healthy subject and a stroke patient. Comparing motion data of the healthy subject and the stroke patient, aspects of the reach-and-grasp movement are expected to vary, such as the symmetry of the reach forward and backward components, degree of variation in movement duration across trials, arm stability, and movement smoothness.

6.4.1 Kalman filter design

Model: The movement was modelled as a periodic one dimensional acceleration along the longitudinal sensor axis (x). For simplicity it was assumed to be represented by the fundamental sinusoid:

$$a_{xm} = A_0.\cos(\omega t) \tag{6.1}$$

State Vector Definition: The state vector X, in equation (6.2), contains the variables to be estimated by the EKF. These are movement velocity (v_{xm}), sensor acceleration measurement (a_x), movement gravity-free acceleration (a_{xm}), mis-alignment sensor mounting angle (which is the angle between the vertical axis of the sensor local coordinate system and gravity (g)) (θ), angular frequency of the overall movement (ω), and an acceleration offset component due to gravity (d). All these variables were estimated for the reach-and-grasp movement along the longitudinal axis.

$$X = [v_{xm} \quad a_x \quad a_{xm} \quad \theta \quad \omega \quad d]^T \tag{6.2}$$

The EKF observations (Z) are the sensor acceleration measurements, as in equation (6.3).

$$Z = [a_x] \text{ where } a_x = g\sin\theta + a_{xm} \tag{6.3}$$

The Kalman filter has a predictor-corrector architecture, so the prediction step is corrected by a fusion of the measurements. Innovation is the difference between the actual filter observation and the predicted observation.

6.4.2 Experiment 1: Robot motion experiment

As explained in Chapter 5 (section 5.5), a 12-camera Vicon (MX F40) system was used to capture motion data from a mobile robot mimicking the one dimensional longitudinal movement representing reach-and-grasp. This experiment was performed so the movement regime could be controlled, and to assess the sensor over the motion regime of interest without mounting artefacts such as skin movement. As shown in Figure 6.3, three (9 mm) passive reflective markers were placed on the robot, in addition to an Xsens sensor containing three dimensional accelerometers. The sensor was also tracked by Vicon through four markers placed on it. Further detail on simulating the movement is provided in section 5.5.

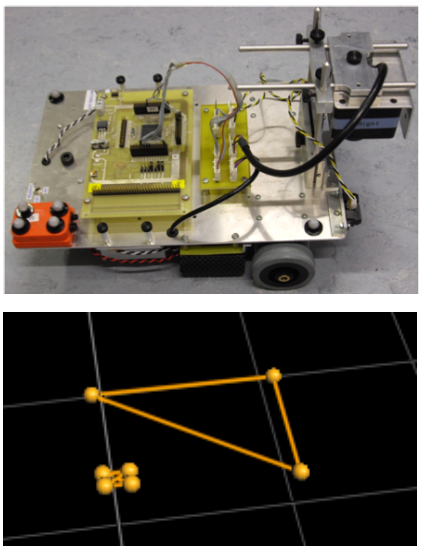

Figure 6.3 A mobile robot with inertial sensor S1: setup, and both as tracked in Vicon

The mobile robot was programmed using CodeWarrior™ (Metrowerks, U.S.) to simulate a reach-and-grasp movement comparable to that of a healthy subject, by controlling the input signal to the motors (i.e. the velocity). Rather than simulating an exact sinusoidal movement, a more general periodic motion was used to test the robustness of the filter algorithm. The calibrated sensor acceleration measurements along the longitudinal axis of the mobile robot in the direction of movement are shown in Figure 6.4. The sensor

calibration defines the global reference for the sensor measurements (the positive direction of x is Magnetic North, y is West, and z positive upwards).

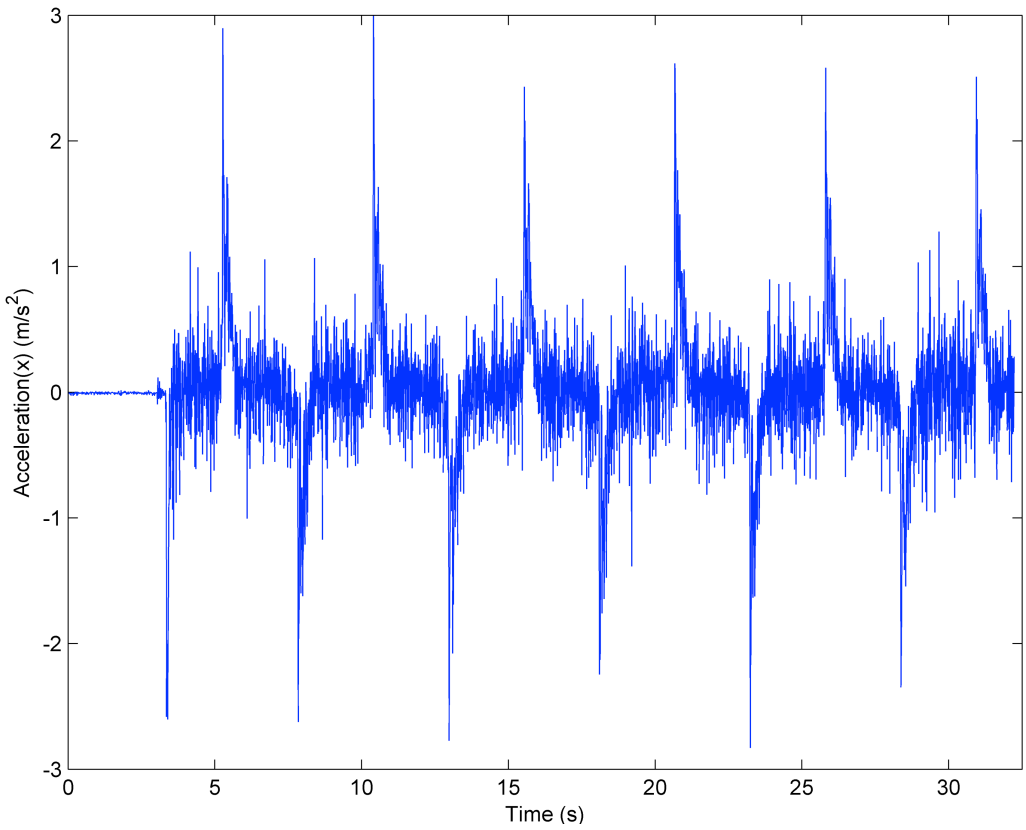

Figure 6.4 Calibrated sensor acceleration measurements along the longitudinal axis of the mobile robot during one dimensional motion. The robot acceleration signal is periodic but not sinusoidal.

The state transition equation for the EKF and the observation/state vector equation are given in equations (6.4) - (6.6). Initialisation of the state vector variables of the EKF, along with the corresponding noise co-variances (with units), is indicated in Table 6.2. These parameters were determined from the motion measurements of the four healthy subjects (given in Table 6.1).

$$\begin{bmatrix} v_{xm} \\ a_x \\ a_{xm} \\ \theta \\ \omega \\ d \end{bmatrix}_{k+1} = \begin{bmatrix} 1 & 0 & \int & 0 & 0 & 0 \\ 0 & 0 & 1 & k_1 & 0 & k_2 \\ 0 & 0 & 0 & 0 & f(\omega) & 0 \\ 0 & 0 & 0 & 1 & 0 & 0 \\ 0 & 0 & 0 & 0 & 1 & 0 \\ 0 & 0 & 0 & 0 & 0 & 1 \end{bmatrix} \begin{bmatrix} v_{xm} \\ a_x \\ a_{xm} \\ \theta \\ \omega \\ d \end{bmatrix}_k + \upsilon(k) \tag{6.4}$$

where $$f(\omega) \sim -A \cdot \cos(\omega t),\ A = 2,\ k_1 = 0,\ k_2 = 1 \tag{6.5}$$

$$\left[a_x\right]_{k+1} = \begin{bmatrix} 0 & 1 & 0 & 0 & 0 & 0 \end{bmatrix} \begin{bmatrix} v_{xm} \\ a_x \\ a_{xm} \\ \theta \\ \omega \\ d \end{bmatrix}_{k+1} + \varpi(k) \tag{6.6}$$

Table 6.2 The Kalman filter: Initialisation of variables (V_I) and noise co-variances (NC_I)

Symbol	Quantity[A]	Robot V_I; NC_I	Healthy V_I; NC_I	Stroke V_I; NC_I
v_{xm}	movement velocity (in m/s)	0; 0.02^2	0; 0.01	0; 0.40^2
a_x	sensor acceleration measurement (in m/s^2)	-0.03; 0.25^2	-0.29; 0.01	2.39; 0.80^2
a_{xm}	movement acceleration (in m/s^2)	0; 0.21^2	0; 0.01	0; 0.60^2
θ	mis-alignment senor mounting angle between z-component of sensor acceleration measurement and gravity (in deg)	0.29; 0.03^2	-0.03; 0.01	(1.6-j0.7); 0.30^2
ω	angular frequency (in rad/s)	(2π/5.14); 0.04^2	(2π/2.51); 0.01	(2π/2.54); 0.40^2
d	offset in sensor acceleration (in m/s^2)	0.03; 0.001^2	0.17; 0.01	4.65; 2.00^2
g	gravity (in m/s^2)	9.8l;N.A.	9.81;N.A.	9.81;N.A.
dT	time difference (in s)	0.01;N.A.	0.01;N.A.	0.01;N.A.
z	sensor acceleration measurement; EKF observation (in m/s^2)	-0.03; 0.30^2	-0.29; 3.00^2	2.39; 1.50^2
$v(k)$	process noise			
$w(k)$	observation noise			

[A] m = meter, s = second, deg = degrees, rad = radians, N.A. = not applicable

** Initialisation of variables:*
- v_{xm} and a_{xm} set to zero
- a_x set to the initial sensor reading
- θ set to $\sin^{-1}(\frac{a_{x\max}}{g})$
- ω set to $\frac{2\pi}{T}$; T set as explained in 6.4.3
- d set to mean(a_x)
- dT set to 0.01 (sampling frequency =100Hz)

** Noise co-variances:*
The noise level is generally assumed to be 10% of the amplitude of a variable. This percentage could change depending on experimental results. For example, it was increased to 15% for ω of the stroke patient, to accommodate for an expected increase in movement duration.

In general, for a sinusoidal motion, the amplitude (A) of the function of movement acceleration (in equation (6.5)) can be determined by the product of the reach distance (p) and square inverse of movement duration (T), as shown in equation (6.7).

$$A = \omega^2 . p = \frac{4\pi^2 p}{T^2}, \tag{6.7}$$

In this experiment, we set $A = 2$, which represents the maximum amplitude of movement acceleration, as it seemed a fair estimate from Figure 6.4. With little sensor motion artefacts (due to the absence of skin), parameter d was sufficient to account for the offset in sensor acceleration measurement caused by gravity. So, k_1 was set to zero, k_2 set to 1, and the mis-alignment sensor mounting angle was assumed to be constant (see equation (6.3)); implying only a translation of the sensor.

6.4.3 Experiment 2: Healthy upper limb reach experiment

As described in detail in Chapter 4 (section 4.2.3), thirty-nine (9 mm) passive reflective markers were placed on the right and left upper limbs, the trunk, and pelvis of a healthy adult female subject (Subject 1, age 25 years), based on the Vicon Plug-in-Gait marker placement protocol. These markers were tracked using a 12-camera Vicon (MX F40) system. In addition, five Xsens sensors were placed on the same anatomical segments (Figure 6.5); these sensors were also tracked by Vicon through three markers placed on each sensor. While seated, the subject reached forward with the dominant arm to pick up a light object (placed centrally, 24 cm away from the edge of a table), moved her arm 15 cm backwards and then forward again to release the object at its original location.

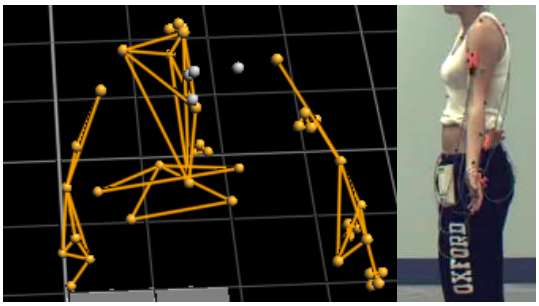

Figure 6.5 The marker/sensor placement on the upper limb of a healthy subject and model in Vicon

The state transition equation and the observation/state vector equation for the EKF are as expressed in equations (6.4) and (6.6) with:

$$f(\omega) \sim A.\cos(\omega t + \pi),\ A = 1,\ k_1 = g\sin(\theta),\ k_2 = 1 \qquad (6.8)$$

In this experiment, we have $A = 1$ as the maximum amplitude of movement acceleration for a healthy subject. This was estimated from equation (6.7) using the known reach distance (measured as 15 cm) and the movement duration from Table 6.1. The movement duration could also be found using the first cycle of sensor motion measurement, or if the sensor data were noisy, this could be supplied by, for example, having the subject touch a pressure pad at each end of the movement. The parameter $k_1 = g\sin(\theta) \neq 0$ as the offset in sensor acceleration is a combination of constant gravity drift *d*, and significant changes in sensor mounting due to skin motion artefact (the latter modelled as a changing θ as in equation (6.3)).

6.4.4 Experiment 3: Upper limb reach experiment for a stroke patient

As described in Chapter 4 (section 4.2.3), thirty-one (9 mm) passive reflective markers were placed on the right and left upper limbs, and the trunk of a male adult patient (age 48 years), 21 months after a stroke. Adjustments to the full marker set previously used were made to adhere with the International Society of Biomechanics recommendations for the upper body, but for consistency the same forearm markers from Experiment 2 were used to track the reach-and-grasp exercise. These markers were tracked using a 12-camera Vicon (TX) system. In addition, three Xsens sensors were placed on the left distal forearm (just above wrist joint), left proximal forearm (just below elbow joint), and left upper arm (Figure 6.6); these sensors were also tracked by Vicon through four markers placed on each sensor. The patient, right side dominant, was asked to reach with his affected left arm to a comfortable position (38 cm away from his body) and then return his arm to the exercise starting point.

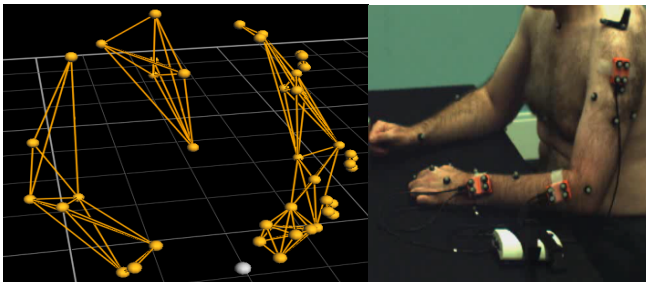

Figure 6.6 The marker/sensor placement on the upper limb of a stroke patient and model in Vicon

The same EKF parameters for Experiment 2 were used, except that some of the state vector noise co-variances were manipulated (values specified in Table 6.2).

6.5 Results

Motion data captured with Vicon for Experiments 1-3 were processed in Vicon Nexus™ 1.4.116, and filtered with the Woltring routine (1995) (see section 4.2.7.3 for more detail). The robot segment movement was tracked with a single marker placed at the top right corner of the mobile robot itself (Figure 6.3). For the healthy subject and the stroke patient, the forearm segment movement was tracked with a marker (as chosen in section 4.4.2, and labelled as RWRB), which is placed on the most caudal-medial point on the ulnar styloid (wrist joint). Data from the sensor mounted on the forearm, near the wrist joint, were used here. Other markers and sensor data were collected for analysis beyond the scope of this work.

6.5.1 Experiment 1: Robot motion experiment

The line (in blue) in Figure 6.7 shows the plot of EKF observations, which are the accelerations of the mobile robot along its longitudinal axis as measured by the sensor. In addition, the EKF prediction of these observations is plotted in red. It is evident that the filter initially makes an error in prediction, but corrects itself within about two seconds (200 samples). This is also shown in the plot of innovation in Figure 6.8, where prediction

errors in acceleration estimation are significantly reduced with time. It should be noted that the small positive peaks of acceleration that occur every 250 samples were not well predicted by the EKF, since these acceleration events were fast so they were perceived as noise by the EKF.

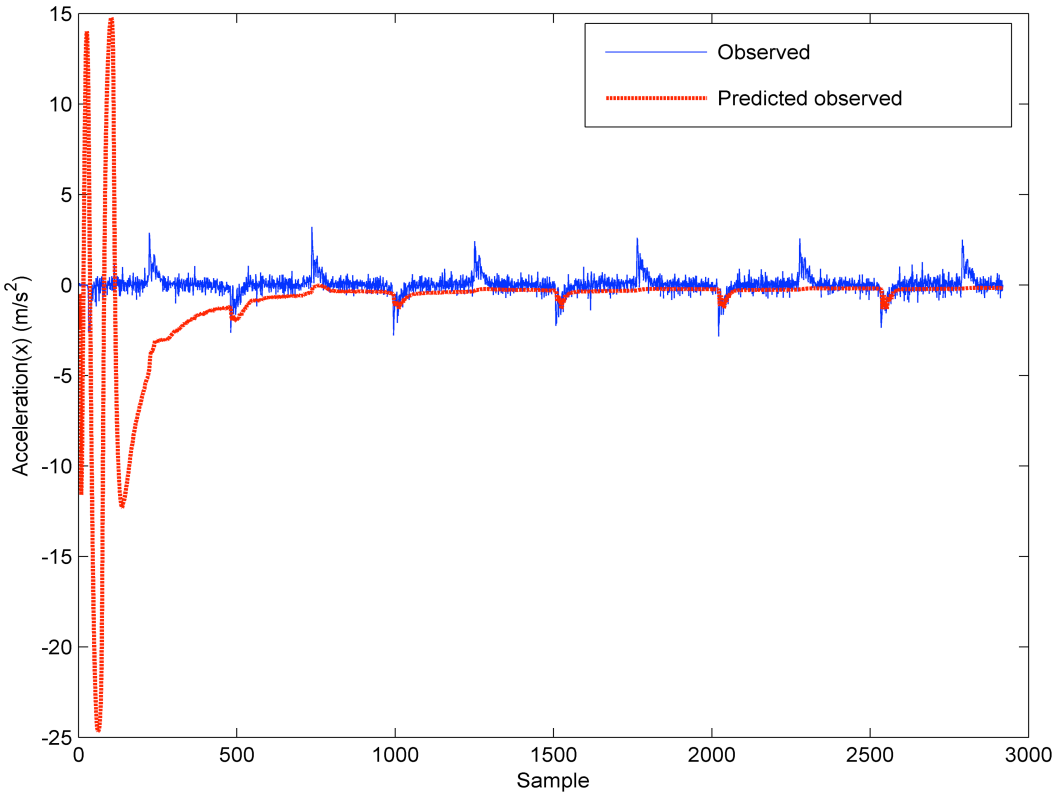

Figure 6.7 Plots of observed (sensor) and Kalman filter predicted accelerations of the mobile robot motion in blue and red lines respectively.

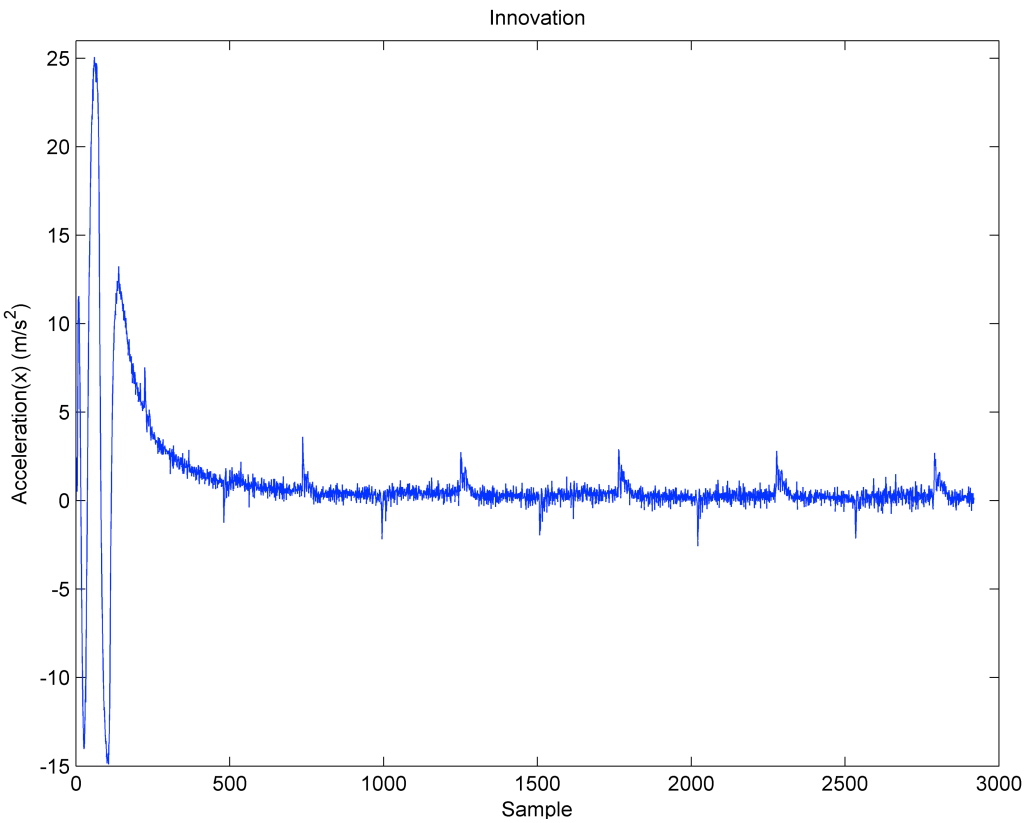

Figure 6.8 Innovation in sensor acceleration of the mobile robot motion. Acceleration prediction error significantly reduces with time.

The Vicon system was considered to be the gold standard for measuring position (Zhou & Hu, 2008), so the reference for comparing velocity estimation for the EKF is the velocity obtained from differentiating positional data obtained by the Vicon system.

Figure 6.9 shows (in blue) the velocity estimate integrated directly from the sensor acceleration observations, independently of the EKF, as compared with the velocity derived from Vicon (in green). Figure 6.10 shows (in red) the velocity estimate from the EKF, again with the Vicon estimate (in green), plotted on the same axes for comparison. Comparing Figure 6.9 and Figure 6.10, it can be seen that the integration drift in velocity was significantly reduced by the EKF. Hence, the EKF appears to perform well on the robot data. The EKF results in Figure 6.10 are similar to those obtained after detrending (Figure 5.35) for the case of the robot, but the EKF is more flexible in its application to non-rigid upper limb movements.

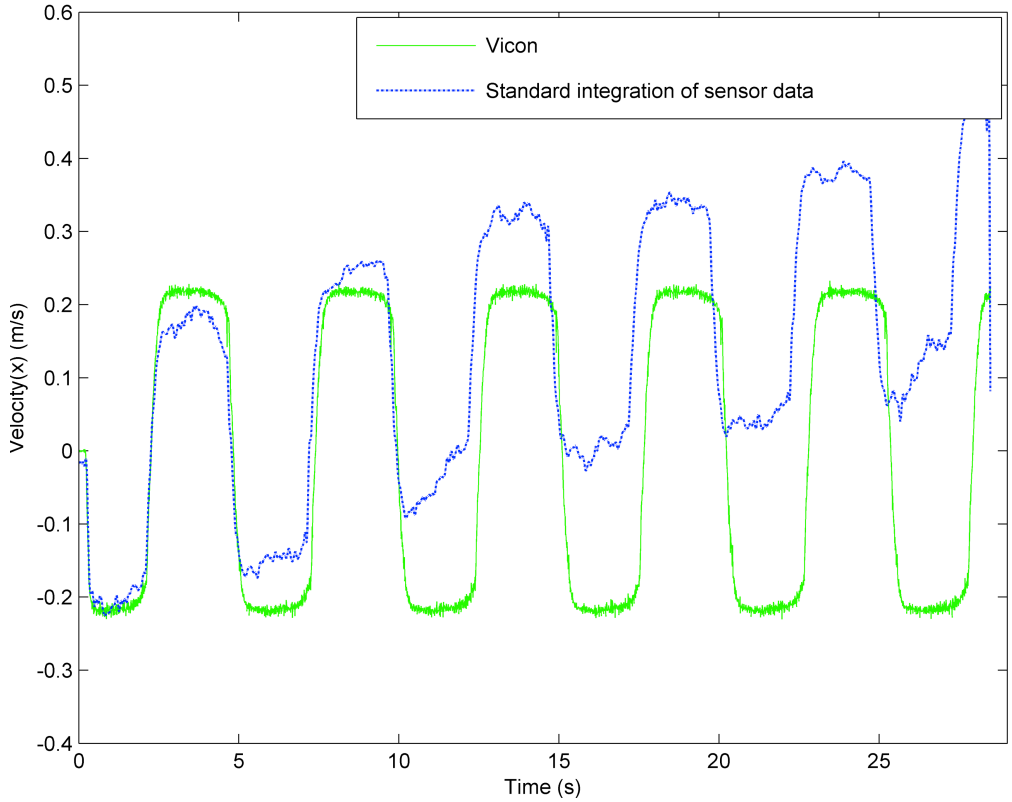

Figure 6.9 Comparison of velocity estimate from the Vicon system (in green) with the standard Simpson integration method (in blue) for the motion of a mobile robot. The difference between the two plots represents integration drift in the velocity estimation.

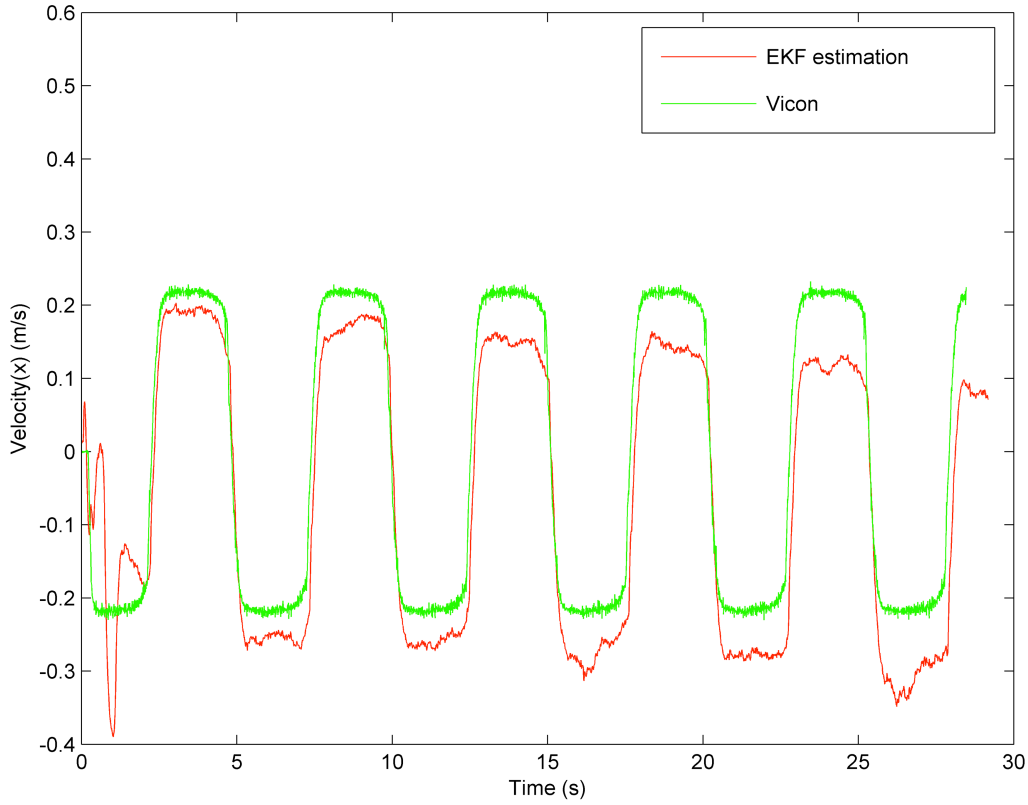

Figure 6.10 Comparison of velocity estimate from the Vicon system (in green) with the Kalman filter (in red) for the motion of a mobile robot. By applying a proper Kalman filter to the sensor robot acceleration data, velocity estimate is stabilised and integration drift has been significantly reduced.

6.5.2 Experiment 2: Healthy upper limb reach experiment

The upper limb reach-and-grasp acceleration data of the healthy subject along the longitudinal axis of the forearm are shown in Figure 6.11 (in blue). Applying the adapted EKF to the forearm reach data, the EKF predicted accelerations are obtained, also shown in Figure 6.11 (in red). It is obvious that some error in amplitude remains, as supported by Figure 6.11 and Figure 6.12. However, the EKF managed to stabilise the velocity estimation for the upper limb data as compared to the velocity estimate from the Vicon system (as shown in Figure 6.12).

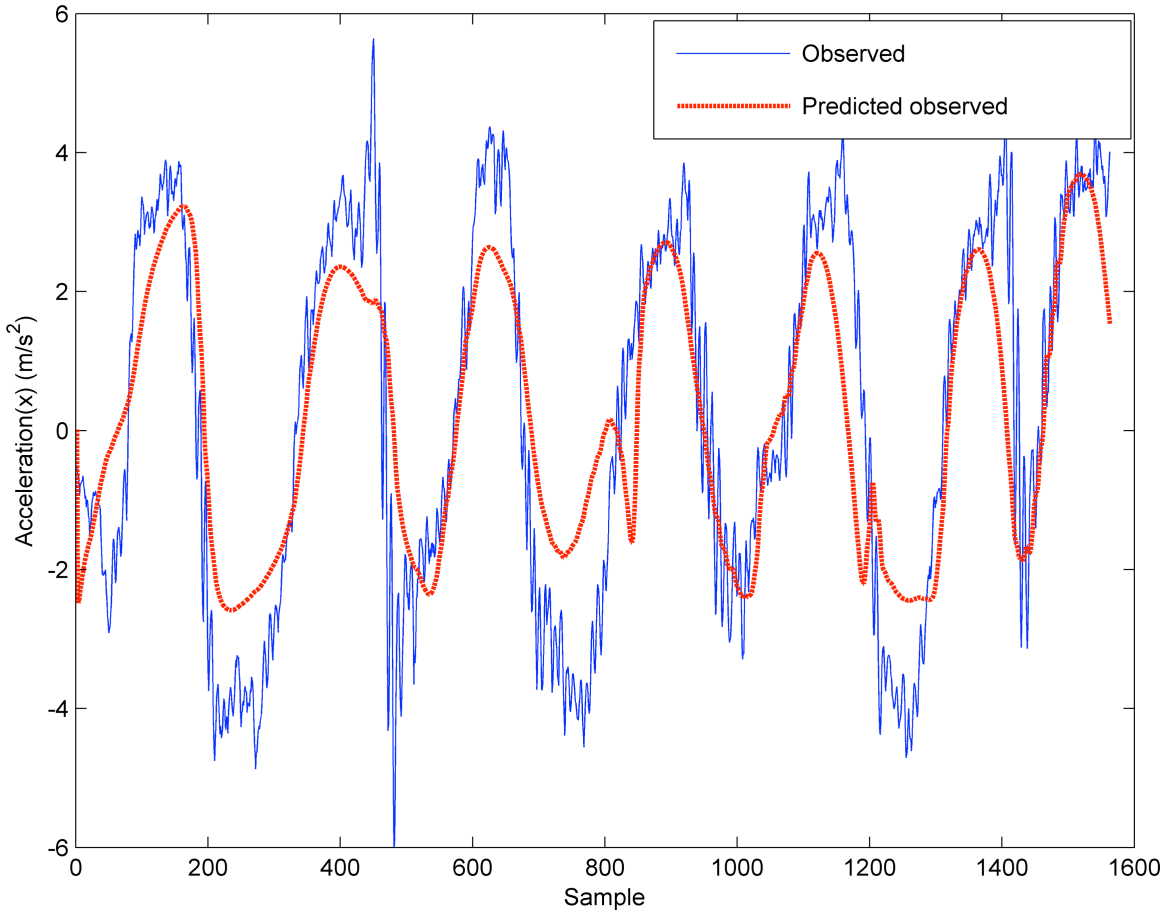

Figure 6.11 Plots of observed (sensor) and Kalman filter predicted accelerations of a healthy subject's forearm reach-and-grasp movement in blue and red respectively.

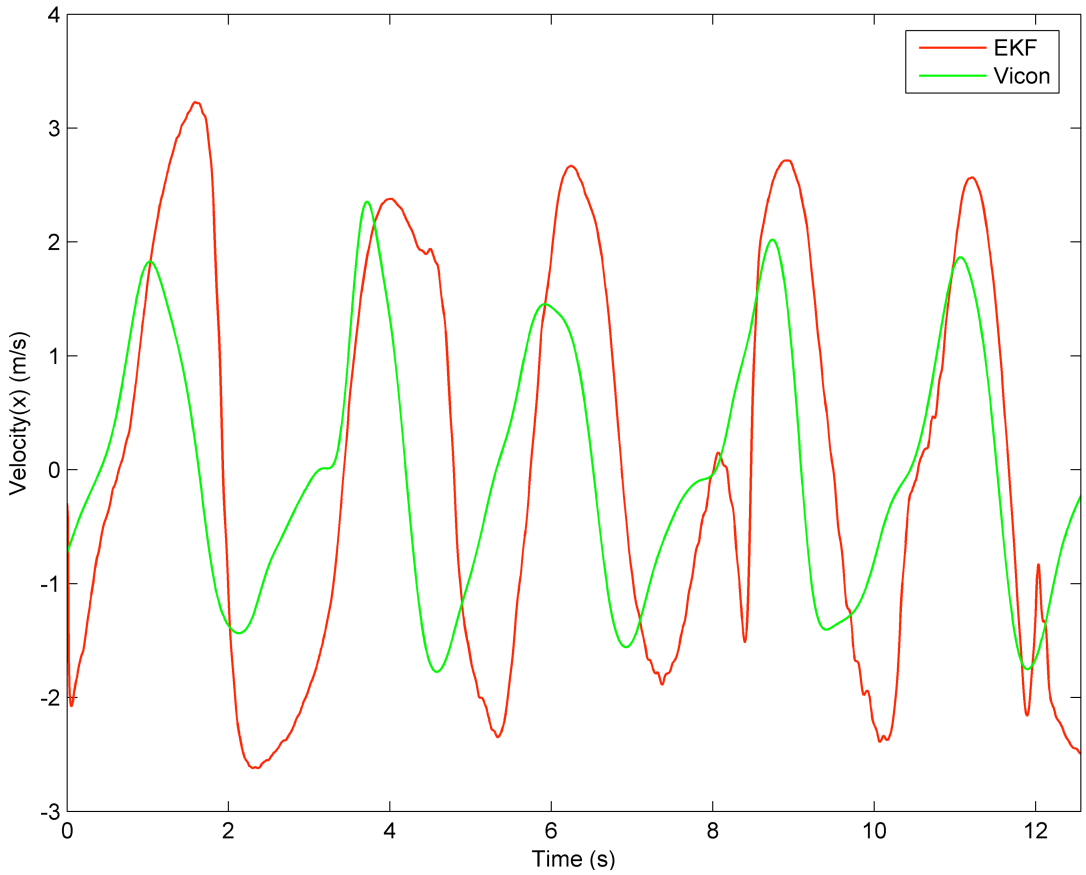

Figure 6.12 Comparison of velocity estimate from the Vicon system (in green) with the Kalman filter (in red) for forearm reach-and-grasp movement of a healthy subject. The velocity estimate is stabilised, but some error in the amplitude remains.

6.5.3 Experiment 3: Upper limb reach experiment for a stroke patient

When the same EKF from Experiment 2 was applied to the forearm reach-and-grasp data of the stroke patient, with some of the state vector noise co-variances manipulated (as specified in Table 6.2), velocity estimation was improved, but not completely stabilised, compared to the observed velocity measurements in Vicon. To address this issue, zero velocity observations were applied at the extremes of the motion (at this stage, the corresponding time instants were estimated from Vicon, but in the absence of Vicon data, this could be supplied by, for example, having the subject touch a pressure pad).

As shown in Figure 6.13, the EKF managed to stabilise the velocity estimation for the upper limb data as compared to the velocity estimate from the Vicon system. A slight phase shift still exists between the two velocity estimates, mainly due a significant difference in the movement duration (hence angular velocity) for the stroke patient between the forward and backward components of the reach movement. Despite a significant stabilisation in the velocity estimate obtained from the EKF, some drift (of mean value -0.56 m/s) continues to exist as an increasing time function. This drift is most apparent after about seven seconds.

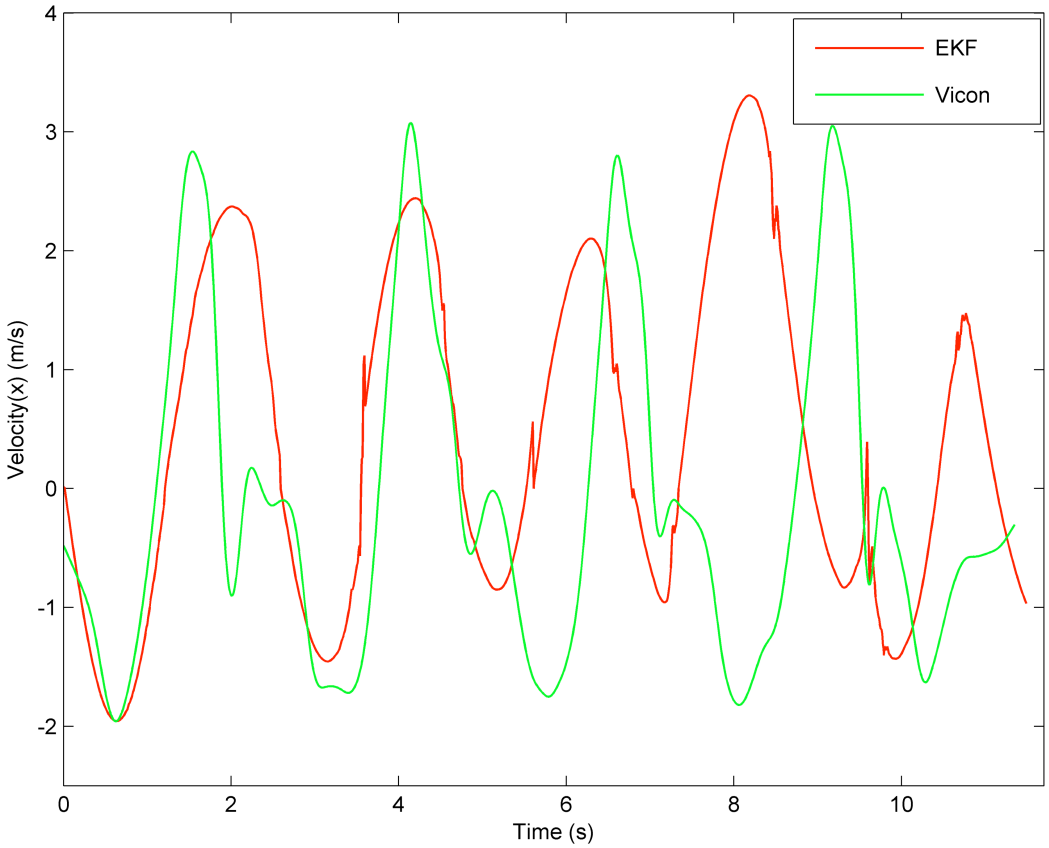

Figure 6.13 Comparison of velocity estimate from the Vicon system (in green) with the Kalman filter (in red) for forearm reach-and-grasp movement of a stroke patient. The velocity estimate is stabilised but further amplitude modulation is required. A slight phase shift exists between the velocity estimates mainly due to a significant difference in movement in the movement duration (hence angular velocity) for the stroke forward and backward components of the reach movement.

Because of the slight time shift between the two signals in Figure 6.13, computing the root mean square error would not be a fair indication of EKF performance. Instead, the velocity

positive peaks were compared before and after Kalman filtering to Vicon's velocity computation. Differences in amplitude are shown in Table 6.3, and indicate that the filter improves drift slightly for cycles 1 and 2; and more so for cycle 4 of the movement. It is worth mentioning that the pre-Kalman filter velocity data given in Table 6.3 are obtained from integrating the sensor accelerometer data after median filtering and detrending. The movement duration and percent time to maximum velocity were not similarly compared at this stage, because of the phase shift in the velocity signals. One possible improvement to address this would be to constrain the movement period.

Table 6.3 Differences in the amplitude of velocity positive peaks before and after Kalman filtering across the four movement cycles

cycle	Amplitude difference of velocity positive peaks [m/s] (as compared to Vicon)	
	Pre-Kalman filter	**Kalman filter**
1	0.465	0.463
2	0.682	0.634
3	0.098	0.701
4	0.873	0.255

6.6 Optimisation estimator

As introduced in section 6.1, a second signal processing method which is based on the least squares theorem and uses optimisation of all available sensor data, is applied to one data set to compare with the performance of the EKF method. The optimisation technique incorporated the uni-axial sensor measurements of acceleration, and a similar sinusoidal, periodic model to the one used by the EKF method, to produce velocity estimation of the motion of the forearm, during repetitive reach-and-grasp motion of a healthy upper limb.

6.6.1 Optimisation estimator design

Model: The movement was modelled as a periodic one dimensional acceleration along the longitudinal sensor axis (x), as in equation (6.1).

Definition of variables: The variables, included in the optimisation estimator are the same as those previously defined in section 6.4.1, along with the time difference between samples (ΔT) and the sample number (k).

Given the sinusoidal assumption of the reach-and-grasp movement acceleration along the longitudinal axis, velocity estimation should ideally follow equation (6.10).

$$\begin{aligned} v_{xm_{k+1}} &= v_{xm_k} + \Delta T . a_{xm} \\ &= v_{xm_k} + \Delta T \cos(\omega . t) \\ &= v_{xm_k} + \Delta T \cos(\omega . k . \Delta T) \end{aligned} \tag{6.9}$$

$$v_{xm_{k+1}} - v_{xm_k} - \Delta T \cos(\omega . k . \Delta T) = 0 \tag{6.10}$$

However, the optimisation algorithm also incorporated all the sensor acceleration-x measurements, (z), from the initial iteration of the algorithm. The relationship between the sensor acceleration measurement and movement velocity is shown in equations (6.11) – (6.13).

$$z = a_x = a_{xm} + g \sin\theta \tag{6.11}$$

$$z_{k+1} = a_{x_{k+1}} = \frac{v_{xm_{k+1}} - v_{xm_k}}{\Delta T} + g \sin(\theta_{k+1}) \tag{6.12}$$

$$a_{x_{k+1}} - \frac{v_{xm_{k+1}} - v_{xm_k}}{\Delta T} - g \sin(\theta_{k+1}) = 0 \tag{6.13}$$

The optimisation is completely described in equation (6.14), given the values of the time difference, gravity constant, and angular frequency of the movement (as in Table 6.2, ΔT = 0.01 second; $\omega \sim 2$ radians/second). The algorithm attempts to estimate velocity accurately, such that the overall errors of the movement model and the observations are minimised.

$$\begin{bmatrix} v_{xm_1} - v_{xm_0} \\ v_{xm_2} - v_{xm_1} - 0.01\cos(0.02) \\ \vdots \\ v_{xm_{k+1}} - v_{xm_k} - 0.01\cos(0.02 * k) \\ \\ a_{x_1} - \dfrac{v_{xm_1} - v_{xm_0}}{0.01} - 9.81\sin(\theta_1) \\ a_{x_2} - \dfrac{v_{xm_2} - v_{xm_1}}{0.01} - 9.81\sin(\theta_2) \\ \vdots \\ a_{x_{k+1}} - \dfrac{v_{xm_{k+1}} - v_{xm_k}}{0.01} - 9.81\sin(\theta_{k+1}) \end{bmatrix} = 0 \qquad (6.14)$$

Velocity samples for the entire movement were initialised in equation (6.14) by integrating all the sensor acceleration measurements following high pass filtering. Samples of the misalignment sensor mounting angle were initialised from the instantaneous rotation matrix, relating the sensor local and global coordinate systems (the rotation matrix was obtained from the updated roll, pitch, and yaw angles estimated by the sensor).

6.6.2 Healthy upper limb reach experiment

To start with, the optimisation algorithm estimated both movement velocity and the misalignment sensor mounting angle, taking into account the corresponding initial values for the entire movement, and all sensor acceleration measurements. Despite achieving convergence in the estimator's solution, allowing the misalignment sensor mounting angle to vary within the solution led to the cancellation of measurement noise. Hence the over-riding influence on the velocity estimation was the movement model itself, producing a perfect sinusoid.

To address this problem in measurement noise cancellation, the misalignment sensor mounting angle was incorporated into the optimisation algorithm shown in equation (6.14), and only movement velocity was estimated. This partially reduced the integration drift in

velocity estimation; however, a substantial drift remained. Zero velocity observations were then applied at the extremes of the motion (as was previously done in section 6.5.3, and found to reduce the remaining drift). Results of the optimisation estimator, shown in red in Figure 6.14, were compared to the velocity estimate from Vicon (Figure 6.14, in green). The velocity estimate from the optimisation method was found to stabilise. Very small integration drift was noticeable (a mean value of -0.076 m/s). The velocity estimate from the optimisation method compared well to the velocity estimate obtained from Vicon over the five trials, in terms of the velocity's peak-to-peak value, movement duration, and percent time to maximum velocity (an error analysis of the optimisation method, as compared to Vicon, is given in Table 6.4). Almost no phase shift was found between the velocity estimate plots (Figure 6.14, in green and red respectively), but there was an offset value of -0.9 m/s, which existed over the entire movement. This offset meant that the optimisation method did not reliably report the amplitude of velocity (the minimum and maximum values). One possible improvement to address this offset and improve the velocity estimation would be to apply boundary constraints to the optimisation.

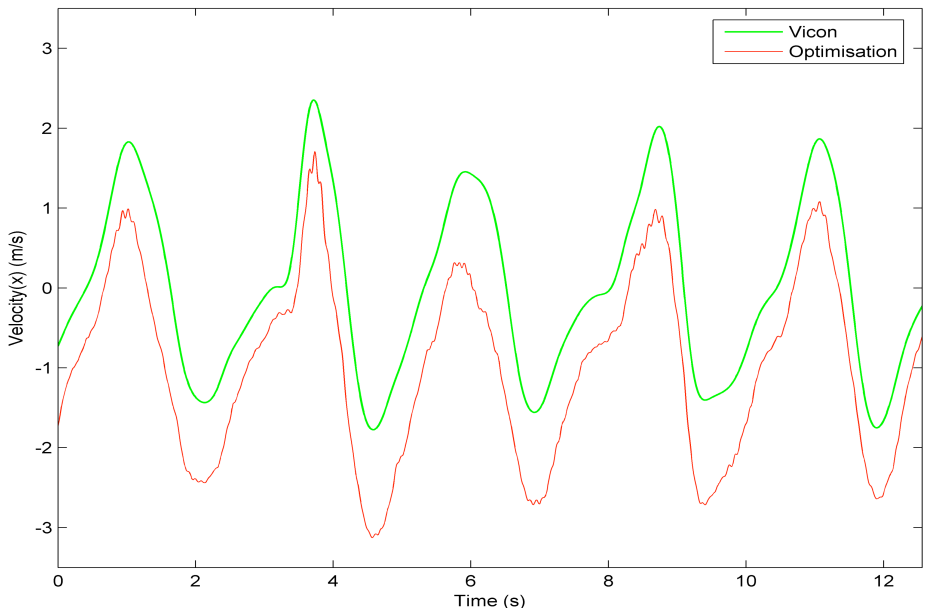

Figure 6.14 Comparison of velocity estimate from the Vicon system (in green) with the optimisation estimator (in red) for forearm reach-and-grasp movement of a healthy subject. The velocity estimate is stabilised, very small integration drift (mean value of -0.076 m/s) remain. Almost no phase shift between the two plots but there is an offset value of -0.9 m/s.

6.7 Comparison of the EKF and optimisation techniques

The performance of the EKF method (section 6.5.2) and optimisation technique (section 6.6.2) for the estimation of velocity was compared for the reach-and-grasp movement. Velocity estimates obtained from Vicon for the healthy subject acted as a gold standard. The values of velocity peak-to-peak and amplitudes of the velocity positive peaks were computed from the velocity estimates of the EKF and optimisation methods. Also, the clinical metrics, movement duration and percent time to maximum velocity, were calculated from the velocity estimates of both methods. These four quantities were then compared for each method to Vicon's computations. Results of the error analysis, computed as the error mean and standard deviation over five consecutive movement cycles are given in Table 6.4.

Overall, the mean and standard deviation of the estimation errors were found to be smaller for the optimisation technique than the EKF method. This was true for all four quantities (as given in Table 6.4), except for the mean error in peak amplitude, which was similar for both methods. This implies that the optimisation technique provided more accurate results than the EKF method, to estimate outcome measures for this data set. Findings were as was expected, given that the optimisation technique bases its velocity estimation on all available sensor measured data at every iteration, and throughout the entire run of the optimisation algorithm. The optimisation technique was also found to produce much smaller integration drift, and a more stable velocity estimate. There was almost no phase shift between the velocity estimate from the optimisation and velocity obtained from Vicon (Figure 6.14), which was an improvement compared to the results of the EKF algorithm (Figure 6.12). However, the EKF method provided an instantaneous estimation of velocity, rather than an offline (batch) estimate, as provided by the optimisation technique.

So the EKF algorithm could be integrated in an interactive system, to respond with the user during exercise, or to provide real-time feedback of exercise performance.

Table 6.4 Error Analysis to compare the performance of the EKF and optimisation techniques (when compared to Vicon)

		Error Analysis (compared to Vicon)	
		EKF	**Optimisation**
Movement duration [sec]	**μ**[a]	0.048	0.020
	σ[a]	0.253	0.066
Percent to maximum velocity [%]	**μ**	5.104	2.087
	σ	4.817	3.810
Velocity positive peak amplitude [m/s]	**μ**	0.808	0.893
	σ	0.535	0.199
Velocity p-p[b] **[m/s]**	**μ**	1.469	0.172
	σ	0.756	0.299

[a] **μ** is the error mean value; **σ** is the error standard deviation for the five cycles
[b] p-p is the peak to peak value defined as the magnitude of range (minimum to maximum value) of a given quantity

6.8 Discussion

Initialisation of the state vector variables of the EKF and corresponding noise co-variances is vital for filter stability. The initialisation adopted in this work (as given in section 6.4.2) is realistic, with parameters attainable either from the movement set-up or the first trial of sensor motion measurements. In this chapter, the reach-and-grasp movement was modelled as a one dimensional motion for simplicity, considering only motion along the longitudinal sensor axis (x). However, a true representation of the upper limb movement would incorporate three dimensional motion. An extension of this work would be to model the three dimensional movement in the state transition equation employed by the Kalman filter. Also, the reach-and-grasp movement has been considered as a primarily linear motion, but it is usually accompanied by a rotation at the elbow (elbow abduction/adduction). So, incorporating the gyroscopic measurements into the EKF observations (to estimate that rotation) could help stabilise the velocity estimate even further.

A strength of the EKF algorithm is that, despite the assumption of simplified sinusoidal movement, the Kalman filter coped well when applied to the mobile robot motion data, which was periodic but not truly sinusoidal (see Figure 6.4). The filter produced encouraging results when applied to human motion data for a healthy subject and a stroke patient, but only after slight modifications. The asymmetry of the reach motion in its forward and backward components for the stroke patient, and an increasing movement duration (i.e. having a non-uniform angular velocity) could be included in the filter; possibly through an adaptive angular velocity of the sinusoidal movement acceleration rather than a constant one, as is the case now.

While the EKF filter helped stabilise movement velocity estimation for the stroke patient, other stroke patients might have movement velocity profiles that are completely non-periodic or extremely jerky, so further testing of the algorithm is needed to see if it is applicable for a broader range of patients.

It should be noted that the Kalman filter did not completely eliminate the drift in velocity estimation, as our assumption of a constant gravity component (thereby constant integration drift in velocity) throughout the entire reach movement was not completely accurate. As shown in Figure 6.9, this drift linearly increases with time. However, this EKF drift estimate could be improved by supplying position information to the filter at particular time points during the reach-and-grasp exercise.

To improve the robustness of the EKF algorithm, the movement model could be improved and refined by taking into account the above points, including manipulating the noise co-variances for the variables in the EKF state vector, and incorporating the gyroscopic

measurements to the filter observations. It would then be worth checking whether the further improved velocity estimate (obtained from the revised EKF) could meet the requirements of the 68% or 95% confidence interval sensitivity tests as in Chapter 5, and allow the monitoring system (inertial sensors and signal processing algorithms) to also report reliably on movement velocity. The performance of the EKF method on other exercises, such as hand-to-mouth and forearm pronation/supination, is also of interest.

In this chapter, an optimisation estimator was also applied to the upper limb motion data of a healthy subject, during repetitive reach-and-grasp motion. The estimator incorporated the sensor acceleration measurements for the entire movement, and the misalignment sensor mounting angles (obtained from the sensor orientation estimation). After zero velocity observations were applied, the estimation of movement velocity stabilised, and very small integration drift was found (mean value of -0.076 m/s). There was a promising lack of phase shift between the velocity estimate from the optimisation and that obtained from Vicon. Also, the optimisation was found to report reliably on the velocity's peak-to-peak value, movement duration and percent time to maximum velocity.

However, an offset was found between the velocity estimate of the optimisation method and data obtained from Vicon. This offset caused the velocity's amplitude (minimum and maximum values) to be inaccurate. The offset could be dealt with, and the estimation of velocity improved, by constraining the optimisation with boundary conditions. Finally, the performance of the optimisation method when applied to the motion data of the stroke patient should be investigated.

6.9 Summary

Gravity has been shown to distort sensor acceleration measurements, with the greatest effect on movement with low acceleration. Eliminating this effect was not straightforward due to changes in the orientation of the sensor over time during any given movement. This led to an erroneous accelerometer reading, hence integration drift when estimating movement velocity by direct integration. However, by applying a proper Kalman filter that exploited the repetitive nature of upper limb movement, like the EKF demonstrated in this chapter, drift was significantly reduced and the velocity estimate stabilised. This EKF was developed from the two dimensional simulated reach-and-grasp movement of a mobile robot. The EKF coped well when applied to the mobile robot motion, which was periodic but not truly sinusoidal.

Encouraging results were also demonstrated on the reach-and-grasp motion data of a healthy subject, and on data of a stroke patient. Velocity estimation was also obtained from an optimisation method, which was applied to healthy upper limb motion data. The optimisation method produced stable velocity estimates (mean integration drift of -0.076 m/s). The optimisation was found to reliably report on velocity peak-to-peak values, movement duration, and percent time to maximum velocity. Almost no phase shift was found between the velocity estimate and the Vicon data, but there was an offset value of -0.9 m/s over the entire movement. This offset meant that the optimisation method did not reliably report on the amplitude of velocity (minimum and maximum values).

Comparing the EKF method and the optimisation technique, the mean and standard deviation of the estimation errors were found to be smaller for the optimisation technique than the EKF method, except for the mean error of the velocity positive peak amplitude,

which was similar for both methods. This implied that the optimisation technique provided more accurate results than the EKF method, to estimate outcome measures for this data set. However, the EKF provided an instantaneous estimation of velocity, compared to the offline (batch) optimisation method.

The two signal processing methods could suit different scenarios and applications. While the instantaneous model-based EKF estimator could offer real-time feedback (for example the use of velocity estimation to monitor stroke patients during their exercises), the optimisation algorithm could possibly give more accurate results as an offline method, but at the expense of real-time feedback.

Further refinement of the EKF is required to improve the performance of the filter, and to allow accurate measurement of movement velocity in a clinical context. Also, the performance of the optimisation could be further improved and tested on the motion data of the stroke patient.

Chapter 7 Conclusions, Recommendations, Limitations and Suggested Further Research

7.1 Conclusions

Research investigating recovery following stroke is an ongoing process, but there is evidence to suggest that recovery of functional movement depends on rehabilitation strategies employed (Mahmood *et al.*, 2009, Van Peppen *et al.*, 2004, Zhou, Hu, Harris *et al.*, 2006). In clinical practice, daily exercises are implemented and reviewed depending on the patient's progress. Current healthcare services that monitor progress in rehabilitation are costly, as upper limb impairment or loss of function is assessed by clinical examination tests, or kinematics computed from laboratory-based motion capture systems. For reasons detailed in Chapter 1, neither method is suitable for use in a non-clinical environment.

There is a need to improve the consistency and objectivity in measuring outcomes, through use of a relatively low cost, compact, and easy-to-use monitoring system. This work exploits the technological improvements in wearable inertial sensors and signal processing algorithms, with a view to augment current rehabilitative interventions, by providing feedback on rehabilitation progress, and supporting rehabilitation in an environment which is accessible to stroke patients. The system (inertial sensors combined with improved

sensor signal processing) would not only be applicable in a clinical research setting, but could potentially be part of a home-based rehabilitation programme.

The primary focus of this thesis was on measuring forearm motion. Three upper limb movements were measured using a laboratory-fixed, multi-camera motion capture system (Vicon) and a number of wearable Xsens inertial sensors. The movements, typical of stroke rehabilitation, were reach-and-grasp, forearm pronation/supination and hand-to-mouth. A surface marker system was selected, and considerations for nominal marker placements to capture upper limb movements were identified. Following this, the forearm was modelled as a single segment, and absolute forearm kinematics were computed to correspond to the absolute sensor measurements obtained at the forearm.

Motion regimes were characterised for four healthy subjects and a stroke patient for the movements (identified above) using Vicon. From this, variables including forearm linear motion (position) and its derivatives, and forearm rotational motion (orientation) and its derivative were calculated. In addition, three clinical kinematic measures were computed - average velocity, movement duration and percent time to maximum velocity. Given the gold standard to compare sensor measurements against was data acquired from Vicon, these motion variables and clinical kinematic measures defined the specifications of accuracy and sensitivity for wearable monitoring of the forearm, while performing the functional movements.

The specifications helped to determine whether the wearable motion sensors were suitable (accurate and sensitive enough) to measure the functional movements, and quantify the movement differences in pre/post- stroke intervention. The dynamic and static

measurement accuracy of Xsens inertial sensors in linear and rotational motion were first determined for rigid body tracking with known movement parameters, particularly for orientation estimation. This was done using a mobile robot simulating a two dimensional "reach" movement of a healthy upper limb, and a bar rotating about its centre at pre-defined requirements of linear and angular velocities (motion regimes representing reach-and-grasp and forearm pronation/supination). The sensor accuracy and sensitivity (68% and 95% confidence error intervals) were also determined for measuring the forearm motion of a stroke patient while performing reach-and-grasp and hand-to-mouth movements. Comparing the sensor accuracy and sensitivity to the accuracy and sensitivity requirements determined earlier, it was shown that the raw sensor measurements could reliably report on acceleration, angular velocity and orientation, but some pre-processing was needed. Simple signal processing methods, such as high-pass filtering and removing the gravity DC offset (bias), were presented to manage the sensor measurement errors, and increase the system's performance.

Results for the stroke patient showed good agreement between the inertial sensors and the Vicon multi-camera system in pre-stroke intervention for both movements. Before pre-processing the sensor data, accelerations contained a gravity bias, hence linear velocity estimation obtained by integrating the sensor accelerations suffered from integration drift. There were errors in orientation estimation by the sensor, mainly when the angle was small, probably caused by a lack of sensor resolution, and from gyroscopic readings (angular velocities) susceptible to drift over time. Detrending or high-pass filtering and detrending were found to be sufficient to reduce these errors in acceleration, orientation and angular velocity.

In addition, the sensor sensitivity was found to be suitable with varying confidence extents for acceleration, angular velocity and orientation measurements for the reach-and-grasp and hand-to-mouth movements, after the simple signal processing methods (detrending or high-pass filtering and detrending) were implemented. Despite the pre-processing of linear velocity, it was not accurately estimated from the sensor accelerometer readings, and was not reliably reported for either movement, even within the lower 68% confidence interval.

In terms of clinical outcome measures, movement duration was accurately estimated from the sensor accelerometer measurements. Also, the change of movement following stroke intervention was detected by the decrease in the standard deviation of movement duration.

However, the problem of integration drift affecting velocity was not resolved. This led to the development of a model-based method, suitable for cyclic movements, to improve the velocity estimation from the accelerometer measurements, for the reach-and-grasp movement. The method employed data integration using Extended Kalman filters (EKF), and application of motion constraints. For simplicity, the reach-and-grasp movement was modelled as a one dimensional sinusoidal motion, mainly considering it along the longitudinal sensor axis (x).

Eliminating the effect of gravity on sensor acceleration measurements was not straightforward, due to changes in the orientation of the sensor over time during any given movement. A strength of the EKF algorithm was that it coped well when applied to the simulated "reach" movement of a mobile robot, which was periodic but not truly sinusoidal. Encouraging results were also demonstrated when the EKF method was applied to healthy, and pathological motion data (of a stroke patient), measured by a sensor on the

forearm while performing reach-and-grasp. This showed that by applying a proper Kalman filter, that exploited the repetitive nature of upper limb movement, integration drift could be significantly reduced, and the velocity estimate stabilised. However, further refinement could improve the performance of the filter even further.

A second technique of signal processing was applied to one data set, to compare with the performance of the EKF method. This optimisation technique was developed on the motion data of a healthy subject. Results indicated a favourable performance, particularly with respect to the values of velocity peak-to-peak, movement duration, and percent time to maximum velocity, as well as a reduction in integration drift in velocity estimation. However, an offset was apparent in the absolute velocity output. This offset could potentially be removed by applying boundary constraints to the optimisation, allowing accurate estimation of absolute velocity.

The two signal processing methods appeared to produce encouraging results in the estimation of velocity, and reduction of integration drift. Given their characteristics, the methods could suit different applications. Further work needs to be done to obtain reliable estimates of velocity, and explore the potential benefits of the two methods.

Long-term or potential outcomes of the work are that the improved sensor measurements may be used to provide a visual display of movement, or to determine kinematic quantities relevant to the performance of the exercise (as in (Caimmi *et al.*, 2008)). Consequently, the system would potentially be able to inform patients and physiotherapists objectively about progress, increasing patient motivation (Caimmi *et al.*, 2008, Cozens & Bhakta, 2002, Maclean *et al.*, 2002), and improving consistency in assessment and reporting of outcomes.

The methods developed in this work are extendable to other limb segments. These methods are also relevant in other areas such as gait analysis, and wearable monitoring and feedback for certain healthy populations (e.g. the elderly), or patients with other cerebro-vascular or neurological diseases (such as cerebral palsy and multiple sclerosis). The methods are also relevant to the area of sports sciences, to monitor the performance of athletes in top condition, or after sports injuries. The movement regimes for the different study groups, and regimes specific of other exercises need to be investigated.

7.2 Thesis contributions and recommendations

7.2.1 Thesis contributions

A computational method was developed and implemented (in Chapter 4) to describe the kinematic associations of the forearm segment. The method was based on motion data measured by Vicon, and applied to the Vicon motion capture system, and a number of Xsens wearable inertial sensors. Motion regimes for the three movements reach-and-grasp, forearm pronation/supination and hand-to-mouth were characterised.

Using the data measured with the Vicon system, specifications of accuracy and sensitivity for wearable devices were determined. The measurement accuracy for accelerometers is recommended to be high. The device should be able to measure accelerations as small as 0.001 m/s^2, with an upper limit of measuring at least 9 m/s^2 for the case of jerky movement. Gyroscopes should also measure angular velocities as small as 2.20 rad/s, and as large as 9.02 rad/s. To detect differences in forearm movement between pre- and post- stroke intervention, the minimum sensitivity requirement for accelerometers and gyroscopes was found to be in the order 0.5 m/s^2 and 0.1 - 0.5 rad/s respectively. Changes in functional movements in pre/post- stroke intervention, due to frequent exercise at home, were

detectable by the two clinical metrics movement duration and percent time to maximum velocity.

The usefulness and reliability of the Xsens system, measured in terms of accuracy and sensitivity, were established to track the movements – reach-and-grasp, forearm pronation/supination, and hand-to-mouth, suggesting it is a suitable monitoring system in a clinical setting, and a potential candidate to be integrated in a home-based rehabilitation programme.

Signal processing methods to reduce the effect of error sources, and improve the raw sensor measurements were recommended. By simply detrending, or detrending and high pass filtering sensor motion data, the sensors were able to reliably report on movement acceleration, angular velocity, and orientation, with varying degrees of confidence. Linear velocity estimation required stabilisation, to reduce integration drift. But model-based estimation (for example EKF filters) and optimisation techniques demonstrated encouraging results to stabilise the velocity estimate for the reach-and-grasp movement, over a limited number of subjects.

Journal Publications

Nour Shublaq, Penny Probert Smith, Julie Stebbins, Jane Burridge, Anne Marie Hughes. Determination of the Measurement Accuracy and Sensitivity of NonInvasive Wearable Inertial Sensors to Measure Pathological Upper Limb Motion of Stroke Patients. *Journal of Dynamic Systems, Measurement and Control* (in preparation).

Nour Shublaq, Penny Probert Smith, Julie Stebbins. Meauring Arm Reach-and-Grasp Movements with Accelerometers in Rehabilitation: A Kalman Filter to Stabilise Velocity Estimate. *The IEEE Journal of Neural Systems and Rehabilitation Engineering* (under review).

Shublaq, N MSc, Smith Probert P Dr, Stebbins J Dr, Buckingham R FRCS. A protocol to assess upper limb movements during stroke rehabilitation, *Gait and Posture*, vol 28, Issue 0, pp. S30 – S31, September 2008

Conference Proceedings/Presentations

N. Shublaq, P. Probert Smith, J. Stebbins. The Reach of a Mobile Robot Modelled Mathematically to Stabilise Velocity Estimate from Accelerometers: Implications in Stroke Rehabilitation. *The 2nd Joint Annual Conference of the European Society for Movement Analysis for Adults and Children Conference ESMAC (19th annual meeting) and Gait & Clinical Movement Analysis Society GCMAS,* 12-15 May 2010 (poster presentation, Hyatt Regency Miami, Miami, Florida, U.S.A.)

Geraldine Fitzpatrick, Madeline Balaam, Lesley Axelrod, Eric Harris, Graham McAllister, Anne Marie Hughes, Jane Burridge, Thomas Nind, Ian Ricketts, Anna Wilkinson, Sue Mawson, Stefan Rennick Egglestone, Tom Rodden, Penny Probert Smith, **Nour Shublaq**, Zoe Robertson. Designing for Rehabilitation at Home, *Proceedings of Workshop on Interactive Systems in Healthcare (WISH@CHI2010),* 11 April 2010 (oral presentation, Atlanta, Georgia, U.S.A.)

Nour Shublaq, Penny Probert Smith, Julie Stebbins. Use of a Mathematical Model to Improve Accelerometer Output during Stroke Rehabilitation, *Proceedings of the 2nd Bioengineering 2009 Conference,* 24-25 September 2009 (oral presentation, Keble College, Oxford, United Kingdom)

N. Shublaq, P. Probert Smith, J. Stebbins. Informing patient, carer, and professional in improved stroke rehabilitation, *Proceedings of the 5th IEEE EMBS UK & Republic of Ireland Postgraduate Conference on Biomedical Engineering and Medical Physics 2009 (PGBioMed'09),* 12-14 July 2009 (oral presentation, Magdalen College, Oxford, United Kingdom)

Nour Shublaq, Penny Probert Smith, Julie Stebbins. Informing patient, carer, and professional in improved stroke rehabilitation: Feedback in the exercise rehabilitation regime, *Proceedings of the International Society of Biomechanics 2009 Conference (ISB 2009),* 5-9 July 2009 (poster presentation, Cape Town, South Africa)

Egglestone, Stefan Rennick; Axelrod, Lesley; Nind, Thomas; Turk, Ruth; Wilkinson, Anna; Burridge, Jane; Fitzpatrick, Geraldine; Mawson, Sue; Robertson, Zoe; Hughes, Anne Marie; Ng, Kher Hui; Pearson, Will; **Shublaq, Nour**; Probert-Smith, Penny; Rickets, Ian; Rodden, Tom. A design framework for a home based stroke rehabilitation system: identifying the key components', *IEEE Conference Proceedings of the 3rd International ICST Conference on Pervasive Computing Technologies for Healthcare 2009,* 1-3 April 2009 (oral presentation, London, United Kingdom)

7.2.2 Recommendations for use of inertial sensors

The effect of environmental conditions, and possible external magnetism on sensor operation and data collection were investigated. Appropriate and practical considerations are provided below, as to the best conditions for sensor operation and data collection.

- To reduce the drift in gyroscopic readings, it is advisable to initially warm up sensor electronics for 15 minutes and leave the sensor for a rest period of two minutes between trials, so gyroscopes can settle down. Also, gyroscopes should not experience a major change in the temperature of the surroundings.

- To help reduce the effect of integration drift on sensor orientation estimation, it is recommended to keep the sensor away from any magnetic disturbance sources. So the force plates should be turned off, and ferromagnetic material should be kept to a minimum.

- To help reduce the bias of sensor accelerometer data due to gravity (and its effect on velocity estimation), particular attention should be given to initial sensor positioning and mounting methods. The use of double-sided tape was established in this work as a suitable sensor mounting method.

- Accelerometers and gyroscopes might require some time to settle down and reach steady state (about one second). So if either were to be used clinically, the settling time should be considered.

The bias of sensor accelerometer data due to gravity could lead to integration drift in the velocity estimation. Therefore, the sensors do not report reliably on velocity, more so for complex exercises. This gravity bias could be dealt with by data pre-processing (high-pass filtering with median filters and detrending), and application of model-based estimation methods (Kalman filters) or optimisation techniques.

Finally, the internal sensor consistency of the accelerometers and gyroscopes was found to be high with a root mean square error of 0.24 m/s^2. For measuring small movements, the sensors could sometimes be more suitable than Vicon, given their limited measurement bandwidth, and the need to attenuate high frequency noise components on motion data from the latter.

7.3 Limitations and suggested further research

7.3.1 Biomechanical modelling and markers

The accuracy of forearm segment characterisation in Vicon, and hence how good is this gold standard, is dependent on accurate marker placement. Marker placement errors can be due to either improper marker attachment on bony landmarks, or marker movement due to skin motion.

A suggested method to determine marker placement errors is to compute the coordinates of particular joints from marker motion data measured in Vicon, and compare these to the joints' real locations using imaging (for example Magnetic Resonance Imaging (MRI)). Assessing intra subject repeatability might also help quantify marker placements errors, when comparing the kinematics of the same individual over multiple testing sessions.

7.3.2 Movements and outcome measures

A better understanding of the clinical relevance of different functional movements, particularly reach-and-grasp, forearm pronation/supination, and hand-to-mouth, should be established. Also, addressing whether the metrics of performance suggested in this work are clinically meaningful, and which metrics - if any - do in fact inform physiotherapists about progress during rehabilitation.

Trunk movement affects stability, a major problem with most stroke patients. It also affects the performance of upper limb tasks. Therefore, trunk movement is worth measuring (as inclination relative to a fixed plane, for example a chair) with the sensors, as it might be a useful feedback metric to patients during their exercises.

7.3.3 Sensor accuracy and sensitivity

It is possible that there are better alternatives to double-sided tape for securing the sensors. The effect of several different mounting methods (Velcro straps, elastic bandages, etc…), and positioning strategies (uncertainty in origin, and orientation) on sensor measurement accuracy and sensitivity requires proper investigation. This could be determined, first on a rigid body and then on a human forearm. A sensor mounting and positioning protocol could then be established for the final setup.

Tremor and fatigue are two common problems affecting upper limb motion in stroke. The effect of tremor and fatigue on the sensor motion data of stroke patients needs to be understood, so a suitable method can be developed to deal with this, if it proves to be problematic. This could be done by identifying measures (for example, amplitude and frequency) to classify noise types that can corrupt the sensor measurements in normal and pathological (stroke) movement. Examples of measurement noise sources are jerk, shaking, motion artefact, and signal offset due to changes in temperature, fluctuations in gain, or general mechanical wear.

In this study, the model used to represent motion assumed rigid body movement. Understanding the effect of soft tissue (skin) and its movement on sensor measurement accuracy is then of interest. A possible experiment would be to compare the sensor performance when attached to a moving solid tube versus a moving solid tube with stiff foam, with the latter modelling the non-rigid nature of anatomical soft tissue and its influence on the rigid skeletal motion. This would provide additional information that could further refine the model suggested here.

7.3.4 Signal processing

The robustness of the EKF algorithm could be improved. The reach-and-grasp movement was modelled as a one dimensional, sinusoidal movement for simplicity, mainly considering motion along the longitudinal sensor axis (x). However, a true representation of the upper limb movement would incorporate three dimensional motion. An extension of this work would be to model the three dimensional movement in the state transition equation employed by the Kalman filter. The movement could be modelled with a more complex function (possibly using a series of sinusoidal functions). Also, the reach-and-grasp movement has been considered as a primarily linear motion, but it is usually accompanied by a rotation at the elbow (elbow abduction/adduction). So, incorporating the gyroscopic measurements into the EKF observations (to estimate that rotation) could help stabilise the velocity estimate even further.

The movement model could be improved by having an adaptive drift component to account for the effect of gravity. The EKF drift estimate could be improved by supplying position information to the filter at particular time points during the reach-and-grasp exercise. The asymmetry of the reach motion in its forward and backward components for the stroke patient, and increasing movement duration (i.e. having a non-uniform angular velocity) could be included in the filter, possibly through an adaptive angular velocity of the sinusoidal movement acceleration rather than a constant one, as is the case now. The movement duration information could be applied at the extremes of the motion by having the subject touch a pressure pad.

Other ways to improve the EKF performance include manipulating the noise co-variances for the variables in the EKF state vector, and more careful modelling of sensor noise. It

would then be worth checking whether the further improved velocity estimate (obtained from the revised EKF) could meet the requirements of the 68% or 95% confidence interval sensitivity tests as in Chapter 5, and allow the monitoring system (sensors and signal processing algorithms) to also report reliably on movement velocity. Computing the mean and standard deviation of percent time to maximum velocity from the revised velocity data, and comparing that to the values determined from Vicon, is of interest.

A possible improvement to the optimisation method would be to address the offset problem, which was found between the method's velocity estimate, and velocity data obtained from Vicon. This could be done by adding boundary constraints to the optimisation algorithm.

7.3.5 Application improvements and more subjects

The movement regimes for other study groups (for example athletes, elderly, and cerebral palsy children) could be investigated. The EKF and optimisation performance on other exercises, such as hand-to-mouth and forearm pronation/supination, is of interest.

The feasibility analysis of using inertial sensors to measure outcomes in stroke rehabilitation was based on motion data of two rigid bodies, four healthy subjects and a patient in pre/post- stroke intervention. Also, while the EKF filter helped stabilise movement velocity estimation for the stroke patient, other stroke patients might have movement velocity profiles that are completely non-periodic or extremely jerky. So further testing of the sensor, as well as the EKF and optimisation performance on more subjects is needed, to confirm findings and see if the work is applicable for a broader range of patients.

List of References

a3bs.com *Human skeleton models,* http://www.a3bs.com/imagelibrary/A46L_L/human-skeleton-models/A46L_L_arm-skeleton-with-scapula-and-clavicle-right.jpg, (accessed on 9 Novemeber 2010)

Adamson, J., Beswick, A. & Ebrahim, S. (2004). Is stroke the most common cause of disability? J Stroke Cerebrovasc Dis. 13, 171-177.

Allard, P., Stokes, I. A. F. & Blanchi, J. (1995). Three-dimensional analysis of human movement, Human Kinematics, Champaign, U.S.A.

Anglin, C. & Wyss, U. P. (2000a). Arm motion and load analysis of sit-to-stand, stand-to-sit, cane walking and lifting. Clin. Biomechanics 15, 441-448.

Anglin, C. & Wyss, U. P. (2000b). Review of arm motion analyses. IMechE 541-555.

Ashby, P., Andrews, C., Knowles, L. & Lance, J. W. (1972). Pyramidal and extrapyramidal control of tonic mechanisms in the cat. Brain 95, 21-30.

Bar-Shalom, Y. & Fortmann, T. E. (1988). Tracking and Data Association. Cambridge, Massachusetts: Academic Press.

Bar-Shalom, Y., Rong Li, X. & Kirubarajan, T. (2001). Estimations with Applications to Tracking and Navigation: Theory, Algorithms and Software. New York, U.S.A.: Wiley-Interscience.

Barker, T. M., Kelly, I. G. & Paul, J. P. (1996). Three-dimensional joint co-ordination strategies of the upper limb during functional activities. Journal of Engineering in Medicine 210 (H1), 17-26.

Baron, J. C., Cohen, L. G., Cramer, S. C., Dobkin, B. H., H., J.-B., Loubinoux, I., Marshall, R. S. & Ward, N. S. (2004). Neuroimaging in stroke recovery. Cerebrovasc Dis. 18, 260-267.

Barshan, B. & Durrant Whyte, H. (1995). Inertial navigation systems for mobile robots. IEEE Trans. on Robotics and Automation 11, 328-342.

Beaulieu, C. F., Hodge, F., Bergman, D. K., Butts, K., Daniel, B. L., Napper, C. L., Darrow, R. D., Domoulin, C. L. & Herfkens, R. J. (1999). Glenohumeral relationships during physiologic shoulder motion and stress testing: initial experience with open MR imaging and active imaging-plane registration. Radiology 212, 699-705.

Beck, C. H. & Chambers, W. W. (1970). Speed, accuracy and strength of forelimb movement after unilateral pyramidotomy in rhesus monkeys. J. Comp Physiol Psychol 70, 1-22.

Bernspang, B. & Fisher, A. G. (1995). Differences between persons with right or left cerebral vascular accident on the assessment of motor and process skills. Arch Phys Med Rehabil 76, 1144-1151.

Biernaskie, J., Chernenko, G. & Corbett, D. (2004). Efficacy of rehabilitative experience declines wiht time after focal ischemic brain injury. J. Neurosci. 24, 1245-1254.

Biryukova, E. V., Roby-Brami, A., Frolov, A. A. & Mokhtari, M. (2000). Kinematics of human arm reconstructed from spatial tracking system recordings. Journal of Biomechanics 33, 985-995.

Blair, E. & Stanley, F. (1985). Interobserver agreement in the classification of cerebral palsy. Dev Med Child Neurol 27, 615-622.

Brandes, M. (2006). Accelerometry based assessment of gait parameters in children. Gait and Posture 24, 482-486.

Brodal, A. (1973). Self-observations and neuro-anatomical considerations after a stroke. Brain 96, 675-694.

Brodie, M. A., Walmsley, A. & Page, W. (2008). Dynamic accuracy of inertial measurement units during simple pendulum motion. Computer Methods in Biomechanics and Biomedical Engineering 11, 235-242.

Brunnstrom, S. (1994). Movement Therapy in Hemiplegia. New York: Chapman & Hill.

Caimmi, M., Carda, S., Giovanzana, C., Maini, E. S., Sabatini, A. M., Smania, N. & Molteni, F. (2008). Using kinematic analysis to evaluate constraint-induced movement therapy in chronic stroke patients. Neurorehabil. Neural Repair 22, 31-39.

Canadian Institute of NeuroSciences, M. H. a. A. (2005). *The Brain from Top to Bottom,* http://thebrain.mcgill.ca/flash/i/i_06/i_06_cl/i_06_cl_mou/i_06_cl_mou.html, (accessed on 5 June 2011)

Cappozzo, A. (1984). Gait analysis methodology. Human Movement Science 3, 27-50.

Carrol, D. (1965). A quantitative test of upper extremity function. J. chron. Dis. 18, 479-491.

Cerveri, P., Borghese, N. A. & Pedotti, A. (1998). Complete calibration of a stereo photogrammetric system through control points of unknown coordinates. Journal of Biomechanics 31, 935-940.

Codd, J. R., Boggs, D. F., Perry, S. F. & Carrier, D. R. (2005). Activity of three muscles associated with the uncinate processes of the giant Canada goose Branta canadensis maximus. The Journal of Experimental Biology 208, 849-857.

Coley, B., Jolles, B. M., Farron, A., Pichonnaz, C., Bassin, J. P. & Aminian, K. (2008). Estimating dominant upper limb segments during daily activity. Gait & Posture 27, 368-375.

Cozens, J. A. & Bhakta, B. B. (2002). Measuring movement irregularity in the upper motor neurone syndrome using normalised average rectified jerk. Journal of Electromyography and kinesiology 13, 73-81.

Craig, J. (2004). Spatial descriptions and transformations, Introduction to Robotics: Mechanics and Control, pp. 19-61. Lebanon, Indiana, U.S.A.: Pearson Prentice-Hall.

Crouter, S. E., Clowers, K. G. & Bassett, J. D. R. (2006). A novel method for using accelerometer data to predict energy expenditure. J Appl Physiol 100, 1324-1331.

Davids, J. R., Peace, L. C., Wagner, L. V., Gidewall, M. A., Blackhurst, D. W. & Roberson, W. M. (2006). Validation of the Shriners Hospital for Children Upper Extremity Evaluation (SHUEE) for children with hemiplegic cerebral palsy. J Bone Joint Surg Am 88, 326-333.

Davis, R. B., Ounpuu, S., Tyburski, D. & Gage, J. R. (1991). A gait analysis collection and reduction technique. Human Movement Science 10, 575-587.

De Quervain, K., Ines, A., Sheldon, S., Leurgans, S., Pease, W. S. & McAllister, D. (1996). Gait pattern in the early recovery period after stroke. Journal of Bone and Joint Surgery 78A, 1506-1514.

de Veries, W. H. K., Veeger, H. E. J., Baten, C. T. M. & Van der Helm, F. C. T. (2009). Magnetic distortion in motion labs, implications for validating inertial magnetic sensors. Gait & Posture 29, 535-541.

Department of Health (2007). National Stroke Strategy, The Department of Health in the UK: The Department of Health in the UK.

Dewald, J. P. A., Pope, P. S., Given, J. D. & Buchanan, T. S. R. (1995). Abnormal muscle coactivation pattern during isometric torque generation at the elbow and shoulder in hemiparetic subjects. Brain 118, 495-510.

Duncan, P. W., Goldstein, L. B., Machtar, D., Divine, G. W. & Feussner, J. (1992). Measurement of motor recovery after stroke: outcome assessment and sample size requirements. Stroke 23, 1084-1089.

Ehara, H., Fujimoto, S., Miyazaki, S., Tanaka, S. & Yamamoto, S. (1995). Comparison of the performance of 3D camera systems. Gait & Posture 3, 166-169.

Ehara, Y. (2002). Comparison Meeting of Motion Analysis Systems. Clinical Gait Analysis Forum of Japan 1-7.

Eliot, B. C., Alderson, J. A. & Denver, E. R. (2007). System and modelling errors in motion analysis: Implications for the measurement of the elbow angle in cricket bowling. Journal of Biomechanics 40, 2679-2685.

Feys, H., De Weerdt, W., Verbeke, G., Steck, G. C., Capiau, C., Kiekens, C., Putman, K., Dejaeger, E., Van Hoydonck, G., Vermeersch, G. & Cras, P. (2004). Early and repetitive stimulation of the arm can substantially improve the long-term outcome after stroke: a 5-year follow-up study of a randomised trial. Stroke 35, 924-929.

Feys, H., Heterbrij, J., Wilms, G., Dom, R. & De Weerdt, W. (2000). Predicting arm recovery following stroke: value of site of lesion. Acta Neurol Scand 102, 371-377.

Foxlin, E., Altshuler, Y., Naimark, L. & Harrington, M. (2004). FlightTracker: A novel optical/inertial tracker for cockpit enhanced vision. *IEEE Symposium on Mixed and Augmented Reality*, pp. 212-221. Washington, D.C.

Furlani, K. M., Miller, P. K. & Mooney, M. A. (2005). Evaluation of wireless sensor node for measuring slope inclination in geotechnical applications. *22nd International Symposium on Automation and Robotics in Construction (ISARC 2005)*, pp. 1-8. Ferrara, Italy

Ghez, C., Krakauer, J. W., Sainburg, R. & Ghilardi, M. F. (2000). Spatial representations and internal models of limb dynamics in motor learning. The New Cognitive Neurosciences 501-514.

Godwin, A., Agnew, M. & Stevenson, J. (2009). Accuracy of inertial motion sensors in static, quasistatic, and complex dynamic motion. Journal of Biomechanical Engineering 131, 1-5.

Goldstein, L. B. & Matchar, D. B. (1994). Clinical Assessment of Stroke. The Journal of the American Medical Association 271, 1114-1120.

Gresham, D. E., Duncan, P. W. & Stason, W. B. (1995). Editor. Post-stroke rehabilitation, 16 ed. Diane Publishing Co.

Hanselman, D. & Littlefield, B. (2004). Mastering MATLAB 7, Cubic Splines, Chapter 21, pp. 336-349. Pearson, Prentice Hall.

Hogan, N. (1985). The mechanics of multi-joint posture and movement control. Biol Cybern 52, 315-331.

Holden, M. & Dyar, T. (2002). Virtual environment training: a new tool for rehabilitation. Neurorehabil. Neural Repair 26, 62-71.

Hollerbach, M. J. & Flash, T. (1982). Dynamic interaction between limb segments during planar arm movement. Biol Cybern 44, 67-77.

Honeywell (2010). *Accelerometers,* http://www.inertialsensor.com/qat160.shtml, (accessed on 7 July 2010)

Hu, H. & Gan, J. Q. (2005). Sensors and data fusion algorithms in mobile robotics. Department of Computer Science, University of Essex, 2-12.

Hwang, J. Y., Kang, J. M., Jang, Y. W. & Kim, H. C. (2004). Development of novel algorithm and real-time monitoring ambulatory system using bluetooth module for

fall detection in the elderly. *Proceedings of the 26th Annual International Conference of the IEEE EMBS*, pp. 2204-2207. San Francisco, CA, USA: IEEE.

Intercollegiate Working Party for Stroke (2004). National clinical guidelines for stroke.

Johansson, G. (1975). Visual motion perception. Sci. Am. 232, 76-88.

Johnson, G. R. & Anderson, J. M. (1990). Measurement of three-dimensional shoulder movement by an electromagnetic sensor. Clinical Biomechanics 5, 131-136.

Kamper, D. G., McKenna-Cole, A. N., Kahn, L. E. & Reinkensmeyer, D. J. (2002). Alterations in reaching after stroke and their relation to movement direction and impairment severity. Arch Phys Med Rehabil 83, 702-702.

Kandel, E. R., Schwartz, J. H. & Jessell, T. M. (2000). Principles of Neural Science, Fourth ed. McGraw-Hill Medical.

Kavanagh, J. J. & Menz, H. B. (2008). Accelerometry: a technique for quantifying movement patterns during walking (review). Gait & Posture 28, 1-15.

Kim, S. G., Ashe, J. & Hendrich, K. (1993). Functional magnetic resonance imaging of motor cortex hemispheric asymmetry and handedness. Science 261, 615-617.

Klingels, K., Jaspers, E., Van de Winckel, A., De Cock, P., Molenaers, G. & Feys, H. (2010). A systematic review of arm activity measures for children with hemiplegic cerebral palsy. Clin Rehabil 8, 887-900.

Ko, B. H., Park, S. H., Hwang, D. S., Kim, Y. Y. & Yoon, Y. S. (2006). Statistical approach to correct pelvic inclination using estimated thickness of soft tissue. *The International Society for Technology in Arthoplasty*. NewYork, USA

Krakauer, J. W. (2005). Arm function after stroke: From physiology to recovery. Seminars in Neurology 25, 384-394.

Krebs, H. I., Hogan, N., Aisen, M. L. & Volpe, B. T. (1998). Robot-aided neurorehabilitation. IEEE Transactions on Rehabilitation Engineering 6, 75-87.

Lance, J. W. (1980). The control of muscle tone, reflexes, and movement: Robert Wartenberg lecture. Neurology 30, 1303-1313.

Laskoski, G. T., Martins, L. D. L., Pichorim, S. F. & Abatti, P. J. (2009). Development of a telemetric goniometer. *World Congress on Medical Physics and Biomedical Engineering*, pp. 227-230. Munich, Germany: Springer.

Latash, M. L. & Levin, M. F. (2004). Effects of age, disorder, and rehabilitation, Vol. 3, Progress in Motor Control, Human Kinetics, Champaign, USA.

Lawrence, D. G. & Kuypers, H. G. J. M. (1968a). The functional organisation of the motor system in the monkey. I: the effects of bilateral pyramidal lesions. Brain 91, 1-14.

Lawrence, D. G. & Kuypers, H. G. J. M. (1968b). The functional organisation of the motor system in the monkey. II: The effects of lesions of the descending brain-stem pathways. Brain 91, 15-36.

Leardini, A., Cappozzo, A., Catani, F., Toksvig-Larsen, S., Petitto, A., Sforza, V., Cassanelli, G. & Giannini, S. (1999). Validation of a functional method for the estimation of the hip joint centre location. Journal of Biomechanics 9, 185-192.

Levin, M. F. (1996). Interjoint coordination during pointing, movements is distrupted in spastic hemiparesis. Brain 119, 281-293.

Liberson, W. T. (1936). Une nouvelle application du quartz piezoelectrique: piezoelectrographie de la marche et des mouvements volontaires. Le Travail Humain 4, 1-7.

Liberson, W. T., Holmquest, H. J. & Halls, A. (1962). Accelerographic study of gait. Arch Phys Med Rehabil 43, 547-551.

Lievesley, R. (2010). Using a 3-D motion capture system to measure forearm pronation and supination. Oxford Gait Laboratory, Nuffield Orthopaedic Centre (Clinical Scientist Portfolio),

Luinge, H. (2002). Inertial sensing of human movement. PhD thesis, Twente University, The Netherlands.

Luinge, H. J. & Vetlink, P. H. (2005). Measuring orientation of human body segments using miniature gyroscopes and accelerometers. Med Bio Eng. Comput. 43, 273-282.

Lum, P. S., Burgar, C. G., Shor, P. C., Majmundar, M. & Van der Loos, M. (2002). Robot-assisted movement training compared with conventional therapy techniques for the rehabilitation of upper-limb motor function after stroke. Arch Phys Med Rehabil 83, 952-959.

Lyle, R. C. (1981). A performance test for assessment of upper limb function in physical rehabilitation treatment and research. Int. J. Rehab. Research 4, 483-492.

Lyons, G., Culhane, K., Hilton, D., Grace, P. & Lyons, D. (2005). A description of an accelerometer-based mobility monitoring technique. Med Eng Phys 27, 497-504.

Maclean, N., Pound, P., Wolfe, C. & Rudd, A. (2002). The concept of patient motivation: A qualitative analysis of stroke professionals. Stroke 33, 444-448.

Mahmood, K., Hossain, M. S. & Rahman, S. (2009). Review of rehabilitation of ischaemic stroke patients. J. Dhaka Med Coll. 18, 169-173.

Masiero, S., Celia, A., Rosati, G. & Armani, M. (2007). Robotic-assisted rehabilitation of the upper limb after acute stroke. Arch Phys Med Rehabil 88, 142-149.

McGRAW-Hill (2003). Dictionary of Engineering, second ed. New York: Licker, Mark D.

Meskers, C. G. M., Fraterman, H., Van der Helm, F. C. T., Vermeulen, H. M. & Rozing, P. M. (1998). In vivo estimation of the glenohumeral joint rotation center from scapular bony landmarks by linear regression. Journal of Biomechanics 31, 93-96.

Molet, T., Huang, Z., Boulic, R. & Thalmann, D. (1997). A real time anatomical converter for human motion capture. *Proceedings of Computer Animation Conference*, pp. 79-94. Lausanne, Switzerland: Springer-Verlag.

Morasso, P. (1981). Spatial control of arm movements. Exp Brain Res 42, 223-227.

Morecki, A., Ekiel, J. & Fidelus, K. (1971). Bionika ruchu (biomechanics and control of human extremities). Panstwowe Wydawnietwo. Naukowe.

Mussa-Ivaldi, F. A. (1999). Modular features of motor control and learning. Curr Opin Neurobiol 9, 713-717.

Nakamura, T., Yabe, Y. & Horiuchi, Y. (1994). A biomechanical analysis of pronation supination of the forearm using magnetic resonance imaging: dynamic changes of the interosseous membrane of the forearm during pronation supination. Nippon Seikeigekagakuai Zasshi.

Nebot, E. & Durrant Whyte, H. (1999). Initial calibration and alignment of low-cost inertial navigation units for land vehicle applications. Journal of Robotic Systems 16, 81-92.

Oppenheim, A. V. & Schafer, R. W. (1989). Discrete-Time Signal Processing. NJ: Prentice-Hall.

Page, S. J., Levine, P. & Leonard, A. C. (2005). Modified constraint -induced therapy in acute stroke: a randomised controlled pilot study. Neurorehabil. Neural Repair 19, 27-32.

Palastanga, N., Field, D. & Soames, R. (1989). Anatomy and Human Movement - Structure and Function. Oxford: Heinemann Medical Books.

Pennec, X., Cachier, P. & Ayache, N. (2001). Tracking brain deformations in time sequences of 3D US images. *Proceedings of International Conference Information Processing in Medical Imaging*.

Peterson, B. (1994). On a model of the upper extremity. *Advances in the Biomechanics of the Hand and Wrist*, edited by F. Schuind, K. N. An, W. P. Cooney III & M. Garcia-Elias, pp. 95-106. Plenum Press, New York.

Platz, T., Pinkowski, C., Van Wijck, F., Kim, I.-H., di Bella, P. & Johnson, G. (2005). Reliability and validity of arm function assessment with standardized guidelines for the Fugl-Meyer Test, Action Research Arm Test, and Box and Block Test: a multi-centre study. Clin Rehabil 19, 404-411.

Pober, D. M., Staudenmayer, J., Raphael, C. & Freedson, P. S. (2006). Development of novel techniques to classify physical activity mode using accelerometers. Med Sci Sports Exer 38, 1626-1634.

Quinn, T. J., Paolucci, S., Sunnerhagen, K., Sivenius, J., Walker, M. F., Toni, D. & Lees, K. R. (2009). Evidence-based stroke rehabilitation: an expanded guidance document from the European Stroke Organisation (ESO) Guidelines for management of ischaemic stroke and transient ischaemic attack 2008. Journal of Rehabil Med 41, 99-111.

Rao, S. S., Bontrager, E. L., Gronley, J. K., Newsam, C. J. & Perry, J. (1996). Three-dimensional kinematics of wheel-chair propulsion. IEEE Trans. Rehab Engng 4, 152-160.

Rau, G., Disselhort-Klug, C. & Schmidt, R. (2000). Movement biomechanics goes upwards: from the leg to the arm. Journal of Biomechanics 33, 1207-1216.

Richards, J. G. (1999). The measurement of human motion: A comparison of commercially available systems. Human Movement Science 18, 589-602.

Roetenberg, D., Luinge, H. & Slycke, P. (2009). Xsens MVN: Full 6DOF Human Motion Tracking Using Miniature Inertial Sensors. Xsens Technologies, 1-6.

Schepers, H. M., Roetenberg, D. & Veltink, P. (2010). Ambulatory human motion tracking by fusion of inertial and magnetic sensing with adaptive actuation. Med Biol Eng Comput 48, 27-37.

Schmidt, R., Disselhort-Klug, C., Silny, J. & Rau, G. (1999). A marker-based measurement procedure for unconstrained wrist and elbow motions. Journal of Biomechanics 32, 615-621.

Seidel, G. K., Marchinda, D. M., Dijkers, M. & Soutas-Little, R. W. (1995). Hip joint centre location from palable bony landmarks - a cadaver study. Journal of Biomechanics 28, 995-998.

Shadmehr, R. & Wise, S. P. (2005). The computational neurobiology of reaching and pointing: a foundation for motor learning. Cambridge, MA.: The MIT Press.

Shelton, F. N. & Reding, M. J. (2001). Effect of lesion location on upper limb motor recovery after stroke. Stroke 32, 107-112.

Shriners Hospital Upper Extremity Evaluation (SHUEE) protocol (2005). Evaluation (SHUEE) for children with hemiplegic cerebral palsy. Dev Med Child Neurol 47, 39–45.

Singh, D. (2005). Transforming Care: Evidence about Improving Care for People with Long Term Conditions. Health Services Management Centre, School of Social Policy, University of Birmingham, 1-73.

Stroke Association (2008). *When a stroke happens,* http://www.stroke.org.uk/document.rm?id=701, (accessed on 6 June 2011)

Stroke Unit Trialists' Collaboration (2001). Organised inpatient (stroke unit) care for stroke. Cochrane Database Syst Rev 3.

Tao, Y., Hu, H. & Zhou, H. (2007). Integration of vision and inertial sensors for 3D arm motion tracking in home based rehabilitation. The International Journal of Robotics Research 26, 607-624.

Teasell, R. W. & Kalra, L. (2005). What's new in stroke rehabilitation: Back to basics. Stroke 36, 215-217.

The Free Dictionary by FARLEX (2010). *The Medical Dictionary,* http://medical-dictionary.thefreedictionary.com, (accessed on 6 June 2011)

The Stroke Association (2009). Physical effects of stroke.

Thilman, A. F., Fellows, S. J. & Garms, E. (1991). The mechanism of spastic muscle hypertonus: variation in reflex gain over the time course of spasticity. Brain 114, 233-244.

Turner-Stokes, L. (2000). Measurement of outcome in rehabilitation, The British Society of Rehabilitation Medicine. 1-14.

Twitchell, T. E. (1950). The restoration of motor function following hemiplegia in man. Brain 74, 443-480.

Van Andel, C. J., Wolterbeek, N., Doorenbosch, C. A. M., Veeger, H. E. J. & Harlaar, J. (2008). Complete 3D kinematics of upper extremity functional tasks. Gait & Posture 27, 120-127.

Van der Helm, F. C. T. (1996). A standardized protocol for the description of shoulder motions. International Shoulder Group 1-7.

Van der Lee, J. H., Smels, I. A. K., Beckerman, H., Lankhorst, G. J., Wagenaar, R. C. & Bouter, L. M. (2001). Exercise therapy for arm function stroke patient: a systematic review of randomised controlled trials. Clinical Rehabil. 15, 20-31.

Van Peppen, P. R. S., Kwakkel, G., Wood-Dauphinee, S., Hendriks, H. J. M., Van der Wees, P. J. H. & Dekker, J. (2004). The impact of physical therapy on functional outcomes after stroke: what's the evidence? Clinical Rehabil. 18, 833-862.

Van Vliet, P. M., Lincoln, N. B. & Robinson, E. (2001). Comparison of the content of two physiotherapy approaches for stroke. Clinical Rehabilitation 15, 398-414.

Veltink, P., Bussmann, H., de Veries, W. H. K., Martens, W. & van Lummel, R. (1996). Detection of static and dynamic activities using uniaxial accelerometers. IEEE transactions on rehabilitation engineering 4, 375-385.

Vicon Motion Systems (2005). System Preparation, Internal Report, Oxford, UK. 1-43.

Vicon Motion Systems (2006). Vicon_MX_questions_answers. 1-8.

Wade, D., R., L.-H., Wood, V. A., Skilbeck, C. E. & Ismail, H. M. (1983). The hemiplegic arm after stroke: measurement and recovery. Journal of Neurology, Neurosurgery, and Psychiatry 46, 521-524.

Ward, N. S., Brown, M. M., Thompson, A. J. & Frackowiak, R. S. (2004). The influence of time after stroke on brain activations during a motor task. Ann Neurol. 55, 829-834.

Weinberg, A., Pietsch, I., Helm, M., Hesselbach, J. & Tscherne, H. (2000). A new kinematic model of pronation and supination of the human forearm. Journal of Biomechanics 33, 487-491.

Whittle, M. W. (1996). Editor. Gait analysis: an introduction, 2nd ed. Oxford, U.K.: Butterworth Heinemann.

WHO (2002). *ICF Introduction,* http://www.who.int/icf, (accessed on 6 June 2011)

Williams, S., Schmidt, R., Disselhort-Klug, C. & Rau, G. (2006). An upper limb model for the kinematical analysis of the joint chain of the human arm. Journal of Biomechanics 39, 2419-2429.

Winstein, C. J. & Pohl, P. S. (1995). Effects of unilateral brain damage on the control of goal-directed hand movements. Exp Brain Res 105, 163-174.

Woltring, H. J. (1995). Smoothing and differentiation techniques applied to 3-D data, Three Dimensional Analysis of Human Movement, Human Kinetics, edited by P. Allard, I. A. F. Stokes & J. Blanchi, p. 79–99. Champaign, IL.

Woltring, H. J. & Huiskes, R. (1990). Stereophotography (Biomechanics of Human Movement: Applications in Rehabilitation, Sports and Ergonomics). Worthington, Ohio: Bertec Corporation.

World Health Organisation (2004). The global burden of disease - 2004 update: The World Health Organisation.

Wu, C.-y., Chen, C.-l., Tang, S. F., Lin, K.-c. & Huang, Y.-y. (2007). Kinematic and clinical analyses of upper-extremity movements after constraint-induced movement therapy in patients with stroke: A randomised controlled trial. Arch Phys Med Rehabil 88, 964-970.

Wu, C.-y., Lin, K.-c., Chen, H.-c., Chen, I.-h. & Hong, W.-h. (2007). Effects of modified constraint-induced movement therapy on movement kinematics and daily functions in patients with stroke: A kinematic study of motor control mechanisms. Neurorehabil. Neural Repair 21, 460-466.

Wu, G., Siegler, S., Allard, P., Kirtley, C., Leardini, A., Rosenbaum, D., Whittle, M., D'Lima, D., Cristofolini, L., Witte, H., Schmid, O. & Stokes, I. (2002). ISB recommendations on definitions of joint coordinate system of various joints for the reporting of human joint motion - part I: ankle, hip, and spine. Journal of Biomechanics 35, 543-548.

Wu, G., Van der Helm, F. C. T., Veeger, H. E. J. D., Makhsous, M., Van Roy, P., Anglin, C., Nagels, J., Karduna, A. R., McQuade, K., Wang, X., Werner, F. W. & Buchholz,

B. (2005). ISB recommendations on definitions of joint coordinate systems of various joints for the reporting of human joint motion - Part II: shoulder, elbow, wrist and hand. Journal of Biomechanics 38, 981-992.

Xsens Technologies (2007). MTi and MTx User Manual and Technical Documentation. 1-57.

You, S., Neumann, U. & Azamu, R. (1999). Hybrid inertial and vision tracking for augmented reality registration. *IEEE Virtual Reality*, pp. 260-267. Houston, TX, USA

Young, J. & Foster, A. (2007). Review of stroke rehabilitation. BMJ 334, 86-90.

Zatsiorsky, V. M. (1998). Kinematics of Human Motion. Champaign, Illinois, U.S.A.: Human Kinematics Publishers.

Zheng, H., Davies, R., Zhou, H., Wilson, S., Hammerton, J., Mawson, S., Ware, P., Black, N., Harris, N., Eccleston, C., Hu, H. & Mountain, G. (2007). SMART rehabilitation: Implementation of ICT platform to support home-based stroke rehabilitation. Universal Access in Human-Computer Interaction. Applications and Services 831-840.

Zhou, H. & Hu, H. (2007). Upper limb motion estimation from inertial measurements. International Journal of Information Technology 13, 1-14.

Zhou, H. & Hu, H. (2008). Human motion tracking for rehabilitation - a survey. Biomedical Signal Processing and Control 3, 1-18.

Zhou, H., Hu, H. & Harris, N. (2005). Application of wearable inertial sensors in stroke rehabilitation. *Proceedings of the 27th Annual International Conference of the Engineering in Medicine and Biology Society (IEEE-EMBS)*, pp. 6825-6828.

Zhou, H., Hu, H., Harris, N. & Hammerton, J. (2006). Application of wearable inertial sensors in estimation of upper limb movements. Biomedical Signal Processing and Control 1, 22-32.

Zhou, H., Hu, H. & Tao, Y. (2006). Inertial measurements of upper limb motion. Med Bio Eng. Comput. 44, 479-487.

Zhou, H., Stone, T., Hu, H. & Harris, N. (2008). Use of multiple wearable inertial sensors in upper limb motion tracking. Medical Engineering & Physics 30, 123-133.

Appendix A Glossary

Definitions of the terms below are taken verbatim from the Medical Dictionary (The Free Dictionary by FARLEX, 2010) – other than those marked with an asterisk (*).

Abduction	the movement of a body segment in a coronal plane away from the midline of the body
Adduction	the movement of a body segment in a coronal plane towards the midline of the body
Advance planning	the preparation of movement in advance of execution
Anterior	toward the front of the body or in front
Articulate	from Articulation, which is a junction between two or more bones of the skeleton
Coronal (frontal) plane	splits the body vertically from top to bottom into front (anterior) and back (posterior) sections, also known as the median vertical
Descending brain stem pathways	nerve fibres originating from the brain stem motor control nuclei and passing down to the spinal cord
Distal	away from the centre of the body or the root of the limb
Dorsal	on or toward the back of the hand or foot
Dorsi-flexion	flexion of the food in an upward direction
Elevation	superior movement of the shoulder girdle (moving the scapula up)
Extension	increasing inner angle of the joint; the moving apart of two opposing body segments in a sagittal plane (e.g. the straightening of the flexed knee or elbow); opposite to flexion
External rotation	Rotation away from the centre of the body; opposite to internal rotation
Flexion	decreasing inner angle of the joint; the bending of adjacent body segments in a sagittal plane so that their two anterior surfaces are approaching as one
Glenoid fossa	the concavity in the head of the scapula that receives the head of the humerus to form the shoulder joint
Hemisphere	either of the lateral halves of the cerebrum in the brain
Infarct	a localised area of tissue in an organ that is dying or dead, having been deprived of its blood supply as a result of an obstruction
Inferior	below
Internal rotation	rotation towards the centre of the body
Latency*	response time
Lateral	away from the midline of the body (the median plane)
Lateral flexion (bending)	bending of the trunk in the coronal plane to one side
Lateral rotation	rotation of a limb segment about its longitudinal axis such that the anterior surface faces away the midline of

	the body
Marker triads*	surface markers placed in a non-collinear triangle to denote a plane
Medial	toward the centre, or midline of the body (the median plane)
Medial rotation	rotation of a limb segment about its longitudinal axis such that the anterior surface faces towards the midline of the body
Muscle tone	continuous and passive contraction of the muscles (residual muscle tension)
Palmar	on or toward the palm of the hand (the grasping side)
Paresis	partial motor paralysis
Plantar	on or toward the sole of the foot (the ground-facing side)
Posterior	toward the back (rear) of the body or behind
Pronation	rotation of the forearm with the palm turning inward
Proprioception	the unconscious perception of movement and spatial orientation arising from stimuli within the body itself
Proximal	toward the centre of the body or the root of the limb
Pyramidal tract	two groups of nerve fibres arising in the brain and passing down through the spinal cord to motor cells
Radial deviation	movement of the hand in the direction of the thumb
Rotation	movement or pivoting around a long axis
Sagittal median plane	splits the body vertically from front to back into symmetrical left and right sections – also known as the anteroposterior plane
Sagittal paramedian plane	any plane parallel to the sagittal median plane (see above)
Superior	above
Supination	rotation of the forearm with the palm turning outward
Tactile	of, relating to, or affecting the sense of touch
Transverse (horizontal) plane	splits the body into upper and lower sections
Volume capture area*	three dimensional workspace in which movements are captured by Vicon

Appendix B
Outcome Measures in Stroke Rehabilitation

A brief description of some of the most widely used outcome measures is given below. The tests are also provided courtesy of the Occupational Therapy department at the Western Community Hospital in Southampton.

1. Action Research Arm Test (ARAT): This is an improved, reorganised and shortened version of the upper extremity function test first described by Carroll (1965). It was modified by Lyle (1981) using a Guttman scale[16], which led to a drastic simplification of test administration (not heavily dependent on language and complex instructions, and does not require much in the way of equipment and test supplies) and scoring, thereby enhancing the ARAT's clinical utility. This is particularly true for studies of upper extremity function in patients at both the early acute and later stages of stroke recovery; where for the latter, patient capacity is often limited (by signs of fatigue).

   The ARAT assesses function of the upper extremity using ordinal scoring on nineteen items, where 0 indicates no movement, and 3 indicates normal movement. Item scores are summed to create four subscale scores: grasp (18 point maximum), grip (12 point maximum), pinch (18 point maximum), and gross motor (9 point

[16] a psychological instrument developed to ensure that the scaling and measurement occurs only on a single trait (a property called uni-dimensionality).

maximum). The total scale score is a maximum of 57, indicating normal performance. It is also a sensitive tool to detect changes in upper extremity function in the early recovery period after stroke.

2. Fugl-Meyer Test: This test is based on the idea that motor recovery follows a sequential pattern. Therefore, a variety of exercises are tested, beginning with reflexes and progressing through synergic collaborative patterns to selective non-synergic movements.

   The maximum total score of this test for the upper extremity is 126 points; the motor function score for the upper extremity ranges from 0 to 66 points. In addition to motor function, the Fugl-Meyer test assesses joint position sense, sensation, passive range of movement, pain during movement, and motor performance judged on a 3 point scale (0 = unable to perform the movement, 1, 2 = partly able at different degrees to perform the movement, 3 = able to perform the movement normally).

3. Motor Function Tests:

   a. Motricity Index: It was developed in 1990 to measure motor loss, primarily for use after stroke but could be useful to look at upper motor neuron weakness. Weighted scores are used for testing six limb movements; pinch grip, elbow *flexion*, shoulder *abduction*, ankle *dorsi-flexion*, knee *extension* and hip flexion. The grading for this test is on how well the task is performed by a limb, and derived following the Medical Research Council (MRC) grading guidelines.

Test validity and reliability have been proven, and sensitivity of change is seen in the test measurements in recovery after stroke.

b. Motor Assessment Scale: This is a general measure of motor impairment which uses eight hierarchical test categories; which are supine to side lying to intact side, supine to sitting over side of bed, balanced sitting, sitting to standing, walking, upper arm function, hand movements, and advanced hand activities.

   Although well studied with good support for validity and reliability, this is a long test with only one section related to upper limb. For that section, there are six tests that aim to measure the capabilities of the shoulder held in *elevation* for some duration of time, then check flexion and extension of the elbow, going to maintaining a joint position with some external rotation. The six tests are done in the order that they are appear in the test sheet and according to the patient's progress within the test, a score is given from 1 to 6.

c. Rivermead Mobility: It is a general test looking at the posture, sensation, and motor function of the body as a whole. It does not directly measure the upper limb. Nonetheless, it is widely used clinically as it is simple to use, clinically applicable and reliable.

d. Nine-hole Peg Test: The test looks at fine finger movements. The idea behind the test is to place as many of the nine wooden pegs on a wood base with nine holes, with a time limit of seven minutes. Grading is taken as the best presented number of seconds taken to place each peg out of three trials.

1. Action Research Arm Test

ACTION RESEARCH ARM TEST

Patient Name: _____

Rater Name: _____

Date: _____

Instructions

There are four subtests: Grasp, Grip, Pinch, Gross Movement. Items in each are ordered so that:

- if the subject passes the first, no more need to be administered and he scores top marks for that subtest;
- if the subject fails the first *and* fails the second, he scores zero, and again no more tests need to be performed in that subtest;
- otherwise he needs to complete all tasks within the subtest

Activity	Score
Grasp	
1. Block, wood, 10 cm cube (If score = 3, total = 18 and to Grip) Pick up a 10 cm block	_____
2. Block, wood, 2.5 cm cube (If score = 0, total = 0 and go to Grip) Pick up 2.5 cm block	_____
3. Block, wood, 5 cm cube	_____
4. Block, wood, 7.5 cm cube	_____
5. Ball (Cricket), 7.5 cm diameter	_____
6. Stone 10 x 2.5 x 1 cm	_____
Coefficient of reproducibility = 0.98	
Coefficient of scalability = 0.94	
Grip	
1. Pour water from glass to glass (If score = 3, total = 12, and go to Pinch)	_____
2. Tube 2.25 cm (If score = 0, total = 0 and go to Pinch)	_____
3. Tube 1 x 16 cm	_____
4. Washer (3.5 cm diameter) over bolt	_____
Coefficient of reproducibility = 0.99	
Coefficient of scalability = 0.98	
Pinch	
1. Ball bearing, 6 mm, 3rd finger and thumb (If score = 3, total = 18 and go to Grossmt)	_____
2. Marble, 1.5 cm, index finger and thumb (If score = 0, total = 0 and go to Grossmt)	_____
3. Ball bearing 2nd finger and thumb	_____
4. Ball bearing 1st finger and thumb	_____
5. Marble 3rd finger and thumb	_____
6. Marble 2nd finger and thumb	_____
Coefficient of reproducibility = 0.99	
Coefficient of scalability = 0.98	
Grossmt (Gross Movement)	
1. Place hand behind head (If score = 3, total = 9 and finish)	_____
2. (If score = 0, total = 0 and finish	_____
3. Place hand on top of head	_____
4. Hand to mouth	_____
Coefficient of reproducibility = 0.98	
Coefficient of scalability = 0.97	

2. Fugl-Meyer Arm Score

FUGL-MEYER ARM SCORE

Primarily assessed side: left ☐ or right ☐

A. SHOULDER-ELBOW-FOREARM		
I REFLEX-ACTIVITY (patient sitting, verbalise the findings) *Biceps, Triceps, Fingerflexors*	- no reflex-activity ☐ 0 - reflex-activity in biceps and/or fingerflexors ☐ 2 - no reflex-activity ☐ 0 - reflex-activity in extensors ☐ 2	**TOTAL** /4
II ACTIVE MOVEMENTS IN SYNERGIES (patient sitting with the back against the backrest) *a) Flexor synergy*: "hand to your (ipsilateral) ear" with shoulder retraction forearm elbow shoulder *b) Extensor synergy:* "knuckles on contralateral knee" from flexor synergy (eventually passive) Ask the patient to place knees apart. Verbalise the findings. forearm elbow shoulder	none / partial / perfect supination: ☐ 0 / ☐ 1 / ☐ 2 flexion: ☐ 0 / ☐ 1 / ☐ 2 outw rotation: ☐ 0 / ☐ 1 / ☐ 2 abduction (90°) ☐ 0 / ☐ 1 / ☐ 2 elevation: ☐ 0 / ☐ 1 / ☐ 2 retraction: ☐ 0 / ☐ 1 / ☐ 2 none / partial / perfect pronation: ☐ 0 / ☐ 1 / ☐ 2 extension: ☐ 0 / ☐ 1 / ☐ 2 adduction + int rotation ☐ 0 / ☐ 1 / ☐ 2	/18
III DYN. FLEXOR+EXTENSOR SYNERGY (patient sitting) *a) Hand to lumbar spine* "bring your hand on your back"	- the specific detail cannot be performed at all ☐ 0 - hand behind ant sup iliac spine but does not reach the spine ☐ 1	
b) Shoulder flexion 0° to 90° elbow extended, forearm in midposition "bring your extended arm up, thumb upwards". The assessor may assist the patient to get into the starting position.	- the detail is performed faultlessly ☐ 2 - arm immediately in abduction or elbow in flexion ☐ 0 - cannot cover full range or shoulder abduction and/or elbow in flexion occurs ☐ 1 - the detail is performed faultlessly ☐ 2	

c) Pro-Supination of the forearm elbow flexed 90°, shoulder 0°	- starting position impossible and/or no pro-supination ☐ 0 - limited pro-supination and/or starting position possible and kept during the movement, ☐ 1 - the detail is performed faultlessly ☐ 2	/6
IV ACTIVE MOVEMENT, WITH LITTLE OR NO SYNERGY (patient sitting)		
a) Shoulder abduction 0° to 90° elbow fully extended and forearm pronated The assessor may assist the patient to get into the starting position.	- immediately supinated and/or elbow flexed ☐ 0 - partly performed or elbow is flexed or forearm can not be kept in pronated position ☐ 1 - the detail is performed faultlessly ☐ 2	
b) Shoulder flexion 90° to 180° arm in adduction, elbow extended and forearm in midposition, "bring extended arm up, thumb up" The assessor may assist the patient to get into the starting position.	- arm immediately in abd. or elbow flexed ☐ 0 - arm not immediately in abduction and/or elbow in flexion ☐ 1 - the detail is performed faultlessly ☐ 2	
c) Pro-Supination of the forearm shoulder 30° - 90° flexion, elbow in extension Score against the passive RoM, don't mistake the rotation of the glenohumeral joint.	- starting position impossible and/or no pro-sup ☐ 0 - starting position possible and kept during the movement, limited pro-sup ☐ 1 - the detail is performed faultlessly ☐ 2	/6
V NORMAL REFLEX-ACTIVITIES Only assessed if in the previous section total score = 6	a) not assessed (because score of A. IV < 6) ☐ 0 b) assessed: - ≥ 2 of 3 reflex-activities are markedly hyperactive ☐ 0 - 1 reflex markedly hyperactive or ≥ 2 lively ☐ 1 - no hyperactive reflexes ☐ 2	/2
B. WRIST		
a) Wrist stability in 15° dorsal flexion shoulder 0°, elbow 90°, forearm fully pronated Assessor may bring and keep the elbow in the required position.	- 15° dorsiflexion not achieved ☐ 0 - wrist dorsiflexion performed, no resistance ☐ 1 - position can be maintained against some (slight) resistance ☐ 2	
b) Max. wrist flexion - extension shoulder in 0°, elbow 90°, forearm pronated Assessor may support the elbow in the required position.	- no active repeated movements ☐ 0 - active movements less than passive range ☐ 1 - detail is fully and adequately performed ☐ 2	
c) Wrist stability in 15° dorsiflexion shoulder slightly flexed and/or abducted, elbow extended, forearm pronated Assessor may support the elbow in this position.	- dorsiflexion to required position not possible ☐ 0 - required wrist position possible, no resistance ☐ 1 - required position can be maintained against some (slight) resistance ☐ 2	

d) Max. wrist flexion - extension shoulder slightly flexed and/or abducted, elbow extended, forearm pronated Assessor may support the elbow if needed.	- no active repeated movements ☐ 0 - active movements smaller than passive movements ☐ 1 - detail is fully and adequately performed ☐ 2	
e) Circumduction of the wrist shoulder 0°, elbow 90°. Assessor may provide support for the forearm but not restrain it.	- circumduction cannot be performed ☐ 0 - jerky or incomplete movements ☐ 1 - detail is fully and adequately performed ☐ 2	/10
C. HAND (assessor may support the elbow in 90° position; not the wrist)		
a) Flexion of the fingers	- no flexion ☐ 0 - some, but not full active flexion ☐ 1 - full active flexion compared with the unaffected hand ☐ 2	
b) Extension of the fingers from the position of full flexion (passive)	- no extension ☐ 0 - some, but not full ext. or release of an active mass flexion grasp ☐ 1 - full active extension, compared with the unaffected hand ☐ 2	
c) Grasp A: extension MCP, flexion PIP and DIP grasp is tested against resistance	- required position not possible ☐ 0 - grasp is weak ☐ 1 - grasp maintained against relatively great resistance ☐ 2	
d) Grasp B: extended index and thumb patient should perform a pure thumb adduction (holding a scrap of paper against a vertical tug)	- the function can not be performed ☐ 0 - scrap of paper kept in place, not against a slight tug ☐ 1 - scrap of paper is held well against a tug ☐ 2	
e) Grasp C: pulpa thumb against the pulpa of the index (holding a pencil against a horizontal tug)	- the function can not be performed ☐ 0 - pencil kept in place, not against a slight tug ☐ 1 - pencil is held well against a tug ☐ 2	
f) Grasp D: volar surface of the thumb and index against each other (holding a cylinder-shaped object against a horizontal tug)	- the function can not be performed ☐ 0 - cylinder kept in place, not against a slight tug ☐ 1 - cylinder is held well against a tug ☐ 2	
g) Grasp E: spherical grasp (grasping a tennisball and holding it against a tug)	- the function can not be performed ☐ 0 - ball grasped, not held against a slight tug ☐ 1 - ball grasped, well held against a tug ☐ 2	/14

D. COORDINATION/ SPEED (no compensation of trunk - head allowed)				
Finger-to-nose test: eyes closed, starting position is abduction, 5 times				
a) *Tremor*	marked ☐ 0	slight ☐ 1	no ☐ 2	
b) Dysmetria	pronounced or unsystematic ☐ 0	slight and systematic ☐ 1	no ☐ 2	
c) Time compare time affected to unaffected side	> 6 sec ☐ 0	2-5 sec ☐ 1	< 2 sec ☐ 2	/6
	time right: sec.	time left: sec.		
	TOTAL MOTOR FUNCTION, UPPER LIMB			.../66

H. SENSATION				
Ask the patient whether she/he feels that light touch on both arms and the palmar surface of the hands gave the same qualitative and quantitative impression. *a) Light touch* Score light touch as follows: 0: anaesthesia 1: hypaesthesia, dysaesthesia 2: normaesthesia				
- volar side of the forearm	0	1	2	
- palmar surface of the hand	0	1	2	

b) Position sense of the joints Patient blindfolded. Score position sense of the joints as follows: 0: absence of sensation 1: considerable difference compared with the joint on the unaffected side, but at least ¾ of the answers correct 2: all answers correct, little or no difference comparing unaffected with affected limb				
- thumb (inter-phalangeal joint)	0	1	2	
- wrist	0	1	2	
- elbow	0	1	2	/12
- glenohumeral joint	0	1	2	
	TOTAL SENSATION, UPPER LIMB			**../12**

***J.* PASSIVE JOINT MOVEMENT/JOINT PAIN**				
a) Passive joint movement Score passive joint movement as follows: 0: only few degrees of range-of-movement 1: decreased passive range-of-movement 2: normal passive range-of-movement				
Shoulder flexion	0	1	2	
abduction to 90 °	0	1	2	
outw. rotation	0	1	2	
inw. rotation	0	1	2	
Elbowflexion	0	1	2	
extension	0	1	2	
Forearm pronation	0	1	2	
supination	0	1	2	
Wrist flexion	0	1	2	
extension	0	1	2	
Fingers flexion	0	1	2	
extension	0	1	2	/24

b) Joint pain Score occurrence of joint pain as follows: 0: pronounced pain during all the movement or very marked pain at the end of the actual range of movement 1: some pain 2: no pain					
Shoulder	flexion	0	1	2	
	abduction to 90 °	0	1	2	
	outw. rotation	0	1	2	
	inw. rotation	0	1	2	
Elbowflexion		0	1	2	
	extension	0	1	2	
Forearm	pronation	0	1	2	
	supination	0	1	2	
Wrist	flexion	0	1	2	
	extension	0	1	2	
Fingers	flexion	0	1	2	/24
	extension	0	1	2	
		TOTAL RANGE OF MOVEMENT AND JOINT PAIN, UPPER LIMB			**../48**

Motricity Index: guidelines

'he patient should be sitting in a chair or on the edge of the bed, but can be tested ying if necessary. The grading is derived from the Medical Research Council (MRC) rades, but weighted scores are used. Six limb movements are tested.

'inch grip
ısk patient to grip a 2.5-cm object (cube) between his thumb and forefinger. Object hould be on a flat surface (for example, a book). Monitor any *forearm* or *small and* muscles.

19 = drops object when lifted (examiner may need to lift wrist)
22 = can hold in air, but easily dislodged

'lbow flexion
lbow flexed to 90 degrees, forearm horizontal and upper arm vertical. Patient sked to bend elbow so that hand touches the shoulder. Examiner resists with hand n wrist. Monitor *biceps*.

14 = *If* no movement seen, may hold elbow out so that arm is *horizontal*.

'houlder abduction
Vith elbow fully flexed and against chest, patient asked to abduct arm. Monitor ontraction of *deltoid*; movement of shoulder girdle does not count—there must be novement of humerus in relation to scapula.

19 = abducted more than 90 degrees beyond horizontal.

ınkle dorsiflexion
'oot relaxed in plantar flexed position. Patient asked to dorsiflex foot ('As if tanding on your heels'). Monitor *tibialis anterior*.

14 = less than full range of dorsiflexion

Knee extension
'oot unsupported, knee at 90 degrees. Patient asked to extend (straighten) knee o touch examiner's hand held level with the knee. Monitor contraction of the *quadriceps*.

14 = less than 50 per cent of full extension (i.e. 45 degrees only)
19 = knee fully extended, but easily pushed down

Hip flexion
Sitting with hip bent at 90 degrees. Patient asked to lift knee towards chin. Check for ıssociated (trick) movement of leaning back, by placing hand behind back and ısking patient not to lean back. Monitor contraction of *illio-psoas* (hip flexors).

14 = less than full range of possible flexion (check passive movement)
19 = fully flexed, but easily pushed down

Trunk Control Test: guidelines

Four movements/functions are tested, with the patient lying on the bed.

Rolling to weak side
From lying on back, rolling over on to weak side. May push/pull on bed with good arm.

Rolling to strong side
From lying on back, bringing weak limbs over
12 if uses good limbs to help

Sitting up from lying down
From lying on back—may use arm(s) to push or pull
12 if pulls on pole, rope, sheets, etc.

Sitting balance
Sitting on edge of bed, feet off ground—balance for 30 sec
12 if needs to touch anything with hands to stay upright
0 if unable to stay up (any way) for 30 sec

References Demeurisse *et al.* (1980); Parker *et al.* (1986); Wade, Langton, and Hewer (1987*b*); Sunderland *et al.* (1989); Collin and Wade (1990); Collen *et al.* (1990)

Comment
A short simple measure of motor loss primarily developed for use after stroke but probably useful in any patient with upper motor neuron weakness. Validity and reliability proven, and sensitive to change seen in recovery after stroke. Although not popular with traditional physiotherapists (and not intended to guide therapy), it is very useful in routine clinical practice. Strongly recommended.

Motor Assessment Scale

General instructions

1. The test should preferably be carried out in a quiet private room or curtained-off area.
2. The test should be carried out when the patient is maximally alert and not when under the influence of hypnotic or sedative drugs. Record if the patient is under the influence of sedative drugs.
3. Patient should be dressed in suitable street clothes with sleeves rolled up and without shoes and socks. Items 1 to 3 inclusive may be scored if necessary with the patient in his right clothes.

4. Each item is recorded on a scale of 0 to 6.
5. All items are to be performed independently by the patient unless otherwise stated. 'Stand-by help' means that the physical therapist stands by and may steady patient but must not actively assist.
6. Items 1 to 8 are recorded according to the patient's responses to specific instructions. General Tonus (item 9) is scored from continuous observations and handling throughout the assessment.
7. Patient should be scored on best performance. Repeat three times unless other specific instructions are given.
8. Because the scale is designed to score the patient's best performance, the physical therapist should give general encouragement but should not give specific feedback on whether response is correct or incorrect. Sensitivity to the patient is necessary to enable him to produce his best performance.
9. Instructions should be repeated and demonstrations given to the patient if necessary.
10. The order of administration of the items can be varied according to convenience.
11. If the patient becomes emotionally labile at any stage during scoring, the physical therapist should wait 15 sec before attempting the following procedures:
    - ask the patient to close his mouth and take a deep breath; and
    - hold the patient's jaw closed and ask the patient to stop crying.

    If patient is unable to control behaviour, the examiner should cease testing him and re-score this item and any other items unscored at a more suitable time.
12. If performance is scored differently on left and right side, the physical therapist may indicate this with an 'L' in one box and an 'R' in another box.
13. The patient should be informed when being timed.
14. You will need: a low, wide plinth, a stopwatch, a polystyrene cup, eight jelly-beans, two teacups, a rubber ball 14 cm (5-in) diameter, a stool, a comb, a top of a pen, a table, a dessert spoon and water, a pen, a prepared sheet for drawing lines, and a cylindrical object such as a jar.

A. *Supine to side lying on to intact side*

1. Pulls himself into side lying.
   Starting position must be supine lying, not knees flexed. Patient pulls himself into side lying with intact arm, moves affected leg with intact leg.
2. Moves leg across actively and lower half of body follows.
   Starting position as above. Arm is left behind.
3. Arm is lifted across body with other arm. Leg is moved actively and body follows in a block.
   Starting position as above.
4. Moves arm across body actively and rest of body follows in a block.
   Starting position as above.
5. Moves arm and leg and rolls to side but overbalances.
   Starting position as above. Shoulder protracts and arm flexes forward.
6. Rolls to side in 3 sec.
   Starting position as above. Must not use hands.

B. *Supine to sitting over side of bed*

1. Side lying, lifts head sideways but cannot sit up.
   Patient assisted to side lying.
2. Side lying to sitting over side of bed.
   Therapist assists patient with movement. Patient controls head position throughout.
3. Side lying to sitting over side of bed.
   Therapist gives stand-by help by assisting legs over side of bed.
4. Side lying to sitting over side of bed.
   With no stand-by help.
5. Supine to sitting over side of bed.
   With no stand-by help.
6. Supine to sitting over side of bed within 10 sec.
   With no stand-by help.

C. *Balanced sitting*

1. Sits only with support.
   Therapist should assist patient into sitting.
2. Sits unsupported for 10 sec.
   Without holding on, knees and feet together, feet can be supported on floor.
3. Sits unsupported with weight well forward and evenly distributed.
   Weight should be well forward at the hips, head and thoracic spine extended, weight evenly distributed on both sides.
4. Sits unsupported, turns head and trunk to look behind.
   Feet supported and together on floor. Do not allow legs to abduct or feet to move. Have hands resting on thighs, do not allow hands to move on to plinth.
5. Sits unsupported, reaches forward to touch floor, and returns to starting position.
   Feet supported on floor. Do not allow patient to hold on. Do not allow legs and feet to move, support affected arm if necessary. Hand must touch floor at least 10 cm (4 in) in front of feet.
6. Sits on stool unsupported, reaches sideways to touch floor, and returns to starting position.
   Feet supported on floor. Do not allow patient to hold on. Do not allow legs and feet to move, support affected arm if necessary. Patient must reach sideways, not forward.

D. *Sitting to standing*

1. Gets to standing position with help from therapist.
   Any method.

2. Gets to standing position with stand-by help.
   Weight unevenly distributed, uses hands for support.
3. Gets to standing position.
   Do not allow uneven weight distribution or help from hands.
4. Gets to standing position and stands for 5 sec with hips and knees extended.
   Do not allow uneven weight distribution.
5. Sitting to standing with no stand-by help.
   Do not allow uneven weight distribution. Full extension of hips and knees.
6. Sitting to standing with no stand-by help three times in 10 sec.
   Do not allow uneven weight distribution.

E. *Walking*

1. Stands on affected leg and steps forward with other leg.
   Weight-bearing hip must be extended. Therapist may give stand-by help.
2. Walks with stand-by help from one person.
3. Walks 3 m (10 ft) alone or uses any aid but no stand-by help.
4. Walks 5 m (16 ft) with no aid in 15 sec.
5. Walks 10 m (33 ft) with no aid, turns around, picks up a small sandbag from floor, and walks back in 25 sec.
   May use either hand.
6. Walks up and down four steps with or without an aid but without holding on to the rail three times in 35 sec.

F. *Upper-arm function*

1. Lying, protract shoulder girdle with arm in elevation.
   Therapist places arm in position and supports it with elbow in extension.
2. Lying, hold extended arm in elevation for 2 sec.
   Therapist should place arm in position and patient must maintain position with some external rotation. Elbow must be within 20 degrees of full extension.
3. Flexion and extension of elbow to take palm to forehead with arm as in 2 above.
   Therapist may assist supination of forearm.
4. Sitting, hold extended arm in forward flexion at 90 degrees to body for 2 sec.
   Therapist should place arm in position and patient must maintain position with some external rotation and elbow extension. Do not allow excess shoulder elevation.
5. Sitting, patient lifts arm to above position, holds it there for 10 seconds, and then lowers it.
   Patient must maintain position with some external rotation. Do not allow pronation.
6. Standing, hand against wall. Maintain arm position while turning body towards wall.
   Have arm abducted to 90 degrees with palm flat against the wall.

G. *Hand movements*

1. Sitting, extension of the wrist.
   Therapist should have patient sitting at table with forearm resting on the table. Therapist places cylindrical object in palm of patient's hand. Patient is asked to lift object off the table by extending the wrist. Do not allow elbow flexion.
2. Sitting, radial deviation of wrist.
   Therapist should place forearm in midpronation–supination (i.e. resting on ulnar side, thumb in line with forearm and wrist in extension, fingers around a cylindrical object). Patient asked to lift hand off table. Do not allow elbow flexion or pronation.
3. Sitting, elbow into side, pronation and supination.
   Elbow unsupported and at a right angle. Three-quarter range is acceptable.
4. Reach forward, pick up large ball of 14 cm (5-in) diameter with both hands and put it down.
   Ball should be on table so far in front of patient who has to extend arms fully to reach it. Shoulders must be protracted, elbows extended, wrist neutral or extended. Palms should be kept in contact with the ball.
5. Pick up a polystyrene cup from table and put it on table across other side of body.
   Do not allow alteration in shape of cup.
6. Continuous opposition of thumb and each finger more than 14 times in 10 sec.
   Each finger in turn taps the thumb, starting with index finger. Do not allow thumb to slide from one finger to the other, or to go backwards.

H. *Advanced hand activities*

1. Picking up the top of a pen and putting it down again.
   Patient stretches arm forward, picks up pen top, releases it on table close to body.
2. Picking up one jellybean from a cup and placing it in another cup.
   Teacup contains eight jellybeans. Both cups must be at arms' length. Left hand takes jellybean from cup on right and releases it in cup on left.
3. Drawing horizontal lines to stop at a vertical line 10 times in 20 sec.
   At least five lines must touch and stop at the vertical line.
4. Holding a pencil, making rapid consecutive dots on a sheet of paper.
   Patient must do at least two dots a second for 5 sec. Patient picks pencil up and positions it without assistance. Patient must hold pen as for writing. Patient must make a dot and not a stroke.
5. Taking a dessert spoon of liquid to the mouth.
   Do not allow head to lower towards spoon. Do not allow liquid to spill.
6. Holding a comb and combing hair at back of head.

4. Nine Hole Peg Test

Southampton City NHS
Primary Care Trust

Nine-Hole PEG Test (NHPT) – Score Sheet

Patients Name: .....

Date of Birth: .....

Hospital No: .....

Diagnosis: .....

Primary Physiotherapist: .....

Dominate Hand: Left / Right

Hand used: Unaffected / Affected

Left / Right

On each repetition of the NHPT, the following data should be recorded:

- The time taken (in seconds) to place each peg
- The time taken to completed the test from start to finish
- The number of pegs which have been successfully placed within a 50 second time limit

	Time Taken to Place Each Peg / Seconds									Total	50s
Date	1	2	3	4	5	6	7	8	9		